

**Alma Mater Studiorum – Università di Bologna**

**DOTTORATO DI RICERCA IN  
CHIMICA**

**Ciclo XXVI**

**Settore Concorsuale di afferenza: 03**

**Settore Scientifico disciplinare: B1**

***CRYSTAL ENGINEERING OF BRIGHT LUMINESCENT COPPER IODIDE CLUSTERS WITH PHOSPHORUS AND NITROGEN-BASED LIGANDS***

**Presentata da:      Paolo Pio Mazzeo**

**Coordinatore Dottorato**

**Prof. Aldo Roda**

**Relatore**

**Prof. Dario Braga**

**Esame finale anno 2014**



*We adore chaos because  
we love to produce order.  
— M.C. Escher*



---

# Index

---

<b>Introduction</b>	<b>1</b>
Photophysical properties of polynuclear copper (I) complexes	2
Geometry landscape: an experimental approach	3
Metal-Organic Frameworks and crystalline device	5
Single phase white-emitting compounds	7
OLED devices	7
<b>Chapter 1   Polymorph and isomer conversion of complexes based on CuI and PPh<sub>3</sub> easily observed via luminescence</b>	<b>11</b>
Introduction	13
Results and Discussions	15
Conclusions	25
Experimental section	25
<b>Chapter 2   Switch on - switch off signal in a MOF-guest crystalline device</b>	<b>31</b>
Introduction	33
Results and Discussions	41
Conclusions	42
Experimental section	43
<b>Chapter 3   Phosphorescence quantum yield enhanced by intermolecular hydrogen bonds in Cu<sub>4</sub>I<sub>4</sub> clusters in the solid state</b>	<b>45</b>
Introduction	47
Results and Discussions	49
Experimental section	58
Conclusions	61
<b>Chapter 4   Mechanochemical preparation of Copper Iodide clusters of interest for luminescent devices</b>	<b>65</b>
Introduction	67
Experimental section	69
Results and Discussions	72
Conclusions	79
<b>Chapter 5   Single-phase white-emitter copper iodide based Metal-Organic Framework</b>	<b>83</b>
Introduction	85
Results and Discussions	86
Conclusions	89
Experimental section	90

---

<b>Chapter 6   Thin Film deposition and OLED preparation</b>	<b>93</b>
Introduction	95
General procedure for thin film high vacuum deposition on glass substrates	95
Direct complex sublimation	96
CuI thin films	97
Gas-solid reactions	99
Layer-by-layer deposition (LBL)	100
OLED design and preparation	101
<b>Chapter 7   Structure determination from X-ray powder diffraction data</b>	<b>105</b>
Introduction	107
Structure determination of Cu <sub>4</sub> I <sub>4</sub> (3-quinoclidinol) <sub>4</sub>	109
Structure determination of catena(bis(μ <sub>3</sub> -iodo(3-aminomethyl)pyridine))-copper(I)	110
Structure solution of CuIPN <sub>3</sub>	111
<b>Chapter 8   Tuning the colour and efficiency in OLEDs by using amorphous or polycrystalline emitting layers</b>	<b>113</b>
Introduction	115
Experimental	116
Results and Discussion	118
Conclusions	129
Conclusions	133
<b>Appendix A</b>	<b>135</b>
<b>Appendix B</b>	<b>143</b>
<b>Appendix C</b>	<b>147</b>
<b>Appendix D</b>	<b>159</b>
<b>Appendix E</b>	<b>163</b>
<b>Appendix F</b>	<b>167</b>

---

## **Relazione finale**

Candidato: Paolo P. Mazzeo

Relatore: Prof. Dario Braga

Curriculum Chimico, indirizzo inorganico

Crystal Engineering of bright luminescent copper iodide clusters with phosphorous and nitrogen-based ligands

Il lavoro del Dott. Paolo P. Mazzeo nel triennio di frequenza del Dottorato in Chimica si è svolto lungo due principali linee di ricerca ovvero la progettazione, sintesi e completa caratterizzazione di complessi luminescenti a base di rame ioduro e la risoluzione di strutture cristalline da dati di diffrazione da polvere.

Sin dal principio del suo percorso dottorale Paolo Mazzeo si è applicato verso la ricerca di complessi luminescenti ad alta efficienza e basso costo, come i complessi di rame (I), progettandoli in modo da aumentarne il rendimento quantico e ottimizzarne l'utilizzo in dispositivi per optoelettronica. Tale dispositivo è stato infine progettato basandosi su questi complessi, mettendo a punto una metodica di preparazione non convenzionale per la preparazione di tali dispositivi e superando il problema legato al basso peso molecolare in condizioni di sublimazione.

I risultati ottenuti hanno, infatti, dimostrato che questi complessi sono idonei per essere utilizzati in dispositivi come OLEDs e possono contribuire alla diffusione di questa tecnologia rendendola più economicamente accessibile.

Nell'ambito della ricerca legata a complessi luminescenti di rame, si è poi studiato come le proprietà luminescenti siano legate alla struttura del complesso finale in stato solido sintetizzando una vasta gamma di complessi a diversa nuclearità fino ad ottenere un MOF (metal-organic framework) la cui emissione globale risulta bianca a temperatura ambiente.

I metal organic frameworks sono stati un argomento caro al dottorando che dopo aver sintetizzato un MOF luminescente si è cimentato nella progettazione di un MOF-guest crystalline-device in cui il guest era capace di interagire con l'impalcatura esterna modificandone le proprietà fisiche a seguito di stimoli elettrici esterni.

Nell'ambito del suo progetto di ricerca, Paolo Mazzeo ha sviluppato una solida conoscenza delle tematiche implicate, acquisendo una completa padronanza delle tecniche sperimentali sviluppando soluzioni originali ai problemi che si sono via via presentati, dimostrando ottime capacità di organizzazione del proprio lavoro coordinandosi in modo ottimale con i colleghi di laboratorio. Ha inoltre svolto attività seminariale presso il Corso di Laurea Magistrale in Fotochimica e Materiali Molecolari, dimostrando buone capacità didattiche.

Nel corso del suo secondo anno di ricerca dottorale Paolo Mazzeo ha trascorso un periodo all'estero presso l'università di Reading sotto la supervisione del Dr. Kenneth Shankland. Durante il suo soggiorno presso tale laboratorio egli ha avuto modo di imparare le tecniche legate risoluzione di strutture cristalline da polveri: dalla preparazione del campione fino al raffinamento della struttura finale. I principali risultati raggiunti nel triennio di ricerca sono documentati da sette articoli scientifici di cui è coautore pubblicati in importanti riviste internazionali, mentre altri articoli sono in fase di preparazione. È in fase di preparazione anche un brevetto al quale il dottorando è stato coinvolto in prima persona. Ha inoltre partecipato a dieci tra convegni e scuole nazionali e internazionali, dove ha presentato comunicazioni poster e orali mostrando ottima padronanza e capacità di organizzazione del materiale scientifico e efficaci doti comunicative. Si è inoltre distinto meritandosi il riconoscimento da parte dell'associazione italiana cristallografia per la sua tesi magistrale in ambito cristallografico.

Nella mia esperienza di supervisore, poche volte ho visto concentrate in una sola persona tante qualità umane e professionali. Mi sento di esprimere un giudizio pienamente positivo del lavoro di Paolo Mazzeo.

Dario Braga



# Introduction

Even after the commercial launch of organic light-emitting diodes (OLEDs) as technology for lighting and display applications some years ago, essential questions remain unsolved. Luminescent metal complexes containing Ir, Pt or Os are widely used as emitters for OLEDs not only because of their colour tunability but also because of their high efficiencies. However, these noble and precious metals are rather expensive and environmentally problematic, which complicates their usage in high-volume productions. To enter mass market applications, luminescent complexes based on more abundant and cost-efficient metals with  $d^{10}$  configuration, such as Cu(I), Ag(I), or Au(I) are currently in the focus of numerous research studies.<sup>1-4</sup>

Among them, copper(I) complexes are favoured as they present several advantages: they are characterized by a large variety of coordination geometries which arise from the many possible combinations of coordination numbers (two, three and four) available for copper(I) and geometries that can be adopted by the halide ions (from terminal to  $\mu^2$ - and up to  $\mu^8$ -bridging);<sup>5,6</sup>

Among several systems, copper(I) halides aggregates represents a prominent and well-investigated family which currently lies at the forefront of both coordination chemistry and crystal engineering research because of the quest of active material for optoelectronic<sup>7-14</sup>.

In this work a panoramic overview of copper(I) complexes photophysical properties will be provided and few different aspects of crystal engineering will be analysed to understand how these complexes could play a key role in the development of optoelectronic field as mass market application.

## Photophysical properties of polynuclear copper (I) complexes

Polynuclear adducts of cuprous halide salt and organic bases of general formula  $\text{Cu}_n\text{X}_n\text{L}_m$  ( $\text{X}=\text{Cl}, \text{Br}$  or  $\text{I}$ ;  $\text{L} = \text{N-}$  or  $\text{P}$ -bound ligand) have been known since the beginning of the 20<sup>th</sup> century<sup>15</sup>. Copper (I) complexes are widely studied cause of the uniqueness of their photophysical properties; in fact, these kind of multinuclear complexes displays two distinct emission bands with marked environmental sensitivity and with relative intensities that vary with excitation source and sharply with temperature. The low-energy (LE) band dominates at room temperature while the high-energy (HE) band becomes more prominent at low temperature. These temperature dependences of emission spectra was first noted in the 1970s by Hardt and co-workers who coined the term *luminescence thermochromism*. Early work on copper(I) halides aggregates, especially the luminescent thermocromism phenomenon, elicited the interest of Ford et al. who continuously embarked on a careful and extensive research project focused on the luminescent properties of  $\text{Cu}_4\text{I}_4\text{py}_4$  and its derivatives, both experimentally<sup>16-18</sup> and theoretically<sup>19, 20</sup>.

These complexes present different luminescent levels which can be ligand centred, charge transfer or, in the case of polynuclear compounds, even metal-centred nature;<sup>18, 21</sup> most of the complexes studied are characterized by a remarkable high quantum yield in solid state;<sup>10, 22, 23</sup> and finally the reagents are cheap and it is relatively easy to obtain the final products.<sup>2, 10</sup>

The luminescent properties of copper(I) halide clusters are strictly related to the geometries adopted by the clusters.<sup>21</sup> In the case of the cubanes  $\text{Cu}_4\text{I}_4\text{L}_4$  and unsaturated ligands for example, two distinct emission bands were observed, the high-energy band attributed to halide-to-ligand charge transfer ( $^3\text{XLCT}$ ), and the low-energy emission band was attributed to a triplet Cu-I Cluster-Centered ( $^3\text{CC}$ ) excited state with the excitation localized to the  $\text{Cu}_4\text{I}_4$  core, only possible in the presence of an interaction between the metal centres. Recently studies have widened the possibility of the emission properties of Copper (I) compounds. Several Cu(I) compounds with  $\text{P}^{\wedge}\text{N}$  ligands present a low singlet-triplet splitting which allows the emission from both the singlet and the triplet excited state depending on the temperature. The singlet excited state, which is slightly higher in energy than the triplet state, can be thermally activated at the expense of the triplet state, leading to the so-called thermally activated delayed fluorescence (TADF). The TADF emission mechanism involves both singlet and triplet states, and therefore, it has been exploited for singlet and triplet excitons for the generation of light in an electroluminescent devices.<sup>22, 24</sup>

## Geometry landscape: an experimental approach

The crystal engineering of copper halides is particularly difficult since in solution, halocuprate complexes are involved in kinetically fast dissociative and associative equilibria<sup>25, 26</sup> and the labile coordination numbers and geometries of both copper(I) and halide ions allows an inner-core variability difficult to predict *a priori*. These complexes are characterized by a flat energy landscape confirmed by the presence of several different copper halides complexes in the CSD<sup>27</sup> which present dramatically different nuclearity of the Cu<sub>x</sub>I<sub>y</sub> cores such as discrete dimers, cubane tetramers, stepped cubane tetramers to infinity polymeric chains (including split stairs, zig-zag, helical, staircase, rack and columnar ones). Although the final structures of the copper(I) halide complexes in crystals could be hardly designed, the reaction stoichiometry allows some degree of control of the copper(I) halide core: reactions with a stoichiometry ratio of CuI/L >>1 higher nuclearity are favoured while CuI/L <<1 promote the formation of monomers.<sup>28</sup> However, to explore all the possible crystal forms it is necessary to vary not only the stoichiometry but also other parameters such as solvent, temperature etc..

In the following chapters different experiments are reported in which CuI has been reacted with triphenylphosphine ligand. Organophosphine copper(I) halides have been extensively studied in the past<sup>29, 30</sup> and several species with different metal coordination numbers and metal:ligand stoichiometries (figure 1.1) have been already reported.

The stoichiometry ratio between the reagents is one of the parameters can be modify to hike the geometry landscape of copper(I) complexes. The 1:1:1 Cu:halogen:ligand complexes CuX(PR<sub>3</sub>) have tetrameric structures which may either be cubane-like (with all copper atoms *pseudo*-tetrahedral and all X atoms serving as μ<sub>3</sub>-bridges) or step-like (with the tetramer containing two *pseudo*-tetrahedral and two three-coordinated copper atoms and two μ<sub>3</sub>- and two μ<sub>2</sub>- iodides). The 1:1:2 adducts CuX(PR<sub>3</sub>)<sub>2</sub> may have either monomeric three-coordinate structures or dimeric *pseudo*-tetrahedral structures. The dimer compounds Cu<sub>2</sub>X<sub>2</sub>(PR<sub>3</sub>)<sub>y</sub> (y=2-4) nicely illustrate the propensity of the organophosphine copper(I) systems to form different polynuclear complexes with similar stabilities with different copper geometries of coordination.<sup>31</sup> At last the 1:1:3 adducts all seem to have monomeric *pseudo*-tetrahedral coordination.<sup>32</sup>

In solution, different complexes are simultaneously present due to the high constant of dissociation of the PPh<sub>3</sub> ligand.<sup>26</sup> Despite the presence of a plethora of complexes in solution, pure compounds can be obtained as precipitates: the stoichiometry ratio determines the nuclearity of the compounds, while the polymorph or isomer outcome can be influenced by the choice of solvent or by the procedure used.

To overcome the problem of the low solubility of the CuI which restricts the possibility of changing the solvent, the reactions can be performed in solid state which can yield to crystal forms hardly or even not obtainable in solution.<sup>33</sup> The reactivity of CuI towards

nitrogen, sulphur or phosphorous based ligands is very high and preliminary work of mechanochemical synthesis with CuI with N-base sature ligands are reported<sup>34, 35</sup> and more extensive studies have been done for Copper thyocyanate complexes,<sup>36-38</sup> in both case mechanochemical synthesis led to the formation of compounds not obtained by solution synthesis.

The main drawbacks in the mecanochemical reactions methods consists in the formation of microcrystalline products, not suitable for X-ray single crystal diffraction. The structural characterization represents a key point to understand the properties and to design new compounds, that is why a great effort will be devoted to tackle this problem. Most of the times traditional crystallizations from solution, but also triple layer crystallizations, or seeding of solutions with microcrystalline powder of the desired compound fail to yield single crystals of amenable size for single crystal diffraction experiments. However the structure can be determined from X-ray powder diffraction data, thanks to the development of “direct space” methods.<sup>39</sup> This approach is particularly suited for materials constructed from well-defined modular building units and it is more challenging for Copper Iodide complexes whose coordination is difficult to control. Spectroscopy techniques such as IR or Solid State NMR can give some insights on the coordination or on the asymmetric units but not assure the solution.<sup>37, 40</sup>

The quest of suitable methods to obtain crystals for structure determination of Copper complexes led us to explore different crystallization processes including those based on solvothermal synthesis. Recently, several zeolites which are commonly obtained by solvothermal synthesis have been reproduced by grinding or ball milling,<sup>41-44</sup> which suggests that the solid state reactions can have several aspects in common with the solvothermal conditions.<sup>36</sup> Although, for large scale preparations nowadays researches try to move from solvothermal to solvent-free reactions in order to reduce environmental impact and energy consumption, solvothermal synthesis can still be exploited to obtain single crystals of the desired compound since the high-temperature and high-pressure environment conditions created, would facilitate the crystallization process of complexes with poor solubility.

### **Structure-properties relationship**

Structure-properties relationship is the key point to design new tailor made compounds with desired properties. In this sense a systematic approach have been proposed in which tetrameric copper (I) iodide cubane clusters with similar-dimension ligands have been studied. As already discussed, the wavelength emission profile is function of metallophilic interaction due to copper–copper distances lower than the sum of van der Walls radii.<sup>45</sup> The quantum yield emission is an important parameter to be taken into account as much as the wavelength emission. All complexes show a cubane Cu<sub>4</sub>I<sub>4</sub> core and are luminescent due to radiative decay of a cluster centred <sup>3</sup>CC emitting state.

However, the photophysical properties of the solids could be very different from those in solution due to the molecular organization through the crystals, which can be expected to affect the energies and/or the kinetics of the excited states.<sup>28, 35, 46</sup> In this respect, polymorphism, (i.e. the existence of different crystal forms for the same molecular or supramolecular entity), could play a key role in determining the final photophysical properties.<sup>28</sup>

Apart from pyridine, we considered only saturated ligands (figure 3.1, page 48) with the aim of excluding photophysical process involving the ligand's  $\pi$  system and determine which parameters affect the cluster-centred characteristics such as basicity, ability to form hydrogen bonds, different groups bonded to the coordinating nitrogen. The different  $pK_b$  values allow to determine if the emission quantum yield in solid is related to the bond strength between ligands and copper atoms. Moreover, the ligands show a progressive rigidity and different ability to form H-bonds and consequently allow to investigate how the vibrations involving the ligand  $\sigma$  backbone can influence the photophysical properties of the complexes.

Quantum yields are in the range of 40-50% for all complexes in solid state apart from a slightly lower 30% for  $Cu_4I_4(3\text{-quinuclidinol})_4$  (compound name are consistent with those reported in chapter 3) and a significantly higher value of 76% for  $Cu_4I_4\text{piperidine}_4$  which, to the best of the authors' knowledge, has never been demonstrated previously for cubane complexes. No significant interactions between the constituting moieties are observed in the crystal structures of the complexes except for compound  $Cu_4I_4\text{piperidine}_4$  where the clusters are held together by hydrogen bonds in pillars. It results that each cluster is involved in eight hydrogen bonds, and clusters are aligned along the *c-axis* to build a stiff columnar structure. We think that these interactions make the cluster extremely rigid and allow to get a very high luminescence quantum yield. On the other side, the less rigid structure of  $Cu_4I_4(3\text{-quinuclidinol})_4$  results in the lowest quantum yield (30%). Desolvation of  $Cu_4I_4(3\text{-quinuclidinol})_4$  leads to loss of crystallinity which goes together with an even more reduced quantum yield (15%).

### Metal-Organic Frameworks and crystalline device

Metal-organic framework are a class of newly developed solid-state materials with infinite extended structures constructed from "connector" (metals) and "linkers" (organic ligands). In recent years, some amendments have been proposed to complement the synthetic principle of "connectors and linkers", and one of the most familiar approach is to introduce inorganic clusters or aggregates as "connectors" in place of single metal ions. It was Champness *et al.* who did the preliminary research and realized the copper halide aggregates could be incorporated in coordination polymers<sup>47-51</sup>. Moreover, the bridging ligand (connecting the copper halide aggregates) gave rise to more complicated copper(I) halide architectures than monodentate or bidentate chelating ligands did. Thus, the crystal engineering of copper(I) halide extended from

only discrete oligomers to one-dimensional (1D) or even two-dimensional (2D) and three-dimensional (3D) architectures.

As already reported in literature, two different luminescent MOFs have been synthesized in our laboratories.<sup>46</sup> The two porous structures were successfully determined and particular emphasis was put on the photophysical aspect. In fact, the two compounds, characterized by the same cluster connectivity both in the inorganic core and in the bridging mode of the bidentate ligand, crystallize in different crystallographic systems with different metal–metal distances which correspond to a different color in emission wavelength. The emission band active in both the compounds was the  $^3\text{CC}$  since the ligand used (DABCO, 1,4-diazabicyclo-[2.2.2]octane) was photophysically inert. The interesting skill of those compounds is that it is possible to transform the MOFs one into the other reversibly.<sup>46</sup>

In that case the conversion was performed by different external stimuli such as VOCs exposition or thermal treatment. Particularly, interest in stimuli-responsive luminescent materials is steadily gaining increasing momentum in the field of smart photofunctional devices.<sup>52</sup> As reported, luminescent behaviors can respond to exterior stimuli such as mechanical grinding (tribochromism),<sup>53</sup> thermal treatment (thermochromism),<sup>17</sup> and fumigating by vapour (vapochromism).<sup>46</sup>

The crystal engineering paradigm has led us to the idea of using this approach to construct crystalline devices. As a device is “a thing made for a particular purpose” which is made of different pieces with different functionalities assembled together, in the same way, a crystalline device is a crystal made of different molecules with different chemical functionalities assembled together to obtain a final material whose properties can be activated by appropriate external stimuli.

In our approach the crystalline device is based on the idea of having a guest molecule trapped into a luminescent MOF which can be subjected to external physical “stimuli” to modify host-guest interactions within the MOF and consequently the host luminescence.<sup>54,55</sup> From this viewpoint a crystalline device can be considered as a higher level step of crystal engineering since the final properties of the device are derived from the tuneable combination of the specific properties of the host and of the guest.

We report on the photochemical and electrochemical properties of one of two MOF previously described,<sup>46</sup> which is made of nodes based on  $\text{Cu}_4\text{I}_4$  cubane clusters and as a secondary building units, loaded with different amounts of  $\text{FeCp}_2$  [ $(\eta^5\text{-C}_5\text{H}_5)_2\text{Fe}^{(\text{II})}$ ] molecules.

Since the ferrocene is widely used as luminescence quencher and electron donor in supramolecular photochemistry, analytical chemistry and biology<sup>56</sup>, as planned, once ferrocene is loaded into the MOF structure, the  $\text{FeCp}_2@\text{MOF}$  luminescence is turned

off; applying an electric potential to the FeCp<sub>2</sub>@MOF deposited onto an ITO glass, Fe<sup>(II)</sup>Cp<sub>2</sub> is oxidized to Fe<sup>(III)</sup>Cp<sub>2</sub><sup>+</sup>, which differently interacts with the excited states of the cage and the luminescence of MOF is partially “turned on” again. Thus FeCp<sub>2</sub>@MOF represents a remarkably simple and reversible switch off/switch on solid state system. It is worth pointing out that, although chemical systems working on “on/off signal” are known in solution in supramolecular chemistry<sup>57-61</sup> this is the first time, to the best of the authors’ knowledge, that luminescence is controlled by external stimuli in an all-sufficient MOF-guest system in the solid state.

### Single phase white-emitting compounds

From the invention of incandescent bulbs, implementation of fluorescent tubes, to the presently fast-growing solid-state lightening, it has been the key fixture in defining the quality of modern life. White organic light-emitting devices (WOLEDs) have been intensively studied in recent years<sup>62, 63</sup> due to their potential for highly efficient and cost effective next generation lighting.<sup>64</sup> In a WOLED, white light is typically generated through the simultaneous emission of multiple emissive materials, which need to be employed in either a single emissive layer with multiple molecular emitters or multiple emissive layers.<sup>65</sup> One of the current academic interests is in the pursuing single white-light phosphors to avoid the intrinsic colour balance, device complication, and high-cost problems when using multiphosphors or multi-LEDs.<sup>66</sup> Examples are rare but still can be found in the research field of organic molecules or polymers,<sup>67-71</sup> metal-doped or hybrid inorganic materials,<sup>72-75</sup> metal complexes,<sup>76-78</sup> and nanomaterials.<sup>79-81</sup>

Here a single phase white emitter copper complex is proposed in which both <sup>3</sup>CC and <sup>3</sup>XLCT are contemporary present at room temperature. The two emission bands are surprisingly complementary in an overall white emission at naked eye.

### OLED device

Luminescent copper (I) complexes are described to be very good candidate for optoelectronics. Few examples are already reported in literature<sup>1-4</sup> with good performance parameters and it is plausible that the use of d<sup>10</sup> complexes will increase in the next years as active material in luminescent devices.

However many problem still remain unsolved. The copper (I) complexes are generically not very soluble and it means that deposition processes such as drop casting or spin coating, which still remain the easiest way to deposit the emission layer, cannot be used in this case.

Volz et al. elude this problem with a series of extraordinary high efficient binuclear copper iodide complexes based on 2-pyridil-bisphosphine ligand.<sup>1, 2</sup> These kind of complexes are soluble in organic solvents and are easily deposited via drop casting.

However if the complexes still remain insoluble in organic solvents (or even in solvents suitable for optoelectronic apparatus) the emissive layer can be deposit by sublimation in a high vacuum chamber. The main problem related to that is the stability of the complex itself in those extreme conditions. It could happen that the ligand moieties can leave the complex during the sublimation process completely or partially and the deposition step will fail. To avoid this problem it is possible to synthesize a “bigger” complex with *ad hoc* designed ligand, with the aim of improving the stability performances of the final complex in the sublimation process.

Herein, our experience on emissive layer deposition is reported as a step-by-step improvement path. Also a new non-conventional layer-by-layer deposition route has been suggested and a preliminary OLED device prototype has been proposed.

## References

1. D. Volz, M. Nieger, J. Friedrichs, T. Baumann and S. Bräse, *Langmuir*, 2013.
2. D. Volz, D. M. Zink, T. Bocksrocker, J. Friedrichs, M. Nieger, T. Baumann, U. Lemmer and S. Bräse, *Chem. Mater.*, 2013, **25**, 3414-3426.
3. D. M. Zink, T. Baumann, J. Friedrichs, M. Nieger and S. Bräse, *Inorg. Chem.*, 2013.
4. D. M. Zink, M. Bachle, T. Baumann, M. Nieger, M. Kuhn, C. Wang, W. Klopper, U. Monkowius, T. Hofbeck, H. Yersin and S. Bräse, *Inorg. Chem.*, 2012, **52**, 2292-2305.
5. L. Maini, P. P. Mazzeo, F. Farinella, V. Fattori and D. Braga, *Faraday Discuss.*, 2014.
6. R. Peng, M. Li and D. Li, *Coord. Chem. Rev.*, 2010, **254**, 1-18.
7. L. Bergmann, J. Friedrichs, M. Mydlak, T. Baumann, M. Nieger and S. Bräse, *Chem. Commun.*, 2013, **49**, 6501-6503.
8. D. M. Zink, T. Baumann, J. Friedrichs, M. Nieger and S. Bräse, *Inorg. Chem.*, 2013.
9. D. M. Zink, D. Volz, T. Baumann, M. Mydlak, H. Flügge, J. Friedrichs, M. Nieger and S. Bräse, *Chem. Mater.*, 2013.
10. Z. Liu, P. I. Djurovich, M. T. Whited and M. E. Thompson, *Inorg. Chem.*, 2011, **51**, 230-236.
11. Z. Liu, M. F. Qayyum, C. Wu, M. T. Whited, P. I. Djurovich, K. O. Hodgson, B. Hedman, E. I. Solomon and M. E. Thompson, *J. Am. Chem. Soc.*, 2011, **133**, 3700-3703.
12. V. A. Krylova, P. I. Djurovich, J. W. Aronson, R. Haiges, M. T. Whited and M. E. Thompson, *Organometallics*, 2012, **31**, 7983-7993.
13. I. Roppolo, E. Celasco, A. Fargues, A. Garcia, A. Revaux, G. Dantelle, F. Maroun, T. Gacoin, J.-P. Boilot, M. Sangermano and S. Perruchas, *J. Mater. Chem.*, 2011, **21**, 19106-19113.
14. P. P. Mazzeo, L. Maini, D. Braga, G. Valenti, F. Paolucci, M. Marcaccio, A. Barbieri and B. Ventura, *Eur. J. Inorg. Chem.*, 2013, **2013**, 4459-4465.
15. H. D. Hardt and H. Gechnizdjani, *Z. Anorg. Allg. Chem. FIELD Full Journal Title:Zeitschrift fuer Anorganische und Allgemeine Chemie*, 1973, **397**, 16-22.
16. P. C. Ford and A. Vogler, *Acc. Chem. Res.*, 1993, **26**, 220-226.
17. P. C. Ford, *Coord. Chem. Rev.*, 1994, **132**, 129-140.
18. M. Vitale and P. C. Ford, *Coord. Chem. Rev.*, 2001, **219-221**, 3-16.
19. M. Vitale, W. E. Palke and P. C. Ford, *J. Phys. Chem.*, 1992, **96**, 8329-8336.
20. F. De Angelis, S. Fantacci, A. Sgamellotti, E. Cariati, R. Ugo and P. C. Ford, *Inorg. Chem.*, 2006, **45**, 10576-10584.
21. P. C. Ford, E. Cariati and J. Bourassa, *Chem. Rev.*, 1999, **99**, 3625-3648.
22. D. M. Zink, M. Bächle, T. Baumann, M. Nieger, M. Kühn, C. Wang, W. Klopper, U. Monkowius, T. Hofbeck, H. Yersin and S. Bräse, *Inorg. Chem.*, 2013, **52**, 2292-2305.
23. R. Czerwieniec, J. Yu and H. Yersin, *Inorg. Chem.*, 2011, **50**, 8293-8301.
24. M. J. Leitl, F.-R. Küchle, H. A. Mayer, L. Wesemann and H. Yersin, *J. Phys. Chem. A*, 2013.
25. C. H. Arnby, S. Jagner and I. Dance, *CrysEngComm*, 2004, **6**, 257-275.

26. D. J. Fife, W. M. Moore and K. W. Morse, *Inorg. Chem.*, 1984, **23**, 1684-1691.
27. *CSD*, (2013), Cambridge Crystallographic Data Centre, UK.
28. L. Maini, D. Braga, P. P. Mazzeo and B. Ventura, *Dalton Trans.*, 2012, **41**, 531-539.
29. M. R. Churchill, B. G. DeBoer and D. J. Donovan, *Inorg. Chem.*, 1975, **14**, 617-623.
30. M. R. Churchill and K. L. Kalra, *Inorg. Chem.*, 1974, **13**, 1065-1071.
31. G. Costa, E. Reisenhofer and L. Stefani, *Journal of Inorganic and Nuclear Chemistry*, 1965, **27**, 2581-2584.
32. P. H. Davis, R. L. Belford and I. C. Paul, *Inorg. Chem.*, 1973, **12**, 213-218.
33. S. L. James, C. J. Adams, C. Bolm, D. Braga, P. Collier, T. Friscic, F. Grepioni, K. D. M. Harris, G. Hyett, W. Jones, A. Krebs, J. Mack, L. Maini, A. G. Orpen, I. P. Parkin, W. C. Shearouse, J. W. Steed and D. C. Waddell, *Chemical Society Reviews*, 2012, **41**, 413-447.
34. D. Braga, L. Maini, P. P. Mazzeo and B. Ventura, *Chem. Eur. J.*, 2010, **16**, 1553-1559.
35. D. Braga, F. Grepioni, L. Maini, P. P. Mazzeo and B. Ventura, *New J. Chem.*, 2011, **35**, 339-344.
36. G. A. Bowmaker, *Chem. Commun.*, 2013, **49**, 334-348.
37. G. A. Bowmaker, J. V. Hanna, R. D. Hart, P. C. Healy, S. P. King, F. Marchetti, C. Pettinari, B. W. Skelton, A. Tabacaru and A. H. White, *Dalton Trans.*, 2012, **41**, 7513-7525.
38. G. A. Bowmaker, J. V. Hanna, B. W. Skelton and A. H. White, *Chem. Commun.*, 2009, 2168-2170.
39. W. I. F. David, K. Shankland, L. M. McCusker and C. Baerlocher, *Structure determination from powder diffraction data* Oxford University Press: New York, 2002.
40. G. A. Bowmaker and J. V. Hanna, *Z.Naturforsch.(B)*, 2009, **64**, 1478-1486.
41. P. J. Beldon, L. Fábián, R. S. Stein, A. Thirumurugan, A. K. Cheetham and T. Friščić, *Angew. Chem. Int. Ed.*, 2010, **49**, 9640-9643.
42. R. E. Morris and S. L. James, *Angew. Chem. Int. Ed.*, 2013, **52**, 2163-2165.
43. Y. Jin, Q. Sun, G. Qi, C. Yang, J. Xu, F. Chen, X. Meng, F. Deng and F.-S. Xiao, *Angew. Chem.*, 2013, **125**, 9342-9345.
44. J. F. Fernández-Bertrán, M. P. Hernández, E. Reguera, H. Yee-Madeira, J. Rodriguez, A. Paneque and J. C. Llopiz, *J. Phys. Chem. Solids*, 2006, **67**, 1612-1617.
45. A. Bondi, *J. Phys. Chem.*, 1964, **68**, 441-451.
46. D. Braga, L. Maini, P. P. Mazzeo and B. Ventura, *Chem. Eur. J.*, 2010, **16**, 1553-1559.
47. A. J. Blake, N. R. Brooks, N. R. Champness, P. A. Cooke, A. M. Deveson, D. Fenske, P. Hubberstey, W. S. Li and M. Schroder, *Journal of the Chemical Society-Dalton Transactions*, 1999, 2103-2110.
48. A. J. Blake, N. R. Brooks, N. R. Champness, M. Crew, L. R. Hanton, P. Hubberstey, P. C. Simon and M. Schroder, *Journal of the Chemical Society-Dalton Transactions*, 1999, 2813-2817.
49. A. J. Blake, N. R. Brooks, N. R. Champness, L. R. Hanton, P. Hubberstey and M. Schroder, *Pure Appl. Chem.*, 1998, **70**, 2351-2357.
50. N. R. Brooks, A. J. Blake, N. R. Champness, P. A. Cooke, P. Hubberstey, D. M. Proserpio, C. Wilson and M. Schroder, *Journal of the Chemical Society-Dalton Transactions*, 2001, 456-465.
51. P. Hubberstey, A. J. Blake, N. R. Brooks, N. R. Champness and M. Schroder, *Abstracts of Papers of the American Chemical Society*, 1999, **217**, U1071-U1071.
52. J.-N. Hao and B. Yan, *Dalton Trans.*, 2014, **43**, 2810-2818.
53. Y. A. Lee and R. Eisenberg, *J. Am. Chem. Soc.*, 2003, **125**, 7778-7779.
54. Y. J. Cui, Y. F. Yue, G. D. Qian and B. L. Chen, *Chem. Rev.*, 2012, **112**, 1126-1162.
55. M. D. Allendorf, C. A. Bauer, R. K. Bhakta and R. J. T. Houk, *Chem. Soc. Rev.*, 2009, **38**, 1330-1352.
56. S. Fery-Forgues and B. Delavaux-Nicot, *Journal of Photochemistry and Photobiology a-Chemistry*, 2000, **132**, 137-159.
57. A. Credi, *Angew. Chem. Int. Edit.*, 2007, **46**, 5472-5475.
58. T. Gunnlaugsson, J. P. Leonard, K. Senechal and A. J. Harte, *J. Am. Chem. Soc.*, 2003, **125**, 12062-12063.
59. L. Flamigni, B. Ventura, A. Barbieri, H. Langhals, F. Wetzel, K. Fuchs and A. Walter, *Chem. Eur. J.*, 2010, **16**, 13406-13416.
60. N. S. Murray, S. P. Jarvis and T. Gunnlaugsson, *Chemical Communications*, 2009, 4959-4961.
61. H. Dube, M. R. Ams and J. Rebek, *J. Am. Chem. Soc.*, 2010, **132**, 9984-9985.
62. T. Justel, H. Nikol and C. Ronda, *Angew. Chem.-Int. Edit.*, 1998, **37**, 3085-3103.
63. C. Feldmann, T. Justel, C. R. Ronda and P. J. Schmidt, *Adv. Funct. Mater.*, 2003, **13**, 511-516.
64. J. Kido, M. Kimura and K. Nagai, *Science*, 1995, **267**, 1332-1334.
65. G. M. Farinola and R. Ragni, *Chemical Society Reviews*, 2011, **40**, 3467-3482.

66. M.-S. Wang, S.-P. Guo, Y. Li, L.-Z. Cai, J.-P. Zou, G. Xu, W.-W. Zhou, F.-K. Zheng and G.-C. Guo, *J. Am. Chem. Soc.*, 2009, **131**, 13572-+.
67. J. Y. Li, D. Liu, C. W. Ma, O. Lengyel, C. S. Lee, C. H. Tung and S. Lee, *Adv. Mater.*, 2004, **16**, 1538-+.
68. M. Mazzeo, V. Vitale, F. Della Sala, M. Anni, G. Barbarella, L. Favaretto, G. Sotgiu, R. Cingolani and G. Gigli, *Adv. Mater.*, 2005, **17**, 34-+.
69. Y. J. Yang, M. Lowry, C. M. Schowalter, S. O. Fakayode, J. O. Escobedo, X. Y. Xu, H. T. Zhang, T. J. Jensen, F. R. Fronczek, I. M. Warner and R. M. Strongin, *J. Am. Chem. Soc.*, 2006, **128**, 14081-14092.
70. J. Luo, X. Z. Li, Q. Hou, J. B. Peng, W. Yang and Y. Cao, *Adv. Mater.*, 2007, **19**, 1113-1117.
71. J. Liu, Y. Cheng, Z. Xie, Y. Geng, L. Wang, X. Jing and F. Wang, *Adv. Mater.*, 2008, **20**, 1357-+.
72. W. H. Green, K. P. Le, J. Grey, T. T. Au and M. J. Sailor, *Science*, 1997, **276**, 1826-1828.
73. T. Hayakawa, Y. Toh, M. Oshima, M. Matsuda, Y. Hatsukawa, N. Shinohara, H. Iimura, T. Shizuma, Y. H. Zhang, M. Sugawara and H. Kusakari, *Phys. Lett. B*, 2003, **551**, 79-85.
74. L. Luo, X. X. Zhang, K. F. Li, K. W. Cheah, H. X. Shi, W. K. Wong and M. L. Gong, *Adv. Mater.*, 2004, **16**, 1664-+.
75. Y. L. Liu, B. F. Lei and C. S. Shi, *Chem. Mater.*, 2005, **17**, 2108-2113.
76. G. J. Zhou, Q. Wang, C. L. Ho, W. Y. Wong, D. G. Ma and L. X. Wang, *Chemical Communications*, 2009, 3574-3576.
77. P. Coppo, M. Duati, V. N. Kozhevnikov, J. W. Hofstraat and L. De Cola, *Angew. Chem.-Int. Edit.*, 2005, **44**, 1806-1810.
78. R.-S. Liu, V. Drozd, N. Bagkar, C.-C. Shen, I. Baginskiy, C.-H. Chen and C. H. Tan, *J. Electrochem. Soc.*, 2008, **155**, P71-P73.
79. H. S. Chen, S. J. J. Wang, C. J. Lo and J. Y. Chi, *Applied Physics Letters*, 2005, **86**.
80. X. M. Sui, C. L. Shao and Y. C. Liu, *Applied Physics Letters*, 2005, **87**.
81. T. Uchino and T. Yamada, *Applied Physics Letters*, 2004, **85**, 1164-1166.

# Chapter 1

## Polymorph and isomer conversion of complexes based on CuI and PPh<sub>3</sub> easily observed *via* luminescence

**Abstract:** Reactions between copper(I) iodide and triphenylphosphine have been explored in solution and in the solid state and six luminescent coordination complexes have been obtained and characterized by X-ray diffraction and UV-Vis spectroscopy. Solid-state reactions of CuI with PPh<sub>3</sub> in different conditions (kneading, vapour digestion) and stoichiometries resulted in the formation of high ratio ligand:metal compounds while tetrameric structures could be obtained only by solution reactions. Crystal structures were determined by single crystal X-ray diffraction while purity of the bulk product was checked by powder diffraction (XRPD). Three different tetrameric structures with 1:1 stoichiometry have been synthesized: two closed cubane-type polymorphs [CuI(PPh<sub>3</sub>)<sub>4</sub>] (form **1a**) and [CuI(PPh<sub>3</sub>)<sub>4</sub>] (form **1b**) and an open step-like isomer [CuI(PPh<sub>3</sub>)<sub>4</sub>] (form **2**). The conversions between the polymorphs and isomers have been studied and characterized by XRPD. The most stable form [CuI(PPh<sub>3</sub>)<sub>4</sub>] (form **1b**) can convert into the open step-like isomer [CuI(PPh<sub>3</sub>)<sub>4</sub>] (form **2**) in a slurry experiment with EtOH or CH<sub>2</sub>Cl<sub>2</sub> or AcCN and converts back into [CuI(PPh<sub>3</sub>)<sub>4</sub>] **1b** when exposed to vapors of toluene. At room temperature all the tetrameric compounds exhibit luminescence in the solid state and, notably, the two polymorphs show a dissimilar dual emission at low temperature. The luminescence features in the solid state seem to be peculiarly related to the presence of the aromatic phosphine ligand and depend on the Cu-Cu distance in the cluster.



## Introduction

Copper(I) halide aggregates constitute a large family of compounds studied for decades for their photochemical and photophysical properties.<sup>1-11</sup> This class of compounds is attracting renewed interest<sup>12-16</sup> because of its potential applications in high-efficiency OLEDs.<sup>17-19</sup> Coordination systems based on copper halides show a remarkable structural diversity,<sup>15</sup> which arises from the many possible combinations of coordination numbers (two, three and four) available for copper(I) and for the geometries that can be adopted by the halide ions (from terminal to  $\mu_2$ - and up to  $\mu_8$ -bridging modes).

Organophosphine copper(I) halides have been extensively studied in the past<sup>20-22</sup> and several species with different metal coordination numbers and metal:ligand stoichiometries (Figure 1) have been already synthesized and the crystal structure determined, while the luminescence properties have been explored only recently without a clear assignment on the nature of the emission bands. With respect to Cu(I) structures with halogens and amine-based ligands,<sup>5, 23, 24</sup> when the organic ligand is an aromatic phosphine, further interactions such as back bonding from the metal to the phosphorous system must be taken into account<sup>25,26</sup> and can play a role in the photophysics of the complexes. Since the organophosphine copper(I) iodide complexes could find applications in light emitting diode technology a full comprehension of the emission bands is essential to tune the emission properties.

The 1:1:1 Cu:halogen:ligand complexes CuX(PR<sub>3</sub>) have tetrameric structures which may either be cubane-like (with all copper atoms *pseudo*-tetrahedral and all X atoms serving as  $\mu_3$ -bridges) or step-like (with the tetramer containing two *pseudo*-tetrahedral and two three-coordinated copper atoms and two  $\mu_3$ - and two  $\mu_2$ -iodides). The 1:1:2 adducts CuX(PR<sub>3</sub>)<sub>2</sub> may have either monomeric three-coordinate structures or dimeric pseudo-tetrahedral structures. The dimer compounds Cu<sub>2</sub>X<sub>2</sub>(PR<sub>3</sub>)<sub>y</sub> (y= 2-4)nicely illustrate the propensity of the organophosphine copper(I) systems to form different polynuclear complexes with similar stabilities with different copper geometries of coordination.<sup>27</sup> At last the 1:1:3 adducts all seem to have monomeric *pseudo*-tetrahedral coordination.<sup>28</sup>

In solution, different complexes are simultaneously present due to the high constant of dissociation of the PPh<sub>3</sub> ligand.<sup>25</sup> Despite the presence of a plethora of complexes in solution, pure compounds can be obtained as precipitates: the stoichiometry ratio determines the nuclearity of the compounds, while the polymorph or isomer outcome can be influenced by the choice of solvent or by the procedure used.

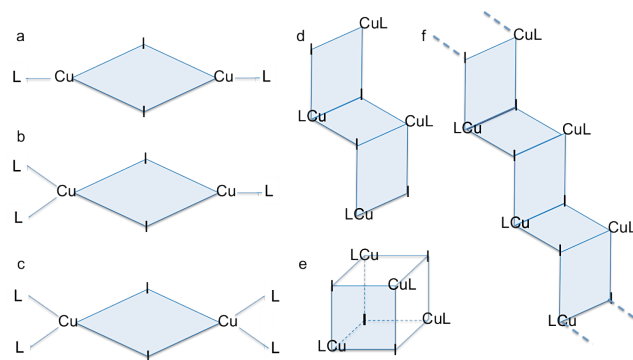


Figure 1.1 | Schematic representation of some examples of different geometries and stoichiometries for CuI aggregates; a)  $[\text{Cu}_2\text{I}_2\text{L}_2]$ ; b)  $[\text{Cu}_2\text{I}_2\text{L}_3]$ ; c)  $[\text{Cu}_2\text{I}_2\text{L}_4]$ ; d)  $[\text{Cu}_4\text{I}_4\text{L}_4]$  step-like; e)  $[\text{Cu}_4\text{I}_4\text{L}_4]$  cubane-like; f)  $[\text{CuIL}]^\infty$  coordination polymer

In this work we report on the synthesis and characterization (both structural and photophysical) of different Cu(I) coordination compounds with the  $\text{PPh}_3$  ligand. All compounds have been obtained either by methods described in literature<sup>29-32</sup> and/or *via* solvent-free reactions such as kneading or vapor digestion.<sup>33, 34</sup> It is well known that these approaches can be a valid alternative to traditional synthetic methods, since they reduce the amount of solvent required and are usually quantitative in yields. Sometimes, non-solution methods also allow the synthesis of different compounds which are not found *via* solvent synthesis.<sup>35</sup> As previously reported in the literature, the synthesis with  $\text{CuI}:\text{PPh}_3$  ratio of 1:3 yielded upon crystallization the monomer  $[\text{CuI}(\text{PPh}_3)_3]$  (form **a**),<sup>29</sup> but we observed also a new polymorph  $[\text{CuI}(\text{PPh}_3)_3]$  (form **b**) which is a metastable form.  $\text{CuI}:\text{PPh}_3$  ratio of 1:2 yielded the dimer  $[\text{CuI}(\text{PPh}_3)_{1.5}]_2$ <sup>32</sup> and, finally, a  $\text{CuI}:\text{PPh}_3$  ratio of 1:1 yielded to the crystallization of the cubane-like compounds  $[\text{CuI}(\text{PPh}_3)]_4$  (form **1b**)<sup>36</sup> and  $[\text{CuI}(\text{PPh}_3)]_4$  (form **1a**)<sup>30</sup> and the step-like compound  $[\text{CuI}(\text{PPh}_3)]_4$  (form **2**).<sup>30</sup> The conversions within the isomers and polymorphs were studied in solution and *via* vapor digestion. We focused our attention on the luminescence properties of the dimer and the tetramers, which exhibit remarkably different emission features depending on the nature of the compound, which make these complexes interesting as sensor-like materials. The photophysical characterization was carried out in the solid and in solution and the results were interpreted on the basis of current theories on the luminescence of Cu(I) cubane clusters<sup>4, 37, 38</sup> with new indications for the specific case of organophosphine based complexes, whose properties have been scarcely investigated up to now.

## Results and Discussions

### Synthesis and structure of [CuI(PPh<sub>3</sub>)<sub>3</sub>] (form a) and [CuI(PPh<sub>3</sub>)<sub>3</sub>] (form b)

Monomeric coordination compounds with a 1:3 molar ratio stoichiometry of CuI salt and PPh<sub>3</sub> were synthesized utilizing the experimental instructions previously reported.<sup>29</sup> The product obtained was a mixture of two concomitant polymorphic forms: [CuI(PPh<sub>3</sub>)<sub>3</sub>] (form **a**), which corresponds to a known structure and [CuI(PPh<sub>3</sub>)<sub>3</sub>] (form **b**) whose structure was determined by us. [CuI(PPh<sub>3</sub>)<sub>3</sub>] (form **b**) (Figure 2a) crystallizes in the monoclinic P2<sub>1</sub>/c space group while [CuI(PPh<sub>3</sub>)<sub>3</sub>] (form **a**) (Figure 2b) crystallizes in a denser structure in the trigonal P3 space group (1.39 g/cm<sup>3</sup> and 1.42 g/cm<sup>3</sup> respectively) which suggests that [CuI(PPh<sub>3</sub>)<sub>3</sub>] (form **a**) is the stable form at room temperature, according to the Kitaigorodsky's density rule.<sup>39</sup> The stability of [CuI(PPh<sub>3</sub>)<sub>3</sub>] (form **a**) was confirmed by an overnight slurry experiment in chloroform where the polymorph **b** converted into form **a**. No further analyses were performed on these two monomeric forms because of the difficulty to obtain them as pure powder.

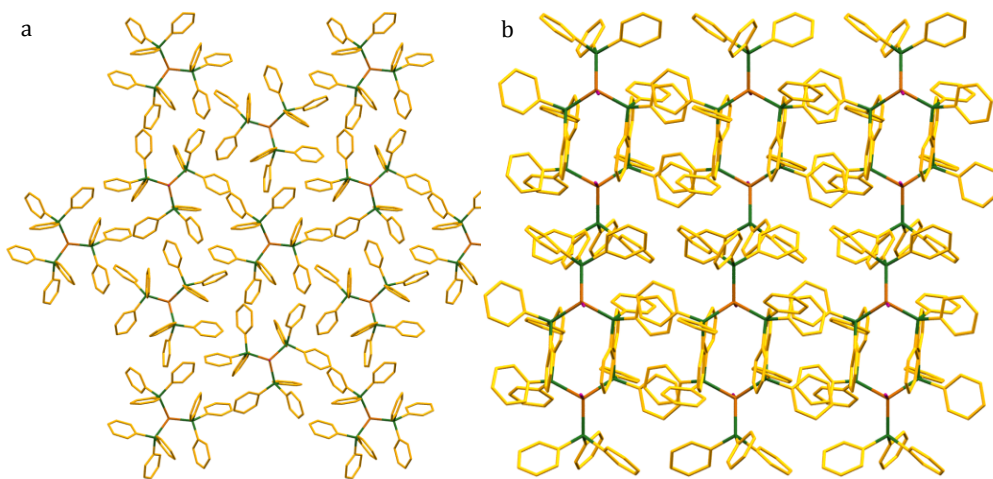


Figure 1.2 | a) [CuI(PPh<sub>3</sub>)<sub>3</sub>] (form **a**) and, b) [CuI(PPh<sub>3</sub>)<sub>3</sub>] (form **b**); hydrogen atoms are omitted for clarity.

### Synthesis and structure of $[\text{CuI}(\text{PPh}_3)_{1.5}]_2$

Dimeric compound  $[\text{CuI}(\text{PPh}_3)_{1.5}]_2$  has been synthesized following the experimental procedure previously reported in the literature.<sup>32</sup> The  $[\text{CuI}(\text{PPh}_3)_{1.5}]_2$  structure consists of a 4-atom ring ( $\text{Cu}_2\text{I}_2$ ), in which the halogen atom acts as a bridge between copper atoms. Different copper coordination numbers are observed in this complex as shown in Figure 3: one copper atom binds two P-based ligands and it has a distorted tetrahedral geometry while the other copper atom has a trigonal geometry. The distance between the two metal atoms is 3.044(5) Å; luminescence features linked to Cu-Cu distances are reported in the following section. We obtained also the solvate species  $[\text{CuI}(\text{PPh}_3)_{1.5}]_2 \cdot \text{CH}_2\text{Cl}_2$  from the crystallization process (see ESI) which shows Cu-Cu distance (3.0444(5) Å) comparable to  $[\text{CuI}(\text{PPh}_3)_{1.5}]_2$  and it is isomorphic to  $[\text{CuCl}(\text{PPh}_3)_{1.5}]_2 \cdot \text{CH}_2\text{Cl}_2$  reported in literature.<sup>40</sup>

---

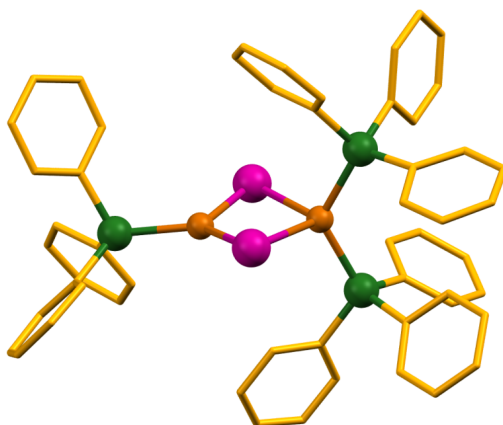


Figure 1.3 | The  $[\text{CuI}(\text{PPh}_3)_{1.5}]_2$  unit; hydrogen atoms are omitted for sake of clarity.

---

### Synthesis and structure of $[\text{CuI}(\text{PPh}_3)]_4$

Compounds with 1:1:1 ratio have been obtained only as in the form of tetrameric units; however it was possible to isolated two polymorphs of  $[\text{CuI}(\text{PPh}_3)]_4$  a cubane-like cluster and a step-like cluster, as shown in Figure 1d-e.

The first synthesis was carried out by following the reported procedure<sup>30</sup> resulting in the expected  $[\text{CuI}(\text{PPh}_3)]_4$  (form **1a**), however, on repeating, the synthesis a second phase appeared which we characterized as form **1b** of  $[\text{CuI}(\text{PPh}_3)]_4$ .<sup>36, 41</sup> Interestingly, once form **1b** had been obtained, a mixture of **1a** and **1b** was subsequently obtained

on repeating the synthesis. At each repetition step, the percentage of form **1b** became predominant and increasing at each reaction, until only form **1b** could be obtained (see Figure 1.4).

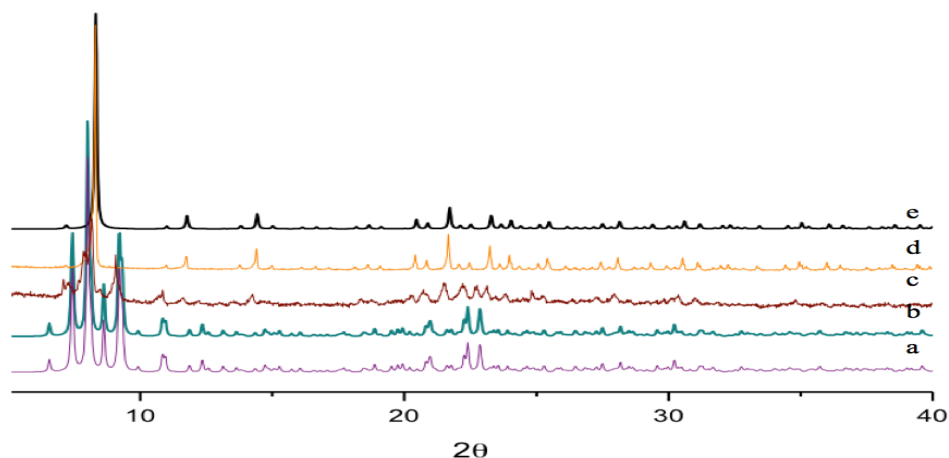


Figure 1.4 | a. calculated X-ray powder pattern of  $[\text{CuI}(\text{PPh}_3)]_4$  (form **1a**); b. X-ray powder diffractogram of compounds obtained from the first synthesis corresponding to  $[\text{CuI}(\text{PPh}_3)]_4$  (form **1a**); c. X-ray powder diffractogram of compounds obtained from the second synthesis both form **1a** and **1b** of phases  $[\text{CuI}(\text{PPh}_3)]_4$  could be recognized; d. X-ray powder diffractogram of compounds obtained in subsequent syntheses corresponding to form **1b**; e. calculated X-ray powder pattern of form **1b**.

The metastable  $[\text{CuI}(\text{PPh}_3)]_4$  (form **1a**) product could no longer be obtained as a pure form in our laboratory, and mixtures of forms **1a** and **1b** were obtained when the synthesis was carried out in a different laboratory and with fast crystallization process. This complex can be counted in as a new example of disappearing polymorphs.<sup>42</sup>

$[\text{CuI}(\text{PPh}_3)]_4$  (form **1a**) is therefore the metastable form at RT, as also suggested by the lower density compared to **1b** ( $1.72 \text{ g/cm}^3$  versus  $1.77 \text{ g/cm}^3$  at RT).<sup>39</sup>

Diffraction data for both polymorphs **1a** and **1b** were collected at RT and 90K and structures were found to be in agreement with those previously reported.<sup>29, 36</sup> The cubane-like clusters of  $[\text{CuI}(\text{PPh}_3)]_4$  form **1a** and **1b** are distorted (see Table 1) with the shortest Cu-Cu distance equal to  $2.839(3) \text{ \AA}$  and  $2.945(4) \text{ \AA}$  respectively at RT which are longer than the Van der Waal distance ( $2.80 \text{ \AA}$ ).<sup>43</sup> All Cu-Cu distances show a dramatic decrease on lowering the temperature with minima Cu-Cu distances equal to  $2.7427(8) \text{ \AA}$  and  $2.828(2) \text{ \AA}$  for **1a** and **1b** at 90K. On the basis of the copper distances, only **1a** at low temperature should shows features ascribable to

cluster-centered interactions while the photophysical behavior suggests the presence of such interactions also at RT for both compounds.

---

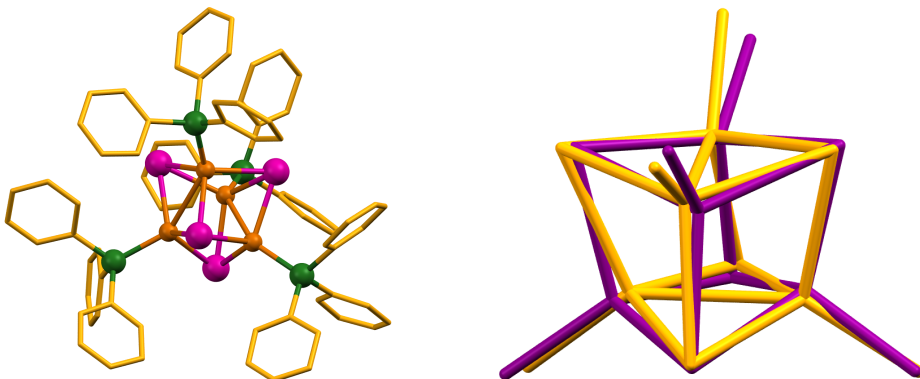


Figure 1.5 | a. The  $[\text{CuI}(\text{PPh}_3)]_4$  cubane-like unit; hydrogen atoms are removed for clarity and in shorter distances Cu atoms are bonded together; b. Overlap between  $\text{Cu}_4\text{I}_4$  clusters in  $[\text{CuI}(\text{PPh}_3)]_4 \mathbf{1a}$  (yellow) and  $[\text{CuI}(\text{PPh}_3)]_4 \mathbf{1b}$  (purple); phenyl rings are removed for clarity

---

The step-like cluster  $[\text{CuI}(\text{PPh}_3)]_4$  form **2** (Figure 1.6) has been obtained according to the reported synthesis<sup>30</sup>. However no single crystals could be obtained and X-ray powder diffraction data was measured at 90K to ascertain that the crystal structure was retained. (Figure A.6.)

The step-like cluster  $[\text{CuI}(\text{PPh}_3)]_4$  form **2** is characterized by two copper atoms *pseudo-tetrahedral* and two three-coordinate copper atoms; although a quite short Cu-Cu distance is observed in the complex (2.834(2) Å at RT) the different coordination around the copper atoms seems to be responsible for the weak luminescence properties of this compound (*vide infra*).

---

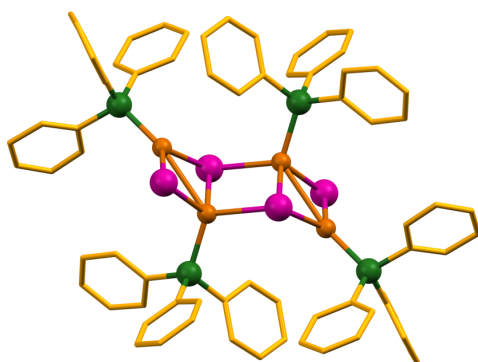


Figure 1.6 | The  $[\text{CuI}(\text{PPh}_3)]_4$  form **2** unit; hydrogen atoms are removed for sake of clarity.

---

Table 1.1 | Cu-Cu distances in cuprous organophosphine compounds. All distances are reported in Å. Labels are in agreement with those reported in Appendix A.

[CuI(PPh <sub>3</sub> ) <sub>1.5</sub> ] <sub>2</sub>	[CuI(PPh <sub>3</sub> ) <sub>4</sub> ] 1a RT	[CuI(PPh <sub>3</sub> ) <sub>4</sub> ] 1a 90K	[CuI(PPh <sub>3</sub> ) <sub>4</sub> ] 1b RT	[CuI(PPh <sub>3</sub> ) <sub>4</sub> ] 1b 90K	[CuI(PPh <sub>3</sub> ) <sub>4</sub> ] 2
Cu <sub>1</sub> Cu <sub>2</sub> 3.0444(5)	Cu1 Cu2 2.928(8)	Cu Cu2 2.7431(4)	Cu Cu1 2.945(3)	Cu1 Cu <sub>1</sub> 2.8281(4) )	Cu Cu1 2.834(2)
Cu <sub>1</sub> Cu3 2.896(6)	Cu Cu3 3.0809(4)	Cu Cu2 3.174(5)	Cu1 Cu <sub>2</sub> 3.1051(4) )	Cu Cu2 3.404(3)	
Cu <sub>1</sub> Cu4 2.873(4)	Cu Cu4 2.7971(8)				
Cu <sub>2</sub> Cu3 2.839(3)	Cu Cu3 2.9985(7)				
Cu <sub>2</sub> Cu4 3.165(3)	Cu Cu4 2.8085(8)				
Cu <sub>3</sub> Cu4 3.109(4)	Cu Cu4 2.8080(9)				

### Solvent free reactions

The possibility of obtaining compounds based on CuI:PPh<sub>3</sub> *via* solvent free reactions with CuI:PPh<sub>3</sub> ratio 1:1, 1:2 and 1:3 was also explored. Kneading process (i.e grinding the physical mixture with a drop of solvent)<sup>33</sup> produced only [CuI(PPh<sub>3</sub>)<sub>4</sub>] (form **2**) irrespectively of the ratio or solvent used.

The physical mixture of between CuI and PPh<sub>3</sub> with different ratios was exposed to vapor of organic solvents and the final products depend on the starting solvents and ratios. Form **2** was obtained with the CuI:PPh<sub>3</sub> 1:1 molar ratio exposed to vapor of acetonitrile; monomeric [CuI(PPh<sub>3</sub>)<sub>3</sub>] (form **a**) was obtained with the CuI:PPh<sub>3</sub>=1:2 molar ratio exposed to acetonitrile vapour while in the all the other cases only the monomer [CuI(PPh<sub>3</sub>)<sub>3</sub>] (form **b**) was observed.

### Interconversions between isomers

The isomer conversion *via* exposure to solvent vapour was also investigated. It has been observed that the two isomeric forms [CuI(pic)]<sub>∞</sub> and [CuI(pic)]<sub>4</sub> interconvert in presence of organic solvent.<sup>24</sup> In our case form **1b** exposed to saturated atmosphere of acetonitrile fully converts into form **2** as confirmed by XRPD measurements. Since solid form **1b** is characterized by a bright green emission while form **2** shows only a very weak emission band (*vide infra*), the conversion between the two isomeric forms produces a switch-on/switch-off signal which can be easily detected by naked eyes. When [CuI(PPh<sub>3</sub>)<sub>4</sub>] (form **1a**) is exposed to vapors of acetonitrile it rapidly converts into form **1b** which subsequently transforms into form **2**. The conversion from **1b** to **2** was observed in other experimental conditions

such as in kneading experiments with acetonitrile or toluene or slurry experiments. The conversion is reversible since it is possible to obtain **1b** from a slurry of form **2** with seeds of form **1b**. All interconversions are summarized in Scheme 1.

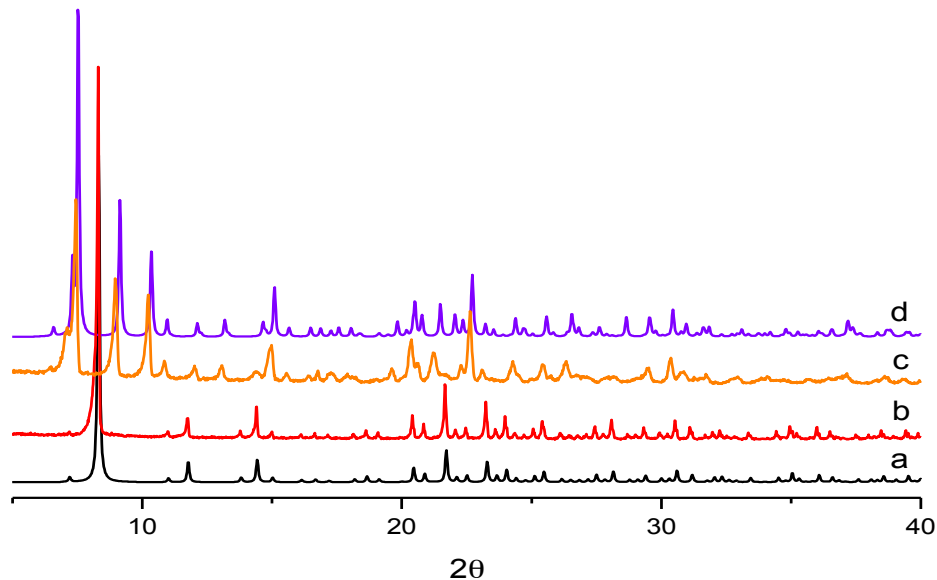
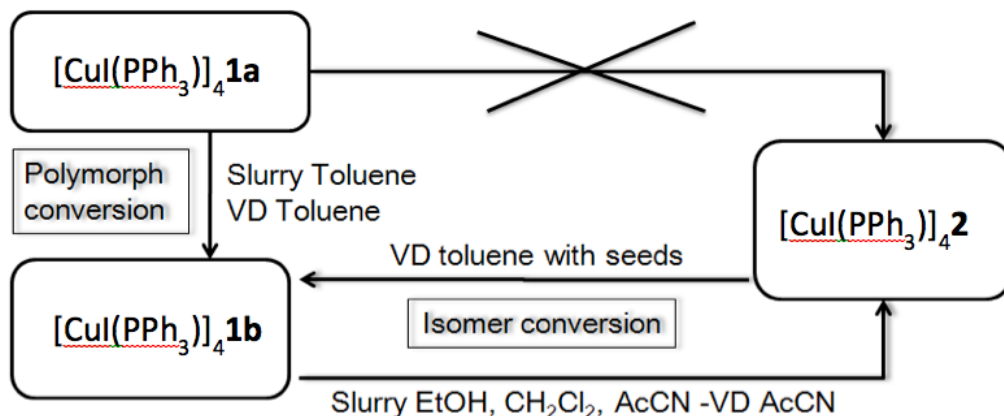


Figure 1.8 | a)  $[\text{CuI}(\text{PPh}_3)_4]$  (form **1b**) calculated; b)  $[\text{CuI}(\text{PPh}_3)_4]$  (form **1b**) experimental; c)  $[\text{CuI}(\text{PPh}_3)_4]$  (form **2**) experimental after conversion; d)  $[\text{CuI}(\text{PPh}_3)_4]$  (form **2**) calculated



Scheme 1.1 | Summary of all interconversions between polymorphic and isomeric forms.

## Photophysical properties

The photophysical properties of compounds **1a**, **1b**, **2** and [CuI(PPh<sub>3</sub>)<sub>1.5</sub>]<sub>2</sub> and of the free ligand PPh<sub>3</sub> have been investigated in solution and in the solid state, both at room temperature and at 77K. The main luminescence data are summarized in Table 2. Toluene has been used as a solvent for **1a**, **1b** and [CuI(PPh<sub>3</sub>)<sub>1.5</sub>]<sub>2</sub>, to retain the main cluster features of the complexes. For the same reason acetonitrile was chosen for the solubilization of [CuI(PPh<sub>3</sub>)<sub>4</sub>] form **2**, but this compound was found to be unstable in solution. It is worth recalling that previous studies on Cu:Cl:PPh<sub>3</sub> complexes in solution have highlighted the presence of different equilibria between various complexes due to ease of exchange of the PPh<sub>3</sub> ligand.<sup>25</sup> The absorption spectra of compounds **1a**, **1b** and [CuI(PPh<sub>3</sub>)<sub>1.5</sub>]<sub>2</sub> in toluene show absorption features extending up to 350-400 nm, ascribable to CT transitions, while the absorption of the free ligand PPh<sub>3</sub> does not exceed 320 nm (see Figure S7).<sup>31,44</sup>

Forms **1a**, **1b** and [CuI(PPh<sub>3</sub>)<sub>1.5</sub>]<sub>2</sub> are non emissive in air equilibrated solutions and display a weak emission centered around 620 nm in air-free toluene at room temperature ( $\phi_{em} = 2-3 \times 10^{-3}$ ), with lifetimes on the order of 200-300 ns (Figure S8 and Table 2). The similarities between the emission features of the three compounds point to a loss of the rigid cluster structure in solution in favor of a comparable pseudo-tetrahedral geometry or to the formation of a similar thermodynamically stable species and the observed luminescence can tentatively be assigned to MLCT (metal-to-ligand charge transfer) excited states.<sup>45</sup> In the dimeric compound [CuI(PPh<sub>3</sub>)<sub>1.5</sub>]<sub>2</sub>, Cu(I) experiences both a trigonal and a tetrahedral geometry, the latter with two phosphine ligands, and the tetrahedral part of the cluster is probably responsible for the emission. Compound **2**, where the tetrahedral coordination of copper includes only one phosphine ligand is instead non-stable in solution, since only a weak emission from PPh<sub>3</sub> was observed.

At 77K in glassy toluene all the three emissive compounds show a luminescence band centered around 415 nm, that is largely hypsochromically shifted in comparison with the room temperature emission, and is blue-shifted also with respect to the low temperature emission of the free PPh<sub>3</sub> ligand (Figure S7 and Table 2). The 77K luminescence of PPh<sub>3</sub>, in fact, is centered at 445 nm with a lifetime of 13.6 ms and is attributed to phosphorescence.<sup>31</sup> The spectral features and the lifetimes, on the order of 200  $\mu$ s, of the luminescence of the complexes at 77K, suggest a ligand contribution to the emission, that can be tentatively assigned to a mixed MLCT/LC (ligand-centered) phosphorescence. A similar long-lived blue

emission in solution at 77K has been recently reported for Ag(I)-bis(diphosphine) complexes, and has been attributed to  $^3\text{MLCT}/^3\text{IL}$  (intra-ligand) states based on tetrahedral geometry.<sup>46</sup> Reflectance spectra of solid samples of PPh<sub>3</sub> and complexes **1a**, **1b**, [CuI(PPh<sub>3</sub>)<sub>1.5</sub>]<sub>2</sub> and **2** (Figure S8), revealed absorption bands below 350 nm for the ligand, with maxima at 212 and 264 nm, ascribable to phenyl-centered and n→π\* phosphorous→phenyl transitions, respectively,<sup>25, 47</sup> and a longer extension of the absorption up to 370 nm for the complexes, with the exception of **2** that tails till 420 nm. A clear band at 300 nm is more pronounced for the two solids **1a** and **1b** while solid [CuI(PPh<sub>3</sub>)<sub>4</sub>] **2** displays a more pronounced absorption around 350 nm.

With respect to the solution case, the solid state luminescence differentiates to a larger extent the four examined complexes. The two polymorphic forms **1a** and **1b**, show different features. Form **1a** displays a bright green-yellow emission at 544 nm at room temperature whereas at 77K a dual emission is clearly observed, with maxima at 410 and 591 nm (see Figure 9a and Table 2), that noticeably render the resultant emission color nearly white. These luminescence features closely resemble the behavior of Cu(I) cubane structures with aromatic amine ligands,<sup>5-8, 23</sup> widely studied by Ford and co-workers, where a dual emission from CC (cluster-centered) and XLCT (iodide to ligand charge transfer) poorly coupled triplet excited states occur. The room temperature emission of form **1a** can thus be attributed to  $^3\text{CC}$  (low energy, LE, emission), and the same band red-shifts at 591 nm at 77K due to the shortening of the Cu-Cu distance at low temperature.<sup>35, 48</sup> The band at 410 nm that appears at 77 K, with a lifetime of 170 μs, can then be ascribed to  $^3\text{XLCT}$  (high energy, HE, emission). This compound presents a Cu-Cu distance in the cluster of 2.839(3) Å at RT, slightly longer than the sum of the orbital radii (2.80 Å), which markedly shorten up to 2.7427(8) Å at 90K. Interestingly, the LE band at 591 nm shows a rise of 7.3 μs, followed by a decay of 26.0 μs (see Figure S9). Ford and co-workers also describe LE rise-times considerably shorter than the HE emission lifetime (ns vs μs range) for Cu<sub>4</sub>I<sub>4</sub>L<sub>4</sub> clusters with pyridinic ligands, speculating on a third higher energy state that directly populates the LE state<sup>5</sup>. Excitation spectra monitored at 590 nm and 410 nm at low temperature and that measured at 544 nm at room temperature (Figure 9a), closely resemble those reported for  $^3\text{XLCT}$  and  $^3\text{CC}$  bands of solid [CuI(py)]<sub>4</sub>.<sup>49</sup> The excitation spectrum measured on the LE band is more confined below 350 nm, also if a clear differentiation is difficult due to the overlap of the two emission bands. Solid **1b** behaves quite differently from its polymorphic form **1a**, showing at room temperature a green emission centered at 518 nm with a lifetime of 3.2 μs, significantly blue-shifted with respect to the room temperature emission of **1a**. At low temperature, then, a dual emission is also

observed, but with one band centered at 434 nm and a less intense band at 516 nm, substantially unshifted with respect to the room temperature case (Figure 9b and Table 2). The description of the dual luminescence of compound **1b** in terms of <sup>3</sup>XLCT and <sup>3</sup>CC is less straightforward, in consideration of the fact that all the Cu-Cu distances estimated in the cluster are longer than 2.80 Å (2.945(4) Å, see Table 1). It is however emerging from recent examples in the literature that organophosphine copper(I) halides with Cu-Cu distances in the range 2.9-3.0 Å show this type of thermochromism, characterized by a dual emission at low temperature with a LE band almost unshifted with respect to the room temperature emission and a blue HE band.<sup>17, 36, 50</sup> The excitation spectra measured at both temperature are similar to those observed for [CuI(PPh<sub>3</sub>)<sub>4</sub>]**1a** (Figure 9b), indicating a similar nature of the excited states and confirming the CC nature of the LE band. The reduced shift in the position of the LE band with temperature can be interpreted considering that at longer Cu-Cu distances the distortion of the CC state with respect to the ground state is reduced<sup>49</sup>. The occurrence of a CC based emission in clusters with Cu-Cu distances longer than 2.8 Å, however, seems to be correlated to the presence of the aromatic phosphine ligand. It is known that the phosphorous-metal bond of triphenylphosphine-transition metal complexes, is not simply describable by the charge donation from the phosphorous lone-pair orbital to the metal, but interactions between the metal d orbitals and the phosphorous-carbon σ orbitals also participate to the bond<sup>26</sup>. We can thus speculate that the involvement of 3d electrons in a “back-bonding” toward the ligand render the d→s,p metal centered contribution to the CC state less effective: the <sup>3</sup>CC emission should be of predominant halide-to-metal charge transfer (XMCT), thus possible also at distances slightly longer than the sum of the van der Waals radii and less sensitive to the contraction of the Cu-Cu cluster occurring when the temperature is decreased. DFT calculations have been performed on Cu<sub>4</sub>X<sub>4</sub>L<sub>4</sub> structures with L=PH<sub>3</sub> or NH<sub>3</sub>,<sup>47</sup> indicating a larger X contribution to the HOMO and a larger Cu contribution to the LUMO when L=PH<sub>3</sub>, but further calculations are required to investigate the nature of the transitions when the phosphine bear aromatic groups. To gain more information about the nature of the luminescence behavior of [CuI(PPh<sub>3</sub>)<sub>4</sub>] form **1b**, the luminescence properties of cubane [CuBr(PPh<sub>3</sub>)<sub>4</sub>], have been investigated, where Cu..Cu distances are between 3.087(2) and 3.541(4) Å at RT.<sup>51</sup> The emission of the solid at room temperature and of both solid and toluene solution at 77 K are reported in Figure S11 and relative data are reported in Table S1. The emission at 620 nm in solution is extremely weak, and the spectral features confirm a <sup>3</sup>MLCT nature of the transition. The solid shows an emission band at 492 nm at room

temperature and a more vibrationally resolved emission that peaks at 442 nm at low temperature, with no strict evidence of dual behavior. The RT spectrum is blue-shifted with respect to form  $[\text{CuI}(\text{PPh}_3)_4]_4$  **1b**, indicating that the substitution of the halogen has effect on the transition, that can be thus of  $^3\text{XMCT}$  (CC) nature. At low temperature the emission appear blue shifted compared to the HE band of form **1b** and with features suggesting a mixed  $^3\text{XLCT/LC}$  character. The LE band in this case can be weak and hidden by the tail of the other band, due to the closeness in energy of the two states. The low temperature emission in solution has a spectral shape coincident with all the other cases, indicating independence from the halogen and confirming a  $^3\text{MLCT}/^3\text{LC}$  nature. Compound  $[\text{CuI}(\text{PPh}_3)_{1.5}]_2$  emits at 482 nm at room temperature and at 414 nm at 77K with no evidence of dual emission (Figure 9c). The Cu-Cu distances in this case are much longer than the sum of the orbital interaction radii (3.044(5) Å) and this leads to describe the luminescence at room temperature in terms of  $^3\text{XLCT}$  phosphorescence; the excitation spectrum recorded at 482 nm is in line with this analysis. The excitation spectrum measured at 414 nm at low temperature, instead, is markedly blue-shifted, suggesting a more pronounced LC nature of the emission, supported also by the long lifetime of 397 $\mu\text{s}$ . It can be noticed that in all the three previously discussed cases the 77K solid state emission (considering the HE bands for polymorphs **1a** and **1b**) is very similar for spectral features and lifetime to that registered in solution at the same temperature and this point to a similar nature of the emitting excited state that clearly involves the ligand orbitals.  $[\text{CuI}(\text{PPh}_3)_4]$  (form **2**), that is non-emissive in solution, shows a very weak luminescence also in the solid state. The room temperature emission, centered at 527 nm with a lifetime of 3.4  $\mu\text{s}$ , slightly blue-shifts at 515 nm at low temperature, with a lifetime of 11.7  $\mu\text{s}$  (Figure 9d and Table 2). The excitation spectrum at room temperature show a sharp absorption at 354 nm, responsible of the observed emission (excitation below 300 nm yielded a more broadened and red-shifted emission). In this compound, the crystal data evidenced the presence of only one Cu-Cu distance in the unit cell of 2.83 Å (Table 1), close to the orbital interaction limit, so the observed weak emission can be tentatively interpreted in terms of  $^3\text{XLCT}$  emission at both temperatures.

Table 1.2 | Luminescence parameters of the ligand and Cu(I) complexes in air-free toluene solutions and in the solid state, at room temperature and at 77 K.

	PPh <sub>3</sub>	Solution	Emission at r.t.			Emission at 77 K	
			$\lambda_{\text{max}}^{\text{a}}/\text{nm}$	$\phi_{\text{em}}^{\text{b}}$	$\tau^{\text{c}}/\mu\text{s}$	$\lambda_{\text{max}}^{\text{a}}/\text{nm}$	$\tau^{\text{c}}/\mu\text{s}$
[CuI(PPh <sub>3</sub> ) <sub>4</sub> 1a]	Solid <sup>c</sup>	468	$6.0 \times 10^{-3}$	$0.6 \times 10^{-3}$		445	$13.6 \times 10^3$
		437		$0.8 \times 10^{-3}$		434	$2.4 \times 10^3$
[CuI(PPh <sub>3</sub> ) <sub>4</sub> 1b]	Solid	628	$2.9 \times 10^{-3}$	0.26		412	224.8
		544		4.7		410, 591	117.3, 26.0 <sup>d</sup>
[CuI(PPh <sub>3</sub> ) <sub>1.5</sub> ] <sub>2</sub>	Solid	628	$1.7 \times 10^{-3}$	0.22		412	190.4
		518		3.2		434, 516	271.8, -
[CuI(PPh <sub>3</sub> ) <sub>1.5</sub> ] <sub>2</sub>	Solution	620	$1.9 \times 10^{-3}$	0.28		412	185.8
		482		7.1		414	397.0
[CuI(PPh <sub>3</sub> ) <sub>4</sub> 2]	Solid	-	-	-		-	-
		527		3.4		515	11.7

<sup>a</sup>From corrected emission spectra.<sup>b</sup> Emission quantum yields in solution, determined by comparing corrected emission spectra, using quinine sulfate in air-equilibrated 1 N H<sub>2</sub>SO<sub>4</sub> ( $\phi_{\text{em}} = 0.546$ )<sup>52</sup> as a standard for PPh<sub>3</sub> and [Ru(bpy)<sub>3</sub>]Cl<sub>2</sub> in air-equilibrated water ( $\phi_{\text{r}} = 0.028$ )<sup>52</sup> as a standard for the complexes, excitation at 300 nm for PPh<sub>3</sub> and at 330 nm for the complexes.<sup>c</sup> Excitation at 278 or 300 nm for PPh<sub>3</sub> and at 331 nm for the complexes.<sup>d</sup> A rise time of 7.3  $\mu\text{s}$  is detected, see text. <sup>e</sup> Emission spectra of PPh<sub>3</sub> in the solid state are shown in Figure A10.

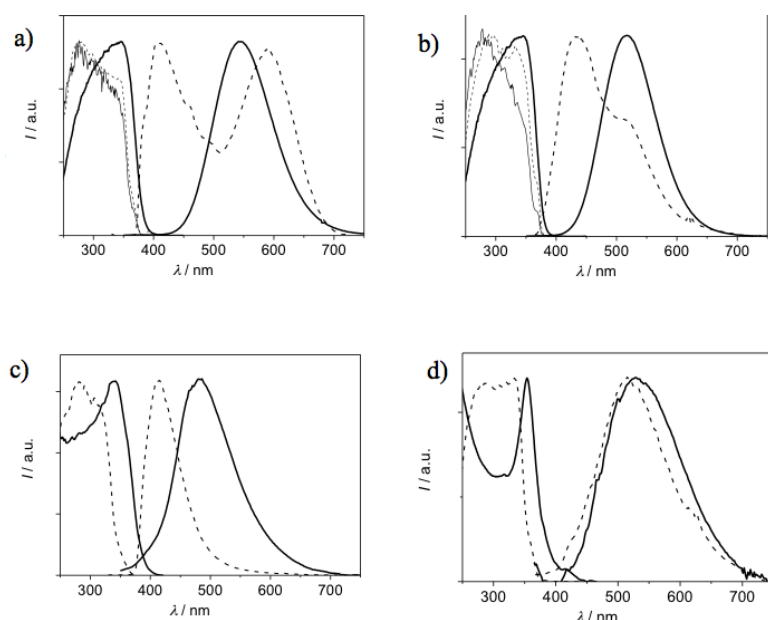


Figure 1.9 | Normalized emission and excitation spectra of solids (a) [CuI(PPh<sub>3</sub>)<sub>4</sub>] form **1a**, (b) [CuI(PPh<sub>3</sub>)<sub>4</sub>] form **1b**, (c) [CuI(PPh<sub>3</sub>)<sub>1.5</sub>]<sub>2</sub> and (d) [CuI(PPh<sub>3</sub>)<sub>4</sub>] form **2**, at room temperature (thick solid lines) and at 77 K (dashed lines). For (a) and (b) the excitation spectra at 77K measured on the HE band are reported as dashed lines whereas those measured on the LE band are reported as thin solid lines.

## Conclusions

Our study confirms the tendency of organophosphine copper(I) iodide compounds to form polynuclear complexes of different structural types but of similar stabilities. On the other hand the observation of the existence of two polymorphs:  $[\text{CuI}(\text{PPh}_3)_3]$  **a** and **b** and  $[\text{CuI}(\text{PPh}_3)]_4$  **1a** and **1b** for both species suggests also the propensity of organophosphine copper(I) iodide compounds to afford polymorphic modifications, probably because of the flexibility of Copper(I) in coordination systems.

The extensive photophysical characterization in solution and solid allowed to a deeper understanding on the nature of the emissive bands. Room temperature emission is postulated to be of  $^3\text{CC}$  nature also in compound  $[\text{CuI}(\text{PPh}_3)]_4$  (form **1b**) which has Cu–Cu distances longer than 2.80 Å, a behavior not observed in similar complexes with nitrogen based ligands. The experimental evidence suggests that the  $^3\text{CC}$  excited state has a predominant halide-to-metal charge transfer (XMCT) nature, which is in agreement with the absence of bathochromic shift in lowering the temperature. The contraction of the cubane cluster  $[\text{CuI}(\text{PPh}_3)]_4$  (form **1a**) at low temperature reduces the distances among the Cu atoms till 2.7431(4) Å, which is shorter than the sum of the van der Waals radii. In this case the  $^3\text{CC}$  emission can be considered of both  $d \rightarrow s,p$  metal centered and XMCT nature, and the red-shift of the LE band at low temperature is indicative of the effect of the shortening of the Cu—Cu distance on the transition. In solution the HE bands are described as mixed  $^3\text{MLCT}/^3\text{LC}$ .

In summary, we have prepared and characterized a rather unusual pair of polymorphs and isomers and studied their interconversion and luminescence properties. Our results have established that  $[\text{CuI}(\text{PPh}_3)_3]$  as form **a** is more stable than as form **b** at RT, while in the case of the tetrameric compounds  $[\text{CuI}(\text{PPh}_3)]_4$  form **1b** is more stable than form **1a**. The relative stability of the isomers, on the other hand, depends on the nature of the solvent.  $[\text{CuI}(\text{PPh}_3)]_4$  as form **1b** converts into form **2** in presence of solvents such as ethanol, acetonitrile and dichloromethane, while the reverse reaction takes place only in slurry in toluene. The conversion can be easily detected by naked eye because forms **1b** and **2** show a dramatic difference in the emission yield and the system could be used as a switch-on/ switch-off signal.

## Experimental Section

### Synthesis of $[\text{CuI}(\text{PPh}_3)_3]$ forms **a** and **b**

The synthesis of the two forms **a** and **b** of compound  $[\text{CuI}(\text{PPh}_3)_3]$  was carried out by utilizing the experimental instruction as previous reported in literature.<sup>29</sup> Stoichiometric quantities of CuI (1 mmol, 0.190 g) and PPh<sub>3</sub> (3 mmol, 0.786 g) were refluxed for 2-4 hours in chloroform and the hot, clear solution has been filtered. On slow cooling and evaporation of the solvent, the products have been separated

as colourless crystal. A mixture of polymorphs **a** and **b** was obtained.

An also different synthetic strategy has been developed to make [CuI(PPh<sub>3</sub>)<sub>3</sub>] **b**: CuI salt (1 mmol; 0.190 g) was dissolved in dimethylchloride under reflux then a solution of PPh<sub>3</sub> (3 mmol; 0.786 g) in n-hexane was added. After two days colourless crystals of [CuI(PPh<sub>3</sub>)<sub>3</sub>] **b** appeared.

Polymorph **b** was also obtained exposing: a) a 1:1 molar ratio physical mixture of CuI and PPh<sub>3</sub> to vapour of toluene; b) a 1:2 molar ratio physical mixture of CuI and PPh<sub>3</sub> to vapour of toluene, acetonitrile and dichloromethane; c) a 1:3 molar ratio physical mixture of CuI and PPh<sub>3</sub> to vapour of toluene, acetonitrile.

### Synthesis of [CuI(PPh<sub>3</sub>)<sub>1.5</sub>]<sub>2</sub>

The synthesis of [CuI(PPh<sub>3</sub>)<sub>1.5</sub>]<sub>2</sub> was previously reported in literature.<sup>32</sup> We report an alternative synthetic strategy. CuI (1 mmol, 0.190 g) was dissolved in 20mL of acetonitrile stirring at 70 °C. Then, a solution of PPh<sub>3</sub> (2 mmol, 0.524g) in AcCN (20 mL) was added to the clear solution. The solution was stirred at 70°C over-night, crystals with prismoidal shape appears after two days.

### Synthesis of [CuI(PPh<sub>3</sub>)<sub>4</sub>] form **1a** e [CuI(PPh<sub>3</sub>)<sub>4</sub>] form **1b**

The synthesis of compound [CuI(PPh<sub>3</sub>)<sub>4</sub>] form **1a** has been made utilizing the experimental instruction as previous reported in literature.<sup>29</sup> CuI (1 mmol, 0.190g) and PPh<sub>3</sub> (1 mmol, 0.262 g) have been refluxed overnight in toluene. Very slow cooling (overnight) of the resultant clear solution to room temperature resulted in well formed crystal of the complex [CuI(PPh<sub>3</sub>)<sub>4</sub>].

As best described in discussion section, we had some difficulties to re-prepare [CuI(PPh<sub>3</sub>)<sub>4</sub>] form **1a**, the second time we followed the above described experimental procedure, we obtained a mixture of polymorph **1a** and **1b**, and from the third time on, we obtained always the most thermodynamically stable polymorph **1b**.

Compound [CuI(PPh<sub>3</sub>)<sub>4</sub>] form **1a** could be re-prepared in drastically kinetic conditions; copper(I) iodide (0.190g, 1 mmol) was dissolved in toluene under reflux and than a solution in toluene of PPh<sub>3</sub> (0.262 g, 1 mmol) has been added, the transparent solution was suddenly evaporated under reduced pressure. The predominant compound was mainly **1a** even if minor quantity of **1b** have been observed.

### Synthesis of [CuI(PPh<sub>3</sub>)<sub>4</sub>] form **2**

The synthesis of compound [CuI(PPh<sub>3</sub>)<sub>4</sub>] form **2** was made utilizing the experimental instruction as previous reported in literature.<sup>20</sup> Stoichiometric quantities of CuI (1 mmol, 0190g) and PPh<sub>3</sub> (1 mmol, 0.262g) were refluxed for 1 hour in chloroform and the hot, clear solution filtered. On slow cooling and solvent evaporation, the product separate as colourless crystal.

The same compound has been obtained grinding physical mixture of CuI and triphenylphosphine in 1:1 molar ratio with two drops of toluene or grinding physical

mixture of CuI and triphenylphosphine in 1:2 and 1:3 molar ratio with two drops of acetonitrile.

**Photophysics:** Solvents used for photophysical determinations were of spectroscopic grade (C. Erba). Dilute solutions were analyzed in 10 mm path length square optical Suprasil Quartz (QS) cuvettes at room temperature, solid samples were placed inside two quartz slides, while capillary tubes immersed in liquid nitrogen in a home-made quartz Dewar were used for measurements at 77 K for both solids and solutions. The absorption spectra of solutions were obtained with a Perkin-Elmer Lambda 950 UV/vis/NIR spectrophotometer, whereas reflectance spectra of solid samples were acquired on a Perkin-Elmer Lambda 9 UV/vis/NIR spectrophotometer equipped with a 60 mm integrating sphere.

Emission and excitation spectra were measured in a SpexFluorolog II spectrofluorimeter, equipped with a Hamamatsu R928 phototube, in right angle mode for solutions and front face mode for solids. Corrected emission spectra are reported, the uncertainty on the band maxima is 2 nm. Luminescence quantum yields in solution were evaluated from the area of the luminescence spectra, corrected for the photomultiplier response, with reference to quinine sulfate in air-equilibrated 1 N H<sub>2</sub>SO<sub>4</sub> ( $\phi_{\text{em}} = 0.546$ )<sup>52</sup> for PPh<sub>3</sub> and to [Ru(bpy)<sub>3</sub>]Cl<sub>2</sub> in air-equilibrated water ( $\phi_{\text{r}} = 0.028$ )<sup>52</sup> for the complexes. The samples, with absorbances < 0.1, were bubbled with Ar for approximately 15 min and sealed in home made 10 mm optical cells. The luminescence tail of toluene emission below 450 nm was previously subtracted from the spectra.

Luminescence lifetimes in the range 0.5 ns – 100 μs were measured with an IBH 5000F time-correlated single-photon counting device, by using pulsed NanoLED excitation sources at 278 or 331 nm (pulse width ≤ 0.6 ns). Longer lifetimes were measured on the same IBH 5000F TCSPC device, by using a pulsed SpectraLED excitation source at 370 nm or on a Perkin-Elmer LS-50B spectrofluorimeter equipped with a pulsed Xe lamp and in a gated detection mode. Analysis of the luminescence decay profiles against time was accomplished with the Decay Analysis Software DAS6 or with the PHOSDecay Software provided by the manufacturers, with an estimated error on the lifetimes of 10%. In some cases the low temperature luminescence of the solid samples showed multiexponential decays; Table 2 reports lifetimes corresponding to pre-exponential factors > 80%.

**X-ray powder diffraction:** X-ray powder diffractograms were collected on a Panalytical X'Pert PRO automated diffractometer with CuKα radiation and X'Celerator detector without a monochromator equipped with a Anton Paar TK 450 chamber to collect data at low temperature. The program PowderCell<sup>53</sup> was used for calculation of X-ray powder patterns.

**Crystal structure determination:** Crystal data for **1a** and **1b** were collected on a

Oxford Xcalibur S with MoK $\alpha$  radiation,  $\lambda = 0.71073$  Å, monochromatorgraphite and equipped with a liquid nitrogen Oxford-Cryostream device.

Crystal data and details of measurements are summarized in Table S2. SHELX97<sup>54</sup> was used for structure solution and refinement based on F<sup>2</sup>. Non-hydrogen atoms were refined anisotropically. Hydrogen atoms bound to carbon atoms were added in calculated positions. Mercury<sup>55</sup> was used for the graphical representation of the results.

### Acknowledgment:

We thank MIUR, the University of Bologna and Italian CNR (Project PM-P04-010 MACOL) for financial support to this research.

### Notes

Supplementary Information (SI) available in appendix A

### References

1. F. G. Mann, D. Purdie and A. F. Wells, *J. Chem. Soc.*, 1936, 447-460.
2. A. E. Arbusow, *J. Russ. Phys. Chem. Soc.*, 1906, **38(ii)**, 293.
3. G. Tartarini, *Gazz. Chim. Ital.*, 1933, **63**, 597-600.
4. N. Armaroli, G. Accorsi, F. Cardinali and A. Listorti, *Top. Curr. Chem.*, 2007, **280**, 69-115.
5. K. R. Kyle, C. K. Ryu, P. C. Ford and J. A. DiBenedetto, *J. Am. Chem. Soc.*, 1991, **113**, 2954-2965.
6. P. C. Ford and A. Vogler, *Acc. Chem. Res.*, 1993, **26**, 220-226.
7. P. C. Ford, *Coord. Chem. Rev.*, 1994, **132**, 129-140.
8. H. D. Hardt and A. Pierre, *Inorg. Chim. Acta*, 1977, **25**, L59-L60.
9. H. D. Hardt and A. Pierre, *Naturwissenschaften*, 1975, **62**, 298.
10. H. D. Hardt, H. Gechnizdjani and A. Pierre, *Naturwissenschaften*, 1972, **59**, 363.
11. H. D. De Ahna and H. D. Hardt, *Z. Anorg. Allg. Chem.*, 1972, **387**, 61-71.
12. R. Peng, S. R. Deng, M. Li, D. Li and Z. Y. Li, *CrystEngComm*, 2008, **10**, 590-597.
13. C. H. Arnby, S. Jagner and I. Dance, *CrystEngComm*, 2004, **6**, 257-275.
14. S. Q. Bai, J. Y. Kwang, L. L. Koh, D. J. Young and T. S. A. Hor, *Dalton Trans.*, 2010, **39**, 2631-2636.
15. R. Peng, M. Li and D. Li, *Coord. Chem. Rev.*, 2010, **254**, 1-18.
16. J. B. Liu, H. H. Li, Z. R. Chen, J. B. Li, X. B. Chen and C. C. Huang, *J. Cluster. Sci.*, 2009, **20**, 515-523.
17. S. Perruchas, X. F. L. Goff, S. Maron, I. Maurin, F. o. Guillen, A. Garcia, T. Gacoin and J.-P. Boilot, *J. Am. Chem. Soc.*, 2010, **132**, 10967-10969.
18. C. Tard, S. Perruchas, S. Maron, X. F. Le Goff, F. Guillen, A. Garcia, J. Vigneron, A. Etcheberry, T. Gacoin and J. P. Boilot, *Chem. Mat.*, 2008, **20**, 7010-7016.
19. Z. Liu, M. F. Qayyum, C. Wu, M. T. Whited, P. I. Djurovich, K. O. Hodgson, B. Hedman, E. I. Solomon and M. E. Thompson, *J. Am. Chem. Soc.*, 2011, **133**, 3700-3703.
20. M. R. Churchill, B. G. DeBoer and D. J. Donovan, *Inorg. Chem.*, 1975, **14**, 617-623.
21. M. R. Churchill and K. L. Kalra, *Inorg. Chem.*, 1974, **13**, 1065-1071.
22. B.-K. Teo and J. C. Calabrese, *Inorg. Chem.*, 1976, **15**, 2467-2474.

23. P. C. Ford, E. Cariati and J. Bourassa, *Chem. Rev.*, 1999, **99**, 3625-3648.
24. E. Cariati, X. H. Bu and P. C. Ford, *Chem. Mat.*, 2000, **12**, 3385-3391.
25. D. J. Fife, W. M. Moore and K. W. Morse, *Inorg. Chem.*, 1984, **23**, 1684-1691.
26. C. Bourg, S. Gamblin and D. Urch, *J. Electron Spectrosc. Relat. Phenom.*, 1995, **73**, 163-172.
27. G. Costa, E. Reisenhofer and L. Stefani, *J. Inorg. Nucl. Chem.*, 1965, **27**, 2581-2584.
28. P. H. Davis, R. L. Belford and I. C. Paul, *Inorg. Chem.*, 1973, **12**, 213-218.
29. P. F. Barron, J. C. Dyason, P. C. Healy, L. M. Engelhardt, C. Pakawatchai, V. A. Patrick and A. H. White, *J. Chem. Soc., Dalton Trans.*, 1987, 1099-1106.
30. J. C. Dyason, P. C. Healy, L. M. Engelhardt, C. Pakawatchai, V. A. Patrick, C. L. Raston and A. H. White, *J. Chem. Soc., Dalton Trans.*, 1985, 831-838.
31. D. J. Fife, W. M. Moore and K. W. Morse, *Inorg. Chem.*, 1984, **23**, 1545-1549.
32. P. G. Eller, G. J. Kubas and R. R. Ryan, *Inorg. Chem.*, 1977, **16**, 2454-2462.
33. D. Braga, S. L. Giuffreda, K. Rubini, F. Grepioni, M. R. Chierotti and R. Gobetto, *CrystEngComm*, 2007, **9**, 39-45.
34. D. Braga, S. L. Giuffreda, F. Grepioni, M. R. Chierotti, R. Gobetto, G. Palladino and M. Polito, *CrystEngComm*, 2007, **9**, 879-881.
35. D. Braga, F. Grepioni, L. Maini, P. P. Mazzeo and B. Ventura, *New J. Chem.*, 2011, **35**, 339-344.
36. H. Kitagawa, Y. Ozawa and K. Toriumi, *Chem. Commun.*, 2010, **46**, 6302-6304.
37. M. Vitale and P. C. Ford, *Coord. Chem. Rev.*, 2001, **219**, 3-16.
38. F. De Angelis, S. Fantacci, A. Sgamellotti, E. Cariati, R. Ugo and P. C. Ford, *Inorg. Chem.*, 2006, **45**, 10576-10584.
39. A. I. Kitaigorodskii, *Organic Chemical Crystallography*, New York.
40. D. J. Dahrenbourg, M. W. Holtcamp, K. K. Klausmeyer and J. H. Reibenspies, *Z. Kristall.*, 1995, **210**, 615-616.
41. Structure of 1b has been published by Kitagawa et al. during the preparation of the manuscript. The nomenclature of the two polymorphs is in agreement with the Kitagwa articles.
42. J. D. Dunitz and J. Bernstein, *Acc. Chem. Res.*, 1995, **28**, 193-200.
43. A. Bondi, *J. Phys. Chem.*, 1964, **68**, 441-451.
44. H. H. Jaffè and L. D. Freedman, *J. Am. Chem. Soc.*, 1952, **74**, 1069-1071.
45. O. Moudam, A. Kaeser, B. Delavaux-Nicot, C. Duhayon, M. Holler, G. Accorsi, N. Armaroli, I. Seguy, J. Navarro, P. Destruel and J.-F. Nierengarten, *Chem. Commun.*, 2007, 3077-3079.
46. K. Matsumoto, T. Shindo, N. Mukasa, T. Tsukuda and T. Tsubomura, *Inorg. Chem.*, 2010, **49**, 805-814.
47. P. A. Grutsch and C. Katal, *J. Am. Chem. Soc.*, 1979, **101**, 4228-4233.
48. D. Braga, L. Maini, P. P. Mazzeo and B. Ventura, *Chem. Eur. J.*, 2010, **16**, 1553-1559.
49. M. Vitale, C. K. Ryu, W. E. Palke and P. C. Ford, *Inorg. Chem.*, 1994, **33**, 561-566.
50. C. Tard, S. Perruchas, S. Maron, X. F. Le Goff, F. o. Guillen, A. Garcia, J. Vigneron, A. Etcheberry, T. Gacoin and J.-P. Boilot, *Chem. Mat.*, 2008, **20**, 7010-7016.
51. P. F. Barron, J. C. Dyason, L. M. Engelhardt, P. C. Healy and A. H. White, *Inorg. Chem.*, 1984, **23**, 3766-3769.
52. M. Montalti, A. Credi, L. Prodi and M. T. Gandolfi, in *Handbook of Photochemistry, Third Edition*, CRC Press, 2006.
53. W. Kraus and G. Nolze, *Powder Cell*, (1999).
54. G. M. Sheldrick, *SHELXL97*, 1997, University of Göttingen, Germany.
55. C. F. Macrae, P. R. Edgington, P. McCabe, E. Pidcock, G. P. Shields, R. Taylor, M. Towler and J. van De Streek, *J. Appl. Crys.*, 2006, **39**, 453-457.

# Chapter 2

## Switch on - switch off signal in a MOF-guest crystalline device

**Abstract:** A metal organic framework (MOF) based on the cluster of  $[\text{Cu}_4\text{I}_4\text{DABCO}_2]$  (**1**) (DABCO=1,4-diazabicyclo[2.2.2]octane), MOF **1**, shows a bright emission with maximum at 556 nm and emission quantum yield of 0.53 in the solid state. When the large cavities of the MOF are loaded, during the synthesis, with different amounts of ferrocene ( $\text{FeCp}_2$ ,  $[(\eta^5\text{-C}_5\text{H}_5)_2\text{Fe}^{(\text{II})}]$ ), MOF **1** luminescence decreases with the increase of ferrocene content, reaching an almost complete quenching for 3.5% w/w of cage loading, corresponding to the complete filling of the MOF cavities. When an electric potential is applied to the  $\text{FeCp}_2@\text{MOF } \mathbf{1}$  deposited onto an ITO glass, the  $\text{Fe}(\text{II})\text{Cp}_2$  is oxidized to  $\text{Fe}(\text{III})\text{Cp}_2^+$ , and the MOF **1** emission is partially switched on again, indicating that a photoinduced electron transfer reaction is contributing to the quenching process.



## Introduction

In the last decades, crystal engineering has developed a new concept of supramolecular chemistry in the solid state. Crystal engineers are devoted to the design and synthesis of new crystalline solids with desired physical and chemical properties starting from an adequate choice of molecular building blocks and framework structures.

The crystal engineering paradigm has led us to the idea of using this approach to construct crystalline devices. As a device is “a thing made for a particular purpose”<sup>[1]</sup> which is made of different pieces with different functionalities assembled together, in the same way, a crystalline device is a crystal made of different molecules with different chemical functionalities assembled together to obtain a final material whose properties can be activated by appropriate external stimuli.

Metal-organic frameworks (MOFs), which are nowadays extensively studied for biology<sup>[2]</sup>, drug delivery<sup>[3]</sup>, gas storage/uptake<sup>[4]</sup>, separation<sup>[5]</sup>, sensing<sup>[6]</sup> and catalysis,<sup>[7]</sup> are good candidates for the construction of such crystalline devices, since they are characterized by a robust framework and cavities to allocate guest molecules. The exploitation of the interactions between host and guest to tune some specific bulk properties (i.e. luminescence, magnetism etc.) is not novel and there is a number of very educative examples.<sup>[8]</sup>

In our approach the crystalline device is based on the idea of having a guest molecule trapped into a luminescent MOF which can be subjected to external physical “stimuli” to modify host-guest interactions within the MOF and consequently the host luminescence.<sup>[9]</sup> From this viewpoint a crystalline device can be considered as a higher level step of crystal engineering since the final properties of the device are derived from the tunable combination of the specific properties of the host and of the guest.

We have focused our attention on MOFs based on CuI clusters since they are characterized by a bright luminescence,<sup>[10]</sup> the metal precursor is cheap and readily available and they are easy to prepare also via solvent free reactions<sup>[11]</sup>. The luminescent properties of copper(I) halide aggregates have been extensively studied by Ford et al.<sup>[12]</sup> who showed that luminescent behaviour and geometry of the aggregate are strictly related, especially when the copper atoms coordinate saturated ligands since the luminescence, arising from the so called “cluster-centred”(CC) excited states, occurs only when the Cu···Cu distance is lower than the sum of the orbital interaction radii.<sup>[12c]</sup> Herein we report on the photochemical and electrochemical properties of MOF **1**, which is made of nodes based on Cu<sub>4</sub>I<sub>4</sub> cubane clusters and a saturated amine (DABCO, 1,4-diazabicyclo-[2.2.2]octane) as a secondary building units, loaded with different amounts of FeCp<sub>2</sub> [ $(\eta^5\text{-C}_5\text{H}_5)_2\text{Fe}^{(\text{II})}$ ] molecules. The overall structure of MOF **1** presents large cavities connected by small channels which permit the exchange of small guest molecules such as ethanol, methanol, acetonitrile etc.<sup>[10]</sup> Otherwise, large guest molecules can be embedded into the framework during the synthesis; these guest molecules are trapped in the cavities without any possibility to leave from the structure.

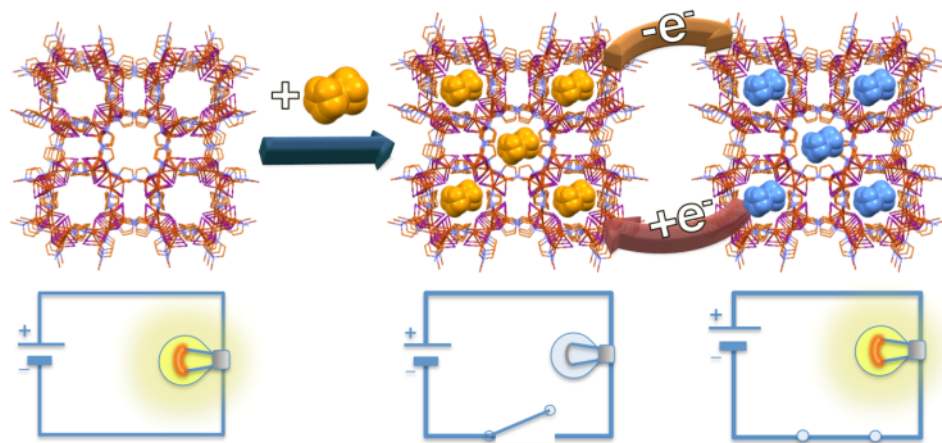


Figure 2.1 | The left side of the figure represents the situation in which the MOF is “turned on” as a light bulb in a closed electrical circuit; on the right part, the electrical circuit is improved with a switch and the MOF is loaded with ferrocene. Upon oxidation/reduction of the ferrocene the MOF luminescence can be turned on/off.

We chose to load the MOF **1** with ferrocene ( $\text{FeCp}_2$ ) since it is an optimum candidate to build a *crystalline device*: in fact,  $\text{FeCp}_2$  can in principle interact with the excited states of the cage. Ferrocene is widely used as luminescence quencher and electron donor in supramolecular photochemistry, analytical chemistry and biology<sup>[13]</sup>. The relatively low energy of its lowest triplet excited state (*ca.* 1.16 eV)<sup>[14]</sup> and a low oxidation potential (*ca.* 0.45 V *vs* SCE in polar solvents),<sup>[15]</sup> allows ferrocene to act as an efficient triplet excited state quencher in triplet-triplet energy transfer processes and as an electron donor in photoinduced electron-transfer reactions.<sup>[16]</sup> In the literature, only few reports describe the occurrence of host-guest photoinduced energy-transfer processes in the solid state between MOF hosts and permanently loaded guests.<sup>[17]</sup> Among these, in two cases ferrocene has been used as guest and the observed luminescence quenching of the  $\text{Tb}(\text{III})$ -based<sup>[17b]</sup> and  $\text{Zn}(\text{II})$ -based<sup>[17c]</sup> MOFs has been interpreted in terms of energy-transfer processes. Additionally  $\text{FeCp}_2$  is characterized by a low oxidation potential, so that it can be easily oxidized by conventional electrochemical techniques (*external stimuli*) and finally it has appropriate dimensions to fit the MOF **1** cavities preserving the original organometallic network. As planned, once ferrocene is loaded into the MOF structure, the  $\text{FeCp}_2@\text{MOF } \mathbf{1}$  luminescence is turned off; applying an electric potential to the  $\text{FeCp}_2@\text{MOF } \mathbf{1}$  deposited onto an ITO glass,  $\text{Fe}^{(\text{II})}\text{Cp}_2$  is oxidized to  $\text{Fe}^{(\text{III})}\text{Cp}_2^+$ , which differently interacts with the excited states of the cage and the luminescence of MOF **1** is partially “turned on” again. Thus  $\text{FeCp}_2@\text{MOF } \mathbf{1}$  represents a remarkably simple and reversible switch off/switch on solid state system. It is worth pointing out that, although chemical systems working on “on/off signal” are known in solution in supramolecular chemistry<sup>[18]</sup> this is the first time, to the best of the authors knowledge, that luminescence is controlled by external stimuli in an all-sufficient MOF-guest system in the solid state.

## Results and Discussion

**Quantification of FeCp<sub>2</sub>@MOF:** MOF **1**, as reported in our previous work,<sup>[10]</sup> is based on Cu<sub>4</sub>I<sub>4</sub> clusters bridged by saturated N-donor DABCO ligands; the crystalline structure presents two mono-dimensional channels that contain disordered solvent molecules. One channel is centred at the origin of the unit cell and it develops along the *c* axes with an accordion-like shape, whereas the second channel is centred on ½ *a* and ½ *b* and is parallel to the first one. The solvent molecules trapped in the channels can be exchanged by exposure of MOF **1** to vapour of different solvents.<sup>[10]</sup>

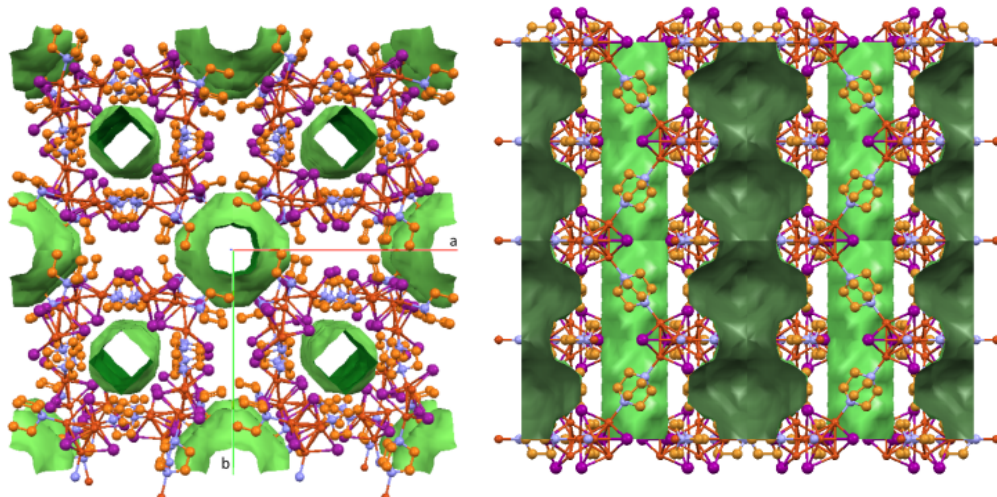


Figure 2.2 | Voids analysis in channels of MOF **1**. View of the crystal structure of MOF **1** along *c* axes (a) and along *b* axes (b). One channel is centred on the origin and is characterized by cavities with a diameter up to 16.18 Å connected by apertures with diameter of 7.06 Å and a total volume of 650 Å<sup>3</sup> per unit cell, whereas the second channel is centred on ½ *a* and ½ *b* and it has a diameter of 7.07 Å with volume of 322 Å<sup>3</sup> per unit cell (distances are measured from diagonally opposite hydrogen atoms in the channel). The channels (highlighted in green) are calculated with Mercury<sup>[19]</sup>: light green is outer surface, dark green is the inner surface.

When the synthesis of MOF **1** is carried out in acetonitrile solution in presence of different amounts of ferrocene, the products obtained present the same powder pattern of MOF **1** (Fig B.1). This suggests that the ferrocene has appropriate dimensions to be accommodated into the cavities without modifying the network structure. Atomic absorption spectroscopy technique (AAS) with external standard method has been used to determine the real amount of ferrocene loaded into the channels for each synthesis. As described in Figure 3, increasing the amount of ferrocene dissolved in solution corresponds to a loading curve of ferrocene into the channels that reaches a plateau at 3.5% w/w of loading, when in the solution is present only 10% in mole of ferrocene

with respect to the amount of CuI used. It derives that 3,5% w/w of loading correspond to the maximum amount of ferrocene that can be accommodated into the cavities in the accordion-like channels and can be reasonably associated to the complete filling of the MOF channels with ferrocene units. The plateau value of loading also corresponds to the almost complete quenching of MOF luminescence, as discussed in details below. The product with the highest percentage of loading (3.51 % w/w) will be indicated in the following text as FeCp<sub>2</sub>@MOF 1.

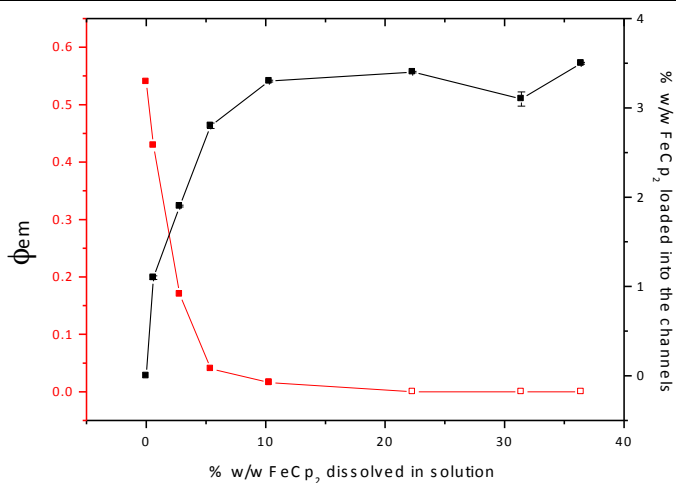


Figure 2.3 | Photochemical behaviour of FeCp<sub>2</sub>@MOF 1 with different FeCp<sub>2</sub> content. Percentage of FeCp<sub>2</sub> dissolved in solution *vs.* percentage of FeCp<sub>2</sub> loaded into the channels (black line) and *vs.* absolute emission quantum yield (red line). The empty red squares refer to  $\phi_{\text{em}}$  values below instrumental resolution.

**Photophysical characterization:** A comprehensive photophysical study has been carried out on MOF 1 and on the ferrocene loaded systems. Reflectance spectra of solid samples of MOF 1 loaded with the different amounts of ferrocene evidence the presence of the guest inside the MOF pores. An absorption band peaking around 430 nm, not present in the spectrum of pristine MOF 1, in fact, gradually appears in the spectra of the ferrocene containing samples (Fig. B.2). This is consistent with the absorption contribution of ferrocene, which shows a main absorption peaks at *ca.* 440 nm ( $\epsilon \cong 100 \text{ M}^{-1} \text{ cm}^{-1}$  in organic solvents).<sup>[16c, 20]</sup> Solid-state photoluminescence of MOF 1 is characterized by a broad luminescence band, peaking at 556 nm, and by an excitation profile in the 250-400 nm region.<sup>[10]</sup> The emission is ascribed to a triplet excited-state of cluster-centered (CC) nature, *i.e.* of mixed iodide-to-copper charge transfer (XMCT) and d→s-p copper-centred (MC) nature; these transitions originate in the Cu<sub>4</sub>I<sub>4</sub> core only when the Cu···Cu distance in the cluster is lower than the sum of the orbital interaction radii. The large Stokes shift (10700 cm<sup>-1</sup>) is explained by the high distortion of the CC state with respect to the ground state.<sup>[12b, 21]</sup>

Table 2.1. Luminescence data of solid MOF **1** loaded with various amounts of FeCp<sub>2</sub> indicated as percentage w/w, as measured by AAS.

% FeCp <sub>2</sub>	$\phi_{\text{em}}^{[a]}$	$\tau / \mu\text{s}^{[b]}$
0	$0.532 \pm 0.015$	14.4
1.10	$0.429 \pm 0.009$	8.0 [d] 9.8 (73%); 3.2 (27%)
1.90	$0.170 \pm 0.022$	4.5 [d] 5.4 (76%); 1.8 (24%)
2.80	$0.041 \pm 0.004$	n.d.
3.30	$0.016 \pm 0.004$	n.d.
3.40	-[c]	-
3.10	-[c]	-
3.51	-[c]	-

[a]Absolute emission quantum yields, excitation at 334 nm. [b] Luminescence lifetimes, excitation at 331 nm. [c] Below instrumental resolution. [d] Weighted average value. n.d. is not detected.

The absolute emission quantum yield of solid MOF **1**, 0.53 (Table 2.1), is a remarkably high value for copper based solid materials. The loading of ferrocene into the MOF pores unequivocally leads to a quenching of MOF **1** luminescence, with a clear inverse relationship between the percentage (w/w) of loaded FeCp<sub>2</sub> and the MOF emission quantum yield (Figure 2.3 and Table 2.1). A visualization of the quenching effect of the ferrocene loading on the photoluminescence of the solid MOF material can be pursued comparing emission spectra of samples characterized by different loadings (Fig. B.3), obtained with the use of an integrating sphere (see Experimental Section for details).

Also the luminescence lifetime of solid MOF **1** (14.4  $\mu\text{s}$ , Table 1) decreases with the increasing amount of ferrocene loaded inside the MOF pores. Whereas the emission of MOF **1** shows a mono-exponential decay, the luminescence of the ferrocene loaded MOF samples show multi-exponential decays that can be reasonably fitted by bi-exponential functions (Table 2.1). This behaviour can be ascribed to a non-homogeneous location of the ferrocene guest molecules inside the MOF structure. Considering a weighted average lifetime for the MOF luminescence in the presence of ferrocene (Table 1), the lifetime quenching roughly follow that of the emission quantum yield. Above 1.90 % (w/w) of loading, the lifetime is not measureable. MOF **1** luminescence decays at different amounts of loading are reported in Figure B.4.

On the basis of the absolute emission quantum yield values, that give a more definite quantification of the quenching effect with respect to the measured lifetimes, a Stern-Volmer analysis has been performed. Mathematical treatments that include static quenching in the pristine Stern-Volmer equation have been afforded for solution cases where both diffusional and static quenching can occur. Generally, static quenching can be due either to the formation at the ground state of a non-fluorescent complex or to a high probability that the chromophore and the quencher happen to be adjacent in space

when the chromophore is excited. This causes an upward deviation from the linearity of the Stern-Volmer relationship and a modified equation, (1), has been derived: [22]

$$\frac{F_0}{F} = (1 + K_D[Q]) \frac{e^{V[Q]}}{Y} \quad (1)$$

$F$  and  $F_0$  are, respectively, the quenched and unquenched emission intensities,  $K_D$  is the dynamic Stern-Volmer constant,  $[Q]$  is the quencher concentration,  $V$  is the active volume surrounding the chromophore where the quencher should exist to have static quenching and  $Y$  is a factor that embodies quenching due to transient effects. In the present case, where diffusion of the quencher is precluded by the crystalline nature of the system, the diffusional term can be neglected ( $K_D = 0$ ) and only the term accounting for the static quenching has to be considered. The concentration of the quencher can be expressed as molar fraction ( $x$ ) of the loaded ferrocene, calculated considering the moles of  $\text{FeCp}_2$  and the moles of the  $[\text{Cu}_4\text{I}_4\text{DABCO}_2]$  cluster in the MOF (Tab. B.1), *i.e.* the minimal photoactive cell in the structure (see below). A plot of  $\phi_0/\phi$  as a function of the ferrocene molar fraction is reported in Figure 4. It can be seen that the fitting based on equation (2) is excellent (Figure 4).

$$\frac{\Phi_0}{\Phi} = \frac{e^{Vx}}{Y} \quad (2)$$

The observed trend is reasonable also considering that a ferrocene molar fraction of 0.16 corresponds to the total loading of the MOF pores with ferrocene (*vide supra*) and that from the crystallographic data it can be estimated that each pore able to host a ferrocene unit is surrounded by eight  $[\text{Cu}_4\text{I}_4\text{DABCO}_2]$  clusters.

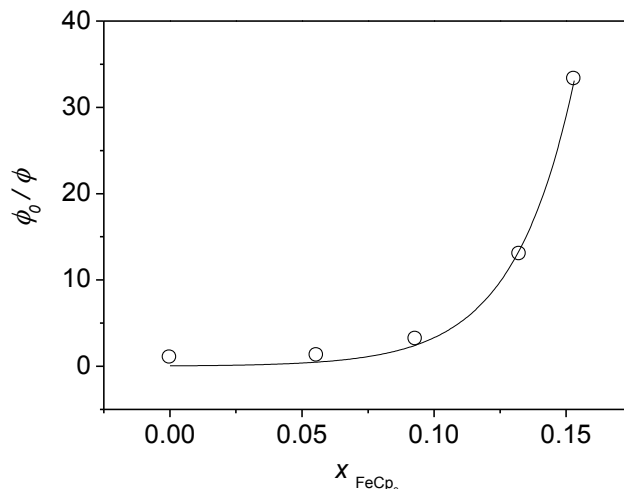


Figure 2.4 | Modified Stern-Volmer Plot of MOF 1 emission quenching as a function of the molar fraction of  $\text{FeCp}_2$  and fitting of the data ( $R^2 = 0.997$ ,  $V = 43.38$ ,  $Y = 23.11$ , solid line) according to equation (2), see text.

**Electrochemical characterization:** The electrochemical properties of MOF **1** and FeCp<sub>2</sub>@MOF **1** films supported onto a conducting substrate have been investigated by cyclic voltammetry (CVs) in various solvents (PBS or acetonitrile). CV is a quite powerful tool for exploring the redox behaviour of MOFs.<sup>[23]</sup> The CV of MOF **1** in acetonitrile, (Figure 5a solid line), shows one large irreversible oxidation peak at 1.3 V (*vs.* SCE). A re-reduction peak located at ~0.5 V is observed in the reverse scan, thus suggesting that the [Cu<sub>4</sub>I<sub>4</sub>DABCO<sub>2</sub>] cluster would undergo a relatively slow but reversible redox process. However, subsequent scans showed the gradual decrease of the CV peaks that was attributed to the irreversible loss of electroactive material associated to degradation of the films upon oxidation of the MOF. Interestingly, the presence of the ferrocene moiety embedded within the MOF structure is clearly evidenced by the different CV behaviour of FeCp<sub>2</sub>@MOF **1** with respect to pristine MOF **1**. In particular, the oxidation process taking place at ~0.4 V (see Figure 5a dashed line) is likely to be associated to the Fe<sup>(III)</sup>Cp<sub>2</sub><sup>+</sup>/Fe<sup>(II)</sup>Cp<sub>2</sub> couple.

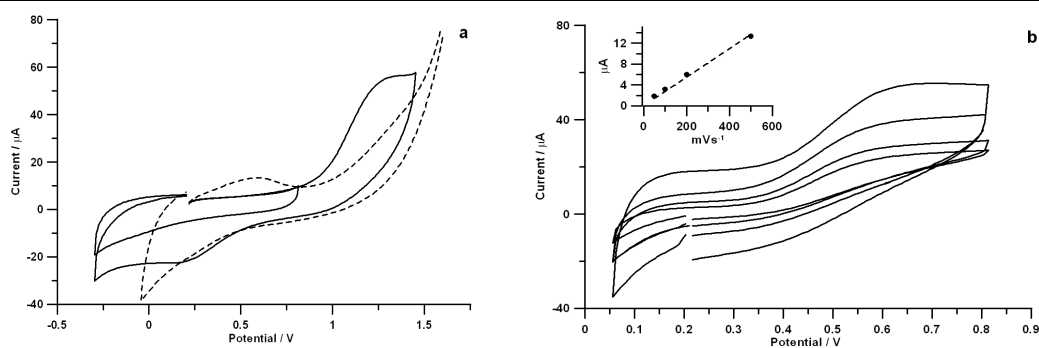


Figure 2.5 | Electrochemical analysis of both MOF **1** and FeCp<sub>2</sub>@MOF **1**. a. Cyclic voltammetry of MOF **1** (solid line) and FeCp<sub>2</sub>@MOF **1** (dashed line) in CH<sub>3</sub>CN, 80 mM TBAH, scan rate 100 mV s<sup>-1</sup>. b. Cyclic voltammetry of FeCp<sub>2</sub>@MOF **1** in PBS solution, scan rate 50-100-200-500 mV s<sup>-1</sup>. Inset: peak current *vs.* scan rate.

In line with this attribution, the peak current of the anodic peak (with  $E_{1/2} = 0.45$  V) displayed in Figure 5b was found to depend linearly on scan rate (see inset in Figure 5b), as typically observed for surface-immobilised species. Furthermore, the large irreversible anodic peak at 1.3 V (and its cathodic counterpart at 0.5 V) in pristine MOF **1** is largely decreased and is replaced, in the case FeCp<sub>2</sub>@MOF **1**, (Figure 5a, dashed line), by a weak shoulder superimposed onto the increasing background current. Such a behaviour was interpreted as the consequence of the electrostatic repulsion induced by the embedded ferrocinium guests that would shift the MOF **1** oxidation towards more positive potentials, *i.e.*, outside the investigated potential window.

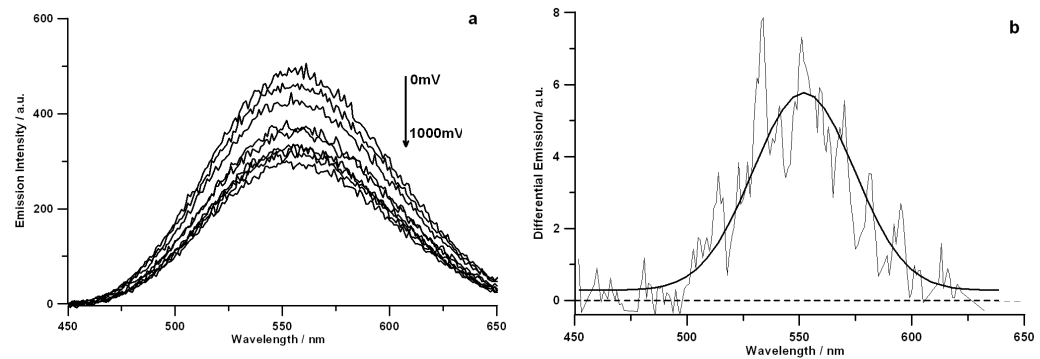


Figure 2.6 | a. Applied potential dependent PL spectra of MOF 1 in PBS solution upon the excitation at 350 nm (applied potential from the top 0-300-400-600-800-900-1000 mV). b. Differential emission spectrum of FeCp<sub>2</sub>@MOF 1 in PBS solution obtained upon oxidation of FeCp<sub>2</sub> (at 0.75 V). PMT bias 750 V. Potential are reported *vs.* SCE.

Significant changes in the emissive properties of MOF 1, were brought about by changes of its redox state carried out electrochemically at MOF 1 drop-cast films onto ITO electrodes. Figure 6a shows the progressive bleaching of MOF 1 emission obtained by the progressive increase of the applied potential, from 0 to 1.0 V. Reversal of the applied potential, however, did not produce any sizeable recovery of emission intensity, in line with the above hypothesis of film degradation under oxidative conditions.

By contrast, in FeCp<sub>2</sub>@MOF 1, where emission is fully quenched in the pristine state (see above), a sizeable - although rather weak - emission was obtained upon oxidation at 0.75 V, that corresponds to the full oxidation of the embedded ferrocene moieties, Figure 6b. From this point of view, FeCp<sub>2</sub>@MOF 1 would then behave as a *crystalline* photo-device where emission is controlled by the redox state of the guest, although the full reversibility of such a process could not be proved under the present conditions due to low stability of films.

### Deactivation of photoexcited FeCp<sub>2</sub>@MOF 1.

**Energy transfer *vs.* electron transfer routes:** The emissive triplet excited state of MOF 1 copper cluster has an energy content of 2.15 eV, value that can be derived from the emission data at 77K.<sup>[10]</sup> An energy-transfer process toward the ferrocene lowest singlet excited state can be excluded by the high energy content of the latter (2.70 eV).<sup>[13]</sup> The lowest triplet excited state of ferrocene can instead come into play; it has been in fact recently reported to lie at 1.16 eV<sup>[14]</sup> compared to *ca.* 1.70 eV of previous assignments.<sup>[13, 20, 24]</sup> Triplet-triplet energy transfer, would be thus strongly exothermic of *ca.* 1.0 eV and spin allowed. This process would probably occur *via* a Dexter type mechanism, although a quantitative discussion on the energy-transfer mechanism is prevented by the lack of data on the absorption profile corresponding to the population of the ferrocene triplet. The occurrence of an electron transfer process leading to the quenching of the emissive excited state of the MOF cluster has also to be considered. In the solid state, at a difference with the solution case, the kinetics and the

thermodynamics of photoinduced electron transfer reactions are less predictable, mainly due to the difficulties in the estimation of the dielectric constant of the medium and in the prediction of its influence on the process.<sup>[25]</sup> Estimation of the energy content of the charge-separated (CS) state can thus be attempted only on the basis of the oxidation and reduction potentials of the donor and the acceptor partners, respectively. In the present case, transfer of an electron from the HOMO of the ferrocene to the partially empty HOMO of the MOF triplet excited state would lead to a CS state characterized by a reduced MOF copper cluster and an oxidised ferrocene unit. The electrochemical data show that FeCp<sub>2</sub> oxidizes easily in FeCp<sub>2</sub>@MOF **1**, at 0.45 V *vs.* SCE (in agreement with literature data),<sup>[15b]</sup> whereas the reduction peak of MOF **1** is not observable in the 0/-0.5 V explored window and this leads to assume a value more negative than -0.5 V for the reduction potential of MOF **1**. The CS energy level can be thus approximately located at a value higher than 0.95 eV, *i.e.* reasonably below the level of the MOF triplet. Both energy transfer and electron transfer can thus contribute to the observed quenching of MOF emission, with a major contribution of the former.

The spectroelectrochemical outcomes evidence that oxidation of the ferrocene inside the MOF produces a sizeable weak recovery of emission. Following the reasoning, the observed recovery can be ascribed to the block of the reductive electron transfer from FeCp<sub>2</sub> to the excited MOF when ferrocene is in its oxidized state. The low value of recovery could be explained considering that: i) the ferrocene units deeply located in the MOF sample are experimentally difficult to oxidize, ii) the energy transfer process, reasonably less affected by the oxidation state of ferrocene, continues to be effective, iii) another quenching mechanism, *i.e.* an oxidative electron transfer from the MOF excited state to the ferrocenium unit, can come into play. The estimated energy of this CS state is, in fact, 0.85 eV (derived from  $E_{\text{ox}(\text{MOF } \mathbf{1})} = 1.30$  V and  $E_{\text{red Fe(III)Cp2+}/\text{Fe(II)Cp2}} = 0.45$  V *vs* SCE): the driving force might render the oxidative electron transfer competitive with the energy transfer process.

## Conclusion

In this paper, the *crystalline device* FeCp<sub>2</sub>@MOF **1** has been prepared and fully characterized. The MOF **1** has been shown to accept ferrocene molecules in the channels as guest molecules in a broad composition range and ferrocene interacts with the MOF structure acting as a luminescence quencher. The emission quantum yield of the MOF can be decreased until a complete switch off as a function of the ferrocene loading. An exhaustive photophysical and electrochemical characterization has been carried out on FeCp<sub>2</sub> loaded MOF **1**. The experimental evidence can be interpreted in terms of both energy and electron transfer processes, with a prevalent contribution from the first. Upon oxidation of the guest the emission can be partially recovered. Importantly, as required for a crystalline device the emission of FeCp<sub>2</sub>@MOF **1** can be

“switched on and off” by applying an *external stimulus*, in our case upon electrochemical oxidation of the embedded ferrocene.

## Experimental Section

**General:** All glassware was dried in an oven set to a temperature of 80 °C for 24 h prior to use. All reagents were purchased from Sigma Aldrich and used without further purification.

**MOF 1:** MOF 1 has been prepared as described in literature.<sup>[10]</sup>

**FeCp<sub>2</sub>@MOF 1:** CuI (0.190 g, 1 mmol) has been dissolved under stirring at 70 °C in a solution of ferrocene in 40 mL of acetonitrile. An acetonitrile solution of DABCO (1.34 g, 1.2 mmol) has been added to the previous one under stirring when all CuI salt has been dissolved. The weight percentage of ferrocene into the MOF is proportionate to the amount of ferrocene dissolved in the solution during the synthesis according to the list in brackets (1.10% = 0.0019 g, 0.01 mmol; 1.90% = 0.009 g, 0.05 mmol; 2.80% = 0.0186 g, 0.10 mmol; 3.30% = 0.0372 g, 0.20 mmol; 3.40% = 0.0930 g, 0.5 mmol, 3.10% = 0.148 g, 0.8 mmol; 3.50% = 0.186 g, 1 mmol). Increasing the amount of FeCp<sub>2</sub> embedded inside the MOF, the powder colour verging turned on yellowy (due to the ferrocene absorption contribution in the 400-500 nm range, see main text).

**AAS:** External standard method has been performed to determine the amount of FeCp<sub>2</sub> trapped into the MOF. The amount of FeCp<sub>2</sub> has been determined by interpolation with the standard line obtained analysing five different standard solutions in HCl 0.5 M with 0.25 ppm, 0.50 ppm, 1.0 ppm, 1.5 ppm, 2.0 ppm and 3.0 ppm of Fe(II) respectively with a Perkin Elmer AAnalyst 400.

**Photophysics:** All determinations made use of powder samples placed inside two quartz slides. Reflectance spectra of solid samples were acquired on a Perkin-Elmer Lambda 9 UV/vis/NIR spectrophotometer equipped with a 60 mm integrating sphere. Each spectrum is the average of 2-3 measurements. Absolute photoluminescence quantum yields were measured according to the method of deMello,<sup>[26]</sup> by using an integrating sphere and an originally developed apparatus.<sup>[27]</sup> The excitation source was composed by a mercury lamp and a band pass interference filter at 334 nm; all measurements were repeated three times. The limit of detection of the system is 2%. Luminescence lifetimes were measured with an IBH 5000F time-correlated single-photon counting apparatus, by using a pulsed NanoLED excitation source at 331 nm. Analysis of the luminescence decay profiles against time was accomplished with the Decay Analysis Software DAS6 provided by the manufacturer, with an estimated error on the lifetimes of 10%. Lifetime measurements have been repeated from three to five times.

**Electrochemistry:** The CV study was carried out on drop-cast films obtained by deposition of 50 µl from an acetonitrile suspension on an optically transparent electrode surfaces (OTE). Electrochemical measurements were carried out with an AUTOLAB

electrochemical station (Ecochemie, Mod. PGSTAT 30). All the electrochemical experiments were carried out in a PTFE cell with a 3 mm diameter aperture and with an O-ring placed on top of the ITO substrate and tightened using two connecting screws. Thin films of the MOF were formed on the working electrodes by applying a drop (~50  $\mu\text{L}$ ) of a 1% (w/v)  $\text{CH}_3\text{CN}$  solution of the MOF to the electrode surface,<sup>[28]</sup> this was allowed to dry in the dark for 12 h, the counter electrode was a platinum spiral and the reference electrode was a SCE electrode.

**Spectroelectrochemistry:** Spectroelectrochemical measurements were performed with a Varian (Cary Eclipse) spectrofluorimeter. Thin films of the MOF were formed as previously described (see electrochemical experimental session). The spectroelectrochemistry measures were carried out in an airtight single-compartment cell described elsewhere,<sup>[29]</sup> using modified ITO as the working, platinum as a counter electrodes and SCE as reference electrode. The potential was set using an AMEL model 552 potentiostat connected to an AMEL model 568 function generator.

### Acknowledgements

This works was supported by University of Bologna and by the CNR Project PM.P04.010 (MACOL).

### References

- [1] from Oxford dictionary.
- [2] A. C. McKinlay, R. E. Morris, P. Horcajada, G. Férey, R. Gref, P. Couvreur, C. Serre, *Angew. Chem. Int. Ed.* **2010**, *49*, 6260-6266.
- [3] P. Horcajada, C. Serre, G. Maurin, N. A. Ramsahye, F. Balas, M. Vallet-Regi, M. Sebban, F. Taulelle, G. Férey, *J. Am. Chem. Soc.* **2008**, *130*, 6774-6780.
- [4] G. Férey, *Chem. Soc. Rev.* **2008**, *37*, 191-214.
- [5] J.-R. Li, R. J. Kuppler, H.-C. Zhou, *Chem. Soc. Rev.* **2009**, *38*, 1477-1504.
- [6] S. Achmann, G. Hagen, J. Kita, I. Malkowsky, C. Kiener, R. Moos, *Sensors* **2009**, *9*, 1574-1589.
- [7] S. Proch, J. Herrmannsdörfer, R. Kempe, C. Kern, A. Jess, L. Seyfarth, J. Senker, *Chem. Eur. J.* **2008**, *14*, 8204-8212.
- [8] a) V. Balzani, A. Credi, M. Venturi, *Molecular Devices and Machines, Concepts and Perspectives for the Nanoworld*, 2nd Edition, Wiley-VCH, Weinheim, **2008**; b) A. Cornia, M. Affronte, A. G. M. Jansen, G. L. Abbati, D. Gatteschi, *Angew. Chem. Int. Ed.* **1999**, *38*, 2264-2266; c) A. Devaux, K. Lutkouskaya, G. Calzaferri, L. Q. Dieu, D. Bruhwiler, L. De Cola, T. Torres, *Chimia* **2007**, *61*, 626-630; d) T. Muraoka, K. Kinbara, T. Aida, *Nature* **2006**, *440*, 512-515.
- [9] a) Y. J. Cui, Y. F. Yue, G. D. Qian, B. L. Chen, *Chem. Rev.* **2012**, *112*, 1126-1162; b) M. D. Allendorf, C. A. Bauer, R. K. Bhakta, R. J. T. Houk, *Chem. Soc. Rev.* **2009**, *38*, 1330-1352.
- [10] D. Braga, L. Maini, P. P. Mazzeo, B. Ventura, *Chem. Eur. J.* **2010**, *16*, 1553-1559.
- [11] a) D. Braga, F. Grepioni, L. Maini, P. P. Mazzeo, B. Ventura, *New J. Chem.* **2011**, *35*, 339-344; b) L. Maini, D. Braga, P. P. Mazzeo, B. Ventura, *Dalton Trans.* **2012**, *41*, 531-539.
- [12] a) P. C. Ford, A. Vogler, *Acc. Chem. Res.* **1993**, *26*, 220-226; b) P. C. Ford, *Coord. Chem. Rev.* **1994**, *132*, 129-140; c) M. Vitale, C. K. Ryu, W. E. Palke, P. C. Ford, *Inorg. Chem.* **1994**, *33*, 561-566; d) C. K. Ryu, K. R. Kyle, P. C. Ford, *Inorg. Chem.* **1991**, *30*, 3982-3986; e) E. Cariati, J. Bourassa, P. C. Ford, *Chem. Commun.* **1998**, 1623-1624; f) P. C. Ford, E. Cariati, J. Bourassa, *Chem. Rev.* **1999**, *99*, 3625-3648.

- [13] S. Fery-Forgues, B. Delavaux-Nicot, *J. Photochem. Photobiol. A: Chem.* **2000**, *132*, 137-159.
- [14] Y. Araki, Y. Yasumura, O. Ito, *J. Phys. Chem. B* **2005**, *109*, 9843-9848.
- [15] a) N. G. Connelly, W. E. Geiger, *Chem. Rev.* **1996**, *96*, 877-910; b) D. Bao, B. Millare, W. Xia, B. G. Steyer, A. A. Gerasimenko, A. Ferreira, A. Contreras, V. I. Vullev, *J. Phys. Chem. A* **2009**, *113*, 1259-1267.
- [16] a) A. S. D. Sandanayaka, H. Sasabe, T. Takata, O. Ito, *J. Photochem. Photobiol. C: Photochem. Rev.* **2010**, *11*, 73-92; b) A. Mateo-Alonso, C. Ehli, G. M. A. Rahman, D. M. Guldi, G. Fioravanti, M. Marcaccio, F. Paolucci, M. Prato, *Angew. Chem. Int. Ed.* **2007**, *46*, 3521-3525; c) T. M. Figueira-Duarte, Y. Rio, A. Listorti, B. Delavaux-Nicot, M. Holler, F. Marchioni, P. Ceroni, N. Armaroli, J.-F. Nierengarten, *New J. Chem.* **2008**, *32*, 54-64.
- [17] a) M. Muller, A. Devaux, C.-H. Yang, L. De Cola, R. A. Fischer, *Photochem. Photobiol. Sci.* **2010**, *9*, 846-853; b) Y. K. Park, S. B. Choi, H. Kim, K. Kim, B.-H. Won, K. Choi, J.-S. Choi, W.-S. Ahn, N. Won, S. Kim, D. H. Jung, S.-H. Choi, G.-H. Kim, S.-S. Cha, Y. H. Jhon, J. K. Yang, J. Kim, *Angew. Chem. Int. Ed.* **2007**, *46*, 8230-8233; c) S. A. Sapchenko, D. G. Samsonenko, D. N. Dybtsev, M. S. Melgunov, V. P. Fedin, *Dalton Trans.* **2011**, *40*, 2196-2203.
- [18] a) A. Credi, *Angew. Chem. Int. Edit.* **2007**, *46*, 5472-5475; b) T. Gunnlaugsson, J. P. Leonard, K. Senechal, A. J. Harte, *J. Am. Chem. Soc.* **2003**, *125*, 12062-12063; c) L. Flamigni, B. Ventura, A. Barbieri, H. Langhals, F. Wetzel, K. Fuchs, A. Walter, *Chem. Eur. J.* **2010**, *16*, 13406-13416; d) N. S. Murray, S. P. Jarvis, T. Gunnlaugsson, *Chem. Commun.* **2009**, 4959-4961; e) H. Dube, M. R. Ams, J. Rebek, *J. Am. Chem. Soc.* **2010**, *132*, 9984-9985.
- [19] C. F. Macrae, I. J. Bruno, J. A. Chisholm, P. R. Edgington, P. McCabe, E. Pidcock, L. Rodriguez-Monge, R. Taylor, J. van de Streek, P. A. Wood, *J. Appl. Crystallogr.* **2008**, *41*, 466-470.
- [20] S. Scuppa, L. Orian, D. Dini, S. Santi, M. Meneghetti, *J. Phys. Chem. A* **2009**, *113*, 9286-9294.
- [21] F. De Angelis, S. Fantacci, A. Sgamellotti, E. Cariati, R. Ugo, P. C. Ford, *Inorg. Chem.* **2006**, *45*, 10576-10584.
- [22] a) M. R. Eftink, *Topics in Fluorescence Spectroscopy Vol. 2: Principles*, Lakowicz, Joseph R. ed., Plenum Press, New York, **1991**; b) J. C. Andre, M. Niclause, W. R. Ware, *Chem. Phys.* **1978**, *28*, 371-377.
- [23] K. F. Babu, M. A. Kulandainathan, I. Katsounaros, L. Rassaei, A. D. Burrows, P. R. Raithby, F. Marken, *Electrochem. Commun.* **2010**, *12*, 632-635.
- [24] W. G. Herkstroeter, *J. Am. Chem. Soc.* **1975**, *97*, 4161-4167.
- [25] A. A. Kornyshev, A. M. Kuznetsov, J. Ulstrup, U. Stimming, *J. Phys. Chem. B* **1997**, *101*, 5917-5935.
- [26] A. Barbieri, G. Accorsi, *EPA Newsletters December 2006*, 26-35.
- [27] C. Aurisicchio, B. Ventura, D. Bonifazi, A. Barbieri, *J. Phys. Chem. C* **2009**, *113*, 17927-17935.
- [28] A. Mateo-Alonso, N. Kulicic, G. Valenti, M. Marcaccio, F. Paolucci, M. Prato, *Chem. Asian J.* **2010**, *5*, 482-485.
- [29] C. Bruno, M. Marcaccio, D. Paolucci, C. Castellarin-Cudia, A. Goldoni, A. V. Streletskaia, T. Drewello, S. Barison, A. Venturini, F. Zerbetto, F. Paolucci, *J. Am. Chem. Soc.* **2008**, *130*, 3788-3796.

# Chapter 3

## Phosphorescence quantum yield enhanced by intermolecular hydrogen bonds in Cu<sub>4</sub>I<sub>4</sub> clusters in the solid state

**Abstract:** Organo-copper(I) halide complexes with a C<sub>4</sub>I<sub>4</sub> cubane core and cyclic amines as ligands have been synthesized and their crystal structures have been defined. Their solid state photophysical properties have been measured and correlated with crystal structure and packing. A unique and remarkably high luminescence quantum yield (76%) has been measured for one of the complexes having the cubane clusters arranged in a columnar structure and hold together by N-H-I hydrogen bonds. This high luminescence quantum yield is correlated with a slow radiationless deactivation rate of the excited state and suggests a rather strong enhancement of the cubane core rigidity bestowed by the hydrogen bonds pattern. Some preliminary thin film deposition experiments show that these compounds could be considered good candidates for applications in electroluminescent devices because of their bright luminescence, low cost and relatively easy synthesis processes



## Introduction

Copper(I) halide complexes constitute a large family of compounds based on a relatively abundant metal element and of relevant photochemical and photophysical interest.<sup>1-11</sup> Relying on their versatile coordination environment these compounds play a unique role in both physical and biological research and application.<sup>3</sup> Recently there has been a surge of interest in studying these complexes, which are currently at the forefront of coordination chemistry and crystal engineering research<sup>12-15</sup> as active material for optoelectronic devices.<sup>16-19</sup>

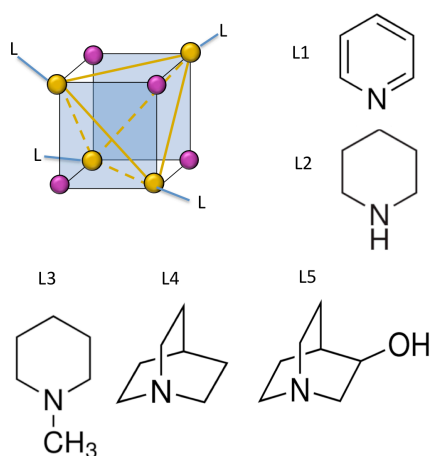
In the past few decades, new concepts for lightning and display applications have been the target of an extensive research<sup>20-22</sup>. Organic Light-Emitting Diodes (OLEDs) are the most promising devices for these tasks, as they can be manufactured with low cost processes and can be purpose-built in thin, flexible and lightweight substrates<sup>23</sup>. Organometallic complexes based on iridium,<sup>24</sup> platinum<sup>25</sup> and osmium<sup>26</sup> are commonly used as materials in OLEDs due to their high emission quantum yield and wavelength tunability while, very recently, copper(I) has appeared in literature as a good candidate to replace such expensive metals for OLEDs.<sup>16, 19, 27</sup>

Whilst the luminescence in solution in halogen-organocopper(I) complexes has been studied for decades,<sup>6, 8</sup> very little work has been done on these complexes in the solid state<sup>19, 27-29</sup>. However, the photophysical properties of the solids could be very different from those in solution due to the molecular organization through the crystals, which can be expected to affect the energies and/or the kinetics of the excited states.<sup>30-32</sup> In this respect, polymorphism, (i.e. the existence of different crystal forms for the same molecular or supramolecular entity), could play a key role in determining the final photophysical properties.<sup>32</sup>

Ford et al. extensively studied the luminescence properties of copper(I) halogen complexes having a Cu<sub>4</sub>X<sub>4</sub> core with cubane -like geometry<sup>6, 33-36</sup> and showed that the luminescence behaviour and environment (solvent or rigid matrix) of the complexes are strictly related.<sup>33</sup> In the case of the cluster Cu<sub>4</sub>I<sub>4</sub>(pyridine)<sub>4</sub>,<sup>4</sup> for example (hereafter **1**), two distinct emission bands were observed in solution, whose high-energy band was attributed to a triplet halide-to-ligand charge transfer (<sup>3</sup>XLCT), while the low-energy emission band was attributed to a triplet Cu-I Cluster-Centred (<sup>3</sup>CC) excited state with the excitation localized to the Cu<sub>4</sub>I<sub>4</sub> core, only possible in the presence of an interaction between the metal centres.<sup>37</sup> The

$^3\text{CC}$  emission band was shown to display a peculiar sensitivity to the temperature and rigidity of the medium.<sup>38</sup>

In this chapter we aim to gain insight into the correlation between photophysics and structure of  $\text{Cu}_4\text{I}_4\text{L}_4$  cubane complexes in which every copper ion binds three iodide atoms and then completes its first coordination sphere with a N-based ligand such as pyridine (L1), piperidine (L2), N-methyl-piperidine (L3), quinuclidine (L4), 3-quinuclidinol (L5) (see scheme 3.1).



Scheme 3.1 | General representation of a  $\text{Cu}_4\text{I}_4\text{L}_4$  cubane cluster; 1=pyridine, 2=piperidine, 3=N-methylpiperidine, 4=quinuclidine, 5=3-quinuclidinol.

Apart from pyridine, we considered only saturated ligands with the aim of excluding photophysical process involving the ligand's  $\pi$  system and determine which parameters affect the cluster-centred characteristics such as basicity, ability to form hydrogen bonds, different groups bonded to the coordinating nitrogen. The different  $\text{pK}_b$  values allow to determine if the emission quantum yield in solid is related to the bond strength between ligands and copper atoms. The substitution of hydrogen with a methyl group on the coordinating nitrogen atom will allow us to verify if the CC excited state radiatioless deactivation due to the N-H bending modes coupling, as hypothesized in solution,<sup>33</sup> can be removed.

Moreover, the ligands show a progressive rigidity and different ability to form H-bonds and consequently allow to investigate how the vibrations involving the ligand  $\sigma$  backbone can influence the photophysical properties of the complexes.

Some preliminary thin film deposition experiments have been carried out in order to envisage applications of these complexes in solid-state optoelectronic devices.

## Results and discussion

Six tetrakis((μ<sub>3</sub>-Iodo)-ligand-copper(I)) cubane complexes have been synthesized: Cu<sub>4</sub>I<sub>4</sub>pyridine<sub>4</sub> (**1**), Cu<sub>4</sub>I<sub>4</sub>piperidine<sub>4</sub> (**2**), Cu<sub>4</sub>I<sub>4</sub>N-methylpiperidine<sub>4</sub> (**3**), Cu<sub>4</sub>I<sub>4</sub>quinuclidine<sub>4</sub> (**4**) and two crystal forms of Cu<sub>4</sub>I<sub>4</sub>(3-quinuclidinol)<sub>4</sub> (**5a** and **5b**). For all complexes, crystal structure and photophysical properties in the solid state have been measured. Complexes **1** and **2** have already been studied and their crystal structure and photophysical data (apart from solid state emission quantum yields) are reported,<sup>4, 33, 38, 39</sup> while **3**, **4**, **5a** and **5b** are here accounted for the first time.

## Synthesis and Crystal Structures

Compounds **1** and **2** were obtained as crystalline powders by following the literature synthesis, **3**, **4**, **5a** and **5b** were obtained by modification of the literature synthesis. Single crystals of **3**, **4**, **5b** were obtained by triple layer crystallization (see experimental part). While no single crystal suitable for SCXR analysis of **5a** could be obtained, its structure has been determined from X-ray powder diffraction data *via* Rietveld refinement of a starting model derived from the single-crystal coordinates of **4** as we found the two structures are isomorphous (see below).

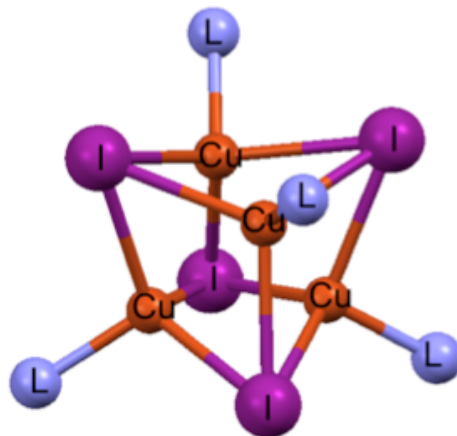


Figure 3.1 | Distorted cubane cluster with nitrogen atoms belonging to the ligand coordinating the copper atoms

The crystal structures of **1–5** are characterized by the presence of distorted cubane clusters (see figure 3.1) and in all compounds the Cu–Cu distances are compatible with metallophilic interactions as, inside the Cu<sub>4</sub>I<sub>4</sub> clusters, they are shorter than two times the van der Waals radius of Cu which has been recently evaluated as 1.92 Å<sup>40, 41</sup> (see table 1). The ligand molecules are located on the vertex of the tetrahedral coordinating copper atoms as sort of blades.

Table 3.1: Interatomic distances in Cu<sub>4</sub>I<sub>4</sub> clusters

	Cu—Cu (Å)	Cu—I (Å)	I—I (Å)
1	2.619(2)	2.630(4)	2.697(4)
	2.684(6)	2.665(3)	4.478(8)
	2.689(3)	2.669(6)	4.488(2)
	2.707(8)	2.670(3)	4.513(2)
	2.719(4)	2.677(5)	4.529(4)
	2.721(1)	2.692(3)	4.594(2)
2	2.595(5)	2.682(3)	4.473(3)
	2.640(1)	2.687(3)	4.584(1)
		2.711(4)	
3	2.868(3)	2.690(1)	4.351(1)
	2.946(2)	2.696(4)	4.480(2)
		2.683(2)	
4	2.671(2) <sup>a</sup>	2.669(2) <sup>a</sup>	4.459(2) <sup>a</sup>
	2.696(3) <sup>a</sup>	2.685(8) <sup>a</sup>	4.493(1) <sup>a</sup>
	2.725(3) <sup>b</sup>	2.695(1) <sup>a</sup>	4.456(1) <sup>b</sup>
		2.682(2) <sup>b</sup>	
5a	2.695(2) <sup>a</sup>	2.692(2) <sup>a</sup>	4.498(1) <sup>a</sup>
	2.720(2) <sup>a</sup>	2.709(3) <sup>a</sup>	4.533(2) <sup>a</sup>
	2.749(3) <sup>b</sup>	2.719(5) <sup>a</sup>	4.496(3) <sup>b</sup>
		2.706(7) <sup>b</sup>	
5b	2.648(3)	2.661(3)	2.696(4)
	2.660(2)	2.679(6)	2.699(6)
	2.662(4)	2.683(3)	2.704(3)
	2.705(4)	2.688(8)	2.715(2)
	2.706(2)	2.689(7)	2.717(4)
	2.745(1)	2.692(2)	2.721(1)
			4.564(2)

<sup>a, b</sup> are referred to crystallographic independent cubane clusters in the structure.

In compound **1**, **2** and **3** the complexes are piled up to form columns, which run parallel to one another. (see figure 3.2). In compound **1** only weak C-H···π interactions are present among the discrete entities, while compound **2** is

characterized by the presence of intermolecular hydrogen bonds. The hydrogen atoms belonging to the nitrogen point to the iodine atoms of an adjacent cluster and form N-H···I interactions. Evidence of the hydrogen bond comes from the alignment of the N-H-I atoms (159°(1)) and the H-I distance (2.935 (3) Å) which is shorter than the sum of the atomic radii (3.16 Å).<sup>42</sup> Since the clusters are piled up, each cubane cluster results to be pinched by eight hydrogen bonds, four in one side and four in the opposite side (see figure 3.2b).

In compound **3** the Cu-Cu distances are about 2.868(3) Å and 2.946(2) Å, slightly longer than the other compounds but it seems not to affect the photophysical properties. As for **2**, in compound **3** the cubane clusters are piled up in columns, but, the tertiary nitrogen atom of the N-methylpiperidine rules out the formation of hydrogen bond interactions among the cubane complexes.

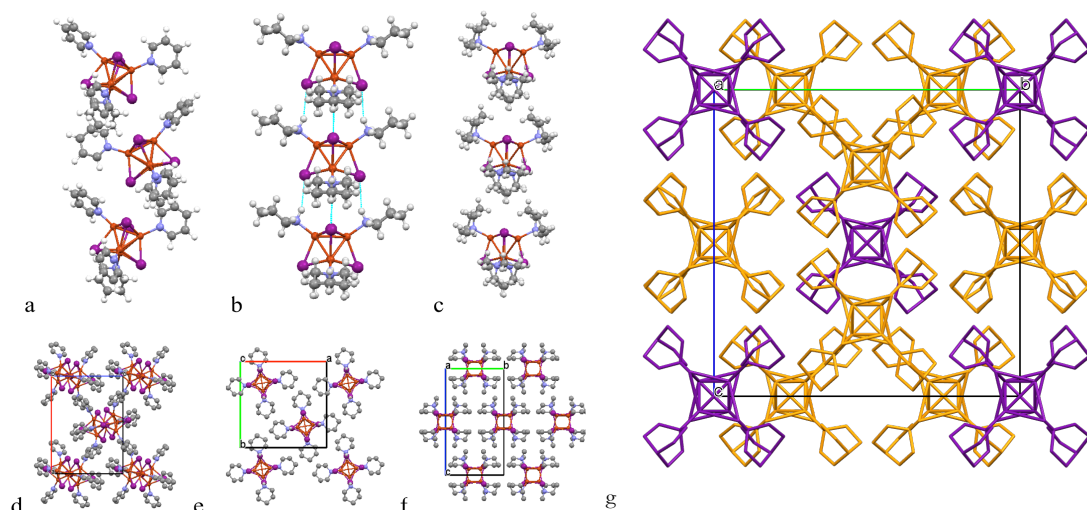


Figure 3.2 | The columns of cubane moieties in compound **1**(a), **2** (b) and **3** (c) and how they pack in the crystal structures **1**(d), **2** (e) and **3** (f). In **2**(b) the N-H···I hydrogen bonds are highlighted in blue. In d, e, f hydrogen atoms are omitted for the sake of clarity. Crystal structure of **4** (g): the two independent cubane moieties are coloured in purple and orange. Hydrogen atoms are omitted.

Compound **4** crystallizes with a cubic lattice and is characterized by two different cubane moieties that are not symmetry related. In the structure one asymmetric cluster occupies the node and the centre of the cell while the second asymmetric

cluster is located on the face. This particular arrangement prevents the formation of columns observed in the previous structures (figure 3.2 a-f).

Two crystal forms **5a** and **5b** have been obtained by reacting CuI with quinuclidinol. Single crystals of **5a** could not be obtained, but its powder X-ray diffraction pattern shows it to be isomorphous with structure **4** (figure 3.3). The unit cell parameter of **5a** was easily refined using the cell parameter of **4** as starting point.

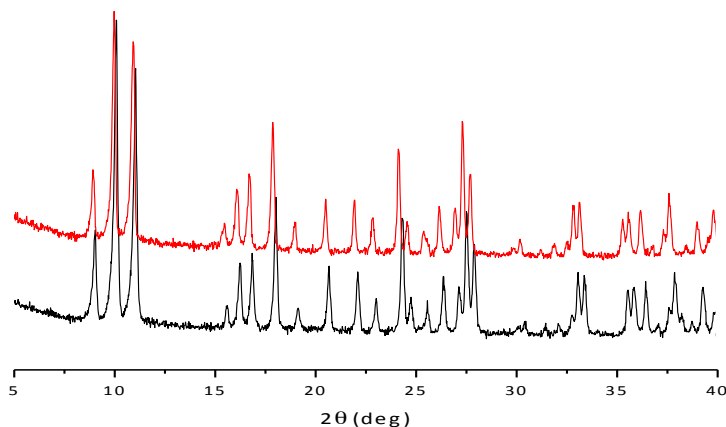


Figure 3.3 | X-ray powder pattern of **5a** (red line) compare with the one of the isomorphic compound **4** (black line)

The structure of **5a** was then solved from the powder data using, as initial coordinates for rigid-body Rietveld refinement, the structure of the compound **4** conveniently modified by changing the H atoms into O-H groups in positions 3, 5 and 8 with respect to N in the quinuclidinol ligand with 1/6 occupancy (because of the rotation along C<sub>3</sub> and of the chirality of the ligand in those positions). The position of the hydroxyl groups results to be disordered and although the hydroxyl groups belonging to different clusters could form hydrogen bonds, a hydrogen bond pattern cannot be identified.

Compound **5b** presents the same complex units as **5a** and in this case, the hydroxyl groups are disordered mainly over two positions. The Cu<sub>4</sub>I<sub>4</sub>L<sub>4</sub> can be described as triangular based pyramids, which are arranged in layers with the parallel bases to form a flat side while the opposite side is characterized by the presence of the vertex of the pyramids. The layers face one another in a complementary way and form curvy monodimensional channels in which disordered solvent molecules are trapped (see figure 3.4). The presence of solvent

molecules in the crystal structure has been confirmed by TGA analysis (see Appendix C).

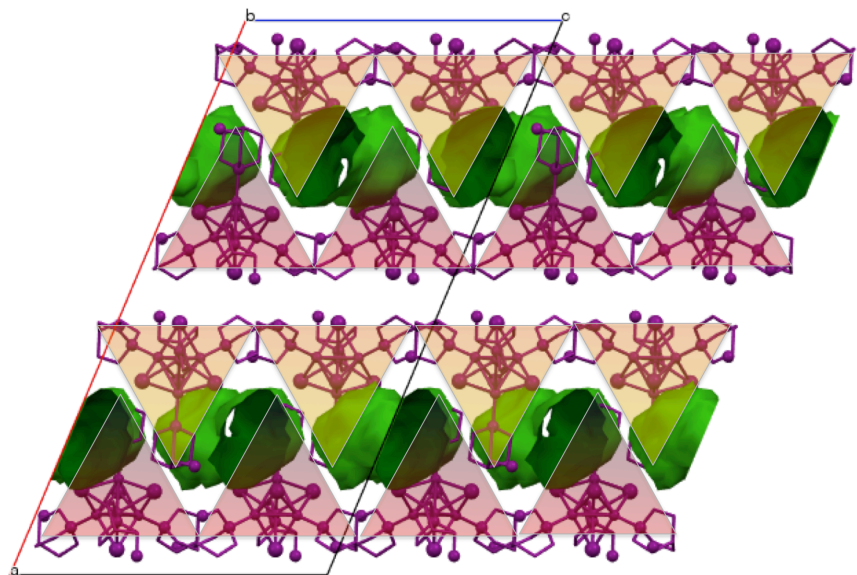


Figure 3.4 | Voids analysis in compound **5b**. Hydrogen atoms are removed for clarity. Curvy monodimensional channels ( $\varnothing$  8.57 Å) are present in the structure along the *b* axis. The cubane moieties are packed along the *bc* plane like pyramidal blocks in complementary sound absorbing panels.

### Conversions

A variable temperature XRPD analysis has been performed on **5b** with *in situ* characterization of the powder. As shown in figure 3.5, on heating up the powder to 100 °C loss of crystallinity is observed due to the release of the disordered solvent molecules trapped into the channels (see Appendix C). At 135°C, peaks of the **5a** phase appear in the diffractogram while the peaks intensities of the **5b** phase decrease. A **5b** to **5a** polymorphic conversion is complete at 150 °C. After cooling down to ambient temperature no recovery of **5b** phase occurs and the phase **5a** remains stable.

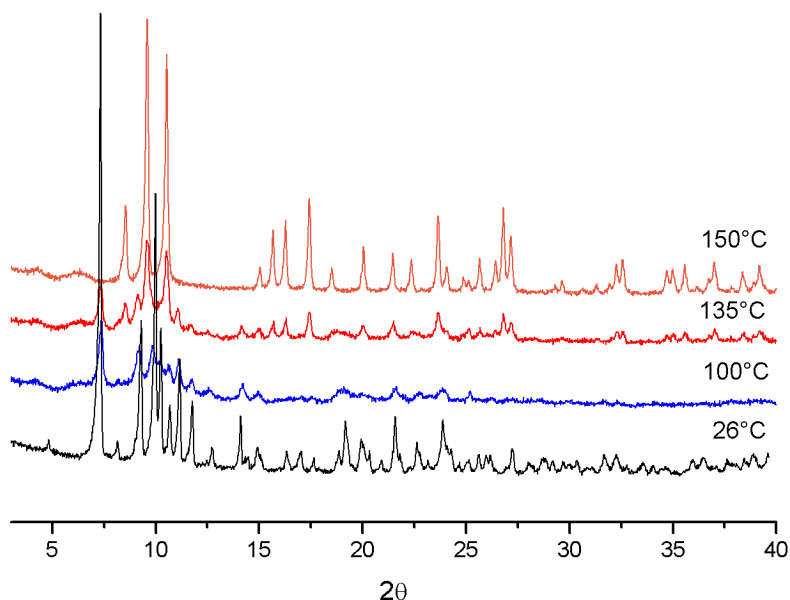


Figure 3.5 | Variable temperature XRPD analysis performed on **5b**, 100 °C: loss of crystallinity due to the solvent release; 135°C: Appearance of peaks of **5a** phase. 150 °C: Complete conversion to form **5a**; Cooling down to rt the phase **5a** remains stable.

### Photophysical properties

All complexes have been characterized by recording excitation and emission spectra and measuring luminescence quantum yields and lifetimes in the solid state. The photophysical data are reported in Table 2. Luminescence behaviour in solution was not investigated since our aim was to evaluate the effect of the crystal structure on the photophysical properties. Moreover, all complexes are poorly soluble and their emission properties are expected to be largely depressed in solution as proved by the big drop of the luminescence quantum yield for **1** and **2** in solution (Table 3.2, in parenthesis, taken from the literature<sup>4</sup>) as a consequence of a big distortion of the excited state respect to the ground state, which is also the reason of the large red shift of the emission band. The fast radiationless deactivation of the excited state in solution, represented by the high value of the decay constant  $k_{nr}$  (Table 3.2), remarkably high for **2**, is associated to an efficient coupling of the ligand vibrations with the electronic transition.<sup>33</sup> Apart from **1**, having an unsaturated ligand whose  $\pi^*$  orbitals are involved in the excitation conferring a  ${}^1\text{XLCT}$  character on the transition, the excitation spectra of all the other complexes are characterized by an envelope of bands extending below 400 nm which are associated with a so-called “cluster centred” ( ${}^1\text{CC}$ )

electronic transitions which goes from HOMOs, localized mainly on the iodide lone pairs, to LUMOs having Cu-Cu bonding and Cu-I antibonding character<sup>37, 43</sup> (figure 3.6). The emission bands have their maxima between 540 nm and 570 nm associated to radiative decay from cluster-centred triplet states (<sup>3</sup>CC) characterized by lifetimes in the 10-15 μs range and highly distorted respect to the ground state geometry as shown by lack of vibrational structure and large Stokes shifts.<sup>37</sup> This picture is consistent with cuprophilic interactions, which are compatible with Cu-Cu distances inside the Cu<sub>4</sub>I<sub>4</sub> clusters shorter than two times the van der Waals radius of Cu which has been recently evaluated as 1.92 Å.<sup>40, 41</sup> Even the rather long Cu-Cu distances in **3** (2.868 Å; 2.946 Å) do not prevent metal-metal interactions and <sup>3</sup>CC emission.

However, although having similar origins, the luminescence transitions occur with different quantum yields for the different compounds. Their values range in the 40-50% for most complexes but a rather higher value for **2** (76%), and somewhat lower value for **5b** (30%) have been measured. The quantum yield is dramatically increased compared to the data reported for **1** and **2** in solution, this behaviour agrees with an increase of the luminescence intensity upon stiffening of the local environment. The quantum yield trend seems to correlate fairly well to the radiationless decay rate constant ( $k_{nr}$ ) which has the lowest value for **2**. Only for this complex the crystalline structure highlights the presence of N-H--I hydrogen bonds between adjacent clusters that assures rigidity to Cu<sub>4</sub>I<sub>4</sub> cubane core preventing vibrations that promote non radiative decay of the excited state. Thus, while **2** in solution has an extremely low quantum yield, it jumps to the highest values as a solid.

The cubane rigidity of this complex has some effect also on the radiative decay constant ( $k_r$ ), which is the highest one, and on the Stokes shift (9500cm<sup>-1</sup>) which is lower than the other clusters values ranging from 10200 to 12400 cm<sup>-1</sup>. Both effects can be correlated to a lower distortion of the excited state respect to the ground state as a direct consequence of N-H--I hydrogen bond which enhances the cubane core stiffness. Accordingly, the more flexible crystal structure of **5b** affects both  $k_r$  and  $k_{nr}$  resulting in a lower luminescence quantum yield. An even lower value has been measured after heating at 80°C and cooling down the complex powder at room temperature (**5b<sup>a</sup>** in Table 1) as the desolvation process goes with a loss of crystallinity. The two isomorphous complexes **5a** and **4** show similar quantum yields and kinetic constants.

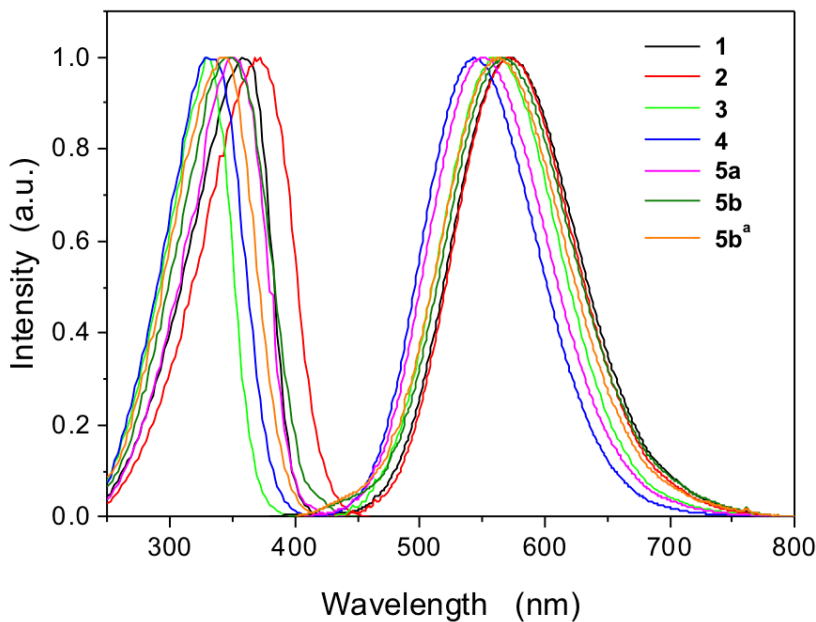


Figure 3.6 | Normalized excitation spectra (250–450 nm, excitation at the emission maximum) and emission spectra (400–800 nm,  $\lambda_{\text{exc}}=350$  nm). All measurements were done on powders at room temperature.

Table 3.2 | Photophysical parameters for compounds **1–5b** as powders at room temperature. In brackets toluene solution data from literature<sup>4</sup>.

	$\lambda_{\text{max}}^{\text{exc}}$ (nm) <sup>b</sup>	$\lambda_{\text{max}}^{\text{em}}$ (nm) <sup>c</sup>	Stokes shift (cm <sup>-1</sup> )	$\Phi$	$\tau$ ( $\mu$ s) <sup>d</sup>	$k_r$ ( $10^4$ s <sup>-1</sup> )	$k_{\text{nr}}$ ( $10^4$ s <sup>-1</sup> )
1	360	570 (690)	10200	0.51 (0.09)	10.5 (10.6)	4.9 (0.8)	4.7 (8.6)
2	370	570 (680)	9500	0.76 (0.0002)	12.3 (0.11)	6.2 (0.2)	2.0 (910)
3	330	560	12400	0.44	10.6	4.2	5.3
4	330	540	11800	0.50	14.2	3.5	3.5
5a	350	550	10400	0.48	14.5	3.3	3.6
5b	350	565	10900	0.30	10.3	2.9	6.8
5b <sup>a</sup>	340	565	11700	0.15	9.8	1.5	8.7

<sup>a</sup> Data related to the compound **5b** once heated at 80 °C and than cooled down to ambient temperature. <sup>b</sup> Excitation maxima, data recorded at maximum emission wavelength. <sup>c</sup> Emission maxima, excitation at 350 nm. <sup>d</sup> Lifetimes, excitation at 331 nm. The kinetic constants  $k_r$  and  $k_{\text{nr}}$  were calculated used the equations  $k_r = \Phi / \tau$  and  $k_{\text{nr}} = (1 - \Phi) /$

### Thin films

Having stated that a solid-vapour reaction occurred when the copper iodide crystalline powder was exposed to the ligand vapours at room temperature, the same reaction was attempted with a CuI thin film. A thin copper iodide layer was deposited on a polished glass slide by high-vacuum sublimation obtaining a polycrystalline, uniform, and smooth layer which showed the characteristic X-ray diffraction (111) peak of the  $\gamma$  phase. Then, the CuI film was exposed to the vapours of the ligand into a closed chamber until complete reaction, as suggested from the absence of any CuI peak in the XRPD analysis (see Appendix C). Our best results have been obtained exposing a 35 nm thick CuI layer to the vapours of quinuclidine and of 3-quinuclidinol at room temperature. The X-ray diffraction analysis directly performed in Bragg-Brentano geometry on these films shows that they are both amorphous. The photoluminescence spectra of both films are in agreement with the emission spectra of the **4** and **5a** powders respectively. A sample obtained by reacting the CuI film with quinuclidine and showing a green luminescence when exposed to UV radiation ( $\lambda=365$  nm) is reported in figure 3.7. When the CuI films were exposed to piperidine and N-methylpiperidine vapours the reaction was too fast due to the higher vapour pressures of these ligands and the samples resulted as blotched and not uniformly emissive layers. More trials are in progress in order to improve the film uniformity by carefully controlling the solid-vapour reaction.

---



Figure 3.7 | Picture of CuI deposited onto silica glass slide after exposition to vapour of quinuclidine under 365 nm UV lamp irradiation.

---

## Experimental Section

### General

All glassware was dried in an oven set to a temperature of 80°C for 24h prior to use. All reagents were purchased from Sigma Aldrich and used without further purification.

### Photophysics

All determinations made use of powder samples placed between two quartz slides and were done at room temperature. Excitation and emission spectra were obtained with a SPEX Fluorolog fluorometer; excitation spectra were monitored at the maximum emission wavelength and emission spectra were recorded exciting all samples at 350nm. Absolute photoluminescence quantum yields were measured according to the method of deMello,<sup>44</sup> by using an integrating sphere customized to fit into the SPEX fluorometer sample compartment. The estimated error on the quantum yield is 10%. Luminescence lifetimes were measured with an IBH 5000F time-correlated single-photon counting apparatus, by using a pulsed NanoLED excitation source at 331 nm. Analysis of the luminescence decay profiles was accomplished with the Decay Analysis Software DAS6 provided by the manufacturer, with an estimated error on the lifetimes of 5%. All decays were monoexponential. The kinetic constants  $k_r$  and  $k_{nr}$  were calculated used the equations  $k_r = \Phi/\tau$  and  $k_{nr} = (1-\Phi)/\tau$ .<sup>45</sup>

### X-Ray powder diffraction

X-Ray powder diffractograms were collected on a Panalytical X’Pert PRO automated diffractometer with CuK $\alpha$  radiation and an X’Celerator equipped with an Anton Paar TTK 450 low-temperature camera. The program Mercury<sup>46</sup> was used for calculation of X-ray powder patterns.

PXRD data of **5a** were collected over the range 3–70° 2θ (2kW; Cu-K $\alpha_1$ , 1.54056 Å step size 0.017 2θ), using a variable count time scheme.<sup>47</sup> The Bruker D8 Advance diffractometer was equipped with a LynxEye detector. The data set was background subtracted and truncated to 50° 2θ for Pawley fitting ( $\chi^2 = 1.9$ ). A scale-only Rietveld refinement against the original data set in the range 4°–65° 2θ to give a good final fit,  $Rwp = 2.89$ .

### Crystal structure determination

Crystal data for **3-4, 5b** were collected on an Oxford Xcalibur S with MoK $\alpha$  radiation,  $\lambda = 0.71073$ , monochromator graphite and equipped with a liquid nitrogen Oxford-Cryostream device. Crystal data and details of measurements are summarized in Table 3. SHELX97<sup>48</sup> was used for the structure solution and refinement based on F<sup>2</sup>. Non-hydrogen atoms were refined anisotropically. The Mercury<sup>46</sup> software package was used for the graphical representation of the resultant structures.

### Synthesis of compound 1

CuI (1 mmol, 0.190g) was dissolved in the minimum amount of a saturated aqueous solution of KI ( $\approx 2\text{mL}$ ). While stirring, pyridine (1.2 mmol, 0.01mL) was added. The product precipitated instantly as a whitish powder that gave yellow emission under UV/Vis radiation. The solid material was recovered by filtration on Buchner funnel and washed with saturated KI aqueous solution and bi-distilled water. Once recovered, the powder has been dried in a desiccator with silica gel.

### Synthesis of compound 2

CuI (1 mmol, 0.190g) was dissolved in the minimum amount of a saturated aqueous solution of KI ( $\approx 2\text{mL}$ ). While stirring, piperidine (1.2 mmol, 0.008 mL) was added. The product precipitated instantly as a whitish powder that gave yellow emission under UV/Vis radiation. The solid material was recovered by filtration on Buchner funnel and washed with saturated KI aqueous solution and bi-distilled water. Once recovered, the powder has been dried in a desiccator with silica gel.

### Synthesis of compound 3

CuI (5 mmol, 0.950 g) were added as solid into a flask were previously have been posed 2 ml of methyl-piperidine. 3 days after, during which the suspension have been taken under stirring at room temperature, the product has been filtered on Buchner funnel and washed with an aqueous saturated solution of KI and bi-distilled cold water. Once recovered, the powder, that gave green emission under UV/Vis radiation, has been dried in a desiccator with silica gel. The titled compound has also been obtained after 10 minute of grinding in an agate mortar 0.190 g of CuI (1mmol) with few drops of methyl-piperidine. As the ligand is

liquid and volatile at rt, the title compound has been obtained also via exposition of CuI to vapour of methyl-piperidine after 2 days. Single crystals were obtained by a three-layer crystallization: the lower layer was CuI dissolved in saturated aqueous solution of KI; the middle layer was pure ethanol and the top layer was a solution of methyl-piperidine in acetone. Crystals appeared after 5–7 days and were chosen with the help of UV lamp.

### Synthesis of compound 4

CuI (0.095 g, 0.5 mmol) was dissolved in the minimum amount of a saturated aqueous solution of KI ( $\approx$  2mL). While stirring, a solution of quinuclidine (0.068 g, 0.6 mmol) in ethanol (1 mL) was added. The product precipitated instantly as a whitish powder with green emission under UV/Vis radiation. The solid material was recovered by filtration on Buchner funnel and washed with saturated KI aqueous solution and bi-distilled water. Once recovered, the powder has been dried in a desiccator with silica gel.

Single crystals were obtained by a three-layer crystallization: the lower layer was CuI dissolved in saturated aqueous solution of KI; the middle layer was pure ethanol and the top layer was a solution of quinuclidine in n-hexane

### Synthesis of compound 5a

Racemic 3-quinuclidinol (0.127 g, 1.2 mmol) was dissolved in methanol (1mL) at 80°C and was added, under stirring, to a saturated KI aqueous solution of CuI (0.190 g, 1 mmol) at 80°C. The product precipitated as a fine white powder, with green emission under UV/Vis radiation; The solid material was recovered by filtration with Buchner funnel and washed with saturated KI aqueous solution and bi-distilled water. Once recovered, the powder was dried in a desiccator with silica gel.

### Synthesis of compound 5b

CuI (1 mmol, 0.190 g) were added as solid into a flask filled with a solution of racemic 3-quinuclidinol (1 mmol, 0.127 g) in methanol (4 mL). 24 hours later the product was filtered on Buchner funnel and washed with an aqueous saturated solution of KI and bi-distilled cold water. Once recovered, the powder was dried in a desiccator with silica gel. The titled compound was also obtain after several hours of grinding in a ball milling a 1:1 physical mixture of the reagents with a catalytic amount of ethanol. Single crystals were obtained by a three-layer crystallization: the lower layer was CuI dissolved in saturated aqueous solution of

KI; the middle layer was pure ethanol and the top layer was a solution of 3-quinuclidinol in water. Crystals appeared after 5–7 days and were chosen with the help of UV lamp.

### Conclusions

Two known (**1** and **2**) and four new (**3**, **4**, **5a** and **5b**) tetrakis((μ<sub>3</sub>-iodo)-ligand-copper(I)) cubane complexes have been synthesized as crystalline powders and their photophysical properties have been measured. The crystal structures of **3**, **4**, **5b** have been determined by single crystal X-ray diffraction while **5a** was solved from the powder data.

All complexes show a cubane Cu<sub>4</sub>I<sub>4</sub> core and are luminescent due to radiative decay of a cluster centred <sup>3</sup>CC emitting state. Quantum yields are in the range of 40–50% for all complexes apart from a slightly lower 30% for **5b** and a significantly higher value of 76% for **2**, which, to the best of the authors' knowledge, has never been demonstrated previously for cubane complexes. No significant interactions between the constituting moieties are observed in the crystal structures of the complexes except for compound **2** where the clusters are held together by hydrogen bonds in pillars. It results that each cluster is involved in eight hydrogen bonds, and clusters are aligned along the c axis to build a stiff columnar structure. We think that these interactions make the cluster extremely rigid and allow to get a very high luminescence quantum yield. On the other side, the less rigid structure of **5b** results in the lowest quantum yield (30%). Desolvation of **5b** leads to loss of crystallinity which goes together with an even more reduced quantum yield (15%).

Some preliminary attempts to obtain thin films of the pure complexes have been performed by using solid-vapour reactions and some uniformly luminescent samples have been obtained. These results may be a first indication of the possibility of an application of these complexes as emissive layers in electroluminescent devices as they do not suffer from concentration quenching and have emissive triplet excited states which are compliant with the “triplet harvesting” frame for high efficiency OLEDs.

### Acknowledgements

We thank MIUR, the University of Bologna and CNR for financial support to this research. PPM thanks the University of Bologna for the Marco Polo fellowship for supporting his visiting period at Reading University.

Table 3.3 | Crystallographic data of compound 1-5.

	<b>1<sup>a</sup></b>	<b>2<sup>b</sup></b>	<b>3</b>	<b>4</b>	<b>5a<sup>[a]</sup></b>	<b>5b</b>
Empirical formula	C <sub>20</sub> H <sub>20</sub> Cu <sub>4</sub> I <sub>4</sub> N <sub>4</sub>	C <sub>20</sub> H <sub>44</sub> Cu <sub>4</sub> I <sub>4</sub> N <sub>4</sub>	C <sub>24</sub> H <sub>56</sub> Cu <sub>4</sub> I <sub>4</sub> N <sub>4</sub>	C <sub>28</sub> H <sub>52</sub> Cu <sub>4</sub> I <sub>4</sub> N <sub>4</sub>	C <sub>28</sub> H <sub>48</sub> Cu <sub>4</sub> I <sub>4</sub> N <sub>4</sub> O <sub>4</sub>	C <sub>28</sub> H <sub>48</sub> Cu <sub>4</sub> I <sub>4</sub> N <sub>4</sub> O <sub>4</sub>
Formula weight	1098.4	1102.39	1162.49	1206.50	1266.46	1266.46
Temperature	293(2) K	293(2) K				
Wavelength	0.71073	0.71073	0.71073	0.71073	1.54056	0.71073
Crystal system	Orthorombic	Tetragonal	Tetragonal	Cubic	Cubic	Monoclinic
Space group	P2 <sub>1</sub> 2 <sub>1</sub> 2 <sub>1</sub>	P4 <sub>2</sub> /n	I-42m	P-43n	P-43n	C 2/c
	a = 16.032(6)	a = 14.589(1)	a = 9.9963(7)	a = 19.7281(6)	a = 19.9032(4)	a = 37.444(4)
	b = 15.510(2)	b = 14.589(1)	b = 9.9963(7)	b = 19.7281(6)	b = 19.9032(4)	b = 12.2662(8)
Unit cell dimensions	c = 11.756(3)	c = 7.538(1)	c = 18.114(2)	c = 19.7281(6)	c = 19.9032(4)	c = 19.9994(19)
	b = 90	b = 113.379(12)				
Volume	2923.2	1604.7	1810.1(3)	7678.1(4)	7884.4 (1)	8431.6(13)
Z	2	2	2	8	8	8

<sup>[a]</sup> data obtained from Rietveld refinement on powder diffraction pattern.

## References

1. F. G. Mann, D. Purdie and A. F. Wells, *J. Chem. Soc.*, 1936, 447-460.
2. G. Tartarini, *Gazz. Chim. Ital.*, 1933, **63**, 597-600.
3. N. Armaroli, G. Accorsi, F. Cardinali and A. Listorti, in *Photochemistry and Photophysics of Coordination Compounds I*, eds. V. Balzani and S. Campagna, Springer-Verlag Berlin, Berlin, 2007, vol. 280, pp. 69-115.
4. K. R. Kyle, C. K. Ryu, P. C. Ford and J. A. DiBenedetto, *J. Am. Chem. Soc.*, 1991, **113**, 2954-2965.
5. P. C. Ford and A. Vogler, *Acc. Chem. Res.*, 1993, **26**, 220-226.
6. P. C. Ford, *Coord. Chem. Rev.*, 1994, **132**, 129-140.
7. H. D. Hardt and A. Pierre, *Inorg. Chim.*, 1977, **25**, L59-L60.
8. H. D. Hardt, H. Gechnizdjan and A. Pierre, *Naturwissenschaften* 1972, **59**, 363.
9. H. D. De Ahna and H. D. Hardt, *Z. Anorg. Allg. Chem.*, 1972, **387**, 61-71.
10. P. C. Ford, E. Cariati and J. Bourassa, *Chem. Rev.*, 1999, **99**, 3625-3648.
11. H. D. Hardt and A. Pierre, *Naturwissenschaften* 1975, **62**, 298.
12. P. P. Mazzeo, L. Maini, D. Braga, G. Valenti, F. Paolucci, M. Marcaccio, A. Barbieri and B. Ventura, *Eur. J. Inorg. Chem.*, 2013, **2013**, 4459-4465.
13. C. H. Arnby, S. Jagner and I. Dance, *CrystEngComm*, 2004, **6**, 257-275.
14. R. Peng, S. R. Deng, M. Li, D. Li and Z. Y. Li, *CrystEngComm*, 2008, **10**, 590-597.
15. S. Q. Bai, J. Y. Kwang, L. L. Koh, D. J. Young and T. S. A. Hor, *Dalton Trans.*, 2010, **39**, 2631-2636.
16. Z. Liu, M. F. Qayyum, C. Wu, M. T. Whited, P. I. Djurovich, K. O. Hodgson, B. Hedman, E. I. Solomon and M. E. Thompson, *J. Am. Chem. Soc.*, 2011, **133**, 3700-3703.
17. Z. Liu, P. I. Djurovich, M. T. Whited and M. E. Thompson, *Inorg. Chem.*, 2011, **51**, 230-236.
18. S. Perruchas, X. F. L. Goff, S. Maron, I. Maurin, F. o. Guillen, A. Garcia, T. Gacoin and J.-P. Boilot, *J. Am. Chem. Soc.*, 2010, **132**, 10967-10969.
19. D. Volz, D. M. Zink, T. Bocksrocker, J. Friedrichs, M. Nieger, T. Baumann, U. Lemmer and S. Bräse, *Chem. Mater.*, 2013, **25**, 3414-3426.
20. N. Thejo Kalyani and S. J. Dhoble, *Renew. Sust. Energ. Rev.*, 2012, **16**, 2696-2723.
21. Y.-L. Chang, Y. Song, Z. Wang, M. G. Helander, J. Qiu, L. Chai, Z. Liu, G. D. Scholes and Z. Lu, *Adv. Funct. Mater.*, 2013, **23**, 705-712.
22. M. C. Gather, A. Köhnen and K. Meerholz, *Adv. Mater.*, 2011, **23**, 233-248.
23. M. Dong and L. Zhong, *IEEE Trans. Mobile Comput.*, 2012, **11**, 1587-1599.
24. J. C. Jeong, H. S. Kim and J. G. Jang, *Mol. Cryst. Liq. Cryst.*, 2010, **530**, 259-265.
25. P. Brulatti, V. Fattori, S. Muzzioli, S. Stagni, P. P. Mazzeo, D. Braga, L. Maini, S. Milita and M. Cocchi, *J. Mater. Chem. C*, 2013, **1**, 1823-1831.
26. Y.-L. Tung, P.-C. Wu, C.-S. Liu, Y. Chi, J.-K. Yu, Y.-H. Hu, P.-T. Chou, S.-M. Peng, G.-H. Lee, Y. Tao, A. J. Carty, C.-F. Shu and F.-I. Wu, *Organometallics*, 2004, **23**, 3745-3748.
27. D. Volz, M. Nieger, J. Friedrichs, T. Baumann and S. Bräse, *Langmuir*, 2013.
28. D. M. Zink, M. Bachle, T. Baumann, M. Nieger, M. Kuhn, C. Wang, W. Klopper, U. Monkowius, T. Hofbeck, H. Yersin and S. Bräse, *Inorg. Chem.*, 2012, **52**, 2292-2305.
29. J. P. Safko, J. E. Kuperstock, S. M. McCullough, A. M. Noviello, X. Li, J. P. Killarney, C. Murphy, H. H. Patterson, C. A. Bayse and R. D. Pike, *Dalton Trans.*, 2012, **41**, 11663-11674.
30. D. Braga, F. Grepioni, L. Maini, P. P. Mazzeo and B. Ventura, *New J. Chem.*, 2011, **35**, 339-344.
31. D. Braga, L. Maini, P. P. Mazzeo and B. Ventura, *Chem. Eur. J.*, 2010, **16**, 1553-1559.
32. L. Maini, D. Braga, P. P. Mazzeo and B. Ventura, *Dalton Trans.*, 2012, **41**, 531-539.
33. M. Vitale and P. C. Ford, *Coord. Chem. Rev.*, 2001, **219-221**, 3-16.
34. M. Vitale, W. E. Palke and P. C. Ford, *J. Phys. Chem.*, 1992, **96**, 8329-8336.
35. C. K. Ryu, M. Vitale and P. C. Ford, *Inorg. Chem.*, 1993, **32**, 869-874.
36. C. K. Ryu, K. R. Kyle and P. C. Ford, *Inorg. Chem.*, 1991, **30**, 3982-3986.
37. F. De Angelis, S. Fantacci, A. Sgamellotti, E. Cariati, R. Ugo and P. C. Ford, *Inorg. Chem.*, 2006, **45**, 10576-10584.
38. D. Tran, J. L. Bourassa and P. C. Ford, *Inorg. Chem.*, 1997, **36**, 439-442.
39. A. Dossing, C. K. Ryu, S. Kudo and P. C. Ford, *J. Am. Chem. Soc.*, 1993, **115**, 5132-5137.
40. S. S. Batsanov, *Inorg. Mater.*, 2001, **37**, 871-885.
41. S. Nag, K. Banerjee and D. Datta, *New J. Chem.*, 2007, **31**, 832-834.
42. L. Brammer, E. A. Bruton and P. Sherwood, *Cryst. Growth Des.*, 2001, **1**, 277-290.
43. A. Vega and J.-Y. Saillard, *Inorg. Chem.*, 2004, **43**, 4012-4018.
44. A. Barbieri and G. Accorsi, *EPA Newsletters*, December 2006, 26-35.

45. J. R. Lakowicz], *Principle of fluorescence Spectroscopy*, 3rd edn., Springer, New York, 2006.
46. C. F. Macrae, I. J. Bruno, J. A. Chisholm, P. R. Edgington, P. McCabe, E. Pidcock, L. Rodriguez-Monge, R. Taylor, J. van de Streek and P. A. Wood, *J. Appl. Crystallogr.*, 2008, **41**, 466-470.
47. K. Shankland, W. I. F. David and D. S. Sivia, *J. Mater. Chem.*, 1997, **7**, 569-572.
48. G. M. Sheldrick, *SHELXL97*, 1997, University of Göttingen, Germany.
49. C. L. Raston and A. H. White, *J. Chem. Soc., Dalton Trans.*, 1976, **0**, 2153-2156.
50. V. Schramm, *Inorg. Chem.*, 1978, **17**, 714-718.

# Chapter 4

## Mechanochemical preparation of Copper Iodide clusters of interest for luminescent devices

**Abstract:** The copper iodide complexes are known for their large variety of coordination geometries. Such diversity while making difficult to predict the final structure, permits the preparation of a great number of copper iodide complexes based on the same ligand. The target of the research was that of thoroughly exploring the chemistry of CuI and the ligand diphenyl-2-pyridyl phosphine PN by varying the stoichiometry ratio and/or the aggregation state. Six different compounds have been identified:  $[\text{Cu}_4\text{I}_4(\text{PN})_2]$ ,  $[\text{Cu}_4\text{I}_4(\text{PN})_2 \cdot (\text{CH}_3\text{CN})]$ ,  $[\text{CuI}(\text{PN})_{0.5}]_\infty$ ,  $[\text{CuI}(\text{PN})_3]$  whose structures have been determined during this study,  $\text{CuI}(\text{PN})_2$  which was characterized by powder diffraction and  $[\text{Cu}_2\text{I}_2(\text{PN})_3]$  which had been already reported. The preparation routes are also different: synthesis in solution yielded  $[\text{Cu}_4\text{I}_4(\text{PN})_2 \cdot (\text{CH}_3\text{CN})]$  and  $[\text{CuI}(\text{PN})_3]$  while  $[\text{CuI}(\text{PN})_{0.5}]_\infty$  and  $\text{CuI}(\text{PN})_2$  were obtained only via solid state reactions. These two latter examples confirmed that mechanochemistry is a valid route to explore the landscape of the possible structures of CuI derivatives. Crystallization by traditional solution procedures failed to give the desired crystal so structure determination of the new compounds was tackled in two ways: by attempting crystal growth *via* solvothermal synthesis and by resolving the structure from X-ray powder diffraction data with “direct space” methods. What is more the photophysical properties of the complexes that could be obtained as sufficiently pure powders, have also been investigated and are herein reported.



## Introduction

The complexes based on Copper Iodide are currently at the forefront of coordination chemistry and crystal engineering research because of the quest of active materials for optoelectronic.<sup>1-8</sup> The interest stems from the increasing demand of more affordable complexes in preference to luminescent metal complexes based on precious (i.e. Platinum group) and rare earth metals, which are often quite expensive and environmentally problematic.<sup>9</sup> The copper iodide complexes present several advantages: they are characterized by a large variety of coordination geometries which arise from the many possible combinations of coordination numbers (two, three and four) available for copper(I) and geometries that can be adopted by the halide ions (from terminal to  $\mu^2$ - and up to  $\mu^8$ -bridging);<sup>10</sup> they present different luminescent levels which can be of ligand centred, charge transfer or, in the case of polynuclear compounds, even metal-centred nature;<sup>11,12</sup> most of the complexes studied are characterized by a remarkable high quantum yield in solid state;<sup>4, 13, 14</sup> and finally the reagents are cheap and it is relatively easy to obtain the final products.<sup>4, 15</sup>

The luminescent properties of copper(I) halide clusters are strictly related to the geometries adopted by the clusters.<sup>12</sup> In the case of the cubanes Cu<sub>4</sub>I<sub>4</sub>L<sub>4</sub> for example, two distinct emission bands were observed, the high-energy band attributed to halide-to-ligand charge transfer (<sup>3</sup>XLCT), and the low-energy emission band was attributed to a triplet Cu-I Cluster-Centered (<sup>3</sup>CC) excited state with the excitation localized to the Cu<sub>4</sub>I<sub>4</sub> core, only possible in the presence of an interaction between the metal centres. Recent studies have widened the possibility of the emission properties of Copper(I) compounds. Several Cu(I) compounds with P<sup>N</sup>N ligands present a low singlet-triplet splitting which allows the emission from both the singlet and the triplet excited state depending on the temperature. The singlet excited state, which is slightly higher in energy than the triplet state, can be thermally activated at the expense of the triplet state, leading to the so-called thermally activated delayed fluorescence (TADF). The TADF emission mechanism allows harvesting of both singlet and triplet excited states generated by charge recombination in electroluminescent devices, therefore light generation efficiency is enhanced.<sup>13, 16</sup>

Due to the increasing interested on CuI(P<sup>N</sup>N ligands) complexes for OLED application and for photochemistry studies,<sup>3, 13, 15, 17</sup> we exploited the reactivity of the CuI towards diphenyl-2-pyridyl phosphine, hereafter PN. Two crucial aspects of the research will be presented: we will first discuss how the synthetic procedure influences the formation of the final product with particular attention to the mechanochemical synthesis; secondly we will address the different strategies to determine the crystal structure when the final product is a crystalline powder.

The crystal engineering of copper halides is particularly difficult since in solution,

halocuprate complexes are involved in kinetically fast dissociative and associative equilibria<sup>18, 19</sup> and the labile coordination numbers and geometries of both copper(I) and halide ions allows an inner-core variability difficult to predict. These complexes are characterized by a flat energy landscape confirmed by the presence of several different copper halides complexes in the CSD<sup>20</sup> which present dramatically different nuclearity of the Cu<sub>x</sub>I<sub>y</sub> cores such as discrete dimers, cubane tetramers, stepped cubane tetramers to infinity polymeric chains (including split stairs, zigzag, helical, staircase, rack and columnar ones). Although the final structures of the copper(I) halide complexes in crystals could be hardly designed, the reaction stoichiometry allows some degree of control of the copper(I) halide core: reactions with a stoichiometry ratio of CuI/L >>1 higher nuclearity are favoured while CuI/L <<1 promote the formation of monomers.<sup>21</sup> However, to explore all the possible crystal forms it is necessary to vary not only the stoichiometry but also other parameters such as solvent, temperature etc.. To overcome the problem of the low solubility of the CuI which restricts the possibility of changing the solvent, the reactions can be performed in solid state which can yield to crystal forms hardly or even not obtainable in solution.<sup>22</sup> The reactivity of CuI towards nitrogen, sulphur or phosphorous based ligands is very high and preliminary work of mechanochemical synthesis with CuI with N-base sature ligands are reported<sup>23, 24</sup> and more extensive studies have been done for Copper thyocyanate complexes,<sup>25-27</sup> in both cases mechanochemical synthesis led to the formation of compounds not obtained by solution synthesis.

The main drawbacks in the mechanochemical reaction methods consist in the formation of microcrystalline products, obviously unsuitable for X-ray single crystal diffraction. The structural characterization is a key point to understand the properties and to design new compounds, that is why a great effort will be devoted to tackle this problem. Most of the times traditional crystallizations from solution, but also triple layer crystallizations, or seeding of solutions with microcrystalline powder of the desired compound fail to yield single crystals of amenable size for single crystal diffraction experiments. However, the structure can be determined from X-ray powder diffraction data, thanks to the development of “direct space” methods.<sup>28</sup> This approach is particularly suited for materials constructed from well-defined modular building units and it is more challenging for Copper Iodide complexes whose coordination is difficult to control. Spectroscopy techniques such as IR or Solid State NMR can give some insights on the coordination or on the asymmetric units but not guarantee the exact structure determination.<sup>26, 29</sup>

The quest of suitable methods to obtain crystals for structure determination of Copper complexes led us to explore different crystallization processes including those based on solvothermal synthesis. Recently, several zeolites, commonly obtained by solvothermal synthesis, have been produced also by grinding or ball milling,<sup>30-33</sup> which suggests that the solid state reactions can have several aspects in

common with the solvothermal conditions.<sup>25</sup> Although, for large scale preparations, nowadays researches try to move from solvothermal to solvent-free reactions in order to reduce environmental impact and energy consumption, solvothermal synthesis can still be exploited to obtain single crystals of the desired compound since the high-temperature and high-pressure environments conditions created, would facilitate the crystallization process of complexes with poor solubility.

Herein we report the synthesis of five new crystal forms of copper iodide with the diphenyl-2-pyridyl phosphine (PN):  $[\text{Cu}_4\text{I}_4(\text{PN})_2]$ ,  $[\text{Cu}_4\text{I}_4(\text{PN})_2 \cdot (\text{CH}_3\text{CN})]$ ,  $[\text{CuI}(\text{PN})_{0.5}]_\infty$ ,  $[\text{CuI}(\text{PN})_3]$  and  $\text{CuI}(\text{PN})_2$ ; as well as that of the known complex  $[\text{Cu}_2\text{I}_2(\text{PN})_3]$ .<sup>14</sup> Mechanochemical synthesis was decisive to obtain the new compounds  $[\text{CuI}(\text{PN})_{0.5}]_\infty$  and  $\text{CuI}(\text{PN})_2$  while the monomer  $[\text{CuI}(\text{PN})_3]$  is formed only by precipitation from solution. Not only the stoichiometry variation but also performing the reaction in solid state or solution allowed us to widen the landscape of crystal forms of copper iodide complexes with PN. The structures of  $[\text{Cu}_4\text{I}_4(\text{PN})_2]$  and  $[\text{CuI}(\text{PN})_{0.5}]_\infty$  have been determined by single crystals obtained from solvothermal synthesis, while the bulk product has been obtained by reaction in solid state or solution. The structure of  $[\text{CuI}(\text{PN})_3]$  was determined by direct methods from X-ray powder diffraction data.

All the compounds obtained are luminescent and the photophysical properties of the complexes that could be obtained as sufficiently pure powders, have been studied and reported.

## Experimentals

### General

All reagents were purchased from Sigma Aldrich and used without further purification.

### Synthesis of $[\text{Cu}_2\text{I}_2(\text{PN})_3]$

Copper(I) iodide (0.380 g; 2 mmol) and the PN ligand (0.789 g; 3 mmol) were suspended under nitrogen atmosphere in dry dichloromethane (10 mL) and stirred for 12 h at room temperature. The yellowish powder obtained was filtered and washed with a saturated solution of  $\text{KI}_{\text{aq}}$  to remove the unreacted CuI and distilled water to remove KI. The same titled compound was obtained by grinding CuI (0.190 g; 1 mmol) and PN (0.394 g; 1.5 mmol) with two drops of acetonitrile in a ball mill for 30 minutes at 20 Hz.

### Synthesis of $[\text{CuI}(\text{PN})_3]$

Copper iodide (0.095 g, 0.5 mmol) was dissolved in saturated aqueous solution of KI (5 mL) then an acetone solution of PN (0,526 g, 2 mmol) was added under stirring. A whitish powder precipitates instantly which was filtered and washed with cold acetone.

### Synthesis of $[\text{CuI}(\text{PN})_2]$

Copper iodide (0.190 g ; 1mmol) and PN ligand (1.052 g; 4 mmol) were ground two drops of AcCN in a ball mill for 60 minutes at 20Hz.

### Synthesis of $[\text{Cu}_4\text{I}_4(\text{PN})_2 \cdot (\text{CH}_3\text{CN})]$

$\text{CuI}$  (0.760 g; 4 mmol) dissolved in 20 mL of  $\text{CH}_3\text{CN}$  at 40°C was added to a solution of PN (0.263 g; 1mmol) in 20 mL of  $\text{CH}_2\text{Cl}_2$ . The clear solution obtained was left standing at room temperature overnight. The brownish powder obtained was filtered and then washed with aqueous saturated solution of  $\text{KI}_{\text{aq}}$  to remove the unreacted  $\text{CuI}$  and with distilled water to remove the  $\text{KI}$ . Ball milling of  $\text{CuI}$  (0.760 g; 4 mmol) and PN (0.263 g; 1 mmol) with two drops of acetonitrile for 60 minutes at 20 Hz leaded to mixture of  $[\text{Cu}_4\text{I}_4(\text{PN})_2 \cdot (\text{CH}_3\text{CN})]$  and  $[\text{CuI}(\text{PN})_{0.5}]_\infty$ .

### Synthesis of $[\text{Cu}_4\text{I}_4(\text{PN})_2]$

$[\text{Cu}_4\text{I}_4(\text{PN})_2]$  can be easily obtained by heating  $[\text{Cu}_4\text{I}_4(\text{PN})_2 \cdot (\text{CH}_3\text{CN})]$  at 170°C.

### Crystallization of $[\text{Cu}_4\text{I}_4(\text{PN})_2]$ and $[\text{CuI}(\text{PN})_{0.5}]_\infty$

Crystals of  $[\text{Cu}_4\text{I}_4(\text{PN})_2]$  suitable for SC-XRD analysis were obtained via solvothermal reaction by mixing 0.2 g of  $\text{CuI}$  with 0.8 g of PN in 1 mL of ethanol at 170°C and slowly cooling down to ambient temperature in 7 days.

Crystals of  $[\text{CuI}(\text{PN})_{0.5}]_\infty$  suitable for SC-XRD were obtained via solvothermal conditions by mixing 0.2 g of  $\text{CuI}$  with 0.6 g of PN in 1 mL of toluene at 140°C and slowly cooling down to ambient temperature in 7 days.

### TGA measurements

TGA measurements were performed using a Perkin Elmer TGA7 in the temperature range 35-700°C under  $\text{N}_2$  gas flow and heating was carried out at 5°C min<sup>-1</sup>.

### Photophysics

All determinations made use of powder samples placed between two quartz slides and were done at room temperature. Excitation and emission spectra were obtained with a SPEX Fluorolog fluorometer; excitation spectra were monitored at the maximum emission wavelength and emission spectra were recorded exciting all samples at 350nm.

### X-Ray powder diffraction

X-Ray powder diffractograms were collected on a Panalytical X'Pert PRO automated diffractometer with  $\text{CuK}\alpha$  radiation and an X'Celerator equipped with an Anton Paar TTK 450 low-temperature camera. The program Mercury<sup>34</sup> was used for calculation of X-ray powder patterns. XRPD data of  $[\text{CuI}(\text{PN})_3]$  were collected over the range 3–70° 2θ with a Bruker D8 Advance diffractometer equipped with a LynxEye detector and focusing mirror.

### Crystal structure determination

Crystal data for  $[\text{Cu}_4\text{I}_4(\text{PN})_2]$  and  $[\text{CuI}(\text{PN})_{0.5}]_\infty$  were collected on an Oxford Xcalibur S with MoK $\alpha$  radiation,  $\lambda = 0.71073$ , monochromator graphite. Crystal data and details of measurements are summarized in Table 1. SHELX97<sup>35</sup> was used for the structure solution and refinement based on  $F^2$ . Non-hydrogen atoms were refined anisotropically. The uniqueness of the crystal of  $[\text{CuI}(\text{PN})_{0.5}]_\infty$ , synthesized by solvothermal reaction, not allowed to obtain better data. Bad quality data due to the poor crystallinity and high mosaicity of the sample.

The Mercury<sup>34</sup> software package was used for the graphical representation of the resultant structures. CCDC 979008-979010 contains the supplementary crystallographic data for this paper. These data can be obtained free of charge from The Cambridge Crystallographic Data Centre via [www.ccdc.cam.ac.uk/data\\_request/cif](http://www.ccdc.cam.ac.uk/data_request/cif).

Table 4.1 | Crystal data

	$[\text{Cu}_4\text{I}_4(\text{PN})_2]$	$[\text{CuI}(\text{PN})_{0.5}]_\infty$	$[\text{CuI}(\text{PN})_3]^a$
Chemical formula	$\text{C}_{34}\text{H}_{28}\text{Cu}_4\text{I}_4\text{N}_2\text{P}_2$	$\text{C}_{17}\text{H}_{14}\text{Cu}_2\text{I}_2\text{N}_1\text{P}_1$	$\text{C}_{51}\text{H}_{42}\text{Cu}_1\text{I}_1\text{N}_3\text{P}_3$
Formula Mass	1288.28	644.15	980.28
Crystal System	Monoclinic	Triclinic	Trigonal
$a/\text{\AA}$	16.7222(3)	7.9805(7)	13.6471(2)
$b/\text{\AA}$	13.9164(3)	8.5298(8)	13.6471(2)
$c/\text{\AA}$	16.4466(3)	14.3667(14)	14.7400(4)
$\alpha/^\circ$	90	78.092(8)	90
$\beta/^\circ$	99.688(2)	85.576(8)	90
$\gamma/^\circ$	90	86.494(7)	120
Volume/ $\text{\AA}^3$	3772.75(13)	953.05(15)	2377.4
Temperature	RT	RT	RT
Space group	P2 <sub>1</sub> /c	P-1	P-3
No. of independent reflections	11078	2594	-
$R_{int}$	0.0534	0.046	-
Final $R_1$ values	0.0489	0.1225	
Final $wR(F^2)$ values	0.0933	0.3395	
Final $R_1$ values (all data)	0.0621	0.1386	

<sup>a</sup> Solved from X-ray powder diffraction.

## Results and discussion

### Synthesis and Crystal Structures

The copper iodide was reacted with PN with different synthetic procedures which differ mainly for the stoichiometric ratio or for the aggregation state (solid state or solution). The reactions in solution are carried out mainly in acetonitrile or saturated aqueous solution of KI in air, while the reactions in solid state were carried out via ball milling with a drop of acetonitrile.

Six different compounds have been isolated so far,  $[\text{Cu}_2\text{I}_2(\text{PN})_3]$  recently described by Zink et al.<sup>13</sup>  $[\text{Cu}_4\text{I}_4(\text{PN})_2]$  and its solvate form  $[\text{Cu}_4\text{I}_4(\text{PN})_2 \cdot (\text{CH}_3\text{CN})]$ ,  $[\text{CuI}(\text{PN})_{0.5}]_\infty$  and  $[\text{CuI}(\text{PN})_3]$  whose structure has been determined during these studies and  $\text{CuI}(\text{PN})_2$ .

The dimer  $[\text{Cu}_2\text{I}_2(\text{PN})_3]$  was easily reproduced by the synthesis described in the literature<sup>13</sup> and it was also obtained by ball milling of CuI and PN with stoichiometry ratio 1:1.5 with a drop of acetonitrile. This complex seems to be very stable and it was obtained as an undesired product in several other reactions (up to stoichiometry ratio CuI:PN 3:1 or 1:3) both in solution and solid state. In many cases to avoid the presence of  $[\text{Cu}_2\text{I}_2(\text{PN})_3]$  the reactions were run with a great excess of one of the reagents. The dimeric core of  $[\text{Cu}_2\text{I}_2(\text{PN})_3]$  is characterized by a butterfly shape due to the presence of a bridging ligand coordinating with both N and P atoms, and a short copper-copper distance ( $2.7694(6)$  Å) consistent with metallophilic interactions (see table 4.2). The two other ligands coordinated only with the P atoms and they are described as ancillary ligands. The complexes interact via C-H---π and in the case of the ancillary ligands also via π-π interactions (see figure 4.1). These weak interactions do not affect the photophysical properties since the compound does not suffer of emission quenching.

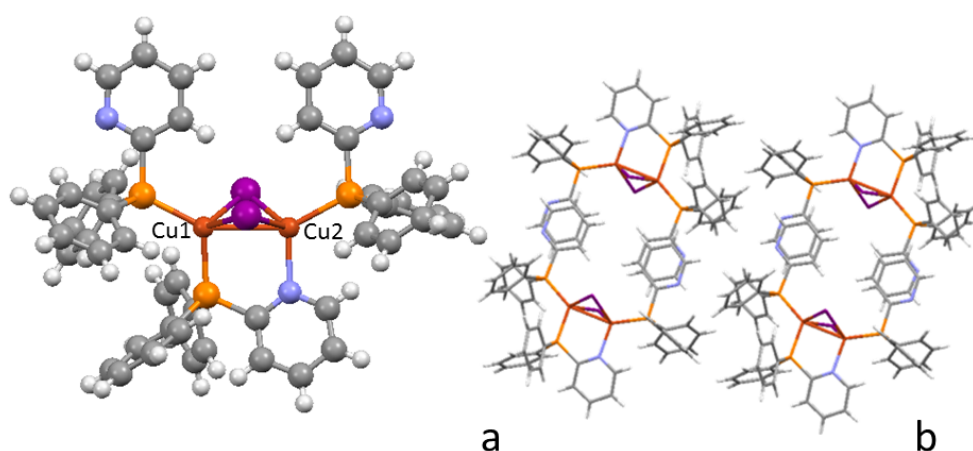


Figure 4.1 | a)  $[\text{Cu}_2\text{I}_2(\text{PN})_3]$  b) π-π interactions present in the crystal packing

---

The reactions carried in excess of CuI (stoichiometry ratio CuI:PN 4:1) leads to the formation of  $[\text{Cu}_4\text{I}_4(\text{PN})_2 \cdot (\text{CH}_3\text{CN})]$ , and  $[\text{CuI}(\text{PN})_{0.5}]_\infty$ ; the pure phase of  $[\text{Cu}_4\text{I}_4(\text{PN})_2 \cdot (\text{CH}_3\text{CN})]$ , is obtained by reaction in solution, while by ball milling a mixture of  $[\text{Cu}_4\text{I}_4(\text{PN})_2 \cdot (\text{CH}_3\text{CN})]$  and  $[\text{CuI}(\text{PN})_{0.5}]_\infty$  is obtained; it was not possible to isolate the pure phase of  $[\text{CuI}(\text{PN})_{0.5}]_\infty$ . Single crystals of  $[\text{Cu}_4\text{I}_4(\text{PN})_2]$  and  $[\text{CuI}(\text{PN})_{0.5}]_\infty$  have been obtained by solvothermal reactions while all other attempts to obtain crystals by triple layer crystallization failed.

Table 4.2 | Copper-copper distances

Compound		Distance/ Å
$[\text{Cu}_2\text{I}_2(\text{PN})_3]$	Cu1-Cu2	2.7694(6)
$[\text{CuI}(\text{PN})_{0.5}]_\infty$	Cu6-Cu7	2.7499(9)
	Cu5-Cu7	2.5883(9)
	Cu6-Cu8	2.574(1)
	Cu5-Cu8	2.699(1)
$[\text{Cu}_4\text{I}_4(\text{PN})_2]$	Cu3-Cu4	2.771(7)
	Cu3-Cu3	2.900(7)
	Cu4-Cu4	3.485(6)

$[\text{Cu}_4\text{I}_4(\text{PN})_2 \cdot (\text{CH}_3\text{CN})]$  presents a powder diffraction pattern very similar to  $[\text{Cu}_4\text{I}_4(\text{PN})_2]$ ; while the structure of the unsolvate form was determined by single crystal X-ray diffraction, it was possible only to index the powder pattern of the  $[\text{Cu}_4\text{I}_4(\text{PN})_2 \cdot (\text{CH}_3\text{CN})]$ . The Pawley refinement converged to  $R_{wp}=6.65\%$  with a monoclinic cell, space group  $P2_1/c$  with parameters  $a=17.4853(5)\text{\AA}$ ,  $b=14.180(2)\text{\AA}$ ,  $c=16.303(2)\text{\AA}$ ,  $\beta=97.07(1)^\circ$  and volume  $4011.5(8)\text{\AA}^3$  which is about  $239\text{\AA}^3$  greater than the volume of  $\text{Cu}_4\text{I}_4(\text{PN})_2$ . The difference in volume can be ascribed to the presence of one acetonitrile molecule in the asymmetric unit. The presence of the solvent was confirmed by the TGA which shows a 3.06% weight loss at  $150^\circ\text{C}$  corresponding to the release of one molecule of acetonitrile (calculated 2.96%) (see figure 4.2a). The transformation of  $[\text{Cu}_4\text{I}_4(\text{PN})_2 \cdot (\text{CH}_3\text{CN})]$  into  $[\text{Cu}_4\text{I}_4(\text{PN})_2]$  was observed also with variable temperature X-ray diffraction (see figure 4.2b). Instead of the common motif of cubane-like clusters, the  $[\text{Cu}_4\text{I}_4(\text{PN})_2]$  cluster adopts an “octahedral” geometry which it has been observed recently by Liu et al.<sup>4</sup> The copper atoms are arranged in a parallelogram with  $\mu^4$ - iodides above and below the parallelogram and  $\mu^2$ - iodides bridging the copper atoms on the short edge. All Cu-Cu distances are lower than the sum of the van der Waals radii (see table 4.2).

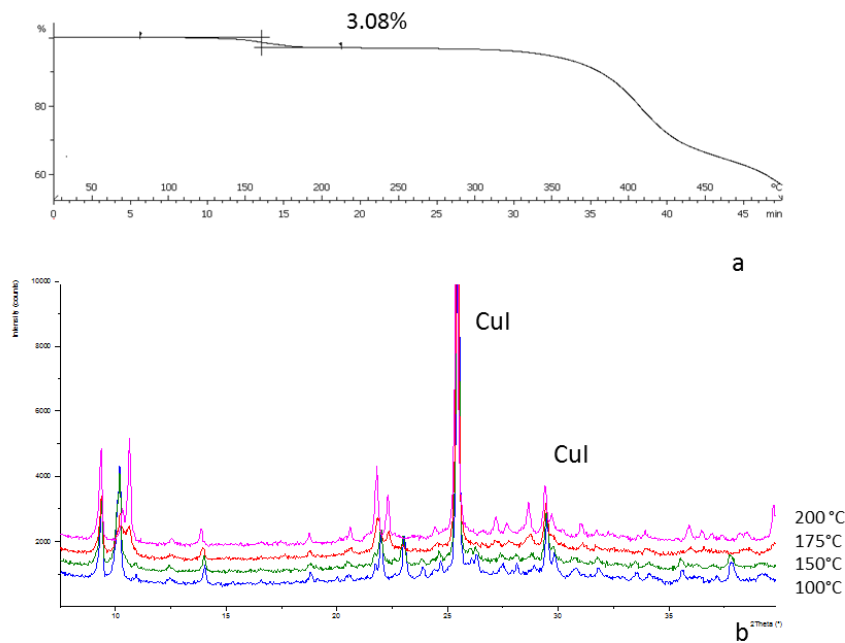


Figure 4.2 | a) TGA curve of  $[\text{Cu}_4\text{I}_4(\text{PN})_2 \cdot (\text{CH}_3\text{CN})]$ , the first step is consistent with the release of one acetonitrile molecule (experimental 3.08%, calculated 2.96%), b) Variable temperature X-ray powder diffraction: pattern reported are at 100°C bottom line, 150°C medium bottom line, 175°C medium top line and 200°C top line. Bragg reflections of unreacted CuI are highlighted with the label.

The aromatic ring interacts mainly via C-H--- $\pi$  interactions and  $\pi$ - $\pi$  interactions involving the pyridine coordinating ring and a phenyl ring (see figure 4.3). The crystal packing suggests that the solvent molecules can be placed in the (1 0 0) plane which is the less dense. Further studies will be done to ascertain the crystal packing of  $[\text{Cu}_4\text{I}_4(\text{PN})_2 \cdot (\text{CH}_3\text{CN})]$ .

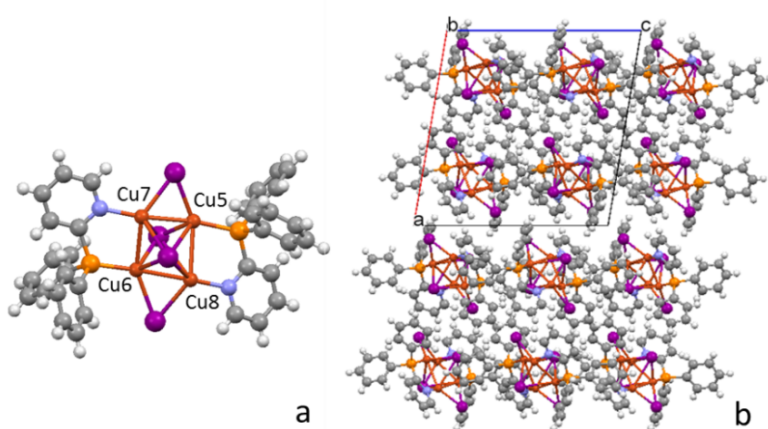


Figure 4.3 | a) Compound  $\text{Cu}_4\text{I}_4(\text{PN})_2$ ; b) crystal packing view along  $b$  axis.

It is worth noting that  $[\text{CuI}(\text{PN})_{0.5}]_\infty$  is easily obtained by mechanosynthesis, although not as a pure phase. Its formation was observed also in solid state reactions with stoichiometry ratio CuI:PN 1:1.5. The low solubility of the compound, which

characterizes all the coordination polymers, seems to preclude its formation from the synthesis in solution, while it seems a driving force in the solid state reactions. The solvothermal conditions (high temperature and high pressure) allow to crystallize phases which are known to be poorly soluble, as well, solid state reactions are known to reach phases which can be hard to obtain in solution as observed for the co-crystals.<sup>36</sup> In our case the solvothermal synthesis were explored in order to obtain a single crystal of the desired phase, since the structure determination by X-ray powder diffraction (XRPD) would be really challenging due to the lack of information on the molecular geometry of the complexes.

Despite of all the structures of CuI(P<sup>N</sup> ligands) described in the literature<sup>1-4, 13, 15, 37</sup> which show discrete complexes, the structure of [CuI(PN)<sub>0.5</sub>]<sub>∞</sub> is characterized by a one-dimensional copper iodide polymeric structure. The infinite double chain of CuI presents short and long copper–copper distances (see table 4.2). Usually the tetrahedral coordination of the copper(I) ions is fulfilled by multidentate bridging ligands to construct a 2D sheet network,<sup>24, 38</sup> in our case the PN ligand bridges two copper atoms but on the same chain and brings the two cooper atoms 3.0716(3) Å apart.

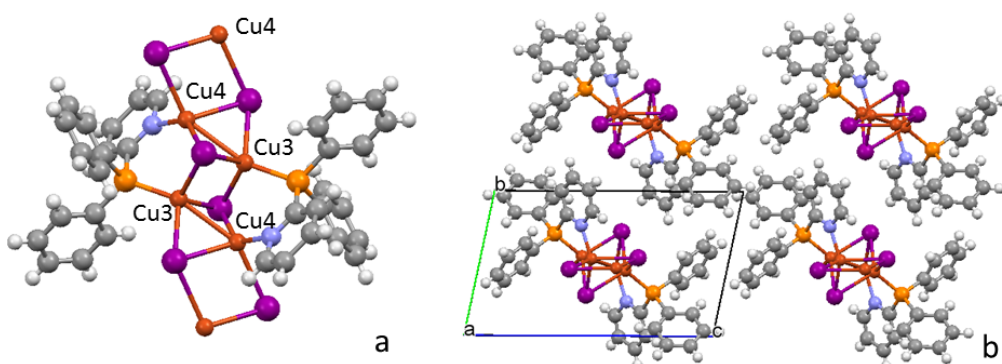


Figure 4.4 | a. Polymeric structure of [CuI(PN)<sub>0.5</sub>]<sub>∞</sub>; b. crystal packing view along *a* axis. Polymeric chains run parallel to each other.

The reactions carried in excess of the ligand leads to the formation of two new phases: [CuI(PN)<sub>3</sub>] and CuI(PN)<sub>2</sub>. The pure compound [CuI(PN)<sub>3</sub>] is obtained only from reaction in solution carried with a stoichiometry ratio CuI:PN 1:4 while when the same reaction is carried out in solid state only CuI(PN)<sub>2</sub> is obtained. The structure of [CuI(PN)<sub>3</sub>] was solved from powder pattern X-ray diffraction data even if the diffractogram acquired shows peaks of unwashed KI salt. The powder pattern is indexed by a trigonal cell with cell axes  $a=13.6471(2)\text{Å}$ ,  $c=14.7400(4)\text{ Å}$  volume =  $2377\text{ Å}^3$  and space group P-3. The volume of the asymmetric unit,  $396\text{ Å}^3$ , is consistent with the volume of the one third of [CuI(PN)<sub>3</sub>]. The solution is possible only if the monomer is located on the 3-fold axis. The structure was solved with a simulated annealing algorithm using as starting model one molecule of the ligand not bounded to the metal atom and the copper atom and the iodide with site occupancy

1/3. The Rietveld refinement converged to a  $R_{wp} = 7.681\%$  and  $R_{exp} = 4.351\%$  (see figure 4.5). The position of the nitrogen atoms was assumed from the structure solution since the packing features or the Rietveld refinement gave no hints on the possible position (see figure 4.6). The crystal packing of  $[CuI(PN)_3]$  does not present important intermolecular interactions. It is worth noting that along the  $c$  axis the molecular disposition create cavities which can host solvent molecules as suggested also by the TGA curve (see figure 4.7a). Several attempts have been made to determine the crystal structure of  $CuI(PN)_2$ , although the diffractogram does not present peaks of the reagents or of other known phases we were not able to index it (see figure 4.7). It is not possible to exclude the presence of more than one phase.

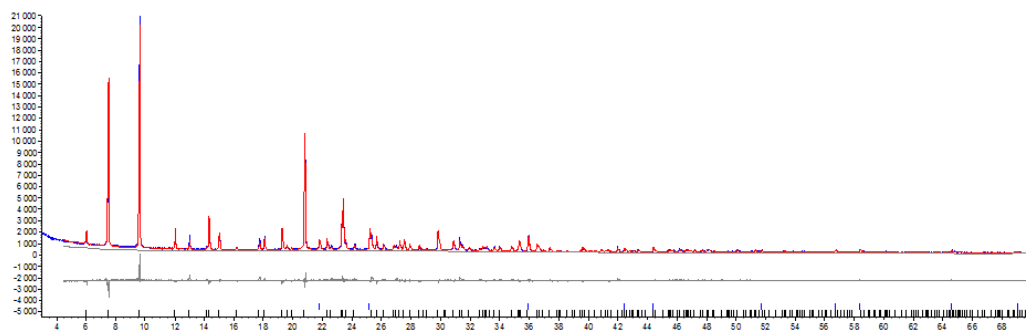


Figure 4.5 | Rietveld refinement of  $[CuI(PN)_3]$ , red line is the calculated diffractogram, blue line observed diffractogram and grey line difference plot. Blue ticks correspond to the Bragg peaks of KI, black ticks correspond to the Bragg peaks of  $[CuI(PN)_3]$ .

The empirical formula is suggested by TGA and VTXRPD (see figure 4.8). X-ray diffraction at variable temperature shows that  $[CuI(PN)_3]$  starts to transform into  $CuI(PN)_2$  at  $180^\circ C$  and the complete transformation accompanied by amorphization is observed at  $250^\circ C$ . In the TGA curve the first step which corresponds to weight lost 0.81% is probably due to some solvent trapped in the crystals, the second step due to the release of one ligand (calculated 26.84% weight lost) which is suddenly followed by decomposition and the release of the second and third ligand.

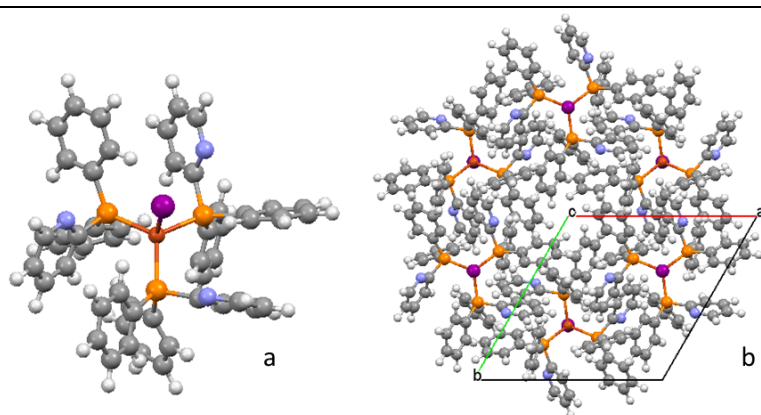


Figure 4.6 | a) Single molecule of  $[CuIPN_3]$ ; b) Packing of  $[CuIPN_3]$  view along the  $c$  axis.

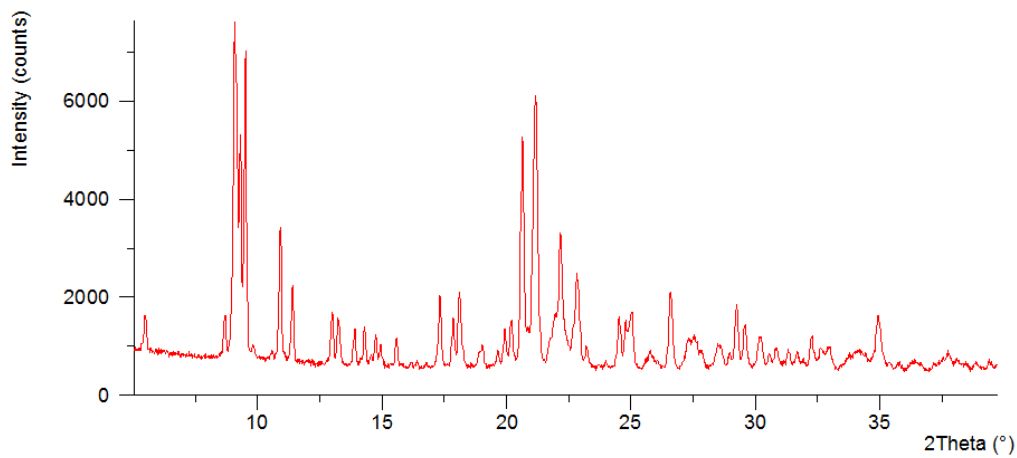


Figure 4.7 | Powder pattern of  $\text{CuI}(\text{PN})_2$  obtained by ball milling.

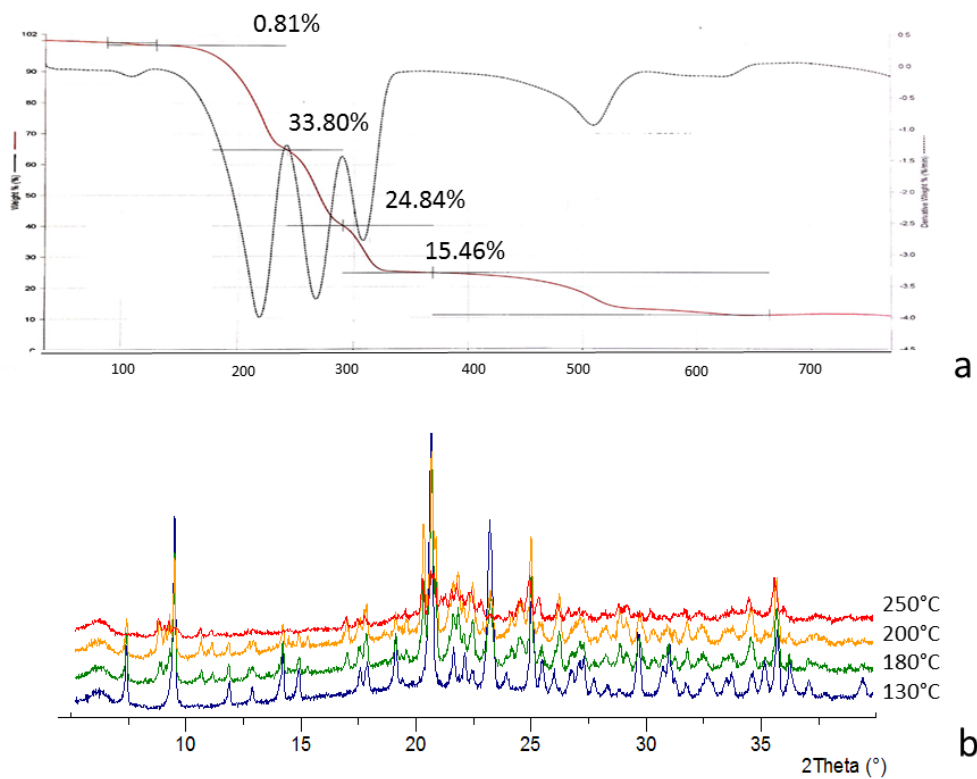


Figure 4.8 | a) TGA curve of  $[\text{CuI}(\text{PN})_3]$ , the first step (0.81%) is due to some solvent release, the second step can be ascribed to the release to one ligand molecule which is suddenly followed by the release of the other ligand molecules; b) VTXRPD of  $[\text{CuI}(\text{PN})_3]$ , at 180°C (green line) the peaks of  $\text{CuI}(\text{PN})_2$  appear, the complete transformation is characterized is observed at 250°C. The powder pattern presents a low crystallinity profile.

## Photophysical properties

All complexes are luminescent in their solid state at room temperature with emissions spanning from green to yellow. The tetrahedral coordination around the copper(I) ion and the stiff molecular structure assured by rigid ligands hamper the Jahn-Teller distortion of the excited state and allow high emission quantum yields.<sup>39,40</sup> Examination of the relevant bond angles reveals an only slightly distorted tetrahedral geometry around the Cu ions, demonstrating the fitting bite angle of the bidentate P<sup>N</sup> ligand in the polynuclear complexes.<sup>13</sup> The lack of concentration quenching make these complexes attractive for applications in solid state devices as OLEDs or LECs. Moreover their emissions stem from excited states populated by fast intersystem crossing, which allow the so-called “triplet harvesting” or “singlet harvesting” that leads to high electroluminescence efficiencies.<sup>13, 16, 41-43</sup>

The emission lifetimes are relatively short, in the order of microseconds, thus preventing the excited state quenching due to triplet-triplet and triplet-charge interaction processes origin of the typical roll-off in the electroluminescence efficiency decay at high currents.<sup>44</sup>

The frontier orbitals involved in electronic transitions have a (X+M)LCT character, only slightly affected by the halogen/metal orbital ratio contributing to the HOMO, and dependent on the Cu<sub>x</sub>I<sub>x</sub> nuclearity, and by the number of bridging ligands that contribute to the LUMO.

The emission spectra of the complexes that could be obtained as sufficiently pure powders are represented in figure 4.9. The dimeric [Cu<sub>2</sub>I<sub>2</sub>(PN)<sub>3</sub>] complex shows an emission band with maximum at 525 nm which has been assigned to a temperature assisted delayed fluorescence (TADF) from a (X+M)LCT singlet excited state in thermal equilibrium with the triplet state lying at a very close energy level.<sup>13</sup>

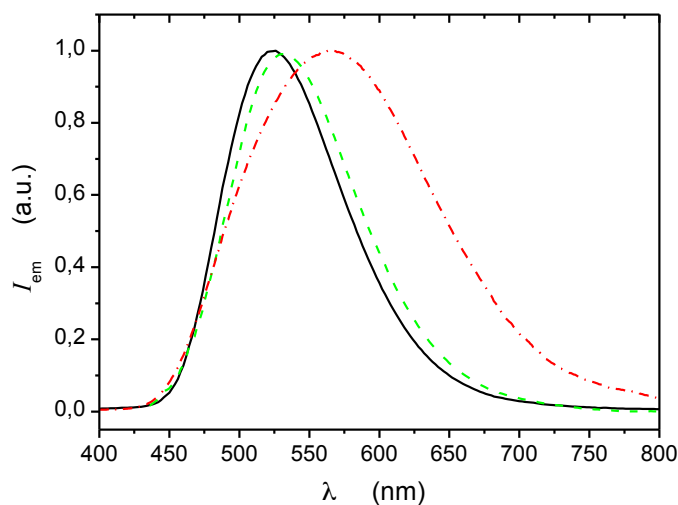


Figure 4.9 | Emission spectra of [Cu<sub>2</sub>I<sub>2</sub>(PN)<sub>3</sub>] (solid, black), [CuI(PN)<sub>3</sub>] (dash, green) and [Cu<sub>4</sub>I<sub>4</sub>(PN)<sub>2</sub>(CH<sub>3</sub>CN)] (dash-dot, red) as crystalline powders at room temperature.

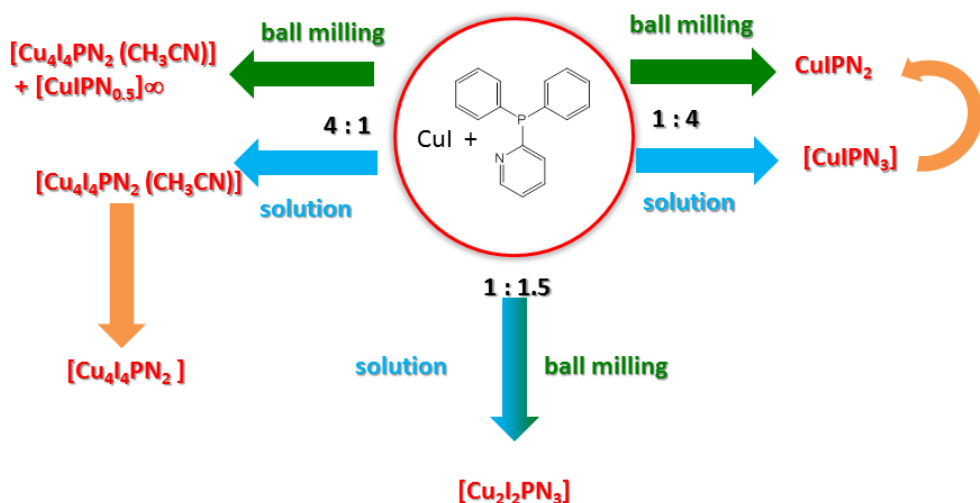
---

The monomer  $[\text{CuI}(\text{PN})_3]$  has a very similar emission band most probably ascribable to a transition akin to the  $[\text{Cu}_2\text{I}_2\text{PN}_3]$  one.

None of the two compounds show radiative decay from excited states generated by cuprophilic interactions. Instead, the red-shifted and broader emission band of the  $[\text{Cu}_4\text{I}_4(\text{PN})_2 \cdot (\text{CH}_3\text{CN})]$  octahedral complex is indicative of a cluster centred (CC) transition at lower energy contributing to the emission.<sup>4</sup>

### Conclusions

The copper iodide complexes are known for their large variety of coordination geometries which allows a great deal of different stoichiometries to be attained with compounds based on the same ligand. One of the targets of the research described in this paper was that of exploring as thoroughly as possible the chemistry of CuI and the ligand diphenyl-2-pyridyl phosphine PN. Five new different compounds have been discussed:  $[\text{Cu}_4\text{I}_4(\text{PN})_2]$ ,  $[\text{Cu}_4\text{I}_4(\text{PN})_2 \cdot (\text{CH}_3\text{CN})]$ ,  $[\text{CuI}(\text{PN})_{0.5}]_\infty$ ,  $[\text{CuI}(\text{PN})_3]$  whose structure has been determined during this study, and  $\text{CuI}(\text{PN})_2$  (see scheme 4.1). Two main synthetic parameters were changed, the stoichiometry and the media in which reactions were carried out, whether in solution or the solid state. Regarding the stoichiometry, we have discovered that only by using great excess of one of the reagents it is possible to move from the dimeric structure  $[\text{Cu}_2\text{I}_2(\text{PN})_3]$  and to obtain new compounds with higher ligand/CuI ratios. In terms of synthetic routes we have shown that solution synthesis yielded  $[\text{Cu}_4\text{I}_4(\text{PN})_2 \cdot (\text{CH}_3\text{CN})]$  and  $[\text{CuI}(\text{PN})_3]$  while  $[\text{CuI}(\text{PN})_{0.5}]_\infty$  and  $\text{CuI}(\text{PN})_2$  were obtained only via solid state reactions, which posed the additional problem of structure determination when only polycrystalline samples are available. One way to circumvent this problem is that of finding an alternative way to grow single crystals of the desired species. This is why in our study we have explored in parallel the solvothermal synthesis with CuI and PN in an attempt to obtain the same species as produced by solid state reactions. In such a way we have obtained single crystals of  $[\text{Cu}_4\text{I}_4(\text{PN})_2]$  and  $[\text{CuI}(\text{PN})_{0.5}]_\infty$  which allowed full identification of this latter mechanochemical products by comparison of observed and simulated patterns. The observation that  $[\text{CuI}(\text{PN})_{0.5}]_\infty$  could be obtained by solid state reaction and by solvothermal method suggests that the two processes can reach similar conditions which are not allowed in the traditional synthesis in solution.  $[\text{Cu}_4\text{I}_4(\text{PN})_2]$  and  $[\text{Cu}_4\text{I}_4(\text{PN})_2 \cdot (\text{CH}_3\text{CN})]$  present a very similar powder patterns which suggests that the solvated compound should maintain the same geometry, upon thermal treatment  $[\text{Cu}_4\text{I}_4(\text{PN})_2 \cdot (\text{CH}_3\text{CN})]$  convert into  $[\text{Cu}_4\text{I}_4(\text{PN})_2]$ . The crystal structure of  $[\text{CuI}(\text{PN})_3]$  was solved from powder pattern X-ray diffraction data. Only the empirical formula of  $\text{CuI}(\text{PN})_2$  was postulate. This compound was obtained by ball milling or upon heating of  $[\text{CuI}(\text{PN})_3]$  at 180°C, which corresponds in the TGA curve, at the release of one ligand. All the compounds obtained are luminescent and the photophysical properties of the complexes that could be obtained as sufficiently pure powders, have been reported.



Scheme 4.1 | Scheme of the compounds obtained and their relationship. Blue arrows indicate synthesis in solution, green arrows synthesis in solid state and orange arrows thermal treatment.

## References

1. L. Bergmann, J. Friedrichs, M. Mydlak, T. Baumann, M. Nieger and S. Bräse, *Chem. Commun.*, 2013, **49**, 6501-6503.
2. D. M. Zink, T. Baumann, J. Friedrichs, M. Nieger and S. Bräse, *Inorg. Chem.*, 2013.
3. D. M. Zink, D. Volz, T. Baumann, M. Mydlak, H. Flügge, J. Friedrichs, M. Nieger and S. Bräse, *Chem. Mater.*, 2013.
4. Z. Liu, P. I. Djurovich, M. T. Whited and M. E. Thompson, *Inorg. Chem.*, 2011, **51**, 230-236.
5. Z. Liu, M. F. Qayyum, C. Wu, M. T. Whited, P. I. Djurovich, K. O. Hodgson, B. Hedman, E. I. Solomon and M. E. Thompson, *J. Am. Chem. Soc.*, 2011, **133**, 3700-3703.
6. V. A. Krylova, P. I. Djurovich, J. W. Aronson, R. Haiges, M. T. Whited and M. E. Thompson, *Organometallics*, 2012, **31**, 7983-7993.
7. I. Roppolo, E. Celasco, A. Fargues, A. Garcia, A. Revaux, G. Dantelle, F. Maroun, T. Gacoin, J.-P. Boilot, M. Sangermano and S. Perruchas, *J. Mater. Chem.*, 2011, **21**, 19106-19113.
8. P. P. Mazzeo, L. Maini, D. Braga, G. Valenti, F. Paolucci, M. Marcaccio, A. Barbieri and B. Ventura, *Eur. J. Inorg. Chem.*, 2013, **2013**, 4459-4465.
9. A. Barbieri, G. Accorsi and N. Armaroli, *Chem. Commun.*, 2008, 2185-2193.
10. R. Peng, M. Li and D. Li, *Coord. Chem. Rev.*, 2010, **254**, 1-18.
11. M. Vitale and P. C. Ford, *Coord. Chem. Rev.*, 2001, **219-221**, 3-16.
12. P. C. Ford, E. Cariati and J. Bourassa, *Chem. Rev.*, 1999, **99**, 3625-3648.
13. D. M. Zink, M. Bächle, T. Baumann, M. Nieger, M. Kühn, C. Wang, W. Klopper, U. Monkowius, T. Hofbeck, H. Yersin and S. Bräse, *Inorg. Chem.*, 2013, **52**, 2292-2305.
14. R. Czerwieniec, J. Yu and H. Yersin, *Inorg. Chem.*, 2011, **50**, 8293-8301.
15. D. Volz, D. M. Zink, T. Bocksrocker, J. Friedrichs, M. Nieger, T. Baumann, U. Lemmer and S. Bräse, *Chem. Mater.*, 2013, **25**, 3414-3426.
16. M. J. Leitl, F.-R. Küchle, H. A. Mayer, L. Wesemann and H. Yersin, *J. Phys. Chem. A*, 2013.
17. D. Volz, M. Nieger, J. Friedrichs, T. Baumann and S. Bräse, *Langmuir*, 2013.
18. C. H. Arnby, S. Jagner and I. Dance, *CrystEngComm*, 2004, **6**, 257-275.

19. D. J. Fife, W. M. Moore and K. W. Morse, *Inorg. Chem.*, 1984, **23**, 1684-1691.
20. *CSD*, (2013 ), Cambridge Crystallographic Data Centre, UK.
21. L. Maini, D. Braga, P. P. Mazzeo and B. Ventura, *Dalton Trans.*, 2012, **41**, 531-539.
22. S. L. James, C. J. Adams, C. Bolm, D. Braga, P. Collier, T. Friscic, F. Grepioni, K. D. M. Harris, G. Hyett, W. Jones, A. Krebs, J. Mack, L. Maini, A. G. Orpen, I. P. Parkin, W. C. Shearouse, J. W. Steed and D. C. Waddell, *Chem. Soc. Rev.*, 2012, **41**, 413-447.
23. D. Braga, L. Maini, P. P. Mazzeo and B. Ventura, *Chem. Eur. J.*, 2010, **16**, 1553-1559.
24. D. Braga, F. Grepioni, L. Maini, P. P. Mazzeo and B. Ventura, *New J. Chem.*, 2011, **35**, 339-344.
25. G. A. Bowmaker, *Chem. Commun.*, 2013, **49**, 334-348.
26. G. A. Bowmaker, J. V. Hanna, R. D. Hart, P. C. Healy, S. P. King, F. Marchetti, C. Pettinari, B. W. Skelton, A. Tabacaru and A. H. White, *Dalton Trans.*, 2012, **41**, 7513-7525.
27. G. A. Bowmaker, J. V. Hanna, B. W. Skelton and A. H. White, *Chem. Commun.*, 2009, 2168-2170.
28. W. I. F. David, K. Shankland, L. M. McCusker and C. Baerlocher, *Structure determination from powder diffraction data* Oxford University Press: New York, 2002.
29. G. A. Bowmaker and J. V. Hanna, *Z.Naturforsch.(B)*, 2009, **64**, 1478-1486.
30. P. J. Beldon, L. Fábián, R. S. Stein, A. Thirumurugan, A. K. Cheetham and T. Friščić, *Angew. Chem. Int. Ed.*, 2010, **49**, 9640-9643.
31. R. E. Morris and S. L. James, *Angew. Chem. Int. Ed.*, 2013, **52**, 2163-2165.
32. Y. Jin, Q. Sun, G. Qi, C. Yang, J. Xu, F. Chen, X. Meng, F. Deng and F.-S. Xiao, *Angew. Chem.*, 2013, **125**, 9342-9345.
33. J. F. Fernández-Bertrán, M. P. Hernández, E. Reguera, H. Yee-Madeira, J. Rodriguez, A. Paneque and J. C. Llopiz, *J. Phys. Chem. Solids*, 2006, **67**, 1612-1617.
34. C. F. Macrae, I. J. Bruno, J. A. Chisholm, P. R. Edgington, P. McCabe, E. Pidcock, L. Rodriguez-Monge, R. Taylor, J. van de Streek and P. A. Wood, *J. Appl. Crystallogr.*, 2008, **41**, 466-470.
35. G. M. Sheldrick, *SHELX97*, 1997, University of Göttingen, Germany.
36. S. L. Childs, N. Rodriguez-Hornedo, L. S. Reddy, A. Jayasankar, C. Maheshwari, L. McCausland, R. Shipplett and B. C. Stahly, *CrystEngComm*, 2008, **10**, 856-864.
37. D. Volz, M. Nieger, J. Friedrichs, T. Baumann and S. Bräse, *Inorg. Chem. Commun.*, 2013, **37**, 106-109.
38. A. J. Blake, N. R. Brooks, N. R. Champness, P. A. Cooke, M. Crew, A. M. Deveson, L. R. Hanton, P. Hubberstey, D. Fenske and M. Schröder, *Crystal Engineering*, 1999, **2**, 181-195.
39. M. Hashimoto, S. Igawa, M. Yashima, I. Kawata, M. Hoshino and M. Osawa, *J. Am. Chem. Soc.*, 2011, **133**, 10348-10351.
40. N. Armaroli, G. Accorsi, F. Cardinali and A. Listorti, *Top. Curr. Chem.*, 2007, **280**, 69-115.
41. M. A. Baldo, S. Lamansky, P. E. Burrows, M. E. Thompson and S. R. Forrest, *Appl. Phys. Lett.*, 1999, **75**, 4-6.
42. M. A. Baldo, D. F. O'Brien, Y. You, A. Shoustikov, S. Sibley, M. E. Thompson and S. R. Forrest, *Nature*, 1998, **395**, 151-154.
43. C.-W. Hsu, C.-C. Lin, M.-W. Chung, Y. Chi, G.-H. Lee, P.-T. Chou, C.-H. Chang and P.-Y. Chen, *J. Am. Chem. Soc.*, 2011, **133**, 12085-12099.
44. H. Yersin, ed., *Highly Efficient OLEDs with Phosphorescent Materials*, Wiley-VCH, Weinheim, 2008.



# Chapter 5

## Single-phase white-emitter copper iodide based Metal-Organic Framework

**Abstract:** Two different compounds based on copper iodide and 3-(aminomethyl)pyridine have been synthesized and characterized.

The structure of the catena(bis( $\mu_3$ -iodo(3-aminomethyl)pyridine))-copper(I) (**1**) consists in a metal-organic framework based on copper iodide coordination polymers bridged by 3-(aminomethyl)pyridine bi-dentate ligands. The structure of **1** has been solved by XRPD data since no single-crystal has been obtained. It showed an overall white emission at ambient temperature due to the co-presence of complementary  $^3\text{CC}$  and  $^3\text{XLCT}$  emission bands. Structure of **2** has not been determined while the stoichiometry  $\text{Cu}_2\text{I}_2(3\text{-}(3\text{-aminomethyl)pyridine})_2$  has been suggest by thermal analysis. A thermal induced transition **2** to **1** has been observed at 150°C as a consequence of one ligand loss in the asymmetric unit.



## Introduction

Lighting has been an indispensable technology in today's 7/24 society. From the invention of incandescent bulbs, implementation of fluorescent tubes, to the presently fast-growing solid-state lightening, it has been the key fixture in defining the quality of modern life. White organic light-emitting devices (WOLEDs) have been intensively studied in recent years<sup>1,2</sup> due to their potential for highly efficient and cost effective next generation lighting.<sup>3</sup> In a WOLED, white light is typically generated through the simultaneous emission of multiple emissive materials, which need to be employed in either a single emissive layer with multiple molecular emitters or multiple emissive layers.<sup>4</sup>

One of the current academic interests is in the pursuing single white-light phosphors to avoid the intrinsic colour balance, device complication, and high-cost problems associating with multiphosphors or multi-LEDs.<sup>5</sup> Examples are rare but still can be found in the research field of organic molecules or polymers,<sup>6-10</sup> metal-doped or hybrid inorganic materials,<sup>11-14</sup> metal complexes,<sup>15-17</sup> and nanomaterials.<sup>18-20</sup>

Significant progress has been achieved in both increasing the efficiency and allowing for colour tuning by use of emitters based on Ir,<sup>21-25</sup> Pt<sup>26,27</sup> and Os<sup>28,29</sup> because with these both triplet and singlet excitons formed upon charge recombination in the emissive layer can be utilized.<sup>30,31</sup> These materials, however, are produced from rather expensive metals, which is one reason why more abundant and cost-efficient metals with d<sup>10</sup> configuration such as Cu(I), Ag(I), or Au(I) have received more attention recently.<sup>5,32-36</sup> Copper(I) halide aggregates constitute a large family of compounds studied for decades for their photochemical and photophysical properties.<sup>37-41</sup>

Particularly, interest in stimuli-responsive luminescent materials is steadily increasing momentum in the field of smart functionalized devices.<sup>42,43</sup> Recently, however, there has been a surge of interest in studying these complexes, which are currently at the forefront of coordination chemistry and crystal engineering research<sup>43-46</sup> as active material for optoelectronic devices.<sup>35,36,47-49</sup>

Since the first and so far the most famous luminescence thermocromic copper(I)-iodide complex, Cu<sub>4</sub>I<sub>4</sub>pyridine<sub>4</sub>, which showed bright yellow luminescence at room temperature and an equally intense blu-violet luminescence when cooled in liquid nitrogen<sup>50</sup>, luminescent thermocromic materials based on copper(I) clusters<sup>49,51</sup> have been enthusiastically pursued due to their excellent luminescence performance and stability<sup>52</sup>.

These compounds exhibit two distinct triplet emission bands: a low energy (LE) and a high energy (HE). The LE band is due to the nature of the complex core and the transition comes from a mixed halogen-to-metal charge transfer and a metal-centred transition and for this reason is known as Cluster Centred transition (<sup>3</sup>CC). It is only possible in the presence of a cuprophilic interaction

when the Cu---Cu distance in the core is shorter than the sum of van der Waals radii.<sup>53</sup> The HE band derive from a halogen-to-ligand charge transfer (<sup>3</sup>XLCT) and it is possible only in presence of ligand accessible  $\pi^*$  or d orbital.

When both requires are contemporary satisfied, the two triplet states are accessible from the same singlet excited state but an energy barrier separates them. The <sup>3</sup>CC state are thermally populated so LE and HE relative intensities change in function of the temperature. This process has known as thermocromic effect. Only recently, in the literature appears CuI pyridine based complexes in which the two emission band are both present at room temperature as the <sup>3</sup>CC is sufficiently populated because the barrier between the XLCT and CC state are enough small to be crossed.<sup>48</sup>

In the past two decades, metal-organic frameworks (MOFs) have received intense interest due to their potential application in gas separation<sup>54</sup> and storage<sup>55, 56</sup>, catalysis<sup>57</sup> and sensors<sup>58</sup>. Studies on the MOF photoluminescence (PL) are still in their infancy<sup>59</sup>; however, novel PL phenomena have been discovered, such as tuneable visible emission<sup>60</sup> or tuneable luminescence intensity driven by the presence/absence of a dynamic guest<sup>61</sup> or by controlling the guest properties by external stimuli as in a crystalline device.<sup>43</sup>

In this chapter, a copper(I) based MOF in which both LE and HE emissions are contemporary observed at room temperature is reported. The ligand used to design the compound was 3-(Aminomethyl)pyridine (=3-picoline) which is characterized by two different N-based binding site.

According to the synthesis used two different compounds with different metal/ligand stoichiometry ratio are easily obtained; the photochemical properties of the two are significantly different.

---

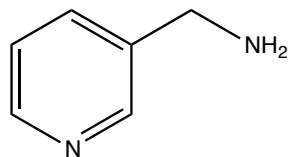


Figure 5.1: Sketch of the (3-aminomethyl)pyridine) (=3-picoline).

---

## Results and Discussion

Two distinct compounds have been obtained according to the synthetic conditions. Catena(bis( $\mu_3$ -iodo(3-aminomethyl)pyridine))-copper(I) (**1**) has been synthesised by reacting a large excess of copper iodide with respect to the ligand used (see experimental). A very interesting room temperature overall white

emission compound has been obtained, the photophysical properties of which are best reported in the section below. No single crystals of the titled compound have been obtained and the structure was solved by XRPD data.

The indexing run was performed with TOPAS 4.1<sup>62</sup> and a centric triclinic lattice parameter set ( $a=9.94(3)$ ,  $b=7.60(2)$ ,  $c=7.63(5)$   $\alpha=99.0(1)$ ,  $\beta=96.25(12)$ ,  $\gamma=108.86(2)$ ) has been proposed. The data set was background modulated with a 6 parameters Chubychev function and truncated to  $50^\circ 2\theta$  for Pawley fitting ( $\chi^2 = 4.4$ ). Structure solution was performed with a rigid body of the ligand not restrained on torsion angle values. Copper and iodine atoms coordinates are refined independently. The crystalline structure results in a non-porous Metal-Organic Framework made by a series of coordination polymers (CPs) that grow along the crystallographic  $c$ -axis.  $\text{Cu}_2\text{I}_2$ (3picolamine) stoichiometry has been found in the asymmetric unit. The castle-like CPs are made by pseudo-tetrahedral copper ions, every of which bonds three iodide ions and then complete its first coordination sphere with the N-based ligand. Metallophobic interactions are present in the structure since the copper-copper distances are  $2.771(3)$  Å,  $2.787(1)$  Å and  $3.123(2)$  Å. The bi-dentate organic ligands bridge the CuI chains in a 3D network. Along the same chain the ligands are in a antiparallel manner and two neighbour copper ions bind the ligands moieties alternatively by pirydic ring and amino group. The bridged CuI columns are wedged together in layers parallel to  $(-110)$  direction separated by  $3.36$  Å due to the inter-layers  $\pi$ - $\pi$  interactions among ligand aromatic rings as reported in figure 5.2. A Rietveld refinement against the original data set in the range  $4^\circ$ – $65^\circ 2\theta$  gave a good final fit,  $R_{wp}=7.2$ . In the refinement step, the ligands torsion angles are restrained to the move along the values range found by CSD statistics and the coordination bonds are forced to be coherent to copper(I) pseudo-tetrahedral geometry.

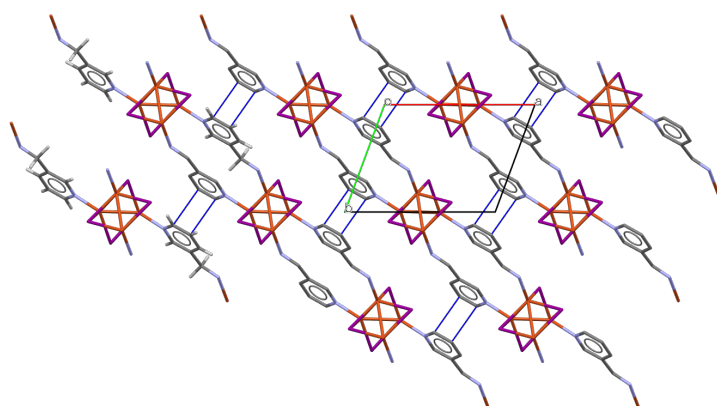


Figure 5.2 | packing of 1 along ab plane. CuI columns are aligned parallel to the  $(-110)$  Miller plane. Inter-layers  $\pi$ - $\pi$  interactions among ligand aromatic rings are highlighted in dashed blue line. Hydrogen atoms are omitted for sake of clarity

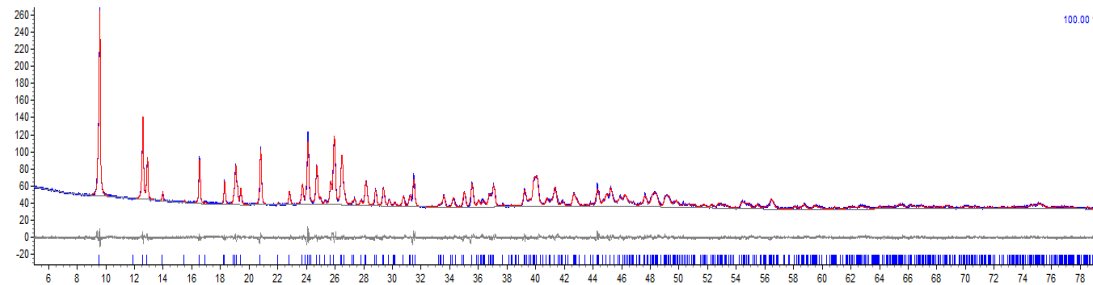


Figure 5.3 | Rietveld analysis plot. red line is the calculated diffractogram, blue line observed diffractogram and grey line difference plot. Blue ticks to the Bragg peaks of **1**.

The emission profile of **1** concerns two distinct emission bands, which are concomitant at ambient temperature. The maxima of the two bands are respectively 470 nm e 690 nm. As reported in figure 5.4, the emission profile is plotted at different temperature and it is evident that the emission intensity of the two bands are inversely proportional to the increase of temperature. To the best of the author knowledge only one example has been reported in literature with a similar emission profile in which both XLCT and CC emission band are present at ambient temperature in copper(I) based compounds.<sup>48</sup> At ambient temperature the CIE diagram coordinates are  $x=0.24$   $y=0.29$  with correlated color temperature = 16600K and with a Color Rendering Index (CRI) = 80.

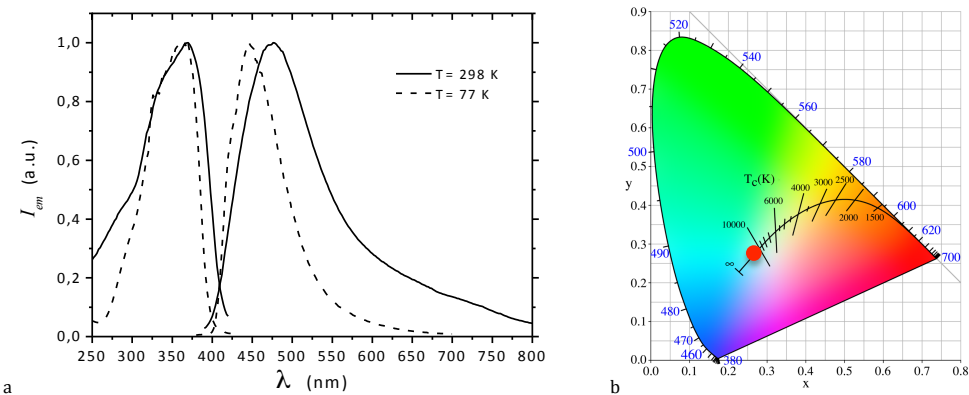


Figure 5.4 | (a) Normalized excitation spectra ( $\lambda_{exc}=365\text{nm}$ ) at 298 K (solid line) and 77 K (dashed line); (b) CIE diagram: the red point localize on the diagram the overall emission colour of the sample at rt.

$[\text{Cu}_2\text{I}_2(3\text{picolamine})_2]$  (**2**) as been obtained by reacting in equimolar stoichiometry the two reactants. The yellowish powder obtained after precipitation (see experimental) gave a high crystalline sample but no single crystal suitable for SCXRD analysis have been obtained by any crystallization process. The structure of the titled compound has not

yet been solved neither by XRPD data. The photophysical behaviour of **2** is summarized in table 5.1. The emission profile shows a unique band with maximum at 496 nm which is ascribable to a  $^3\text{CC}$  transition. According to that, it is presumable that metallophyllic interactions are present in the structure. The metal/ligand stoichiometry ratio has been determined by TGA analysis that shows a weigh loss of 17.7% consistent with the loss of one ligand molecule from an asymmetric unit of  $\text{Cu}_2\text{I}_2(3\text{picolamine})_2$  (see Appendix E). Once **2** has been heated up to 130°C it start to convert into **1** until a complete transformation has been achieved at 180°C as best described in VT-XRPD analysis reported in figure 5.6. The phase **1** was still stable once the sample has been cooled at rt.

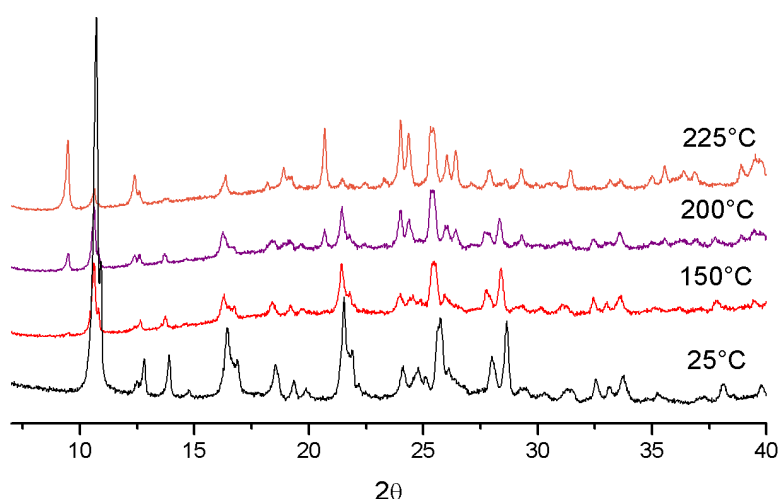


Figure 5.6 | VT-XRPD analysis plot; at 150°C **2** starts convert into **1**; at 225°C **2** completely transforms into **1** that is still stable once cooled at ambient temperature.

## Conclusion

Two different compounds based on copper iodide and 3-(aminomethyl)pyridine have been synthesized and characterized.

The structure of the **1** consists in a metal-organic framework based on copper iodide coordination polymers bridged by 3-(aminomethyl)pyridine bi-dentate ligands. The layers of **1** has been solved by XRPD data. It showed an overall white emission at ambient temperature due to the co-presence of complementary  $^3\text{CC}$  and  $^3\text{XLCT}$  emission bands. A thermal induced transition **2** to **1** has been observed at 150°C as a consequence of one ligand loss in the asymmetric unit.

## Experimental Section

### General

All glassware was dried in an oven set to a temperature of 80°C for 24h prior to use. All reagents were purchased from Sigma Aldrich and used without further purification.

### Synthesis of catena(bis( $\mu_3$ -iodo(3-aminomethyl)pyridine))-copper(I)

CuI (3mmol; 0.570 gr) was dissolved in 50mL or acetonitrile at 80°C, when the solution turned limpid, the ligand (1mmol; 100 $\mu$ L) was added whit a syringe under stirring for 30 second. A high crystalline whitish powder precipitated at the bottom of the flask, than it was filtered on a bucker funnel and washed with acetonitrile.

### Synthesis of Cu<sub>2</sub>I<sub>2</sub>(3-picoline)<sub>2</sub>

CuI (1mmol; 0.190 gr) was dissolved in minimum amount of KI saturated aqueous solution at rt, when the solution turned limpid, the ligand (1mmol; 100 $\mu$ L) was added whit a syringe under stirring. A high crystalline yellowish powder precipitated at the bottom of the flask, than it was filtered on a bucker funnel and washed with acetonitrile.

### X-ray diffraction analysis

X-Ray powder diffractograms were collected over the range 3–70° 2θ (40mW-40mA; Cu-K $\alpha_1$ , 1.54056 Å step size 0.017 2θ) on a Panalytical X'Pert PRO automated diffractometer with CuK $\alpha$  radiation and an X'Celerator equipped with an Anton Paar TTK 450 low/high-temperature camera.

### Photophysics

All determinations made use of powder samples placed between two quartz slides and were done at room temperature. Excitation and emission spectra were obtained with a SPEX Fluorolog fluorometer; excitation spectra were monitored at the maximum emission wavelength and emission spectra were recorded exciting all samples at 350nm. Absolute photoluminescence quantum yields were measured according to the method of deMello,<sup>63</sup> by using an integrating sphere customized to fit into the SPEX fluorometer sample compartment. The estimated error on the quantum yield is 10%. Luminescence lifetimes were measured with an IBH 5000F time-correlated single-photon counting apparatus, by using a pulsed NanoLED excitation source at 331 nm. Analysis of the luminescence decay profiles was accomplished with the Decay Analysis Software DAS6 provided by the manufacturer, with an estimated error on the lifetimes of 5%. All decays were monoexponential.

## References

1. T. Justel, H. Nikol and C. Ronda, *Angew. Chem.-Int. Edit.*, 1998, **37**, 3085-3103.
2. C. Feldmann, T. Justel, C. R. Ronda and P. J. Schmidt, *Adv. Funct. Mater.*, 2003, **13**, 511-516.
3. J. Kido, M. Kimura and K. Nagai, *Science*, 1995, **267**, 1332-1334.
4. G. M. Farinola and R. Ragni, *Chemical Society Reviews*, 2011, **40**, 3467-3482.
5. M.-S. Wang, S.-P. Guo, Y. Li, L.-Z. Cai, J.-P. Zou, G. Xu, W.-W. Zhou, F.-K. Zheng and G.-C. Guo, *J. Am. Chem. Soc.*, 2009, **131**, 13572-+.
6. J. Y. Li, D. Liu, C. W. Ma, O. Lengyel, C. S. Lee, C. H. Tung and S. Lee, *Adv. Mater.*, 2004, **16**, 1538-+.
7. M. Mazzeo, V. Vitale, F. Della Sala, M. Anni, G. Barbarella, L. Favaretto, G. Sotgiu, R. Cingolani and G. Gigli, *Adv. Mater.*, 2005, **17**, 34-+.
8. Y. J. Yang, M. Lowry, C. M. Schowalter, S. O. Fakayode, J. O. Escobedo, X. Y. Xu, H. T. Zhang, T. J. Jensen, F. R. Fronczek, I. M. Warner and R. M. Strongin, *J. Am. Chem. Soc.*, 2006, **128**, 14081-14092.
9. J. Luo, X. Z. Li, Q. Hou, J. B. Peng, W. Yang and Y. Cao, *Adv. Mater.*, 2007, **19**, 1113-1117.
10. J. Liu, Y. Cheng, Z. Xie, Y. Geng, L. Wang, X. Jing and F. Wang, *Adv. Mater.*, 2008, **20**, 1357-+.
11. W. H. Green, K. P. Le, J. Grey, T. T. Au and M. J. Sailor, *Science*, 1997, **276**, 1826-1828.
12. T. Hayakawa, Y. Toh, M. Oshima, M. Matsuda, Y. Hatsukawa, N. Shinohara, H. Iimura, T. Shizuma, Y. H. Zhang, M. Sugawara and H. Kusakari, *Phys. Lett. B*, 2003, **551**, 79-85.
13. L. Luo, X. X. Zhang, K. F. Li, K. W. Cheah, H. X. Shi, W. K. Wong and M. L. Gong, *Adv. Mater.*, 2004, **16**, 1664-+.
14. Y. L. Liu, B. F. Lei and C. S. Shi, *Chem. Mater.*, 2005, **17**, 2108-2113.
15. G. J. Zhou, Q. Wang, C. L. Ho, W. Y. Wong, D. G. Ma and L. X. Wang, *Chemical Communications*, 2009, 3574-3576.
16. P. Coppo, M. Duati, V. N. Kozhevnikov, J. W. Hofstraat and L. De Cola, *Angew. Chem.-Int. Edit.*, 2005, **44**, 1806-1810.
17. R.-S. Liu, V. Drozd, N. Bagkar, C.-C. Shen, I. Baginskiy, C.-H. Chen and C. H. Tan, *J. Electrochem. Soc.*, 2008, **155**, P71-P73.
18. H. S. Chen, S. J. J. Wang, C. J. Lo and J. Y. Chi, *Applied Physics Letters*, 2005, **86**.
19. X. M. Sui, C. L. Shao and Y. C. Liu, *Applied Physics Letters*, 2005, **87**.
20. T. Uchino and T. Yamada, *Applied Physics Letters*, 2004, **85**, 1164-1166.
21. L. He, J. Qiao, L. Duan, G. Dong, D. Zhang, L. Wang and Y. Qiu, *Adv. Funct. Mater.*, 2009, **19**, 2950-2960.
22. T. Tsuzuki, Y. Nakayama, J. Nakamura, T. Iwata and S. Tokito, *Applied Physics Letters*, 2006, **88**, 243511-243513.
23. C.-H. Yang, Y.-M. Cheng, Y. Chi, C.-J. Hsu, F.-C. Fang, K.-T. Wong, P.-T. Chou, C.-H. Chang, M.-H. Tsai and C.-C. Wu, *Angew. Chem.-Int. Edit.*, 2007, **46**, 2418-2421.
24. L. Flamigni, A. Barbieri, C. Sabatini, B. Ventura and F. Barigelli, in *Photochemistry and Photophysics of Coordination Compounds II*, eds. V. Balzani and S. Campagna, 2007, vol. 281, pp. 143-203.
25. T. Hofbeck and H. Yersin, *Inorg. Chem.*, 2010, **49**, 9290-9299.
26. W. Y. Wong, Z. He, S. K. So, K. L. Tong and Z. Y. Lin, *Organometallics*, 2005, **24**, 4079-4082.
27. P. Brulatti, V. Fattori, S. Muzzioli, S. Stagni, P. P. Mazzeo, D. Braga, L. Maini, S. Milita and M. Cocchi, *J. Mater. Chem. C*, 2013, **1**, 1823-1831.
28. J. H. Kim, M. S. Liu, A. K. Y. Jen, B. Carlson, L. R. Dalton, C. F. Shu and R. Dodda, *Applied Physics Letters*, 2003, **83**, 776-778.
29. P.-T. Chou and Y. Chi, *Eur. J. Inorg. Chem.*, 2006, 3319-3332.
30. H. Yersin, *Highly Efficient OLEDs with Phosphorescent Materials*, Wiley-VCH, Weinheim, 2008.
31. H. Yersin, *Transition Metal and Rare Earth Compounds III*, 2004, **241**, 1-26.
32. A. Barbieri, G. Accorsi and N. Armaroli, *Chemical Communications*, 2008, 2185-2193.
33. C.-W. Hsu, C.-C. Lin, M.-W. Chung, Y. Chi, G.-H. Lee, P.-T. Chou, C.-H. Chang and P.-Y. Chen, *J. Am. Chem. Soc.*, 2011, **133**, 12085-12099.
34. D. Volz, D. M. Zink, T. Bocksrocker, J. Friedrichs, M. Nieger, T. Baumann, U. Lemmer and S. Bräse, *Chem. Mater.*, 2013, **25**, 3414-3426.
35. D. M. Zink, M. Bachle, T. Baumann, M. Nieger, M. Kuhn, C. Wang, W. Klopper, U. Monkowius, T. Hofbeck, H. Yersin and S. Bräse, *Inorg. Chem.*, 2012, **52**, 2292-2305.
36. D. M. Zink, T. Baumann, J. Friedrichs, M. Nieger and S. Bräse, *Inorg. Chem.*, 2013.

37. F. De Angelis, S. Fantacci, A. Sgamellotti, E. Cariati, R. Ugo and P. C. Ford, *Inorg. Chem.*, 2006, **45**, 10576-10584.
38. P. C. Ford, *Coord. Chem. Rev.*, 1994, **132**, 129-140.
39. M. Vitale and P. C. Ford, *Coord. Chem. Rev.*, 2001, **219-221**, 3-16.
40. H. D. Hardt and H. Gechnizdjani, *Z. Anorg. Allg. Chem.*, 1973, **397**, 23-30.
41. H. D. Hardt and A. Pierre, *Inorg. Chim.*, 1977, **25**, L59-L60.
42. Y. Cui, H. Xu, Y. Yue, Z. Guo, J. Yu, Z. Chen, J. Gao, Y. Yang, G. Qian and B. Chen, *J. Am. Chem. Soc.*, 2012, **134**, 3979-3982.
43. P. P. Mazzeo, L. Maini, D. Braga, G. Valenti, F. Paolucci, M. Marcaccio, A. Barbieri and B. Ventura, *Eur. J. Inorg. Chem.*, 2013, **2013**, 4459-4465.
44. C. H. Arnby, S. Jagner and I. Dance, *CrystEngComm*, 2004, **6**, 257-275.
45. R. Peng, S. R. Deng, M. Li, D. Li and Z. Y. Li, *CrystEngComm*, 2008, **10**, 590-597.
46. S. Q. Bai, J. Y. Kwang, L. L. Koh, D. J. Young and T. S. A. Hor, *Dalton Trans.*, 2010, **39**, 2631-2636.
47. Z. Liu, M. F. Qayyum, C. Wu, M. T. Whited, P. I. Djurovich, K. O. Hodgson, B. Hedman, E. I. Solomon and M. E. Thompson, *J. Am. Chem. Soc.*, 2011, **133**, 3700-3703.
48. Z. Liu, P. I. Djurovich, M. T. Whited and M. E. Thompson, *Inorg. Chem.*, 2011, **51**, 230-236.
49. S. Perruchas, X. F. L. Goff, S. Maron, I. Maurin, F. o. Guillen, A. Garcia, T. Gacoin and J.-P. Boilot, *J. Am. Chem. Soc.*, 2010, **132**, 10967-10969.
50. H. D. Hardt and A. Pierre, *Fresenius' Z. Anal. Chem. FIELD Full Journal Title:Fresenius' Zeitschrift fuer Analytische Chemie*, 1973, **265**, 337-339.
51. C. Tard, S. Perruchas, S. Maron, X. F. Le Goff, F. Guillen, A. Garcia, J. Vigneron, A. Etcheberry, T. Gacoin and J. P. Boilot, *Chem. Mater.*, 2008, **20**, 7010-7016.
52. D. Sun, S. Yuan, H. Wang, H.-F. Lu, S.-Y. Feng and D.-F. Sun, *Chemical Communications*, 2013, **49**, 6152-6154.
53. A. Bondi, *J. Phys. Chem.*, 1964, **68**, 441-451.
54. J.-R. Li, R. J. Kuppler and H.-C. Zhou, *Chemical Society Reviews*, 2009, **38**, 1477-1504.
55. L. J. Murray, M. Dinca and J. R. Long, *Chemical Society Reviews*, 2009, **38**, 1294-1314.
56. S. Ma and H.-C. Zhou, *Chemical Communications*, 2010, **46**, 44-53.
57. L. Ma, C. Abney and W. Lin, *Chemical Society Reviews*, 2009, **38**, 1248-1256.
58. S. Achmann, G. Hagen, J. Kita, I. Malkowsky, C. Kiener and R. Moos, *Sensors*, 2009, **9**, 1574-1589.
59. M. D. Allendorf, C. A. Bauer, R. K. Bhakta and R. J. T. Houk, *Chemical Society Reviews*, 2009, **38**, 1330-1352.
60. D. Braga, L. Maini, P. P. Mazzeo and B. Ventura, *Chem. Eur. J.*, 2010, **16**, 1553-1559.
61. S. A. Sapchenko, D. G. Samsonenko, D. N. Dybtsev, M. S. Melgunov and V. P. Fedin, *Dalton Trans.*, 2011, **40**, 2196-2203.
62. Bruker AXS, Karlsruhe, Germany, 2008, *TOPAS v.4.2: General Profile and Structure Analysis Software for Powder Diffraction Data*.
63. A. Barbieri and G. Accorsi, *EPA Newsletters*, December 2006, 26-35.

# Chapter 6

Thin Film deposition and  
OLED preparation



## Introduction

Copper (I) complexes are abundantly described in the previous chapter as good candidate for OLED devices. Few examples are already reported in literature<sup>1-4</sup> with good performance parameters and it is plausible to think that the use of d<sup>10</sup> complexes will increase in the next years as active material in luminescent devices. However many problems still remain unsolved. The copper (I) complexes are generically not very soluble and it means that deposition processes such as drop casting or spin coating, which still remain the easiest way to deposit the emission layer, cannot be used in this case. Volz *et al.* elude this problems with a series of extraordinary high efficient binuclear copper iodide complexes based on 2-pyridil-bisphosphine ligand in which one ligand molecule binds in chelating mode the two metal atoms while other two ancillary ligands bond just one metal atom each.<sup>1,2</sup> These kinds of complexes are soluble in organic solvents and are easily deposited via drop casting. However if the complexes still remain insoluble in organic solvents (or even soluble in not-suitable solvent for optoelectronic apparatus) the emissive layer can be deposit by sublimation in a high vacuum chamber. The complex stability to those extreme conditions (high temperature/ low pressure) treatment still remains the key problem to the applicability of this method. To avoid this problem it is possible to synthesize “bigger” complexes with *ad hoc* designed ligand (usually to enhance the lone pair back donation from the ligand to the metal d-orbital), with the aim of improve the stability performances of the complex in the sublimation process.

Herein, our experience on emissive layer deposition is reported as a step-by-step improvement path. Also a new non-conventional layer-by-layer deposition route has been suggested and a preliminary OLED device prototype has been proposed.

## General procedure for thin film high vacuum deposition on glass substrates

A microscope glass slide was cut in a 2.5 cm square plate. The glass surface has to be carefully cleaned before to be used as substrate for film deposition in order to obtain a much more uniform film and decrease the roughness of the deposited layer. First of all the glass were cleaned mechanically with a powder-free paper and acetone to roughly take out powder particles than, the slide were held by a acetone filled sample holder and placed in a ultrasonic bath for 20 minutes. To complete the cleaning step, the glass slide were then bring in a “clean room” where were exposed to a very low wavelength ultraviolet beam to remove all the impurities and to prepare the surface to the film grafting. The clean room is a special laboratory in where the inner atmosphere has filtered to prevent the powder particles creation particularly on the glass slide. In the clean room a special work wear is required to prevent the air pollution.

The vapour deposition was performed with sublimation equipment. Few milligrams of the solid material that have to be deposited on the glass slide were put inside a tungsten boat placed in between the two electrodes. The glass substrate was located on an appropriate sample holder right above the sublimation source, in the range of the sublimation cone (figure 6.1). The space gap between the sample holder and the sublimation source has optimized to deposit a good and uniform coverage of the glass slide and to limit the film roughness. After checked the sample and the substrate were place in the right position, a  $2 \times 10^{-6}$  mBar pressure were obtained by a vacuum pumping system.

Once the desired pressure was reached, the voltage applied to the electrodes was gently increased to get a constant rate of sublimation as deposition (usually in the range of 0.2-0.4 nm s<sup>-1</sup>). A really sophisticated balance, based on the resonance frequency of quartz crystal, fixed at a known distance from the glass substrate, records the amount of material that is being deposited and the instantaneous deposition rate. All depositions were made in the same experimental conditions of pressure and deposition rate.

---

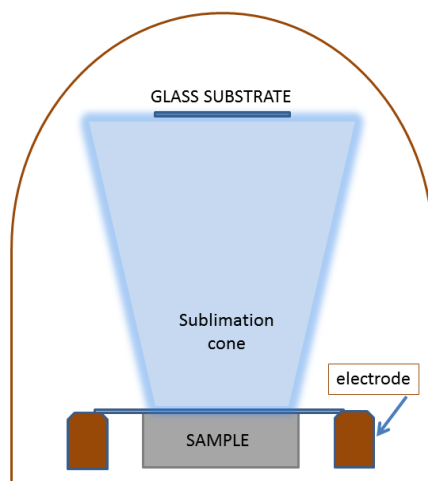


Figure 6.1 | Schematic representation of sample and substrate disposition inside the sublimation's bell

---

### Direct complex sublimation

Direct vacuum sublimation of complex Cu<sub>2</sub>I<sub>2</sub>PN<sub>3</sub> (PN=2-pyridyl(bisphenylphosphine)) (Chapter 4) on a glass substrate produced an heterogeneous and non-uniform white film. We select the titled compounds since it was very well characterized (both by us and by Baumann *et. al*)<sup>1</sup> and it get a fantastic high emission quantum yield value approximately in the range between 80 and 90%. Even if the absorption spectrum could not be obtained directly on then sample deposited on the glass slide because of the large scattering due to the non-uniformity of the film, in the Figure 6.2b are shown the

excitation and emission spectra. The emission band is centered at 518 nm with a shoulder near 700 nm. In the excitation spectrum both the complex absorption at around 350 nm and the CuI absorption at around 420 nm are present.

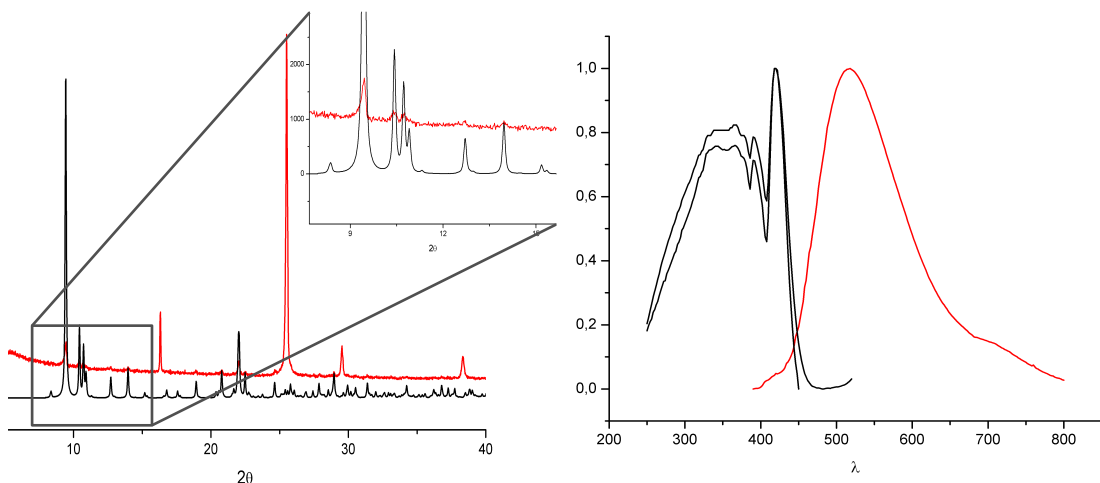


Figure 6.2| (a) Comparison between the sublimation product (red line) and the calculated pattern of Cu<sub>4</sub>I<sub>4</sub>PN<sub>2</sub> (black line). Low angle diffraction is magnified in the box (left); (b) Normalized excitation (black line) and emission (red line) spectra for the sublimation of the complex Cu<sub>2</sub>I<sub>2</sub>PN<sub>3</sub> (right)

### CuI thin films

Direct deposition of the complex into film was unsuccessful due to the degradation of the complex at high temperature and low pressure. Having stated that a solid-vapour reaction occurred when the copper iodide crystalline powder was exposed to the ligand vapours at room temperature, the same gas-solid reaction was attempted with a CuI thin film. This procedure has, of course, lots of experimental parameters that might be optimized also to increase the reproducibility of the process (e.g. distance between the glass support and the ligand powder, the temperature of the system which is directly linked to the reaction rate etc.)

There are many papers in literature speaking about copper iodide thin films<sup>5-11</sup>, and we decided to sublime CuI in a high vacuum chamber. A thin copper iodide layer was deposited on a polished glass slide by high-vacuum sublimation obtaining a polycrystalline, uniform, and smooth layer. The X-ray diffraction analysis performed on the sample (Figure 6.3) has shown us a unique peak at  $\approx 25^\circ$  2θ which correspond to a  $\gamma$ -CuI preferred oriented (111) Miller plane<sup>12</sup>.

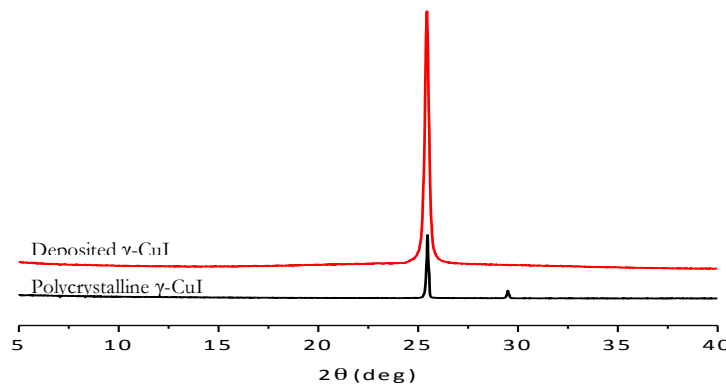


Figure 6.3 | Comparison between polycrystalline and sublimed  $\gamma$ -CuI samples.

The  $\gamma$ -phase is the stable until 350°C and it is the commercial form we usually used also in wet reactions. The transmission spectrum (Figure 6.4a) was recorded on a 100 nm thick CuI sample and it is coherent with the previously reported on polycrystalline material<sup>7</sup>. Two peaks are shown in the spectrum: the main one at 406 nm (3.06 eV), the less intense at 336 nm (3.69 eV). The band gap is calculated approximately at 3.1 eV<sup>13, 14</sup>. The energy difference between the two bands (0.63 eV) is coherent with the spin-orbit splitting of the higher CuI valence band ( $\Gamma_{15,2}$ ) reported in literature (0.64 eV)<sup>3</sup>. The evaluation of the sample roughness has been performed by AFM analysis (Figure 6.4b). On 35nm thick samples, the mean value of roughness is about 3 nm, so less than 10%. A so high value was also due to the glass support.

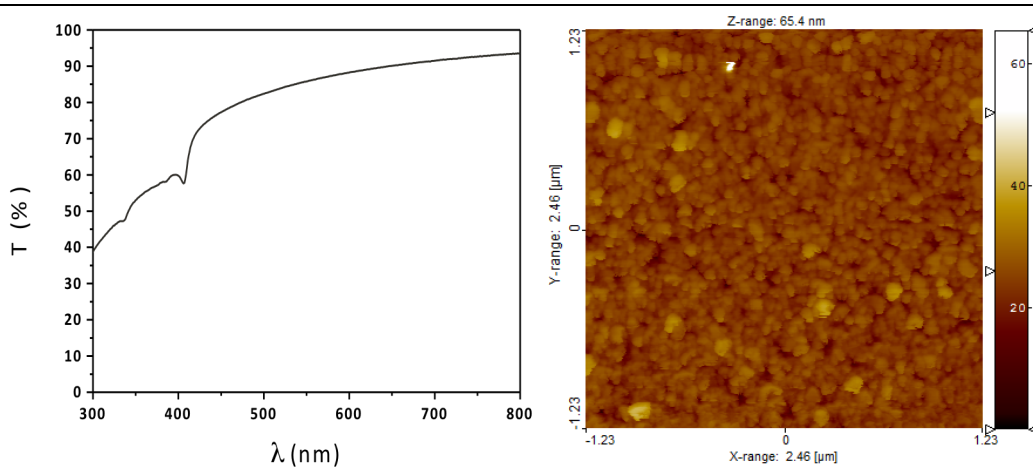
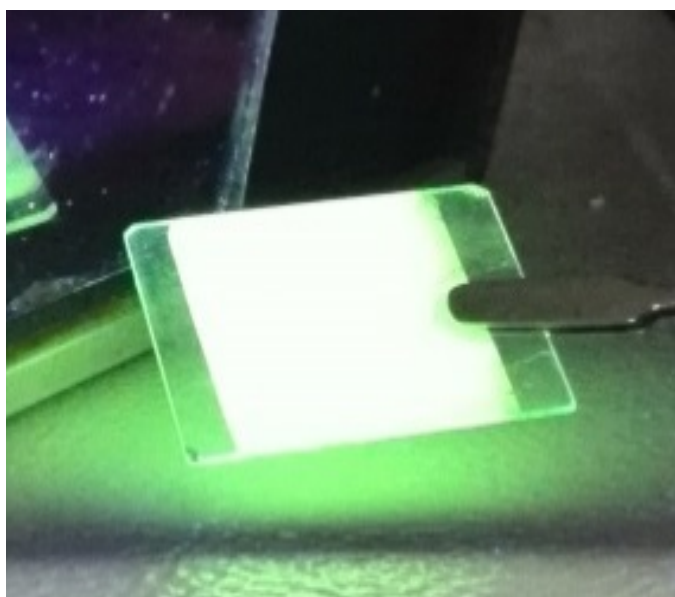


Figure 6.4 | (a) (left) Transmission spectrum of the 100nm thick CuI samples. The two peaks at 336 and 406 are shown. A long range of transparency in the visible region is recorded; (b) (right) AFM analysis performed on 35nm thick CuI samples deposited on glass slide.

### Gas-solid reactions

The CuI film was exposed to ligand vapours into a closed chamber until complete reaction, as suggested from the absence of any CuI peak in the XRPD analysis. Our best results have been obtained exposing a 35 nm thick CuI layer to the vapours of quinuclidine and of 3-quinuclidinol at room temperature. The X-ray diffraction analysis directly performed in Bragg-Brentano geometry on these films shows that they are both amorphous. The photoluminescence spectra of both films are in agreement with the emission spectra of the  $\text{Cu}_4\text{I}_4\text{quinuclidine}_4$  (**4** in chapter 3) and  $\text{Cu}_4\text{I}_4(3\text{-quinuclidinol})_4$  form **a** (**5a** in chapter 3) powders respectively. A sample obtained by reacting the CuI film with quinuclidine and showing a green luminescence when exposed to UV radiation ( $\lambda=365$  nm) is reported in figure 3.7.

An alternative procedure has been attempted to deposit a thin film of the complex. Once the copper iodide has been sublimed on a glass slide, it was dipped in a ligand ethanol solution. In this case, the ligand use was 2-pyridin(bisphenylphosphine) (PN) and, since the sample was characterized by a very high luminescence (Figure 6.5), it was however characterized by a too high roughness value to be used in a OLED device.



---

Figure 6.5 | First result obtained by dipping of the CuI in an ethanol solution of the ligand. Exposed under UV-light at 365 nm

### Layer-by-layer deposition (*LBL*)

The improvement of the complex deposition experiment was done subliming sequentially CuI and the ligand. For this procedure we decided to use 2-pyridin(bisphenylphosphine) as ligand. A 80 nm thick layer of copper iodide has been deposited as previously described and 40 nm of ligand have been sequentially deposited on top. The emission spectra of the sample (**A**) was coherent with the one of  $\text{Cu}_2\text{I}_2\text{PN}_3$  complex which definitely points out that the solid-gas reaction has taken place.

---

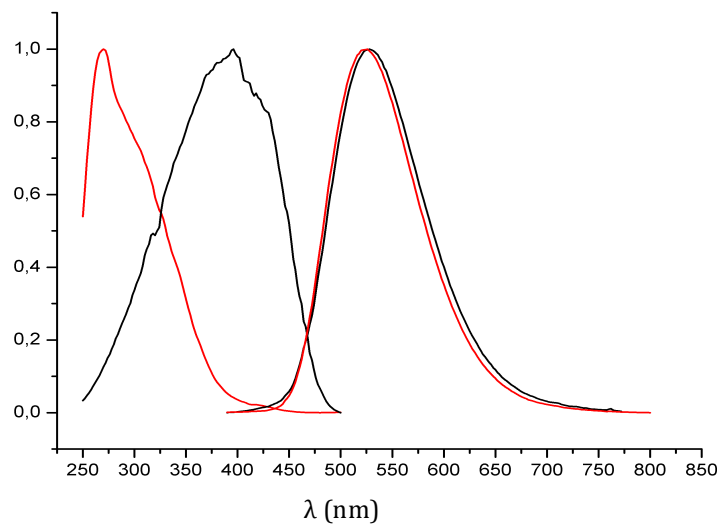


Figure 6.6 | Excitation and Emission spectra of polycrystalline  $\text{Cu}_2\text{I}_2\text{PN}_3$  (black line), and after layer-by-layer deposition of reagents (red line)

---

The excitation spectrum (red curve in figure 6.6) does not show any appreciable absorption by the very thin layer of the complex. Instead, it is representative of the 80 nm thick CuI film and proves the sensitization of the complex emission by energy transfer from CuI. To increase the complex film thickness, a layer-by-layer deposition has been performed. To maintain the CuI-PN stoichiometry ratio 1:1.5 as in the complex, simply mass consideration has been taken into account as different reagent density ( $\rho(\text{CuI}) = 5.7 \text{ g/cm}^3$ ;  $\rho(\text{PN}) = 1.4 \text{ g/cm}^3$ ) and the consequently different number of molecules deposited in a volume unit by sublimation process. The result suggests that to maintain the 1:1.5 stoichiometry ratio between the reagents, a ratio of 1:8 in thickness respectively of CuI and PN has to be used in the sublimation process. So that, 2 nm thick CuI layer has been deposited on top of the samples (**A**) and 16 nm thick PN layer followed it. This procedure was repeated two times (**B** and **C**). The emission spectra reported in figure 6.7a show a progressive increase of the complex emission intensity. Since the CuI emission intensity increases as well, we can estimate that not all the copper iodide deposited sequentially reacts with the ligand and it kick up the complex emission by layer-by-layer energy transfer process. The XRD analysis performed on the final

sample (C) has shown the preferred oriented (001) miller plane of the complex  $\text{Cu}_2\text{I}_2\text{PN}_3$  which suggest the lattice was deposited along the crystallographic c-axis as represented in figure 6.8.

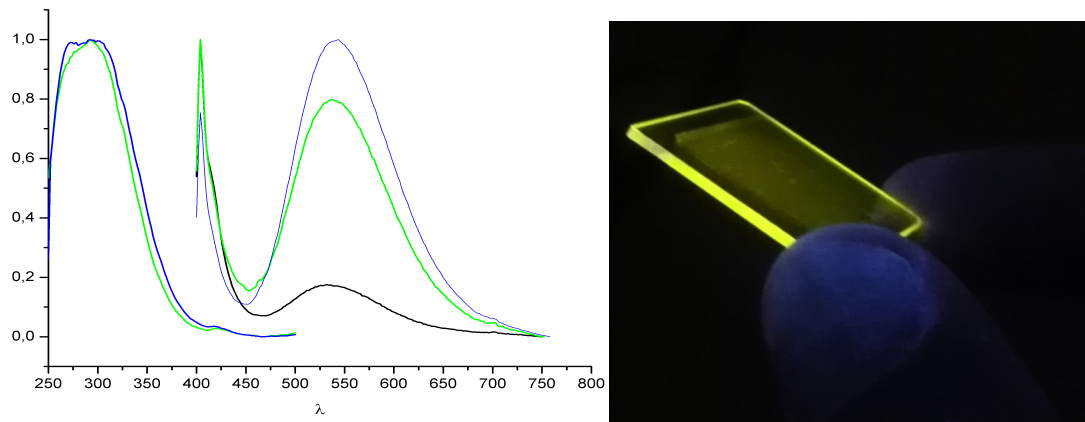


Figure 6.7 | (a) (left) Normalized excitation emission spectra for the samples with different layers: emission spectrum for sample (A) with 80nm copper iodide and 40 nm PN (black line), excitation and emission spectra for the sample with more 2 nm CuI layer and 16 nm PN layer deposited once (B) (green line) and two times (C) (blue line); (b) (right) Crystalline film obtained with layer-by-layer deposition of CuI and PN under UV-light at 254 nm.

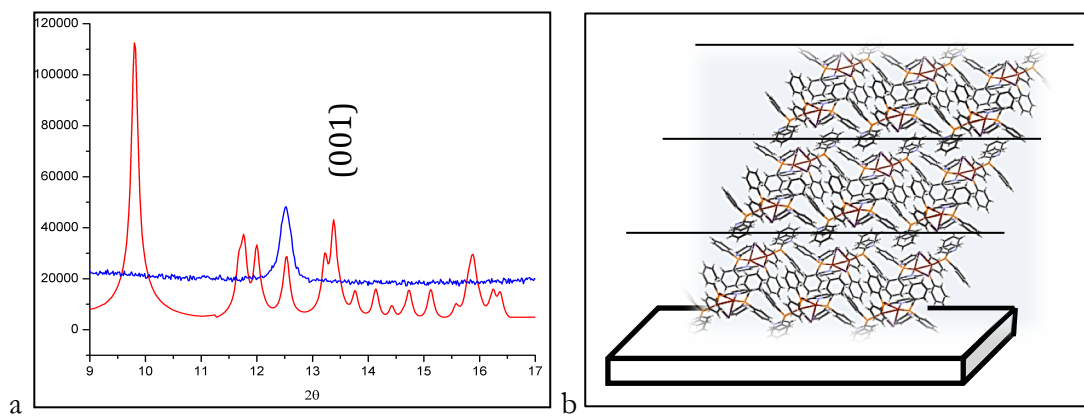


Figure 6.8| (a) X-ray powder pattern of polycrystalline  $\text{Cu}_2\text{I}_2\text{PN}_3$  (red line) and the sample (C) deposited on glass slide (blue line); (b) Schematic rappresentation of how the molecules crsytallize on the slide during the sublimation process.

## OLED design and preparation

The preparation of an OLED device consists in a step-by-step deposition of different layers with different functions. We proposed an example that might be optimized. The

substrate was prepared cutting a 2.5cm square piece from a bigger glass slide covered by ITO on one side. It was, than, scraped off by etching process: the central zone was sheltered by an insoluble foil while it was treated with an “*aqua regia*” solution to remove the ITO from the bordering, non-covered zone. The substrate for OLED was obtained as shown in figure 6.9. Afterwards the substrate was cleaned as described before (see general procedure). The layers were deposit by LBL deposition: a schematic representation of the layers is reported in figure 6.10.

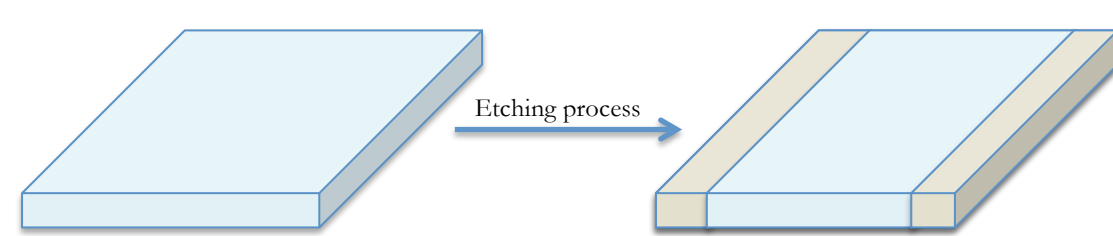


Figure 6.9 | Substrate schematic representation before (left) and after (right) etching. The cyan area represent the ITO on the substrate.

The first 80 nm CuI layer plays a double role of both *hole transport layer* and reactant for the formation of the complex with the followed 40 nm of PN. As better described in the previous paragraph, to increase the emission intensity from the *emitting layer*, layer-by-layer deposition of 2nm CuI and 16 nm PN layers has been done twice. A 25nm of TPBI (1,3,5-tris(N-phenylbenzimidazole-2-yl)benzene) and 0.5 LiF have been added respectively as *electron transport layer* and *electron injection layer*. The last 100nm thick Aluminum layer has deposited as *counter electrode*

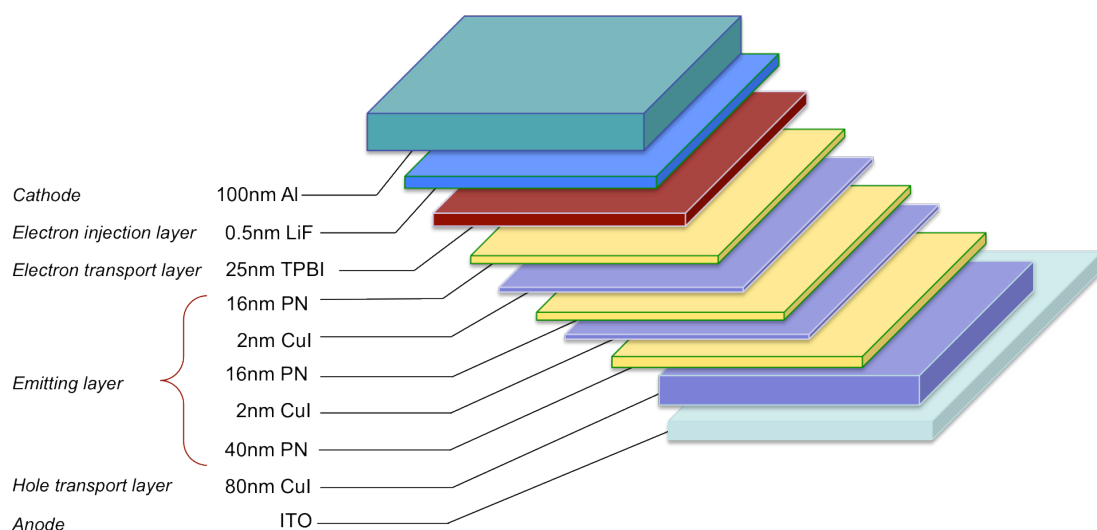


Figure 6.10 | Schematic representation of OLED device based on LBL deposition process

When a low voltage (2-4 V) was applied to the OLED a rather large current flow was recorded and some light output was observed as short blinks. No continuous light emission could be observed. This behavior is maybe due to a large non uniformity of the deposited film which results in a non-uniform applied electric field that can rise to a very high current flows with high temperature and device damage in the thinnest parts. Moreover the CuI conductivity is rather high and a larger layer thickness is needed to have a better charge balance in the emitting layer. More experiments are needed to improve the film deposition and try different device architectures (thicknesses, types of electron transport layer, cathodes etc.)

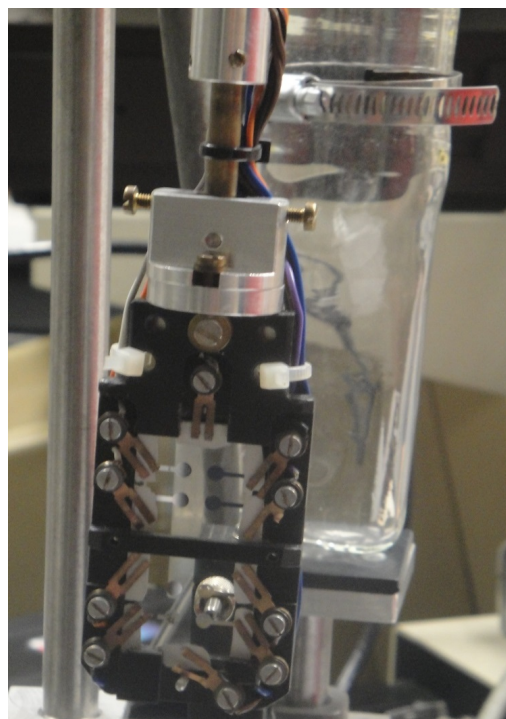


Figure 6.11 | Device for the characterization of the OLED; in background, the glass container for Ar atmosphere.

## References

1. D. Volz, M. Nieger, J. Friedrichs, T. Baumann and S. Bräse, *Langmuir*, 2013.
2. D. Volz, D. M. Zink, T. Bocksrocker, J. Friedrichs, M. Nieger, T. Baumann, U. Lemmer and S. Bräse, *Chem. Mater.*, 2013, **25**, 3414-3426.
3. D. M. Zink, M. Bachle, T. Baumann, M. Nieger, M. Kuhn, C. Wang, W. Klopper, U. Monkowius, T. Hofbeck, H. Yersin and S. Bräse, *Inorg. Chem.*, 2012, **52**, 2292-2305.
4. D. M. Zink, T. Baumann, J. Friedrichs, M. Nieger and S. Bräse, *Inorg. Chem.*, 2013.
5. T. Tanaka, K. Kawabata and M. Hirose, *Thin Solid Films*, 1996, **281**, 179-181.
6. D. Kim, M. Nakayama, O. Kojima, I. Tanaka, H. Ichida, T. Nakanishi and H. Nishimura, *Physical Review B*, 1999, **60**, 13879-13884.
7. P. M. Sirimanne, M. Rusop, T. Shirata, T. Soga and T. Jimbo, *Chem. Phys. Lett.*, 2002, **366**, 485-489.

8. Yang and Q. Gao, *Langmuir*, 2005, **21**, 6866-6871.
9. X. Hu, J. C. Yu, J. Gong and Q. Li, *Cryst. Growth Des.*, 2007, **7**, 262-267.
10. Z. Zheng, A. Liu, S. Wang, B. Huang, K. W. Wong, X. Zhang, S. K. Hark and W. M. Lau, *J. Mater. Chem.*, 2008, **18**, 852-854.
11. H. Kang, R. Liu, K. Chen, Y. Zheng and Z. Xu, *Electrochim. Acta*, 2010, **55**, 8121-8125.
12. P. M. Sirimanne, M. Rusop, T. Shirata, T. Soga and T. Jimbo, *Mater. Chem. Phys.*, 2003, **80**, 461-465.
13. W. Sekkal and A. Zaoui, *Physica B: Condensed Matter*, 2002, **315**, 201-209.
14. M. Certier, M. Soltani, O. Pages, A. Zaoui, W. Sekkal and H. Aourag, *Materials Science and Engineering: B*, 1999, **58**, 234-237.

# Chapter 7

Structure determination from X-ray powder  
diffraction data (SDXRPD)



## Introduction

The art of solving from powder diffraction data has developed rapidly and powder diffraction itself has played a central role in structural chemistry, physics and material sciences over the past ten years. Important advantages in structural studies of materials, ranging from high temperature superconductor to molecular hydrogen storage to luminescent materials, have relied heavily on the powder diffraction techniques. If taking into account both the developments of molecular materials and the consequent need of a deeper knowledge of how these materials work at the atomic level, it becomes clear that structure determination represents a key procedure to understand their properties and to design new tailor made compounds. For these reasons a great effort has been devoted to tackle this problem. Structure determination is the bread and butter of a solid state scientist. Solving the 3D-structure of a molecular material by performing a single crystal X-ray diffraction analysis is nowadays, relatively easy. However, having at least a single crystal suitable in dimensions and purity is a prerequisite for this analysis. This still remains the bottleneck step and, in the worst case, even if a single crystal has been obtained, it might not correspond to the interesting bulk powder<sup>1</sup>

In fact, the developments in powder diffraction have been driven by a growing need for tools that are able to probe the structures of materials that are only available in powder form, or can only be studied as powders (e.g. under difficult *in situ* conditions). In these ill-fated cases, structure solution from powder data seems to be the only way to win the day, even if the route to a successful structure determination is still by no means as straightforward and routine as it is with single-crystal diffraction. Unfortunately, structure determination from powder diffraction data is much more complex than from single crystal data: this is associated almost entirely with the collapse of the three dimensions of crystallographic information onto the single dimension of the powder pattern.<sup>2</sup>

The aim of this chapter is not to teach how to achieve the right and successful strategy to solve structure by powder diffraction data or even to evaluate the best route one can hike over all the possibilities (for that I could recommend to read the book *Structure determination from powder data* edited by W. David, K. Shankland, L. McCusker, Ch. Baerlocher that was my bible and my source of inspiration during the last years), but to contextualize the use of this technique into my research area. The structure determination process can be considered a search for the successful way through a maze, sometimes the best one could be neither the shortest nor the simplest one. Although there are many paths leading to the center, which represents, in our consideration, the target of the molecular structure, they are not all appropriate or even practicable for a given problem and the user experience could play a key role to finally solve the structure.

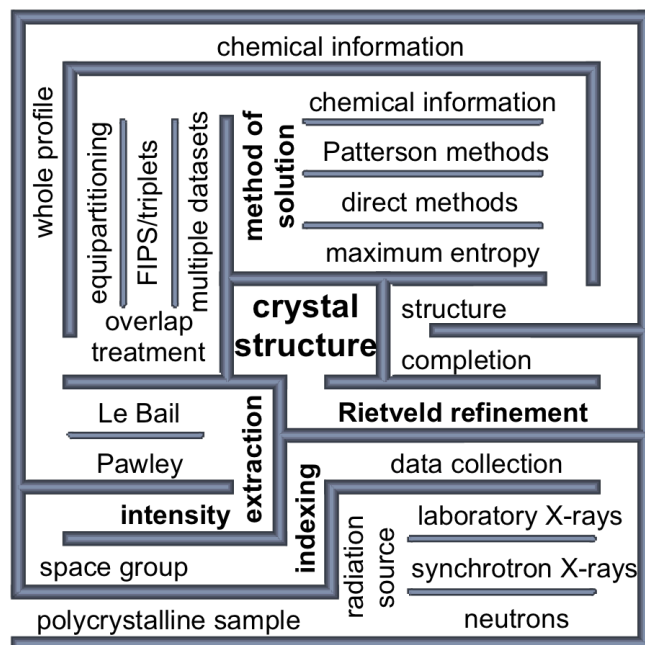


Figure 7.1 | The structure determination maze.

As I already reported in previous chapters, since the introduction paragraph, the copper iodide complexes are characterized by a plethora of coordination geometries which arise from the many possible combinations of coordination numbers (two, three and four) available for copper(I) and geometries that can be adopted by the halide ions (from terminal to  $\mu^2$ - and up to  $\mu^8$ -bridging)<sup>3</sup>.

Predicting *a priori* the geometry of the complex synthesized, still remains a tricky step. Although in our previous works, we synthesized lots of these kinds of complexes, and nowadays we have the feeling to approach this problem, the only knowledge of the reaction conditions, like solvent and reactants ratio used, is still not sufficient to predict the final product geometry, even if they influence it dramatically. In our routine, before starting to solve the complexes structure by XRPD data, the powder itself is characterized as much as possible by thermal analysis like DSC and TGA to try, at least, to clarify the ratio between the metal atoms and the ligand molecules. Elemental analysis could also be recommended. More routine-less analyses are suggested to understand the right coordination pattern like SS-NMR or FTIR.

When the stoichiometry ratio is determined unequivocally, the following step is to work on sample: as McCusker suggested in her work, “*everything depends upon the sample itself; [...] time invested in producing a high quality polycrystalline sample (e.g. high purity and crystallinity) prior to a structural investigation is time well spent*”. The grade of success will depend upon the

quality of the data and these, in turn, depend in quality of the sample. So, come back to the lab to improve, recipe in the hand, the sample purity and crystallinity and, once hit the target, the data collection is performed as best as possible increasing the exposition time and reducing the step size.

Working with lab data (and with  $\text{K}\alpha_1$  and  $\text{K}\alpha_2$  Cu radiation source) makes indexing step ever more tricky than it actually is and the determination of the correct lattice parameters comes out from several considerations. The golden rule is that the lattice volume should be coherent with the stoichiometry previously found and than, it is a good practice to use different indexing algorithms: if they give the same lattice parameters, it could be a signal that it is the right path.

Before moving to the solution step, other few considerations have to be done:

1. the space group have to be determined and even if it is suggested by the indexing software it has to be reasonable with the hypothesized geometry.
2. once the stoichiometry have been defined, the coordination pattern have to be theorized according to symmetry elements in the SP, since, copper iodide complexes could arrange in the different way with the same stoichiometry (e.g. closed or open cubane clusters, di- or tetranuclear clusters)
3. the coordination patter will be dramatically influenced by the number of the active binding sites: for multidentate ligands the discrimination of the number of the effective binding sites they used to bound the metal centre with will be a good starting point for preliminary z-matrix writing.

The complexity could increase much more than this considering that copper iodide compounds are well known also to grow in mono-dimensional polymeric chains or bi-dimensional layers<sup>4</sup> or even in metal-organic frameworks (porous or not)<sup>5</sup>.

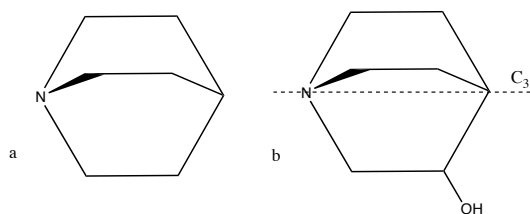
The aim of these questions does not want to be to discourage to solve structure of copper iodide complexes from powder diffraction data but to underline how challenging it is and to justify the small number of copper(I) complexes solved by XRPD reported in literature. In the previous chapters few examples of structure solution from powder data of copper(I) complexes have been reported (chapter 3, 4 and 5) without any emphasis on the strategy used to solve the structure. In those cases different approach have been followed to hit the mark and in the next paragraphs I just want to sum up the step list has been carried on.

### Structure determination of $\text{Cu}_4\text{I}_4(3\text{-quinuclidinol})_4$

Two crystal forms of  $\text{Cu}_4\text{I}_4(3\text{-quinuclidinol})_4$  (**5a** and **5b**) (name are consistent with those reported in chapter 3) have been obtained by reacting CuI with 3-quinuclidinol. Single crystals of **5a** could not be obtained, but its powder X-ray

diffraction pattern shows it to be isomorphous with Cu<sub>4</sub>I<sub>4</sub>quinuclidine<sub>4</sub> structure (**4**) (Figure 3.3 page 52). The unit cell parameter of **5a** was easily refined using the cell parameter of **4** as starting point. The structure of **5a** was then solved from the powder data using, as initial coordinates for rigid-body Rietveld refinement, the structure of the compound **4** conveniently modified by changing the H atoms into O-H groups in positions 3, 5 and 8 with respect to N in the quinuclidinol ligand with 1/6 occupancy (because of the rotation along C<sub>3</sub> and of the chirality of the ligand in those positions).

---



---

Figure 7.2 | Sketches of a) quinuclidine and b) 3-quinuclidinol

---

The position of the hydroxyl groups results to be disordered and although the hydroxyl groups belonging to different clusters could form hydrogen bonds, a hydrogen bond pattern cannot be identified.

PXRD data of **5a** were collected over the range 3–70° 2θ (2kW; Cu-Kα<sub>1</sub>, 1.54056 Å step size 0.017 2θ), using a variable count time scheme.<sup>2</sup> The Bruker D8 Advance diffractometer was equipped with a LynxEye detector. The data set was background modelled with a 6 parameters Chubychev function and truncated to 50° 2θ for Pawley fitting ( $\chi^2 = 1.9$ ). A scale-only Rietveld refinement against the original data set in the range 4°–65° 2θ to give a good final fit,  $R_{wp} = 2.89$ .

### Structure determination of catena(bis(μ<sub>3</sub>-iodo(3-aminomethyl)pyridine))-copper(I)

The powder of the titled compound has been obtained by mixing together a large excess of copper(I) iodide with respect to ligand used in a refluxing acetonitrile solution (see experimental section in chapter 5 page 90). After the two components have reacted, a highly crystalline whitish powder has been obtained that was then collected in Bragg-Brentano geometry on a flat sample stage.

The indexing run was performed with TOPAS 4.1<sup>6</sup> and a centric triclinic lattice parameter set (a=9.94(4) Å, b=7.60(1) Å, c=7.63(6) Å, α=99.01(1), β=96.25(4), γ

=108.86(2); volume=531.4 Å<sup>3</sup>) has been proposed. The data set was background subtracted and truncated to 50° 2θ for Pawley fitting ( $\chi^2 = 4.4$ ). The lattice volume suggested is coherent with a stoichiometry CuI:L=2:1 since the volume of CuI and 3-picolinamine are respectively 61 Å<sup>3</sup> and ≈ 144 Å<sup>3</sup> therefore, assumed P-1 as space-group (Z=2), the lattice content will be Cu<sub>4</sub>I<sub>4</sub>(3-picoline)<sub>2</sub>. As a consequence of the volume considerations, the ligand has to bind two different copper atoms in bridging mode with both pyridinic and amino nitrogen atoms but there are not sufficient information to know a priori neither how the ligand links the copper atoms nor the inorganic part nuclearity.

Structure solution was performed with a rigid body of the ligand not restrained on torsion angle. DASH<sup>7</sup> software was used to write the z-matrix of the organic ligand. The fragment used was taken by single crystal structure on CDS, conveniently modified. Copper and iodine atoms coordinates are refined independently without further restraints.

The crystalline structure results in a non-porous Metal-Organic Framework made by a series of coordination polymers (CPs) that grow along the crystallographic *c*-axis. Cu<sub>2</sub>I<sub>2</sub>(3picolamine) stoichiometry has been found in the asymmetric unit. The castle-like CPs are made by pseudo-tetrahedral copper ions, every of which bonds three iodide ions and than complete its first coordination sphere with the N-based ligand. Metallophobic interactions are present in the structure since the copper-copper distances are 2.771(3) Å, 2.787(1) Å and 3.123(2) Å. The bi-dentate organic ligands bridge the CuI chains in a 3D network. Along the same chain the ligand are put in a antiparallel manner and two neighbour copper ions bind the ligands moieties alternatively by pyridinic ring and amino group. The bridged CuI columns are wedged together in layers parallel to (-110) direction separated by 3.36 Å due to the inter-layers π- π interactions among ligand aromatic rings as reported in figure 5.2 (chapter 5, page 87). A Rietveld refinement against the original data set in the range 4°–65° 2θ gave a good final fit, Rwp = 7.2. In refinement step, the ligands torsion angles are restrained to the move along the values range found by CSD statistics and the coordination bonds are forced to be coherent to copper(I) pseudo-tetrahedral geometry.

### Structure solution of CuIPN<sub>3</sub>

The structure of [CuI(PN)<sub>3</sub>] (Chapter 4) was solved from powder pattern X-ray diffraction data even if the diffractogram acquired shows peaks of unwashed KI salt came out from the last synthetic step.

The powder pattern was indexed by a trigonal cell with crystallographic parameters of  $a=13.6471(2)$  Å,  $c=14.7400(4)$  Å volume = 2377 Å<sup>3</sup> and space group P-3. The volume of the asymmetric unit, 396 Å<sup>3</sup>, is consistent with the volume of the one third of [CuI(PN)<sub>3</sub>]. The solution is possible only if the

monomer is located on the 3-fold axis with copper and iodine atoms on special position (1/3, 1/3, z). Even if it is not usual for the PN ligand to bind copper ions only by phosphor atom (with nitrogen atom not involved in any coordination bond), this monomeric geometry was supposed as similar to the  $\beta$  form of CuI(PPh<sub>3</sub>)<sub>3</sub><sup>8</sup> (chapter 1), which crystallizes in the same crystallographic space group. In that case, the triphenylphosphine ligands bind the copper atom which stay on the rotational axis as the iodine atom. The powder pattern shows the presence of unwashed KI salt due to last synthetic step. The indexing run was performed taking apart the KI phase peaks, while all the following steps were all performed in the presence of a *scale-only* Rietveld refinement of KI phase. The structure was solved with a simulated annealing algorithm using as starting model one molecule of the ligand describer as rigid body in which torsion angles of the phenyl groups are left free to move along all the positions. In our description the ligand molecules are not preliminary bounded to the metal atom and the copper and the iodide ions are restrained to move along the C<sub>3</sub> axis with 1/3 site occupancy. The Rietveld refinement converged to a R<sub>wp</sub>= 7.681% and R<sub>exp</sub>= 4.351% (see figure 4.5). The position of the nitrogen atoms was assumed from the structure solution since the packing features or the Rietveld refinement gave no hints on the possible position (see figure 4.6). The crystal packing of [CuI(PN)<sub>3</sub>] does not present important intermolecular interactions. It is worth noting that along the c axis the molecular disposition create cavities, which can host solvent molecules as suggested also by the TGA curve (see figure 4.7a).

## References

1. W. I. F. David, K. Shankland, L. M. McCusker and C. Baerlocher, *Structure determination from powder diffraction data* Oxford University Press: New York, 2002.
2. K. Shankland, W. I. F. David and D. S. Sivia, *J. Mater. Chem.*, 1997, **7**, 569-572.
3. R. Peng, M. Li and D. Li, *Coord. Chem. Rev.*, 2010, **254**, 1-18.
4. D. Braga, F. Grepioni, L. Maini, P. P. Mazzeo and B. Ventura, *New J. Chem.*, 2011, **35**, 339-344.
5. D. Braga, L. Maini, P. P. Mazzeo and B. Ventura, *Chem. Eur. J.*, 2010, **16**, 1553-1559.
6. Bruker AXS, Karlsruhe, Germany, 2008, TOPAS v.4.2: General Profile and Structure Analysis Software for Powder Diffraction Data.
7. W. I. F. David, K. Shankland, J. van de Streek, E. Pidcock, W. D. S. Motherwell and J. C. Cole, *J. Appl. Crystallogr.*, 2006, **39**, 910-915.
8. L. Maini, D. Braga, P. P. Mazzeo and B. Ventura, *Dalton Trans.*, 2012, **41**, 531-539.

# Chapter 8

## Tuning the colour and efficiency in OLEDs by using amorphous or polycrystalline emitting layers

In the following chapter my contribution was about the carachterization of the sample as polycrystalline powders and glass-deposited thin films. I report the published paper as it is in Journal of Material Chemistry, C. 2013, 1, 1823-1831.

**Abstract:** We investigated the nature of the emissive states in newly synthesized cyclometallated Pt complexes containing a chelating 2-pyridyl tetrazolate (2-PTZ) ligand, namely Pt(ppy)(2-PTZ) and Pt(F<sub>2</sub>ppy)(2-PTZ) as solid-state phosphor, by examining their structural properties versus their phosphorescence (PH) and electroluminescence (EL) characteristics. It is found that the observed tuning of both PH and EL spectra, their red shift and shortening decay with increasing concentration in the complex blends is due to a competition between three emissive states: monomer, excimer and dimer. The pure dimer emission appeared in neat films, reaching high PH quantum yield of about 75% and external EL efficiency approaching 10% for the OLED based on neat Pt(F<sub>2</sub>ppy)(2-PTZ) complex film as emitting layer (EML). X-ray diffraction proved high structural order of the latter thin film. These findings have direct impact on the design of a new OLED generation based on single phosphor multi-emission controlled by structural order degree of the EML.



## Introduction

The efficient parallel phosphorescent emissions from bi-molecular (B-M) and mono-molecular (M-M) excited states<sup>1</sup> render the Pt complexes very attractive for organic optoelectronics.<sup>2</sup> Among others, they allow the colour and efficiency of organic light-emitting devices (OLEDs) to be effectively tuned.<sup>3</sup> The square planar structures enable the Pt complex molecules to facially aggregate through attractive intermolecular interactions of Pt-Pt or ligand-ligand or a combination of these, thereby facilitating formation of (B-M) states, either in the ground state (dimers) or in the excited states (excimers). Emission from (B-M) states are normally associated with a low quantum yield. This is due to an increase in the rate of radiationless relaxation of the excited state, arising from increased intermolecular phonon interactions in extended molecular systems, and an overall reduction in the oscillator strength of the dimer due to the fact that only a fraction of the oscillator strength of the dimer transition is derived from the parent monomer transition.<sup>4</sup> There have been, however, reports on molecules exhibiting high singlet excimer efficiency (~75%),<sup>5</sup> though triplet excimer efficiencies have long remained very low,<sup>6</sup> only recently high PH and EL efficiencies, from triplet excimers formed on heavy organometallic phosphor molecules, have been reported. For example, red and near-infrared light-emitting devices were demonstrated with maximum external quantum efficiencies of  $\varphi_{\text{EL}}=2.4\%$  (at 0.05 mA/cm<sup>2</sup>) based on a neat film FPt1 complex as triplet aggregate emitter<sup>7</sup> and of  $\varphi_{\text{EL}}=14.5\%$  (at 1 mA/cm<sup>2</sup>) based on a neat film PtL<sup>2</sup>Cl complex as triplet excimer emitter<sup>8</sup> showing photoluminescence (PL) efficiency of  $\varphi_{\text{PL}}(\text{excimer}) \approx 35\%.$ <sup>9</sup> Moreover,  $\varphi_{\text{PL}}(\text{excimer}) = 74\% > \varphi_{\text{PL}}(\text{monomer}) = 49\%$  has recently been reported for another Pt complex (PtL<sup>26</sup>Cl).<sup>10</sup> Broad featureless emission from B-M excited states (excimers and dimers) becomes therefore even more attractive to the manufacturing of efficient red and NIR OLEDs<sup>7,8,11</sup> as well as to the improvement of white OLEDs (WOLEDs) where a combination of phosphorescent molecule with the red-shifted excimer PH yields emission approaching white light based on single emissive dopant.<sup>12</sup>

Within the framework of our recent studies dealing with the use of Ir(III)-tetrazolate complexes as highly efficient emitters for OLED-type devices,<sup>13</sup> we now describe the first examples of very luminescent Pt(II)-tetrazolate phosphors in which the colour tuning of their emissions is due to the formation of two different B-M aggregates induced by the phosphor concentration. We demonstrate highly efficient OLEDs employing novel materials Pt(ppy)(2-PTZ) and Pt(F<sub>2</sub>ppy)(2-PTZ), where 2-PTZ stands for the chelating 5-(2-pyridyl)tetrazolate anion and ppy and F<sub>2</sub>ppy represent the cyclometalating ligands deriving from 2-phenylpyridine and 2-(2,4-difluorophenyl)pyridine, respectively. These complexes (Scheme 8.1 for molecular

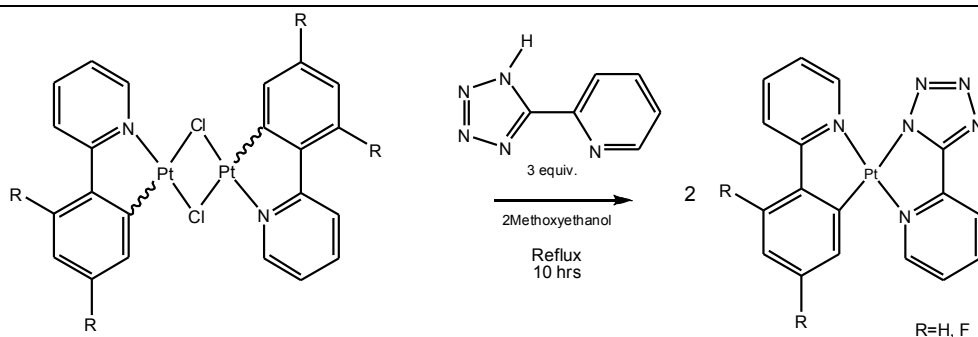
structures) are used as single dopant emitter in the emissive layers (EMLs). They take part in constituting a relatively simple device structure (Experimental section and Fig. F.2) which allows colour change from green to red as the phosphorous concentration increases. However, their concentration-imposed successive red shift is due to three different radiative states: monomer, excimer and dimer. A substantial part of this work is dedicated to elucidate the presence of two phosphorescent B-M aggregates in solid thin films through optical and structural characterizations and their correlations.

## Experimental

### Synthetic procedure for the target Pt(II) complexes

The preparation of the target cyclometalated Pt(II) complexes was accomplished by a two step procedure involving the preliminary synthesis of the chloride-bridged Pt(II) dimers  $[\text{Pt}(\text{ppy})(\mu\text{-Cl})]_2$  and  $[\text{Pt}(\text{F}_2\text{ppy})(\mu\text{-Cl})]_2$ , which were obtained by the reaction of the metal reagent  $\text{K}_2\text{PtCl}_4$  with one equivalent of the appropriate cyclometalating ligand in a 3/1(v/v) 2-methoxyethanol/water mixture.<sup>14</sup> Then, the obtained Pt(II) dimers were treated with an excess (3 equiv.) of 2-(1H tetrazol-5-yl)pyridine without the need of acid scavengers. The product complexes displayed very low solubility in all the common solvents. In particular, in the case of  $[\text{Pt}(\text{F}_2\text{ppy})(2\text{-PTZ})]$  it was not possible to record any NMR spectrum and the confirmation of the composition was provided only by the analysis of the ESI mass spectral data that displayed ion peaks patterns consistent with the expected formulation.

In principle, the reactions might lead to the formation of two different geometric isomers. However, according to reports dealing with similar cyclometalated Pt(II) derivatives,<sup>15</sup> we believe that the pronounced *trans* effect induced by the cyclometalating carbon might rule the formation of the isomer depicted in the scheme S1 as the predominant species.



Scheme 8.1 | Synthesis of  $[\text{Pt}(\text{ppy})(2\text{-PTZ})]$  ( $\text{R} = \text{H}$ ) and  $[\text{Pt}(\text{F}_2\text{ppy})(2\text{-PTZ})]$  ( $\text{R} = \text{F}$ )

### General Procedure for the synthesis of the cyclometalated Pt(II) complexes

A 100 mL round-bottomed flask was charged with 0.25 mmol (1 equiv.) of the appropriate Pt dimer,  $[\text{Pt}(\text{ppy})(\mu\text{-Cl})]_2$  or  $[\text{Pt}(\text{F}_2\text{ppy})(\mu\text{-Cl})]_2$ , and 0.4 mmol (1 equiv) and 0.75 mmol (1.5 equiv) of 2 (*1,H* tetrazol-5-yl)pyridine (2-PTZH). Then, 15 mL of 2-methoxyethanol were added and the stirred suspension was kept at the reflux temperature for 10 hours. After this time, the orange (in the case of  $[\text{Pt}(\text{ppy})(2\text{-PTZ})]$ ) or purple (as for  $[\text{Pt}(\text{F}_2\text{ppy})(2\text{-PTZ})]$ ) precipitate that had formed was removed by suction filtration and washed with several 10 mL portions of diethyl ether. In the case of  $[\text{Pt}(\text{ppy})(2\text{-PTZ})]$  an additional aliquot of the product could be obtained by extracting the filtrate with three 20 mL portions of dichloromethane. The organic layers were combined and dried over  $\text{MgSO}_4$ , and the solvent was removed in vacuum,, to afford  $[\text{Pt}(\text{ppy})(2\text{-PTZ})]$  (0.120 g, 48%) as an orange powder or  $[\text{Pt}(\text{F}_2\text{ppy})(2\text{-PTZ})]$  (0.105 g, 40%) as a purple microcrystalline powder.

### Characterization of both cyclometalated Pt(II) complexes:

**[Pt(ppy)(2-PTZ)]** (orange powder, 0.120 g, 48%). ESI-MS:  $m/\tilde{\chi}$  496  $[\text{M}+\text{H}]^+$ .  $^1\text{H}$  NMR ( $\text{CDCl}_3$ , 400 MHz): 10.21 (d, 1H,  $J=5.6$  Hz); 9.17 (d, 1H,  $J=5.6$  Hz), 8.29 (d, 1H,  $J=8$  Hz); 8.12 (t, 1H,  $J=7.2$  Hz); 7.86 (t, 1H,  $J=7.2$  Hz), 7.63 (d, 1H,  $J=8$  Hz), 7.48-7.45 (m, 2H), 7.34 (d, 1H,  $J=8$  Hz), 7.27-7.14 (m, 3H) $\text{H}_\text{v}$  ppm.  $^{13}\text{C}$  NMR ( $\text{CDCl}_3$ , 100 MHz): 153.7, 151.65, 140.2, 139.6, 132.9, 130.0, 125.6, 125.1, 124.3, 123.3, 122.7, 118.8 ppm.

**[Pt(F<sub>2</sub>ppy)(2-PTZ)]** (dark purple powder, 0.105 g, 40%) ESI-MS:  $m/\tilde{\chi}$  554  $[\text{M}+\text{Na}]^+$ . NMR data are not available because of the very low solubility in all common solvents.

### X-ray diffraction

X-ray powder diffractograms were collected on a Panalytical X'Pert PRO automated diffractometer with CuKa radiation and X'Celerator. All measurements were collected with Bragg-Brentano geometry. Peak positions were determined with Highscore Plus. Grazing incidence (GID) in-plane measurements were performed by using a SmartLab-Rigaku diffractometer, equipped with a rotating anode (CuKa radiation) followed by a parabolic mirror, to collimate the incident beam, and a series of variable slits (placed after the sample position).

### Photoluminescence in films

The samples in PMMA matrix were prepared by drop casting dichloromethane solutions of Pt complex and PMMA while thin films in TCTA blend and neat Pt complex films were prepared by codeposition in high vacuum ( $10^{-6}$  hPa) of two components or single deposition of Pt complex, respectively. Absorption and emission spectra were recorded using a Perkin Elmer Lambda 950 UV/Vis spectrophotometer

and an Edinburgh FLS920 spectrofluorometer, respectively. The photoluminescence quantum yields were measured by a custom integrating sphere system applied to the same Edinburgh spectrofluorometer and using DeMello's method. Time resolved luminescence measurements were obtained with an Single-photon IBH model 5000 counter.

### OLED preparation and experimental procedures

OLEDs were fabricated by growing a sequence of thin layers on clean glass substrates pre-coated with a 120 nm-thick layer of indium tin oxide (ITO) with a sheet resistance of  $20\ \Omega$  per square. A 60 nm thick hole transporting layer of [N,N'-diphenyl-N,N'-bis(3-methyl)-1,1'-biphenyl-4,4' diamine (TPD)] 75 wt%: [bisphenolpol-A-polycarbonate (MW 32000-36000) (PC)]25wt% (Aldrich and Polysciences Inc., respectively) blend was spun on top of the ITO from a 10 mg/ml dichloromethane solution at room temperature. All remaining organic layers were deposited in succession by thermal evaporation under vacuum of  $\sim 10^{-6}$  hPa, followed by high vacuum ( $\sim 10^{-6}$  hPa) thermal-evaporation of the cathode layer consisting of 0.5 nm-thick LiF and by a 100 nm-thick Al cap. The emitting layer (EML) was evaporated by co-deposition of the Pt complex and 4,4',4''-tris(N-carbazolyl-triphenylamine (TCTA) to form a 30nm-thick blend film (5w% Pt complex : 95w% TCTA) or by single deposition of Pt complex to form a 30nm neat film. The performance of the emissive layer has been optimized by locating the EML between exciton blocking layers of TCTA (10 nm) and 3-phenyl-4-(1'-naphthyl)-5-phenyl-1,2,4-triazole (TAZ), the latter acting also as an electron transporting and hole-blocking layer (30 nm). The current-voltage characteristics were measured with a Keithley Source-Measure unit, model 236, under continuous operation mode, while the light output power was measured with an EG&G power meter and electroluminescence (EL) spectra by StellarNet spectroradiometer. All measurements were carried out at room temperature under argon atmosphere and were reproduced for many runs, excluding any irreversible chemical and morphological changes in the devices.

## Results and Discussion

### B-M Aggregates : excimer and dimer

It is well known that the square planar configuration of Pt(II) complexes often leads to stacking and formation of aggregates which quenches the monomer luminescence.<sup>16</sup> The resulting species may display their own, red-shifted photoluminescence and electroluminescence.<sup>17</sup>

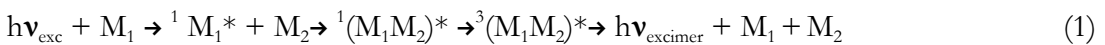
The broad band phosphorescence from Pt(II) organic complexes is often assigned to

the radiative decay of the bimolecular excited triplet states constituting quantum mechanical entities, excimers, which are a result of excitonic (EX) and charge-transfer (CT) resonances imposed optically or electrically between two nearest-neighbour molecules ( $M_1, M_2$ ) and can be described by a function:<sup>18</sup>

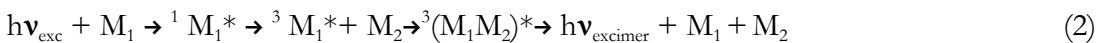
$${}^3|M_1M_2\rangle^* = c_1 {}^3|M_1M_2\rangle_{\text{EX}}^* + c_2 {}^3|M_1M_2\rangle_{\text{CT}}^*$$

Whereas the coefficients  $c_1$  and  $c_2$  determine the contributions of the EX and CT interaction components to the excimer. The relation between amplitudes of function, thus the excimer energy, depends on the distance between molecules  $M_1$  and  $M_2$  and their mutual orientation.

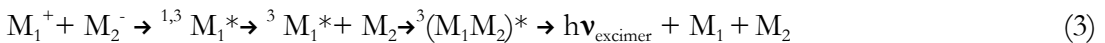
Phosphorescent excimer can be formed indirectly by optical excitation of the single molecule,  $M_1$  or  $M_2$ :



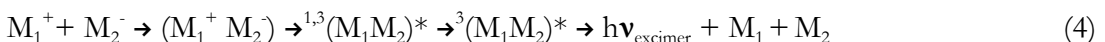
or



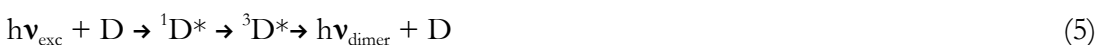
In electroluminescence (EL) by charge recombination:



or directly from charge pair precursor



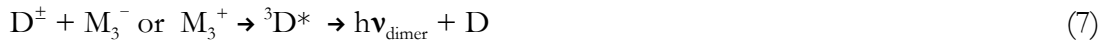
Alternatively, phosphorescent aggregate states can be formed by the direct optical excitation of the ground-state, dimers,  $D \equiv (M_1M_2)$ :



and/or by their excitation as a result of the energy transfer from monomolecular triplet states:



In EL, the dimer-localized charge carriers can serve as recombination centres (charge traps), leading to the excited dimers as a result of direct recombination process on them



or through energy transfer from  ${}^3M_1^*$  generated by the recombination  $M_1^+ + M_2^- (M_3^-)$ , where  $M_3$  represents either the dopant or matrix molecule. The triplet dimer emission has been observed in neat films of Pt(II) porphyrin.<sup>19</sup>

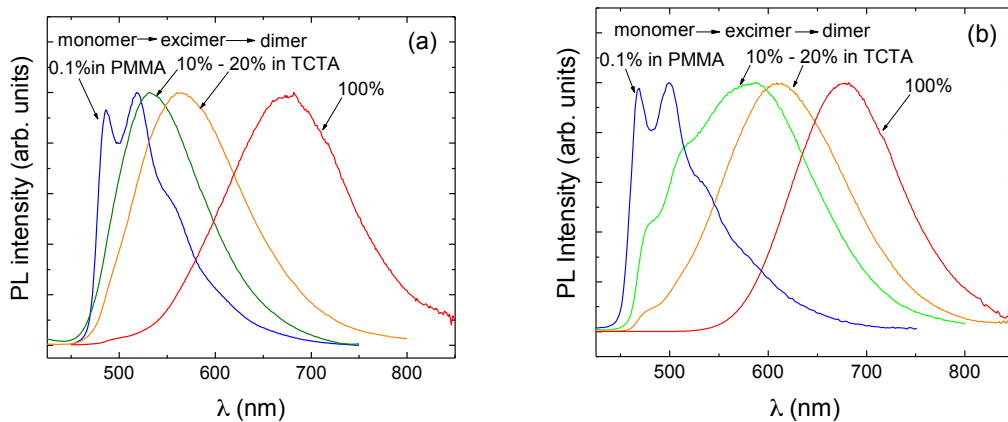


Figure 8.1 | Molecular structures of the Pt complexes studied in this work (top), and photoluminescence (PL) spectra of Pt(ppy)(2-PTZ) (a) and of Pt(F<sub>2</sub>ppy)(2-PTZ) (b) in solid state (bottom). In addition to structured molecular phosphorescence (monomer emission) below 480-500 nm, broad longer-wavelength emission bands appear when the concentration of both complexes is increased. They are attributed to radiative transitions from bi-molecular (B-M) species: excimer and dimer with the emission maxima at shorter and longer wavelengths, respectively.

## Photo-physical properties

The two complexes have been studied in solid-state matrix, namely a blend of the Pt complex in 4,4',4''-Tris(N-Carbazolyl-TriphenylAmine (TCTA) or Poly(Methyl MethAcrylate) (PMMA), and the neat film. Photoluminescence (PL), absorption (Abs) and photoexcitation (PE) spectra are displayed in Figures 8.1, 8.2 and 8.3. The influence of varying the concentration on the ability of the compounds to form bi-molecular species, and on the nature of such species, has been probed. From Figure 8.1 remarkable difference is apparent in the PL spectra of the complexes at different concentration in PMMA and TCTA matrix. In addition to structured molecular phosphorescence (monomer emission) around 500 nm and a broad longer-wavelength emission band located immediately behind it (about 550-600 nm), a still longer-

wavelength broad band around 670 nm appears in neat film (high concentration) for both complexes.

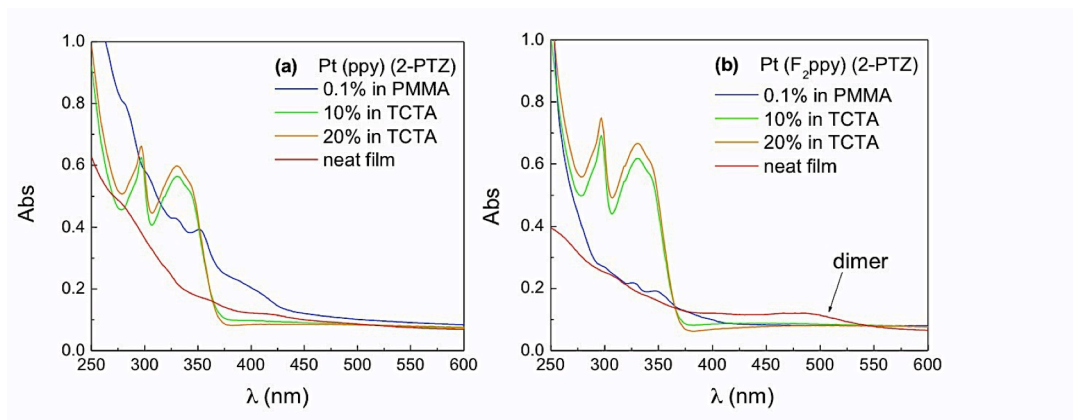


Figure 8.2 | Absorption (Abs) spectra of  $\text{Pt}(\text{ppy})(\text{2-PTZ})$  (a) and  $\text{Pt}(\text{F}_2\text{ppy})(\text{2-PTZ})$  (b) at different concentration in PMMA or TCTA matrix.

The excimeric emissions of the 10% and 20% of Pt complex in TCTA (Fig. 8.1) are confirmed by the PE and Abs spectra (Fig. 8.2 and 8.3). In fact these spectra correspond, except for a little Pt complexes contribution (Fig. 8.2 and 3, 0.1% Pt complex in PMMA), to that to the TCTA pure film. The absence of additional lower-energy bands indicates excitation of isolated molecules that subsequently form the triplet emissive excimer species undergoing reaction (1) and/or (2). In both reactions, excimer phosphorescence is produced. However, beyond a certain point, a new even lower energy broad-band appears in neat film, which has a different excitation spectrum (Fig. 8.2b and 8.3b, PE spectra). We believe that this is due to an excited ground state dimer,  $\text{D}^*$  [see reactions (5),(6)]. The emergence of a new low-energy band in the Abs and/or in the PE spectrum is consistent with the behavior displayed by well-known aggregating Pt complexes such as  $\text{Pt}(\text{bpy})\text{Cl}_2$  or  $\text{Pt}(\text{en})\text{Cl}_2$ <sup>20</sup>. The long-wavelengths detected PE spectra differ from the absorption spectra as could be expected for a relatively low concentration of dimers. A straightforward conclusion is that we are dealing with molecular aggregates, in which the dimer formation can proceed due to shorter intermolecular distances and/or favorable intermolecular configurations. However, the dimerization is often the initial stage of crystallization and it is difficult to distinguish emission by randomly formed dimers from that of larger molecular aggregates or nano/microcrystals. To prove these latter assumptions a structural characterization of our solid samples is reported in the next section.

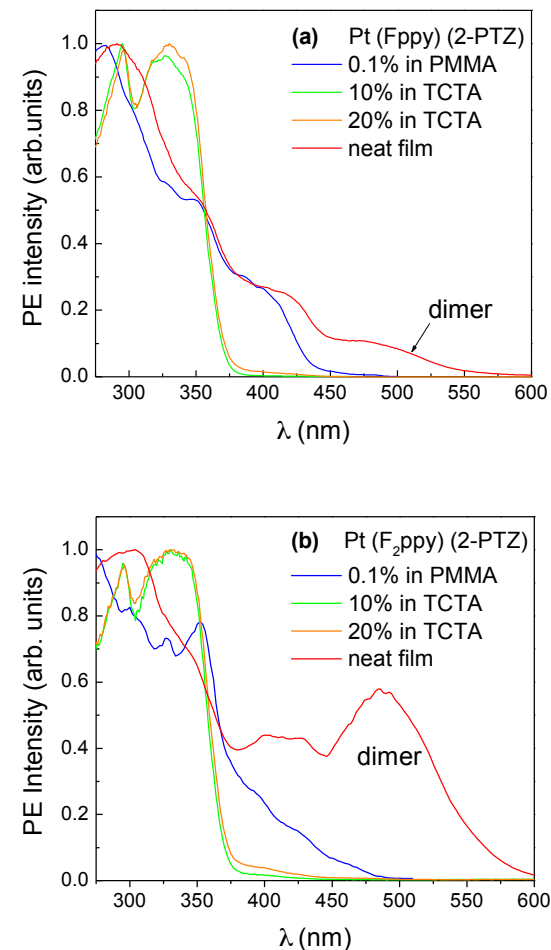


Figure 8.3 | Photo-Excitation (PE) spectra of Pt(ppy)(2-PTZ) (a) and Pt(F<sub>2</sub>ppy)(2-PTZ) (b) at different concentration in PMMA or TCTA matrix. PE spectra were detected at the monomer, excimer and dimer emission regions. While they are identical in TCTA matrix, distinct difference is apparent in case of both Pt complex neat films, attributable to the formation of dimers or higher aggregates.

In order to integrate the optical properties of both platinum complexes, decay times of solid films of Pt(ppy)(2-PTZ) and Pt(F<sub>2</sub>ppy)(2-PTZ) were measured and they are reported in Table 1. Mono-exponential transient decays are observed for (a) low-concentration 0.1% Pt complex: PMMA matrix (for both complexes), (b) 10 wt% for Pt(ppy)(2-PTZ) in TCTA, (c) 20 wt% for Pt(F<sub>2</sub>ppy)(2-PTZ) in TCTA and (d) for both neat films on the microsecond scale (Fig. F.3). The lifetimes of the emissive species, obtained from exponential decay fits, show a decrease from  $\tau_m = 6.6$ ; 8.1  $\mu$ s to  $\tau_{\text{excimer}} = 3.8$ ; 1.4  $\mu$ s and finally to  $\tau_{\text{dimer}} = 0.7$ ; 0.5  $\mu$ s for these three different specimens, respectively.

Table M.1 | Photophysical properties of Pt complexes at different concentrations.

	film	$\lambda_{\text{max}}$ [nm]	$\varphi_{\text{PL}}$ [%]	$\tau$ [ $\mu\text{s}$ ]	$K_r$ [ $\text{s}^{-1}$ ] <sup>a</sup>	$K_{\text{nr}}$ [ $\text{s}^{-1}$ ] <sup>a</sup>
<b>Pt (ppy) (2-PTZ)</b>	0.1% in PMMA (monomer)	486,518, 550	20	6.6	$3.0 \times 10^4$	$1.2 \times 10^5$
	10% in TCTA (excimer)	535	45	3.8	$1.2 \times 10^5$	$1.4 \times 10^5$
	20% in TCTA (excimer&dimer)	565	40	3.5 [87%] 0.7 [13%]	-	-
	Neat film (dimer)	675	30	0.7	$4.3 \times 10^5$	$1.0 \times 10^6$
<b>Pt (F<sub>2</sub>ppy) (2-PTZ)</b>	0.1% in PMMA (monomer)	470, 500, 530	10	8.1	$1.2 \times 10^4$	$1.2 \times 10^5$
	10% in TCTA (monomer&excimer)	585	35	3.1 [30%] 1.4 [70%]	-	-
	20% in TCTA (excimer)	610	52	1.4	$3.7 \times 10^5$	$3.4 \times 10^5$
	Neat film (dimer)	678	75	0.5	$1.4 \times 10^6$	$6.0 \times 10^5$

[a] Radiative ( $K_r$ ) and nonradiative ( $K_{\text{nr}}$ ) rate constants calculated from  $\tau$  and  $\varphi_{\text{PL}}$  values; estimated uncertainty  $\pm 10\%$ .

The dimer phosphorescence response function of the neat films (d) can be well approximated by a function:<sup>6a</sup>

$$P_E(t) = A(e^{-t/\tau_d} - e^{-t/\tau_r})$$

with  $\tau_r = 7$  and 11 ns and  $\tau_d = 0.7$  and 0.5  $\mu\text{s}$  for Pt(ppy)(2-PTZ) and Pt(F<sub>2</sub>ppy)(2-PTZ) respectively (Fig. F.3d). This indicates that the dimer excitation rate constant  $\tau_r$  exceeds largely the monomolecular decay rate constant,  $\tau^{-1}$ . The obtained value of  $\tau_r$  is too long to reflect the rapid intersystem crossing from <sup>1</sup>M\* to <sup>3</sup>M\* (at a probable rate  $10^{12} \text{ s}^{-1}$ ),<sup>21</sup> and suggests that only selected intermolecular arrangements can serve as the dimer forming sites at which the configuration of adjacent parallel molecules ensures a good overlap; the molecular excitons need around 10 ns to transfer the excitation energy to these sites.

It is interesting to note that the measured decay time of the monomer emission is much longer than the decay time of the B-M emissions. Both the radiative ( $k_r$ ) and overall non-radiative ( $k_{\text{nr}}$ ) rate constants can be extracted from the quantum yield and the above lifetime data by means of the following relationships:

$$\tau = (k_r + k_{nr})^{-1}$$

$$\varphi_{PL} = k_r / (k_r + k_{nr}) = k_r \tau$$

In table M.1 all these photophysical parameters are listed. The data indicate that the reduced lifetime of the excited B-M states, compared to that of the M-M transitions, is due mainly to their ten or hundred-fold increased  $k_r$ . This indicates that either the B-M phosphorescence transitions of both Pt complexes are less forbidden than its monomer transition. The understanding of the relation  $K_r^{(B-M)} \gg K_r^{(M-M)}$  is not straightforward, but a possible explanation could be that the B-M emissions can be originated from excited states with MMLCT (metal-metal-to-ligand charge transfer) character through Pt-Pt bimetallic interaction.<sup>11b,22</sup> In addition we also have to take into consideration the fact that these B-M states could be less susceptible to energy migration quenching by chemical impurity or physical defects, which may lead to increase their  $k_r$ -to- $k_{nr}$  ratio compared to that of M-M excited states.

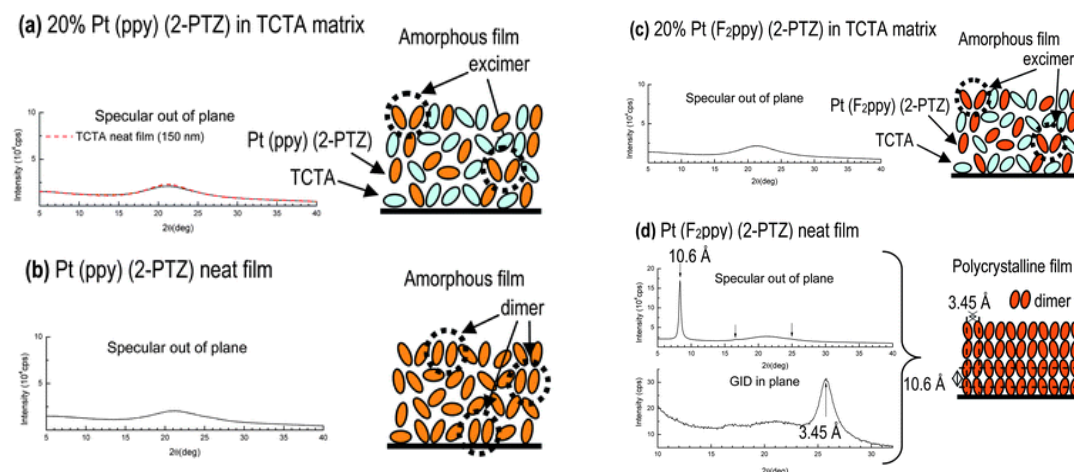


Figure 8.4 | X-ray patterns of thin films with simple scheme of the film structure: (a) 20 % Pt(ppy)(2-PTZ) in TCTA matrix and TCTA neat film, (b) Pt(ppy)(2-PTZ) neat film , (c) 20 % Pt(F<sub>2</sub>ppy)(2-PTZ) in TCTA matrix, (d) Pt(F<sub>2</sub>ppy)(2-PTZ) neat film . The big bump centered at  $2\theta=21^\circ$  is due to the quartz substrate.

The Pt complex concentration-imposed successive red shift is accompanied by a non-monotonous variation in the PL efficiency showing a maximum of  $\varphi_{PL} = 45\%$  at the concentration  $c=10$  wt% and is lowered to 30% for the neat film of Pt(ppy)(2-PTZ) complex. Whereas in the case of Pt(F<sub>2</sub>ppy)(2-PTZ), the PL efficiency increases

monotonously with Pt concentration from  $\varphi_{PL} = 10\%$  for 0.1% Pt complex: PMMA blend, to  $\varphi_{PL} = 75\%$  for the neat film (Table 1).

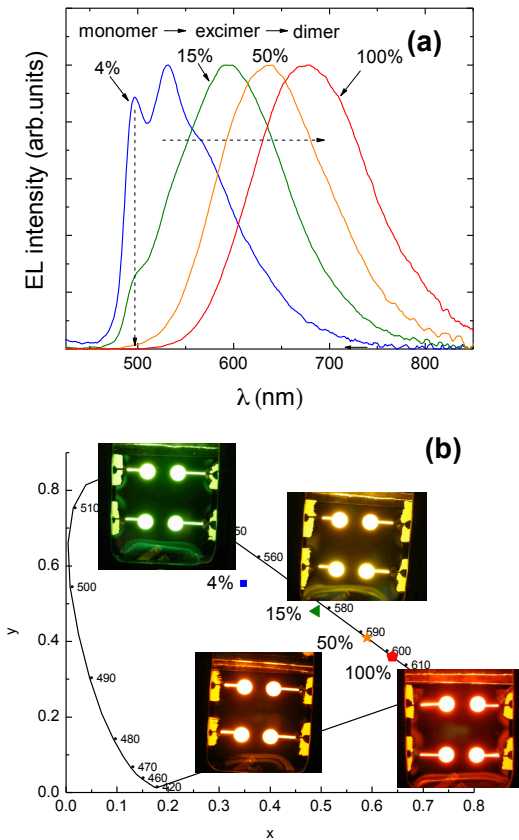


Figure 8.5 | Electroluminescence spectra (a) and CIE diagram (b) for OLEDs with different concentrations of Pt(ppy)(2-PTZ) in the EML. To show the real colour tuning, CIE coordinates and photographs of OLEDs are given.

### Structural characterization

Pt(ppy)(2-PTZ) and Pt(F<sub>2</sub>ppy)(2-PTZ) powder materials and thin films sublimed on quartz substrate have been structurally characterized by means of X-ray diffraction and DSC techniques.

DSC reveals that the crystalline powder of Pt(ppy)(2-PTZ) -light orange- and of Pt(F<sub>2</sub>ppy)(2-PTZ) - pink- decompose respectively at 270 °C, and at 320 °C.

Neat thin films and a series of films having different Pt complex concentration wt % in

TCTA matrix have been studied. All the Pt(ppy)(2-PTZ) thin films consist of amorphous material (Figure 8.4a,b). Pt(F<sub>2</sub>ppy)(2-PTZ) thin films in TCTA matrix are amorphous (Figure 8.4c), on the other hand the as-deposited Pt(F<sub>2</sub>ppy)(2-PTZ) neat thin films result to be polycrystalline (Figure 8.4d). Complementary information on the structure of the Pt(F<sub>2</sub>ppy)(2-PTZ) polycrystalline films could be achieved by combining X-ray diffraction measurements collected in specular out-of-plane and grazing incidence in-plane geometries: the former detects the periodicities parallel to the substrate and the latter those perpendicular. The specular XRD pattern shows, together with a broad halo coming from the amorphous quartz substrate, the presence of three peaks (Figure 8.4d). The first peak corresponds to a interplanar distance equal to  $d=10.6 \text{ \AA}$  and the others to the second and third order of diffraction of the same lattice planes (their values are  $d/2$  and  $d/3$ ).

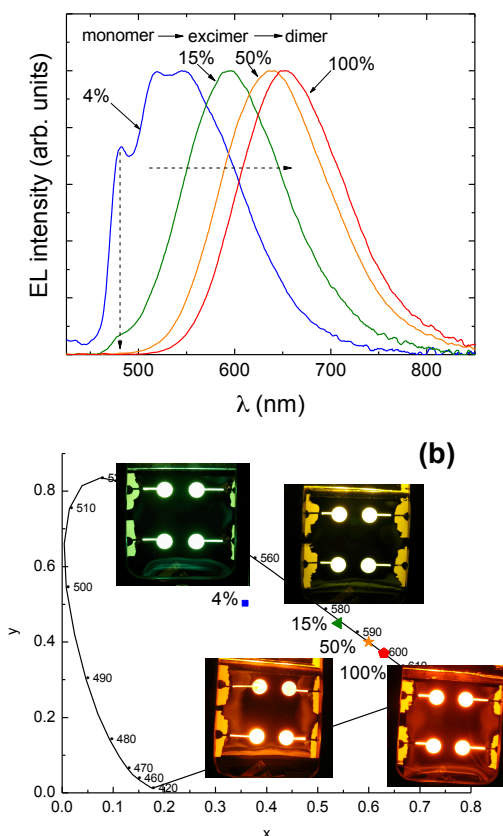


Figure 8.6 | Electroluminescence spectra (a) and CIE diagram (b) for OLEDs with different concentrations of Pt(F<sub>2</sub>ppy)(2-PTZ) in the EML. To show the real colour tuning, CIE coordinates and photographs of OLEDs are given.

The lack of other reflections indicates a strong texturing of the film with the molecular stacking along the surface normal, and the d-spacing value suggests the molecules lie with the long axis approximately perpendicular to the surface.

This molecular configuration is consistent with the periodicity revealed in-plane diffraction pattern (Figure 8.4d), where the detected peak, corresponding to  $d=3.45\text{ \AA}$ , is consistent with the presence of Pt-Pt metallophilic interactions, such as those observed in several dimeric structures of cyclometallated Pt(II) complexes in single crystal.<sup>11b,22,23</sup> The diffractogram of the  $\text{Pt}(\text{F}_2\text{ppy})(2\text{-PTZ})$  film differs to those of the powder material (see Fig. F.5 and F.6), indicating the presence of a dimorphic system, as observed in several Pt(II) complexes.<sup>24</sup>

### OLEDs spectra and performances

The devices consist of an indium tin oxide (ITO) coated glass anode transparent to the light generated in the emitter layer (EML) which consists of  $\text{Pt}(\text{ppy})(2\text{-PTZ})$  or  $\text{Pt}(\text{F}_2\text{ppy})(2\text{-PTZ})$  ( $x$  wt%) – doped TCTA blend. Holes are injected from the ITO anode, and pass through (TPD:PC) and TCTA hole-transporting layers (HTL), and recombine in the EML with electrons that were injected from a Al/LiF cathode and transported through the electron transporting layer (ETL) of a triazole derivative (TAZ). The 10 nm-thick TCTA layer, characterized by a triplet exciton energy  $E_T$  of 2.85 eV, has been used to block triplet exciton transfer from the Pt complexes ( $E_T=2.55\text{--}2.60\text{ eV}$ ) to the non-radiative triplet of TPD ( $E_T=2.45\text{ eV}$ ). The 30 nm-thick layer of TAZ ( $E_T=2.75\text{ eV}$ ) plays a similar role of inhibiting quenching of the Pt complex triplet excitons at the cathode while at the same time blocking holes. These last two properties enable the recombination process to be confined to a 30 nm-thick EML layer (Fig. F. 2). Such an OLED architecture allowed us to maximize its performance parameters . In both OLED series the Pt complex concentration-imposed successive red shift is accompanied by a non-monotonous variation in the external EL quantum efficiency (QE) showing a maximum of  $\varphi_{\text{EL}}\approx10\%$  at the concentration  $c=15\text{ wt\%}$  and then decreasing down to  $\sim2\%$  and 8% for the  $c=100\text{ wt\%}$  (neat film) of  $\text{Pt}(\text{ppy})(2\text{-PTZ})$  and  $\text{Pt}(\text{F}_2\text{ppy})(2\text{-PTZ})$  respectively. At the same time, the EL QE from high dopant concentration EMLs exceeds that from monomer emitting samples (see table 8.1).

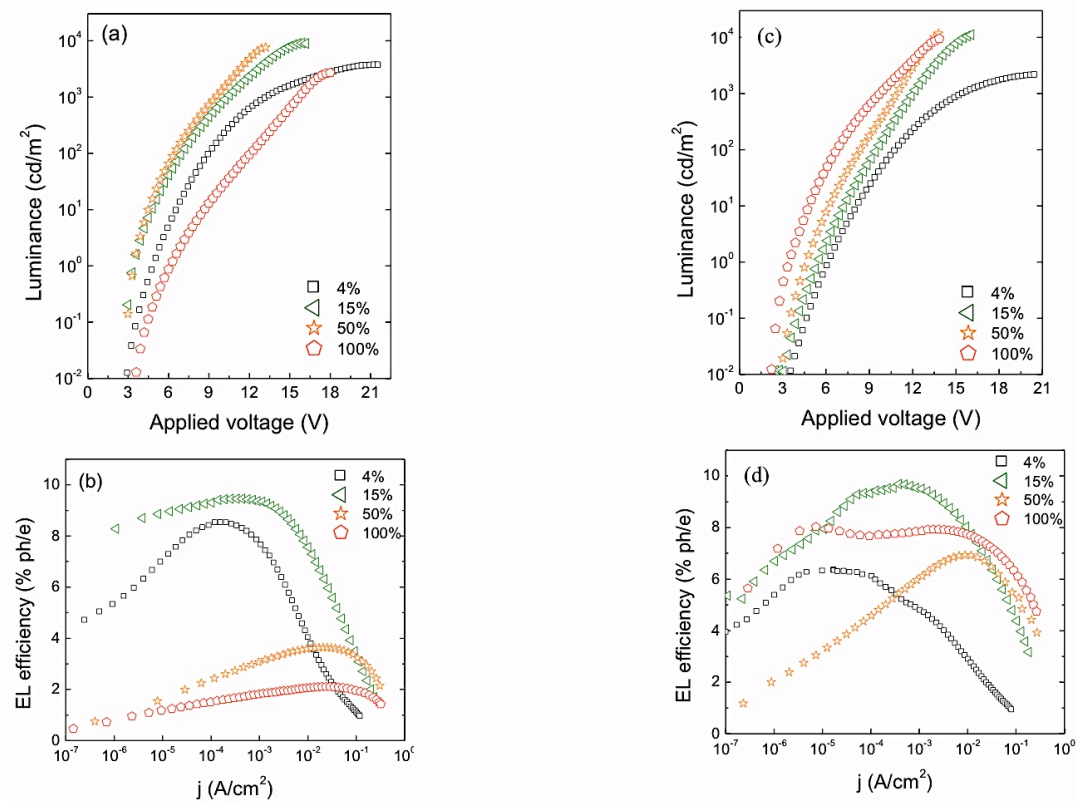


Figure 8.7 | Luminance vs applied voltage (a) and EL efficiency vs current density (b) of  $\text{Pt}(\text{ppy})(2\text{-PTZ})$  at different concentrations in the EML. Luminance vs applied voltage (c) and EL efficiency vs current density (d) of  $\text{Pt}(\text{F}_2\text{ppy})(2\text{-PTZ})$  at different concentrations in the EML.

Figures 8.5a and 8.6a show EL spectra of OLEDs for the Pt complexes at different dopant concentrations. It is clear that a reduction in its concentration in the EML leads to a relative increase of the green light emission band originating from the radiative decay of molecular triplet excitons of the isolated phosphorescent molecules of the Pt complex. On the other hand by reassigning the amount of the dopant concentration, the contribution of the broad yellow and red light bands emanating from the phosphorescent emission of the two Pt complex aggregates, excimer and dimer respectively, can be increased [see reaction (3) or (4) and (7)]. These emission bands have the main maxima at  $\lambda \approx 600$  nm for both Pt complexes at 15 wt% concentration and  $\lambda \approx 675$  and 655 nm for 100wt% of  $\text{Pt}(\text{ppy})(2\text{-PTZ})$  and  $\text{Pt}(\text{F}_2\text{ppy})(2\text{-PTZ})$ , respectively. The CIE coordinates for the OLEDs of 4, 15, 50, 100 wt% concentrations of both Pt complexes in their EML, show how varying the doping provides a simple way of tuning colour over a wide range from green to red (Figure 8.5b and 8.6b).

Figures 8.7a and 8.7c show the voltage dependence of luminance for the devices with different Pt complex concentrations. Luminance (B) increases monotonically with increasing dopant concentration (up to ca 10000 cd/m<sup>2</sup>), always showing a tendency to saturation associated with the typical OLEDs high-voltage roll-off in the EL quantum efficiency (Figures 8.7b and 8.7d). A detailed examination of the B(V) and EL QE(j) characteristics show a distinct increase in luminance at 15 and 50 wt% of the Pt complexes, while for neat films the EL behaviors become quite different due to the great difference of their PH quantum yields , about 30% and 75% for Pt(ppy)(2-PTZ) and Pt(F<sub>2</sub>ppy)(2-PTZ) respectively, and different electronic properties of their aggregates, that certainly influence the charge carrier recombination and quenching probabilities.

The minor roll-off effect observed in neat film EMLs may be due to the fact that only emissive dimers are generated, and these emissive species are subject to weaker quenching as compared with quenching of monomolecular excitons. Indeed for all voltage range, the luminance of neat Pt(F<sub>2</sub>ppy)(2-PTZ) film-based devices is greater than that for blend-based ones, showing higher efficiency at high current density (high electric field) as shown in Figure 8.7c-d.

## Conclusions

We have shown that both photoluminescence and electroluminescence from thin organic neat and blended films of cyclometallated Pt(II)-tetrazolate complexes constitute in general a combination of light generated by the phosphorescent decay of monomolecular and two different bi-molecular aggregates, “excimer” and “dimer”, that are formed either through the absorption of exciting photons or by recombination of holes and electrons when used as emitters of the EL devices. We examined the formation of phosphorescent states in blend and pure solid state phase (films) using the absorption, photoexcited and electroluminescent emission, and excitation spectra of a couple of Pt(II) complexes, Pt(ppy)(2-PTZ) and Pt(F<sub>2</sub>ppy)(2-PTZ), that differ for the structure of the cyclometalating ligand. We find that the spectral composition of the emission from either blends or pure solid state specimens exhibits strong material dependence changing the bands positions and their relative intensity, depending on the interaction character and relative molecular packing. While the emission from low-concentration samples (4-15wt%) is dominated by monomer and/or excimer emissions (450-600 nm) with weak inter-molecular interaction, the principal emission from high-concentration samples (50-100wt%) originates from dimers (600-800 nm) with strong inter-molecular interaction.

The structural characterization reveals that Pt(ppy)(2-PTZ) neat film is amorphous (no

peaks in X-ray diffractogram are present), while the fluorinated complex Pt(F<sub>2</sub>ppy)(2-PTZ) neat film consists of crystallites having a pronounced preferential orientation with respect to the substrate: the lattice planes parallel to the susbtrate have 10.6 Å, spacing, which is close to the molecular length, and those perpendicular to the substrate a periodicity of 3.45 Å which is consistent with an effective Pt-Pt interaction. Coupling the structural and optical properties we can conclude that the concentration of phosphorescent triplet dimers is much higher in neat crystalline film of Pt(F<sub>2</sub>ppy)(2-PTZ), by the presence of the dimers regularly distributed in the thin film, compared to the dimer concentration in the neat amorphous film of Pt(ppy)(2-PTZ) where dimers are randomly formed. The -F substituents on Pt(F<sub>2</sub>ppy)(2-PTZ) promote the molecular self-assembly into more uniform ordered structures along the thin film. Moreover the crystal packing in the “*thin film*“ form plays a fundamental role in promoting the radiative decay of the aggregate state and the dimer is characterized by a surprisingly high PL efficiency ( $\phi_{PL}=75\%$ ). In fact we believe that a strong correlation between polycrystalline structures and Pt-Pt interaction could play a fundamental role in promoting the radiative decay of the aggregate excited state.

The doping concentration of the phosphor complex in the conductive molecular matrix in blended films determines the relative monomer-excimer-dimer EL emission ratio and hence the colour of the emitted light can be tuned from green to red with high efficiency. Furthermore, phosphorescent dimer OLED based on neat polycrystalline film as emitter layer has been shown to be a new route for realizing efficient systems.

### Acknowledgements

This work was supported by Consorzio MIST E-R (project FESR-Tecnopolis AMBIMAT), and by Italian MISE (project Industria 2015 “ALADIN”).

### Notes and references

Electronic Supplementary Information (ESI) available: electrochemistry, OLED configuration, Transient decay analysis, X ray diffraction. See Appendix F

## References

- 1 J. Kalinowski, *J. Non-Cryst. Solids*, 2008, **354**, 4170.
- 2 (a) B. D'Andrade, *Nature Photonics*, 2007, **1**, 33; (b) S. Reineke, F. Lindner, G. Schwartz, N. Seidler, K. Walzer, B. Lüssem, K. Leo, *Nature*, 2009, **459**, 234; (c) R. Capelli, S. Toffanin, G. Generali, H. Usta, A. Facchetti, M. Muccini, *Nature Materials*, 2010, **9**, 496.
- 3 (a) M. Cocchi, J. Kalinowski, L. Murphy, J. A. G. Williams, V. Fattori, *Org. Electron.*, 2010, **11**, 388; (b) J. Kalinowski, V. Fattori, M. Cocchi, J. A. G. Williams, *Chem. Coord. Rev.*, 2011, **255**, 2401; (c) B. Ma, P. I. Djurovich, S. Garon, B. Alleyne, M. E. Thompson, *Adv. Funct. Mater.*, 2006, **16**, 2438.
- 4 M. Pope, C. E. Swenberg, in *Electronic Processes in Organic Crystals*, Clarendon, Oxford 1982.
- 5 J. B. Birks, D. J. Dyson, I. H. Munro, *Proc. Roy. Soc. A*, 1963, **275**, 575.
- 6 (a) J. B. Birks, in *Photophysics of Aromatic Molecules*, Wiley-Interscience, London 1970; (b) X. Wang, W. G. Kofron, S. Kong, C. S. Rajesh, D. A. Modarelli, E. C. Lim, *J. Phys. Chem. A*, 2000, **104**, 1461.
- 7 B. D'Andrade, S. R. Forrest, *Chem. Phys.*, 2000, **256**, 321.
- 8 M. Cocchi, J. Kalinowski, D. Virgili, J. A. G. Williams, *Appl. Phys. Lett.*, 2008, **92**, 113302.
- 9 M. Cocchi, J. Kalinowski, D. Virgili, V. Fattori, J. A. G. Williams, *Appl. Phys. Lett.*, 2007, **90**, 023506.
- 10 J. Kalinowski, M. Cocchi, L. Murphy, J. A. G. Williams, V. Fattori, *Chem. Phys.*, 2010, **378**, 47.
- 11 (a) E. Rossi, L. Murphy, P. L. Brothwood, A. Colombo, C. Dragonetti, D. Roberto, R. Ugo, M. Cocchi, J. A. G. Williams, *J. Mater. Chem.*, 2011, **21**, 15501; (b) E. Rossi, A. Colombo, C. Dragonetti, D. Roberto, F. Demartin, M. Cocchi, P. Brulatti, V. Fattori, J. A. G. Williams, *Chem. Commun.*, 2012, **48**, 3182.
- 12 B. W. D'Andrade, J. Brooks, V. Adamovich, M. E. Thompson, S. R. Forrest, *Adv. Mater.*, 2002, **14**, 1032; (b) V. Adamovich, J. Brooks, A. Tamayo, A. M. Alexander, P. I. Djurovich, B. W. D'Andrade, C. Adachi, S. R. Forrest, M. E. Thompson, *New J. Chem.*, 2002, **26**, 1171; (c) E. L. Williams, K. Haavisto, J. Li, G. E. Jabbour, *Adv. Mater.*, 2007, **19**, 197; (d) Cocchi, M., J. Kalinowski, D. Virgili, V. Fattori, S. Develay, J. A. G. Williams, *Appl. Phys. Lett.*, 2007, **90**, 163508; (e) J. Kalinowski, M. Cocchi, D. Virgili, V. Fattori, J. A. G. Williams, *Adv. Mater.*, 2007, **19**, 4000; (f) M. Cocchi, J. Kalinowski, V. Fattori, J. A. G. Williams, L. Murphy, *Appl. Phys. Lett.*, 2009, **94**, 073309; (g) L. Murphy, P. Brulatti, V. Fattori, M. Cocchi, J. A. G. Williams, *Chem. Commun.*, 2012, **48**, 5817.
- 13 M. Cocchi, J. Kalinowski, S. Stagni, S. Muzzioli, *Appl. Phys. Lett.*, 2009, **94**, 083306.
- 14 M. Ghedini, T. Pugliese, M. La Deda, N. Godbert, I. Aiello, M. Amati, S. Belviso, F. Lelj, G. Accorsi, F. Barigelli, *Dalton Trans.*, 2008, 4303.
- 15 S.-Y. Chang, Y.-M. Cheng, Y. Chi, Y.-C. Lin, C.-M. Jiang, G.-H. Lee, P.-T. Chou, *Dalton Trans.* 2008, 6901.
- 16 (a) S-C. Chan, M. C. W. Chan, Y. Wang, C-M. Che, K-K. Cheung, N. Zhu, *Chem. A-Eur. J.*, 2001, **7**, 4180; (b) M. Hissler, J. E. McGarrah, W. B. Connick, D. K. Geiger, S. Cummings, *Coord. Chem. Rev.*, 2000, **208**, 115; (c) E. Rossi, A. colombo, C. Dragonetti, D. Roberto, R. Ugo, A. Valore, L. Falciola, P. Brulatti, M. Cocchi, J. A. G. Williams, *J. Mater. Chem.*, 2012, **22**, 10650.
- 17 (a) B. W. D'Andrade, S. R. Forrest, *Adv. Mater.*, 2004, **16**, 1585; (b) H-F. Xiang, S-C. Chan, K. K-Y. Wu, C-M. Che, P. T. Lai, *Chem. Commun.*, 2005, **11**, 1408.
- 18 J. Kalinowski, in *Organic Light Emitting Diodes: Principles, Characteristics, and Processes*, Marcel Dekker, New York, 2005.
- 19 J. Kalinowski, W. Stampor, J. Szmytkowski, M. Cocchi, D. Virgili, V. Fattori, P. Di Marco, *J. Chem. Phys.*, 2005, **122**, 154710.
- 20 (a) V. M. Miskowski, V. H. Houlding, *Inorg. Chem.*, 1991, **30**, 4446; (b) J. A. G. Williams, *Top. Curr. Chem.*, 2007, **281**, 205.

- 21 E. O. Danilov, I. E. Pomestchenko, S. Kinayigit, P. L. Gentili, M. Hissler, R. Ziessel, F. Castellano, *J. Phys. Chem. A*, 2005, **109**, 2465.
- 22 (a) S. Chang, J. Kavitha, S. Li, C. Hsu , Y. Chi, Y. Yen, P. Chou, G. Lee, A. Cart, Y. Tao, C. Chien, *Inorg. Chem.*, 2006, **45**, 137; (b) J. Ni, X. Zhang, N. Qiu, Y. Wu, L. Zhang, J. Zhang, Z. Chen, *Inorg. Chem.*, 2011, **50**, 9090; (c) C. Chen, F. Wu, Y. Tsai, C. Cheng, *Adv. Func. Mater.*, 2011, **21**, 3150.
- 23 (a) L. Chassot, E. Muller, A. Von Zelewsky, *Inorg. Chem.*, 1984, **23**, 4249; (b) J. Bailey, V. Miskowski, H. Gray, *Inorg. Chem.*, 1993, **32**, 369; (c) W. B. Connick, L. M. Henling, R. E. Marsh, H. B. Gray, *Inorg. Chem.*, 1996, **35**, 6261; (d) B. Ma, J. Li, P. I. Djurovich, M. Yousufuddin, R. Bau, M. E. Thompson, *J. Am. Chem. Soc.*, 2005, **127**, 28.
- 24 A. Santoro, A. Whitwood, J. A. G. Williams, V. N. Kozhevnikov, D. W. Bruce, *Chem. Mater.*, 2009, **21**, 3871.

---

# Conclusions

At the end of this work I want just to sum up chronologically all the activities I have done during my ph.D. period and the paper published in the last three years.

I have attended two International School of Crystallography in Erice (The power of powder diffraction 2011 and The Future of Dynamic Structural Science 2013) where I presented my results by posters presentations, The Zurich school of Crystallography (2011) where I have been awarded the best student prize and the AIC International school of Crystallography in Trento (2012)

I have attended the 5<sup>th</sup>, the 6<sup>th</sup>, and the 7<sup>th</sup> editions of the workshop Crystal forms @ Bologna where I presented my results by poster presentations.

I have attended the 2012 AIC congress in Verona, where I have been awarded the best master thesis in crystallography and the 2013 MISSCA congress in Como where I presented my results by oral presentation.

I spent a 4-month period at the Reading University under the supervision of Dr. Kenneth Shankland with a project based on structure solution by X-ray powder diffraction data. In the same period I have also attended a X-ray user meeting in Orford at the Agilent Technologies department

The list of patent and publications about this work is reported below:

1. Lucia Maini, Dario Braga, Paolo P. Mazzeo and Barbara Ventura, *Polymorph and isomer conversion of complexes based on CuI and PPh<sub>3</sub> easily observed via luminescence*, Dalton Trans., (2012), **41**, 531;
2. Pierpaolo Brulatti, Valeria Fattori, Sara Muzzioli, Stefano Stagni, Paolo Pio Mazzeo, Dario Braga, Lucia Maini, Silvia Milita and Massimo Cocchi, *Tuning the colour and efficiency in OLEDs by using amorphous or polycrystalline emitting layers*, J. Mater. Chem. C, (2013), **1**, 1823-1831;
3. Paolo P. Mazzeo, Lucia Maini, Dario Braga, Giovanni Valenti, Francesco Paolucci, Massimo Marcaccio, Andrea Barbieri, and Barbara Ventura, *Switch On/Switch Off Signal in an MOF-Guest Crystalline Device*, Eur. J. Inorg. Chem., (2013), 4459–4465;
4. Lucia Maini, Paolo Pio Mazzeo, Francesco Farinella, Valeria Fattori and Dario Braga, *Mechanochemical preparation of Copper Iodide clusters of interest for luminescent devices*, Faraday Discussions, (2014), Accepted manuscript;
5. Paolo P. Mazzeo, Lucia Maini, Alex Petrolati, Valeria Fattori, Kenneth Shankland, and Dario Braga, *Phosphorescence quantum yield enhanced by intermolecular hydrogen bonds in Cu<sub>4</sub>I<sub>4</sub> clusters in the solid state*, Dalton Trans. (2014) Submitted paper;
6. Paolo P. Mazzeo, Lucia Maini, Valeria Fattori and Dario Braga, *Single-phase white-emitter copper iodide based Metal-Organic Framework*, in preparation;
7. Dario Braga, Lucia Maini, Paolo P. Mazzeo, Emettitore di luce bianca in fase cristallina singola, Patent in preparation.



# Appendix A

Polymorph and isomer conversion of  
complexes based on CuI and PPh<sub>3</sub> easily  
observed *via* luminescence

Supplementary information

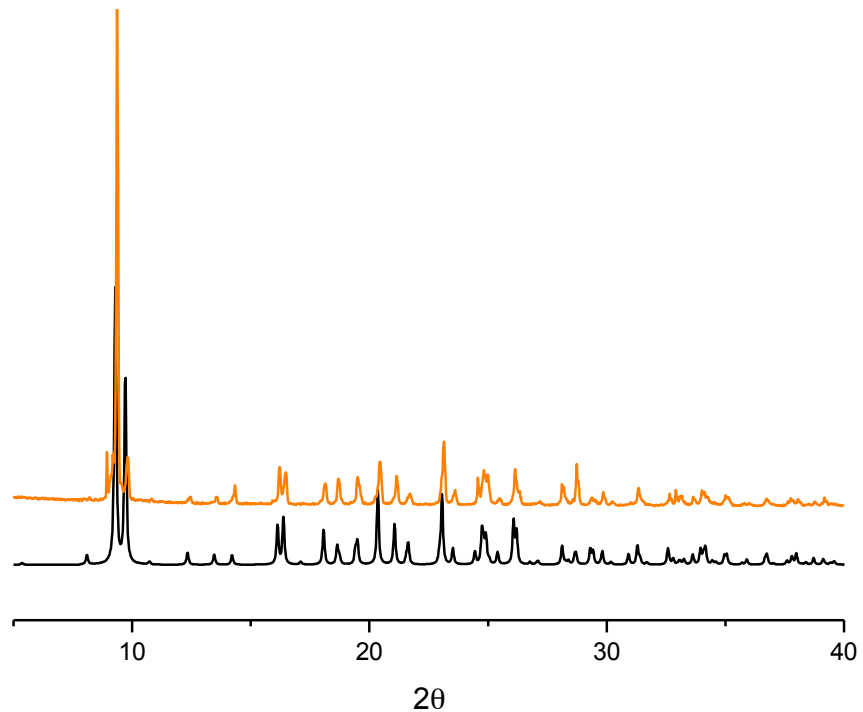


Figure A.1 | experimental and calculated diffraction pattern comparison for  $[\text{CuI}(\text{PPh}_3)_3]\alpha$

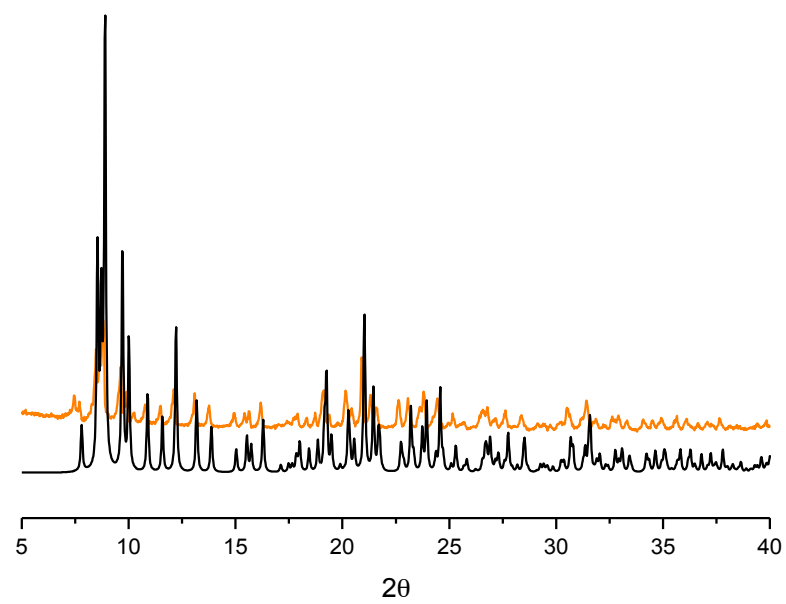


Figure A.2 | experimental and calculated diffraction pattern comparison for  $[\text{Cu}_2\text{I}_2(\text{PPh}_3)_3]$

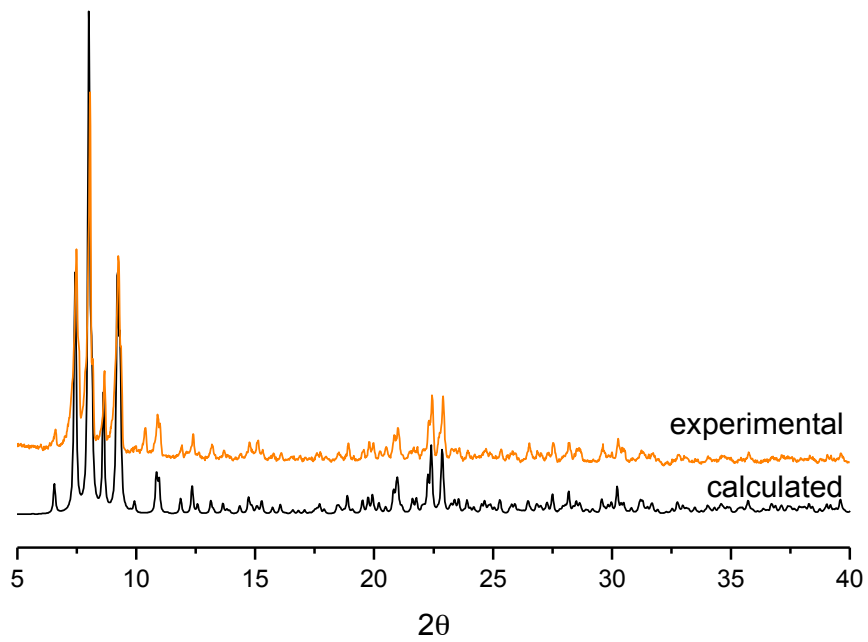


Figure A.3 | experimental and calculated pattern comparison for  $[\text{CuI}(\text{PPh}_3)]_4 \mathbf{1a}$

---

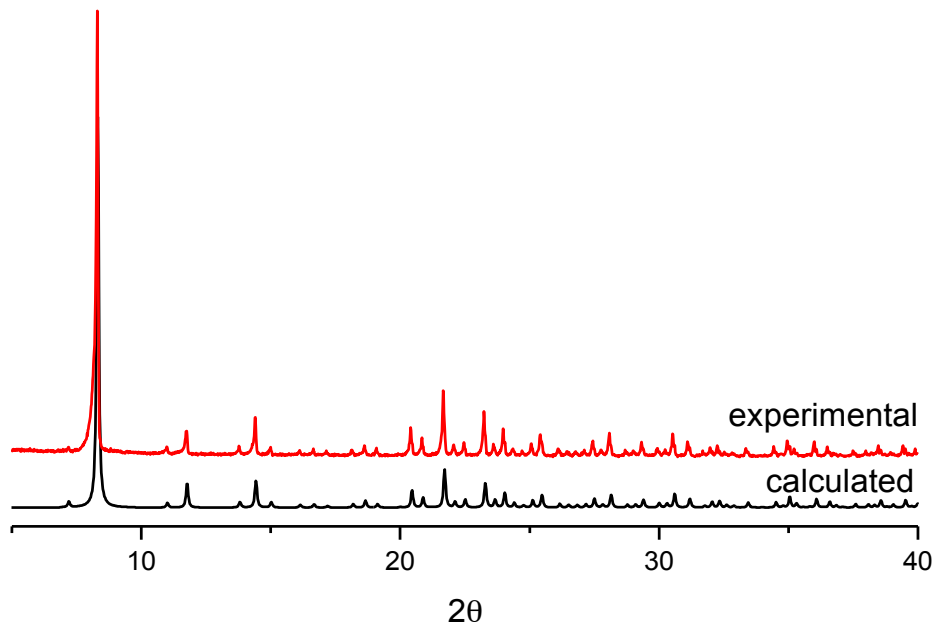


Figure A.4 | experimental and calculated pattern comparison for  $[\text{CuI}(\text{PPh}_3)]_4 \mathbf{1b}$

---

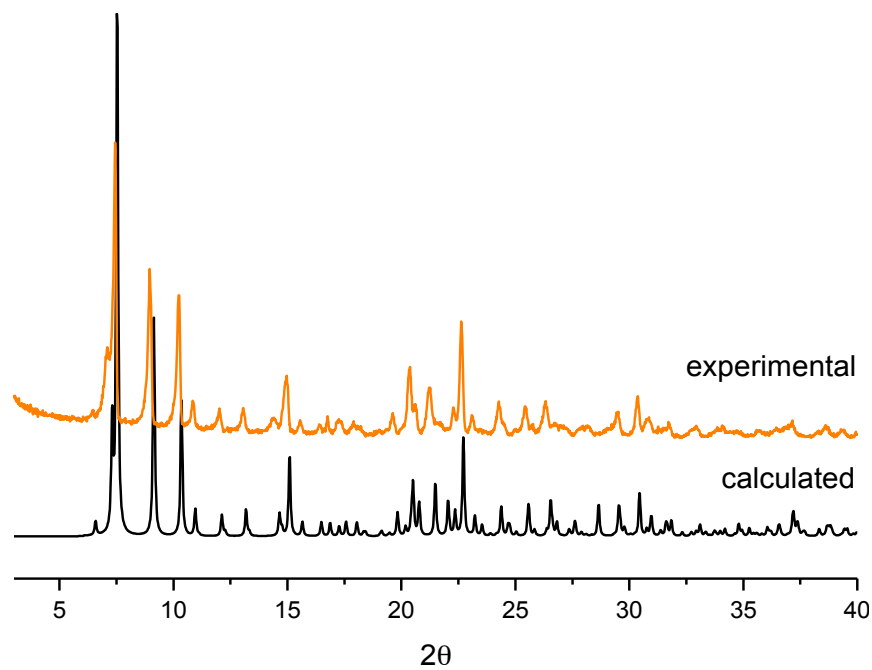


Figure A.5 | experimental and calculated patter comparison for  $[\text{CuI}(\text{PPh}_3)_4]_2$

---

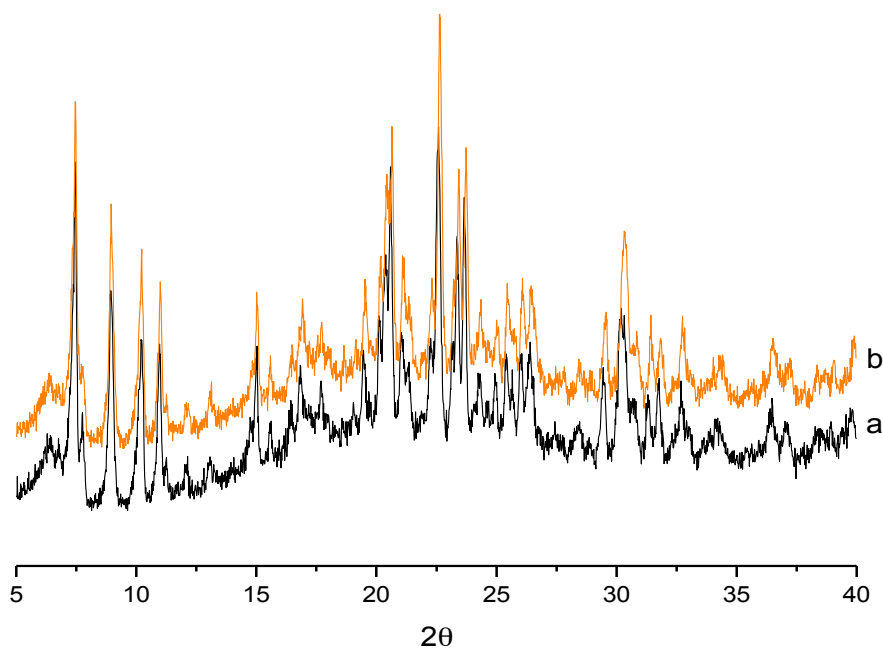


Figure A.6 | experimental and calculated patter comparison for  $[\text{CuI}(\text{PPh}_3)_4]_2$

---

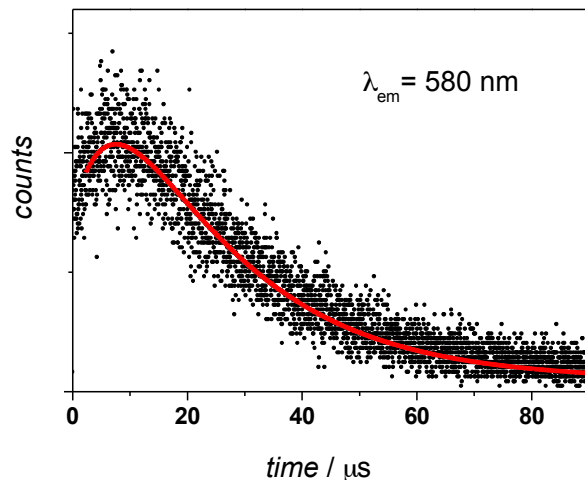


Figure S7. Luminescence profile at 580 nm of solid  $[\text{Cu}_4\text{I}_4(\text{PPh}_3)_4]$  **1b** at 77 K and the bi-exponential fitting (red).

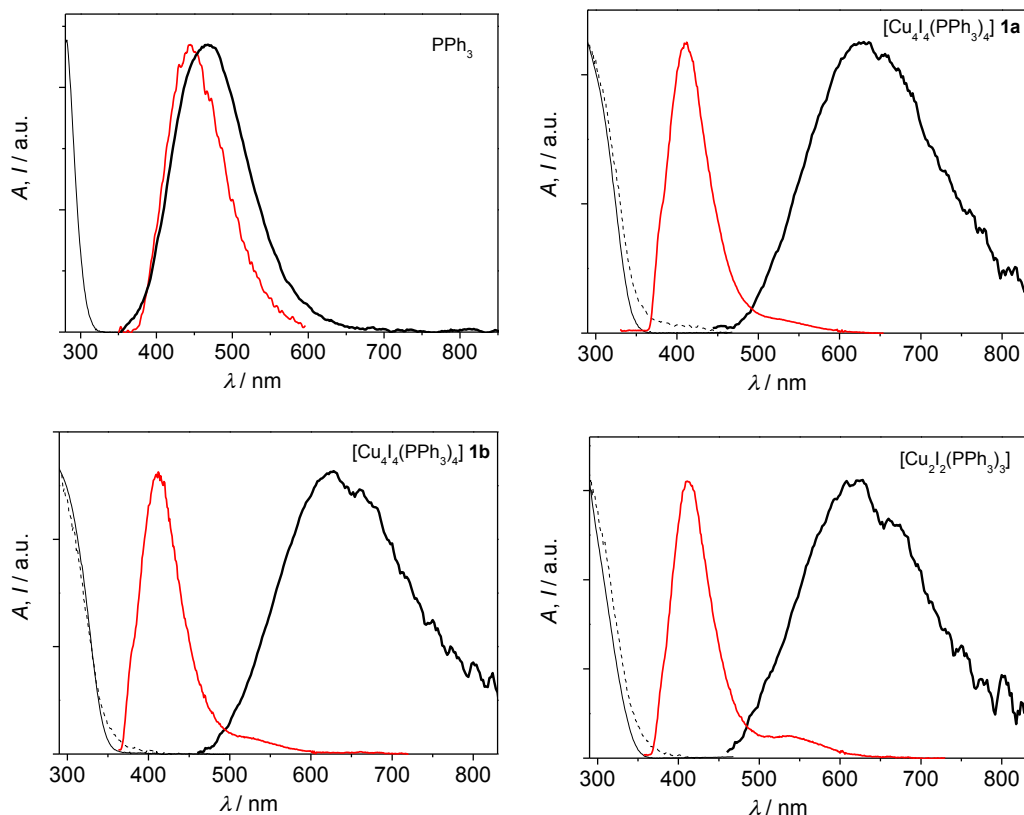


Figure A.8 | Arbitrarily scaled absorption (black thin) and room temperature (black thick) and 77K (red) corrected emission spectra of toluene solutions of  $\text{PPh}_3$  and compounds  $[\text{Cu}_4\text{I}_4(\text{PPh}_3)_4]$  **1a**,  $[\text{Cu}_4\text{I}_4(\text{PPh}_3)_4]$  **1b** and  $[\text{Cu}_2\text{I}_2(\text{PPh}_3)_3]$ ; excitation at 300 nm for  $\text{PPh}_3$  and 330 nm for the Cu(I) complexes. The room temperature excitation spectra of the complexes measured at 600 nm are also reported (dash).

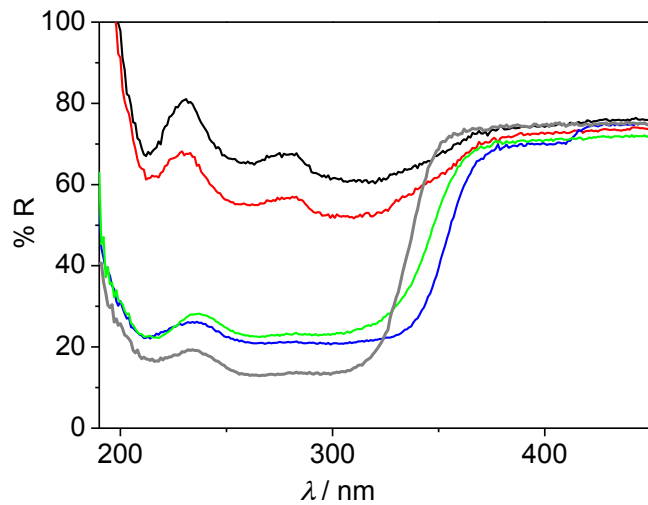


Figure A.9 | Reflectance spectra of solid samples of PPh<sub>3</sub> (grey), [Cu<sub>4</sub>I<sub>4</sub>(PPh<sub>3</sub>)<sub>4</sub>]1a (black), [Cu<sub>4</sub>I<sub>4</sub>(PPh<sub>3</sub>)<sub>4</sub>]1b (red), [Cu<sub>4</sub>I<sub>4</sub>(PPh<sub>3</sub>)<sub>4</sub>]2 (blue) and [Cu<sub>2</sub>I<sub>2</sub>(PPh<sub>3</sub>)<sub>3</sub>] (green).

---

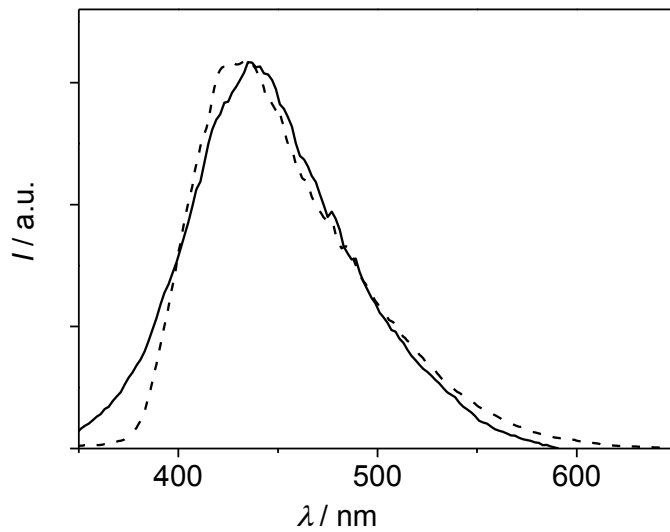


Figure A.10 | Normalized corrected emission spectra of solid PPh<sub>3</sub> at room temperature (solid line) and 77 K (dashed line). Excitation at 300 nm.

---

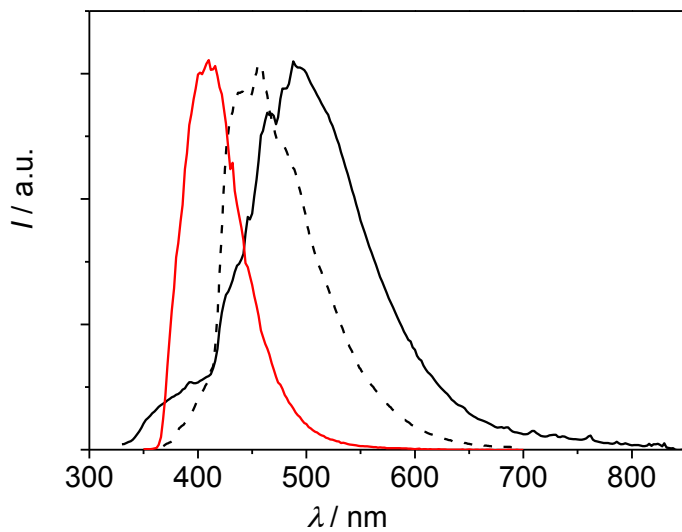


Figure A.11 | Normalized corrected emission spectra of solid Cu<sub>4</sub>Br<sub>4</sub>(PPh<sub>3</sub>)<sub>4</sub> at room temperature (solid black line) and at 77 K (dashed black line) and of a toluene solution at 77K (red line). Excitation at 300 nm.

Table A.1. Luminescence parameters of Cu<sub>4</sub>Br<sub>4</sub>(PPh<sub>3</sub>)<sub>4</sub> in air-free toluene solution and in the solid state, at room temperature and at 77 K.

	Emission at r.t.			Emission at 77 K		
	$\lambda_{max}^a /$	$\phi_{em}^b$	$\tau^c / \mu s$	$\lambda_{max}^a /$	$\tau^c / \mu s$	
Cu <sub>4</sub> Br <sub>4</sub> (PPh <sub>3</sub> ) <sub>4</sub>	Solution	620	9 ×	29.1 ×	410	511.1 (40%), 1.2 ×
	Solid	492	10 <sup>-4</sup>	10 <sup>-3</sup>	442	10 <sup>3</sup> (60%)

<sup>a</sup>From uncorrected emission spectra. <sup>b</sup> Emission quantum yield in solution, determined by comparing corrected emission spectra, using quinine sulfate in air-equilibrated 1 N H<sub>2</sub>SO<sub>4</sub> ( $\phi_{em}$  = 0.546) as a standard, excitation at 330 nm. <sup>c</sup> Excitation at 331 nm.<sup>d</sup> Large uncertainties due to the weakness of the emission.

Table A.2 | Crystal data and details of measurement for compound crystallized in this work.

	<b>[CuI(PPh<sub>3</sub>)<sub>3</sub>]b</b>	<b>[Cu<sub>4</sub>I<sub>4</sub>(PPh<sub>3</sub>)<sub>4</sub>]1a</b>	<b>[Cu<sub>4</sub>I<sub>4</sub>(PPh<sub>3</sub>)<sub>4</sub>]1b</b>	<b>[CuI(PPh<sub>3</sub>)<sub>2</sub>]<sub>1.5</sub>*CH<sub>2</sub>Cl<sub>2</sub></b>
Chemical formula	C <sub>54</sub> H <sub>45</sub> CuIP <sub>3</sub>	C <sub>72</sub> H <sub>60</sub> Cu <sub>4</sub> I <sub>4</sub> P <sub>4</sub>	C <sub>72</sub> H <sub>60</sub> Cu <sub>4</sub> I <sub>4</sub> P <sub>4</sub>	C <sub>55</sub> H <sub>47</sub> Cl <sub>2</sub> Cu <sub>2</sub> I <sub>2</sub> P <sub>3</sub>
M <sub>r</sub>	977.25	1811.85	1810.84	1252.62
Crystal system	Monoclinic	Monoclinic	Cubic	Monoclinic
Space group	P2 <sub>1</sub> /c	P2 <sub>1</sub> /n	I-43d	P2 <sub>1</sub> /c
T [K]	RT	90	90	RT
a [Å]	13.2375 (5),	13.4237 (10)	29.7864 (3)	15.7252(6)
b [Å]	18.5976 (7)	26.406 (3)		19.5305(7)
c [Å]	18.9297 (7)	19.4266 (11)		17.6410(8)
β (°)	93.953 (4)	99.531 (7)		110.473(5)
V (Å <sup>3</sup> )	4649.1 (3)	6791.0 (9)	26427.4 (5)	5075.7(4)
Z	4	4	16	4
F (000)	1984	3524	14080	2480
θ range [°]	2.68 – 29.02	2.78 – 29.18	2.56 – 29.01	2.68 – 29.09
Radiation type	Mo Kα	Mo Kα	Mo Kα	Mo Kα
μ (mm <sup>-1</sup> )	1.27	3.19	3.28	2.29
Measured reflns	24269	35458	13317	32388
Unique reflns	10549	15590	4275	11167
Parameters	424	758	253	578
GOF on F <sup>2</sup>	0.76	1.04	1.02	1.23
R <sub>int</sub>	0.035	0.100	0.046	0.072
R <sub>1</sub> (on F,  F  > 2σ(F))	0.044	0.046	0.038	0.106
wR(F <sup>2</sup> )	0.130	0.112	0.061	0.323

# Appendix B

## Switch on - switch off signal in a MOF-guest crystalline device

Supplementary informations

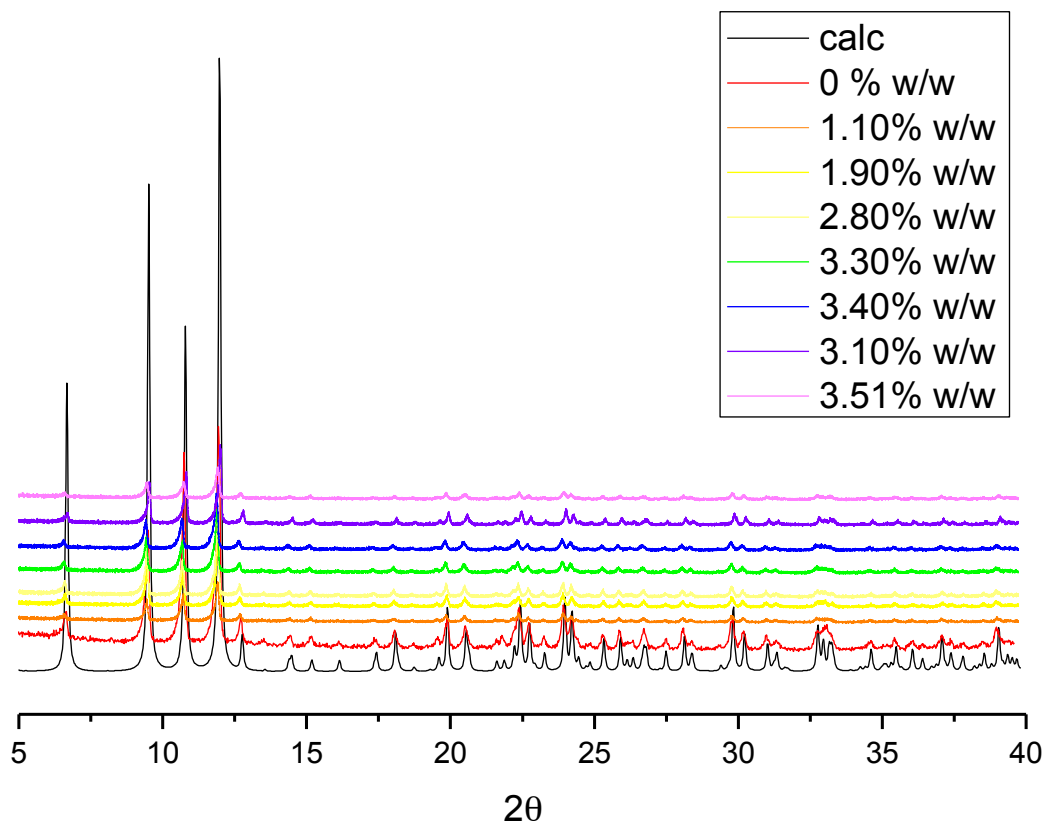


Figure B.1 | XRPD analysis of MOF 1 (red line) combined with FeCp<sub>2</sub>@MOF 1 with different loading content of guest molecule in host structure; labels represent the percentage of FeCp<sub>2</sub> w/w in FeCp<sub>2</sub>@MOF 1 (orange to pink lines). Black line represents the calculated XRPD pattern from SCXRD analysis performed on MOF 1.

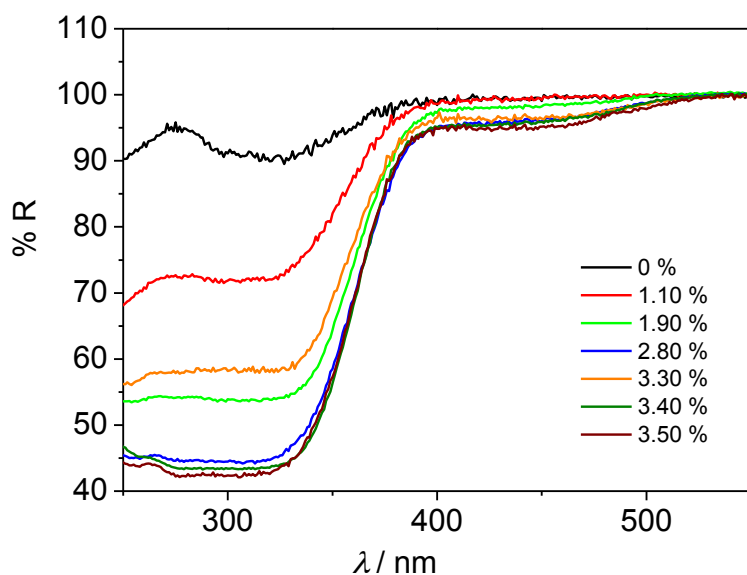


Figure B.2 | Reflectance spectra of solid samples of MOF 1 with different loadings of FeCp<sub>2</sub> (% w/w, as measured by AAS).

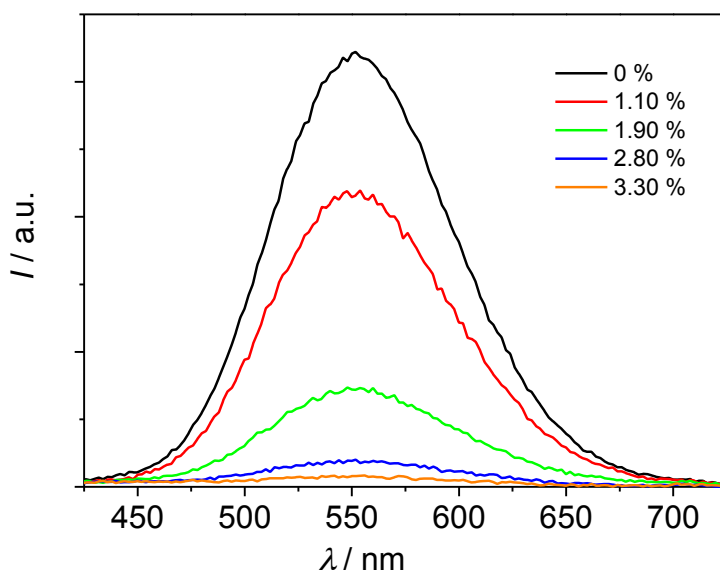


Figure B.3 | Raw emission profiles of solid samples of MOF **1** with different loadings of FeCp<sub>2</sub> (% wt/wt) obtained with the use of an integrating sphere and corrected for the absorption coefficient (see text).

Figure B.3 reports the emission profiles of the samples placed in the sphere upon direct hit of the excitation beam,<sup>1</sup> corrected for the absorption coefficient of the sample at the excitation wavelength, estimated by the use of the integrating sphere.<sup>2</sup> It can be noticed that each determination of the value of the absolute emission quantum yield is a stand-alone measurement and Figure B.3 only furnishes an immediate visual estimation of the effect of the ferrocene loading on MOF **1** emission.

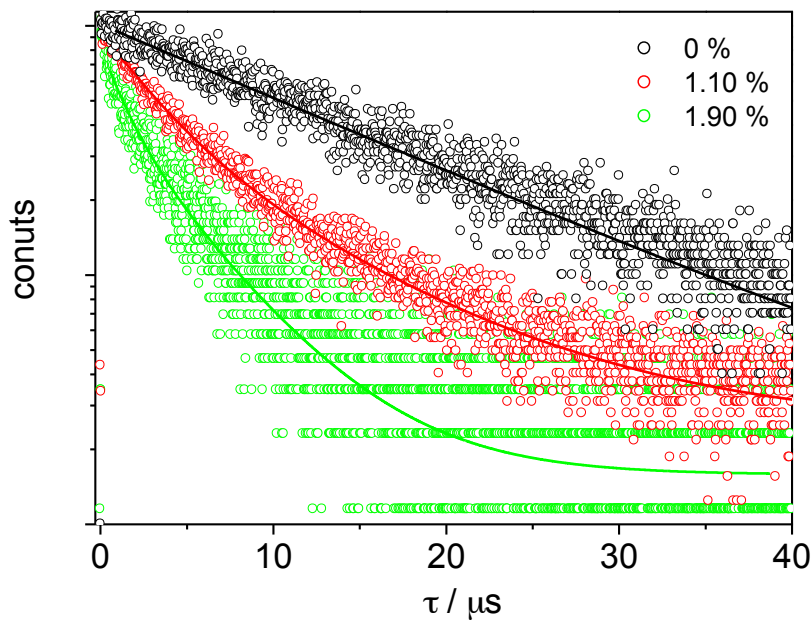


Figure B.4 | Luminescence decays, on a semi-log scale, of MOF **1** at different amounts of FeCp<sub>2</sub> loading and relative fittings

**Table B.1|** Conversion of guest/host weight ratio in guest/host molar ratio. ( $\text{FeCp}_2=186\text{g/mol}$ ;  $\text{Cu}_4\text{I}_4(\text{DABCO})_2=985\text{g/mol}$ ). According to the CC emission band,  $\text{Cu}_4\text{I}_4(\text{DABCO})_2$  has been chosen as the minimal emitting portion in MOF structure.

Guest/Host (w/w)	$\text{FeCp}_2$ (mol)	$\text{Cu}_4\text{I}_4(\text{DABCO})_2$ (mol)	Guest/Host (mol/mol)
1.10%	0.59%	10.04%	6%
1.90%	1.02%	9.96%	10%
2.80%	1.51%	9.87%	15%
3.30%	1.77%	9.82%	18%
3.40%	1.83%	9.81%	19%
3.10%	1.67%	9.84%	17%
3.50%	1.88%	9.80%	19%

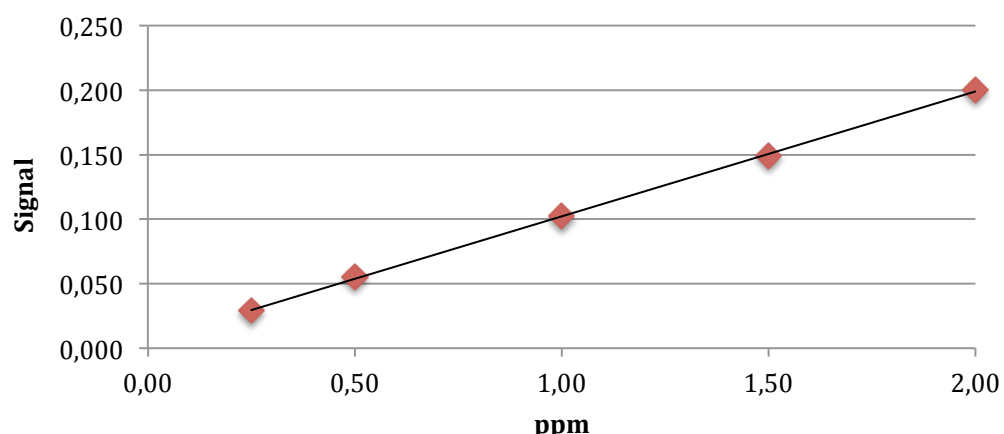


Figure B.5 | Calibration line for AAS experiment ( $R^2=0.99972$ , black line). Iron standard solutions have been prepared in concentration of 0.25 ppm, 0.50 ppm, 1.0 ppm, 1.50 ppm, 2.00 ppm. The iron concentration in samples of  $\text{FeCp}_2@\text{MOF } \mathbf{1}$  has been taken in the range of calibration line.

- 1 Barbieri, A. & Accorsi, G. *Absolute photoluminescence quantum yield determination of solid-state samples*. EPA Newsletters, 26-35 (December 2006).
- 2 Aurisicchio, C., Ventura, B., Bonifazi, D. & Barbieri, A. *Photophysical Properties of Tolan Wavelength Shifters in Solution and Embedded in Polymeric Organic Thin Films*. J. Phys. Chem. C **113**, 17927-17935 (2009).

# Appendix C

Phosphorescence quantum yield enhanced by  
intermolecular hydrogen bonds in Cu<sub>4</sub>I<sub>4</sub>  
clusters in the solid state

Supporting information

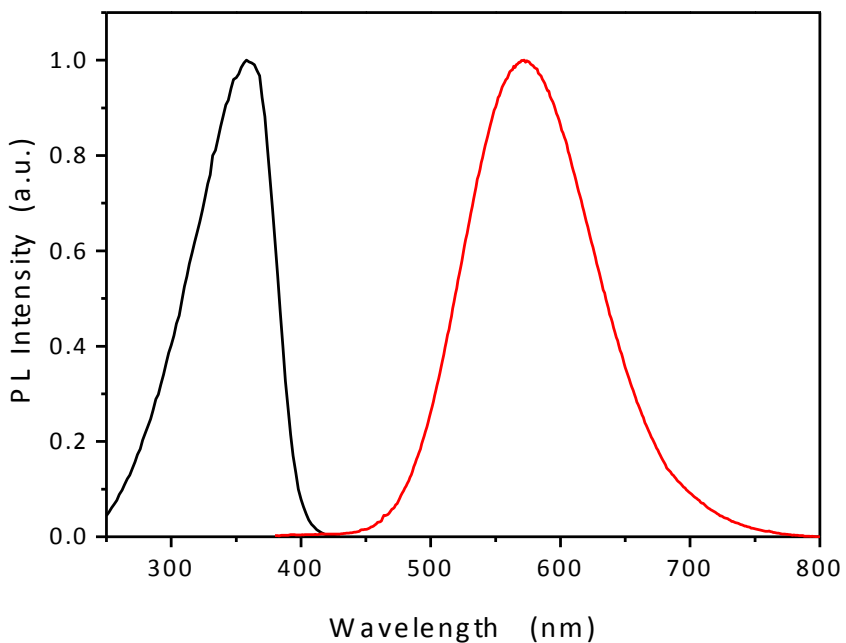


Figure C.1 | Normalized excitation (black) and emission (red) spectra recorded on microcrystalline powder of **1**.

---

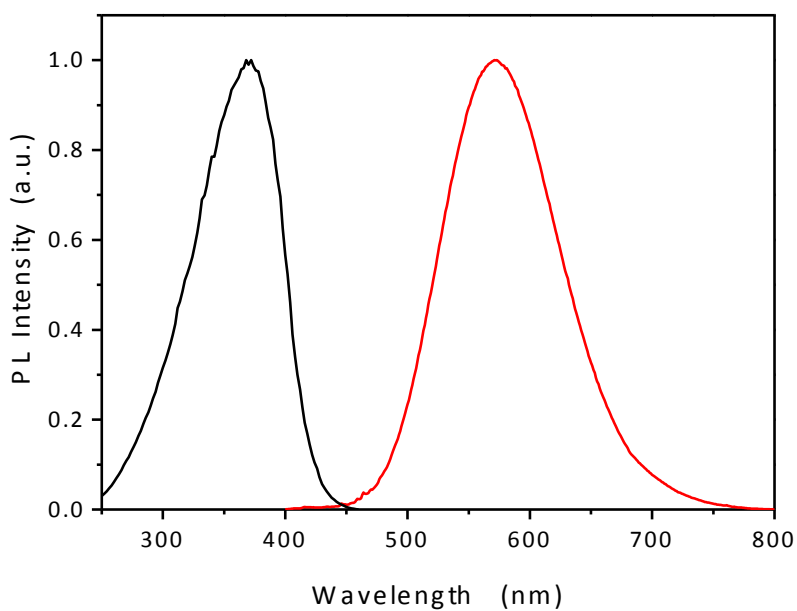


Figure C.2 | Normalized excitation (black) and emission (red) spectra recorded on microcrystalline powder of **2**.

---

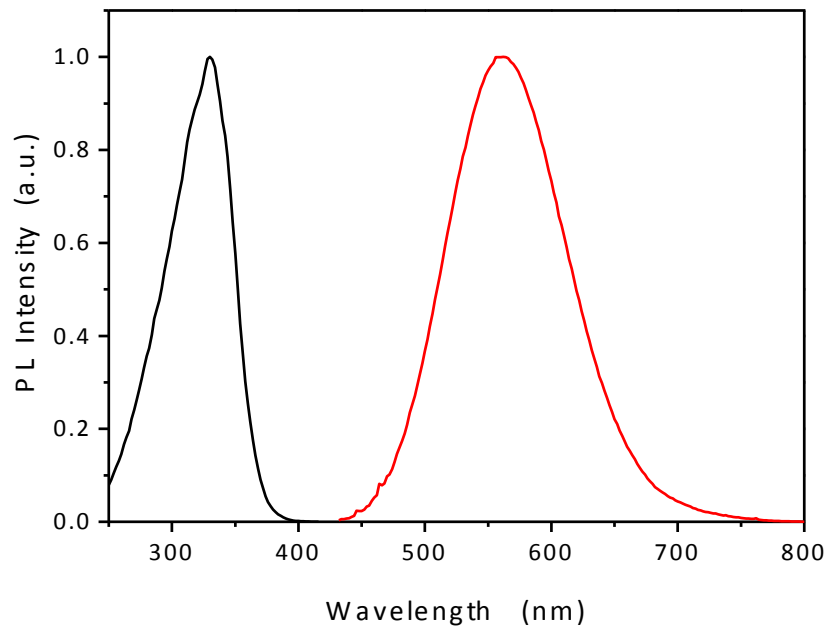


Figure C.3 | Normalized excitation (black) and emission (red) spectra recorded on microcrystalline powder of **3**.

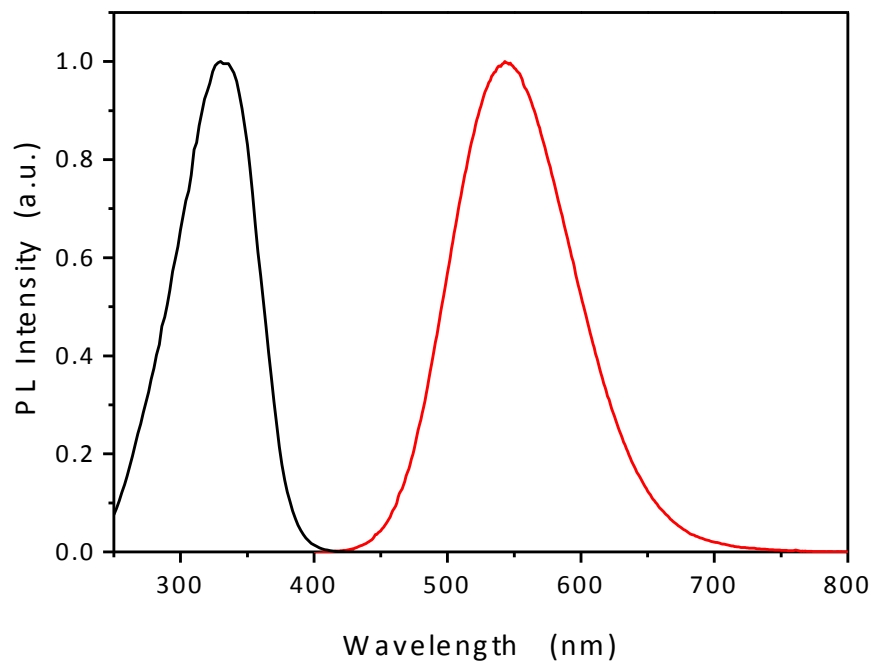


Figure C.4 | Normalized excitation (black) and emission (red) spectra recorded on microcrystalline powder of **4**.

---

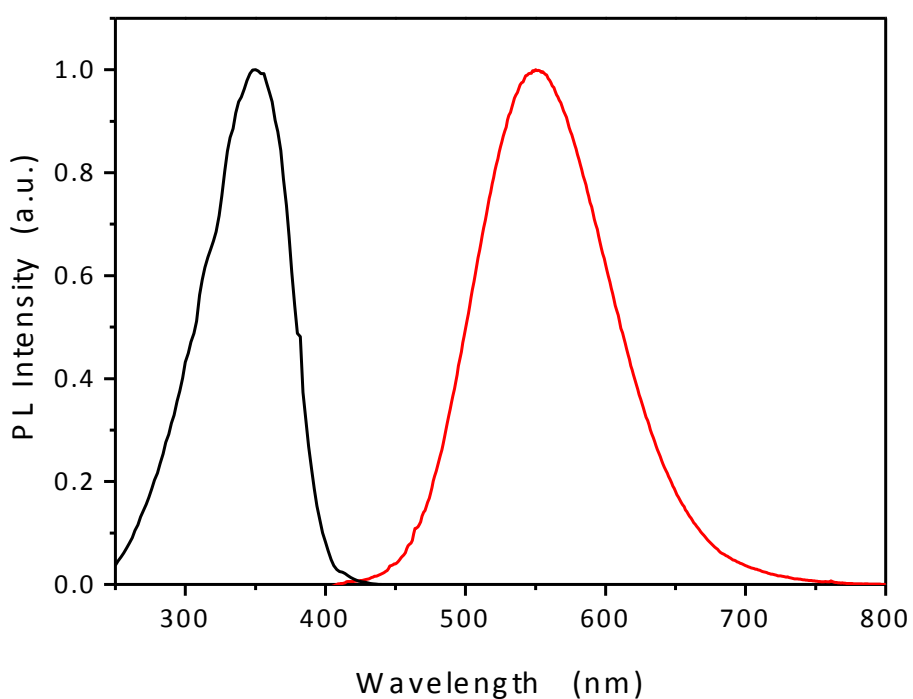


Figure C.5 | Normalized excitation (black) and emission (red) spectra recorded on microcrystalline powder of **5a**.

---

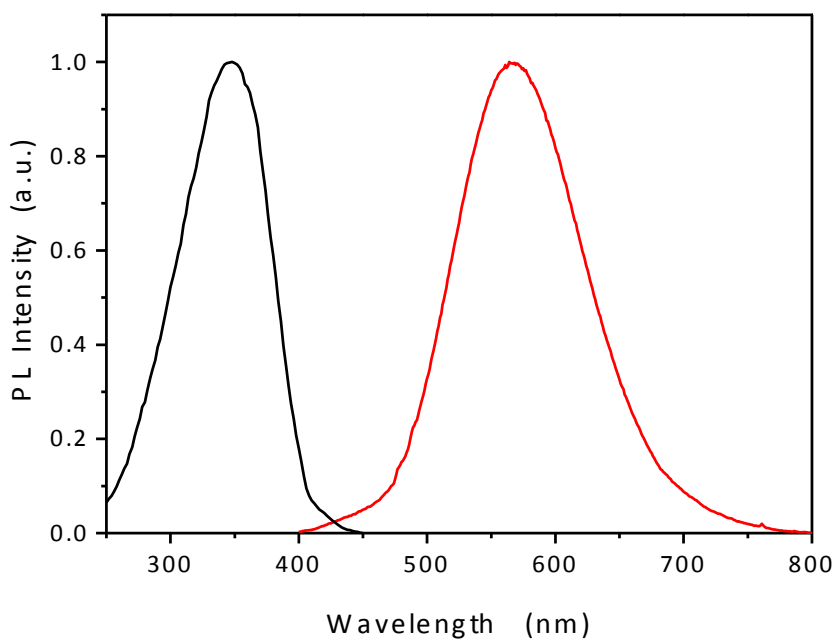


Figure C.6 | Normalized excitation (black) and emission (red) spectra recorded on microcrystalline powder of **5b**.

---

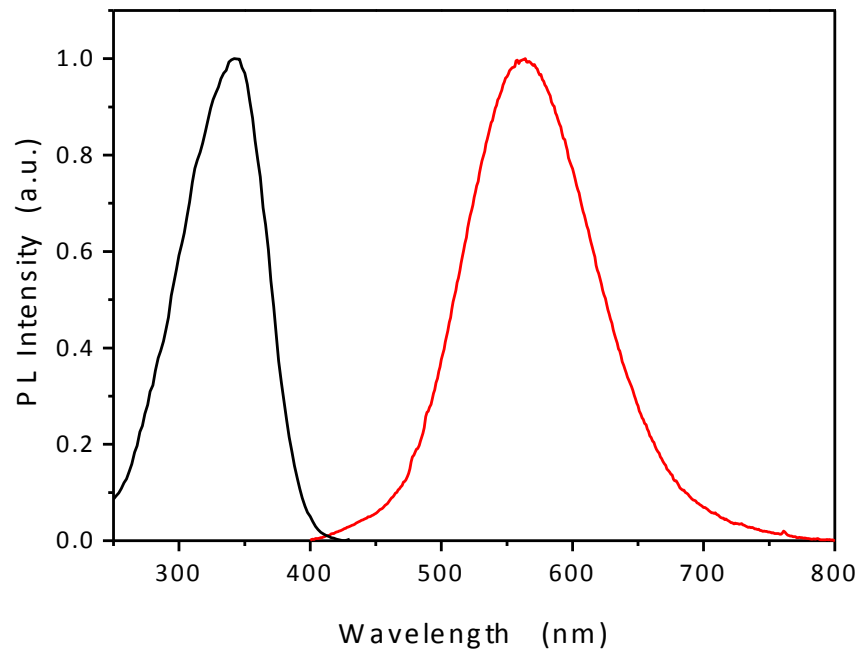


Figure C.7 | Normalized excitation (black) and emission (red) spectra recorded on microcrystalline powder of **5b** (desolvated).

---

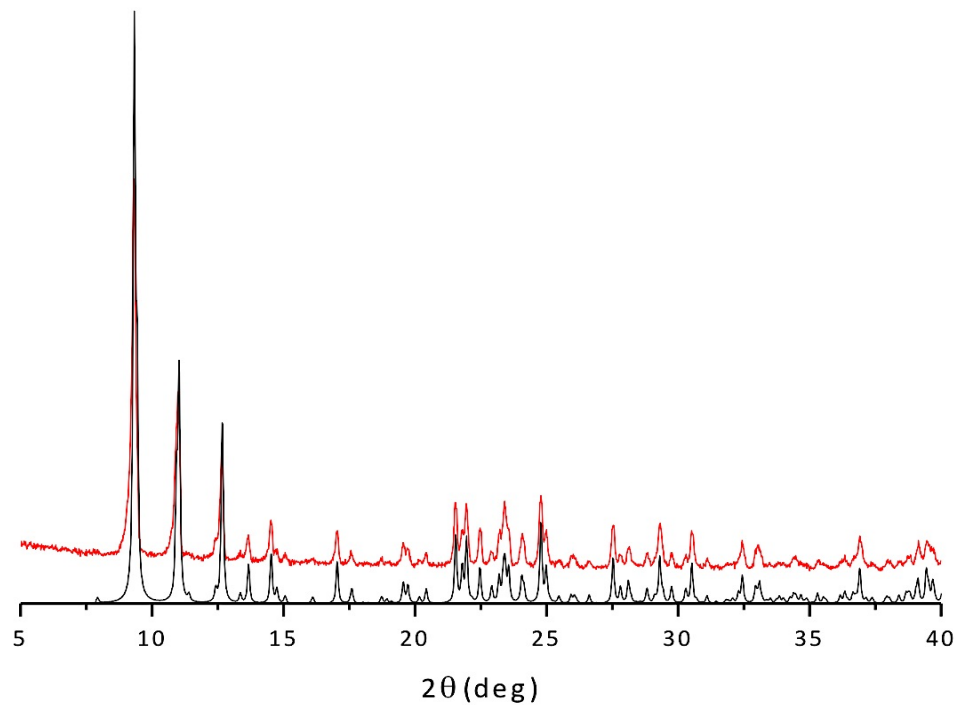


Figure C.8 | Experimental (red line) and calculated (black line) powder pattern comparison of **1**

---

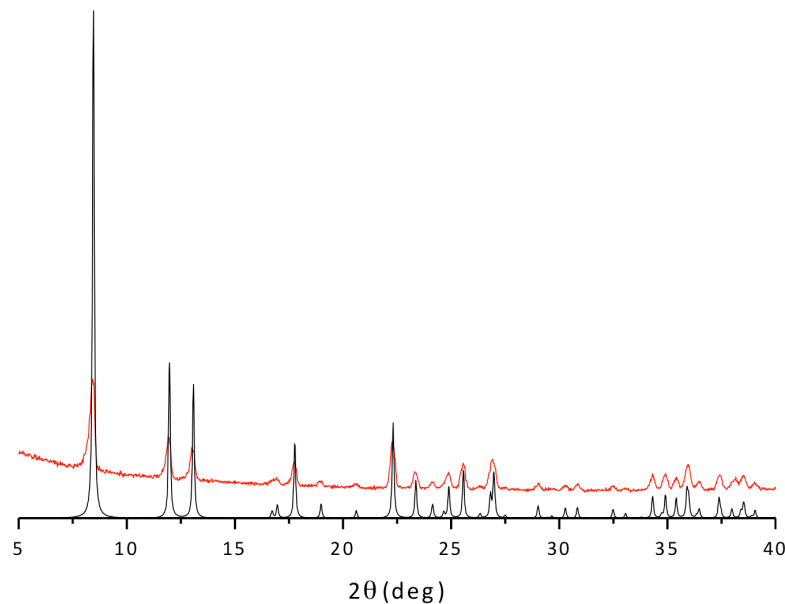


Figure C.9 | Experimental (red line) and calculated (black line) powder pattern comparison of **2**

---

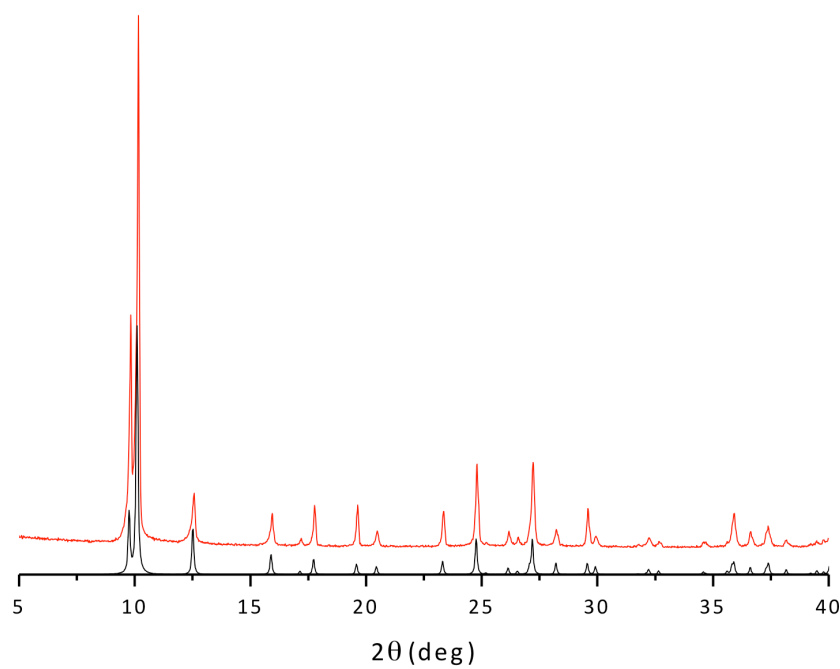


Figure C.10 | Experimental (red line) and calculated (black line) powder pattern comparison of **3**

---

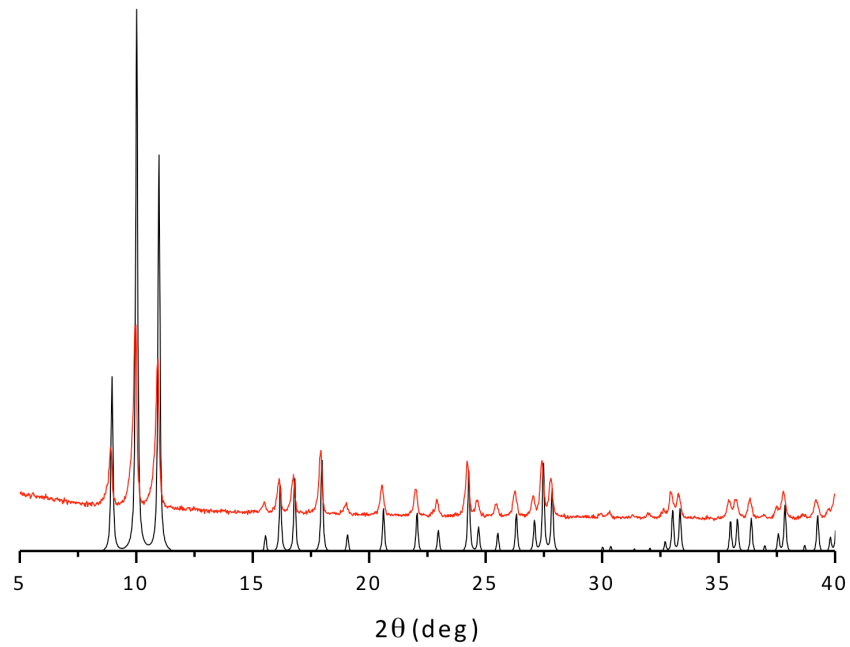


Figure C.11 | Experimental (red line) and calculated (black line) powder pattern comparison of 4

---

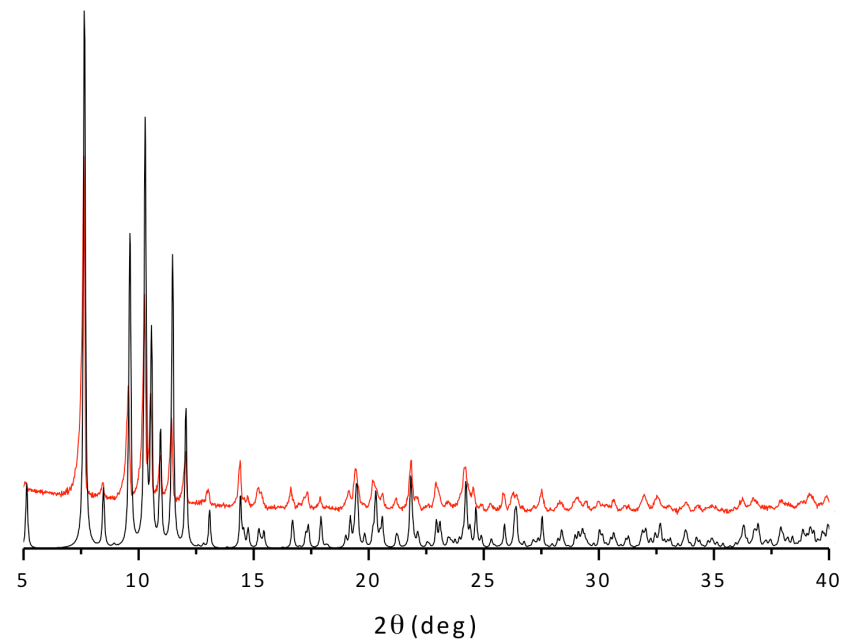


Figure C.12 | Experimental (red line) and calculated (black line) powder pattern comparison of 5b

---

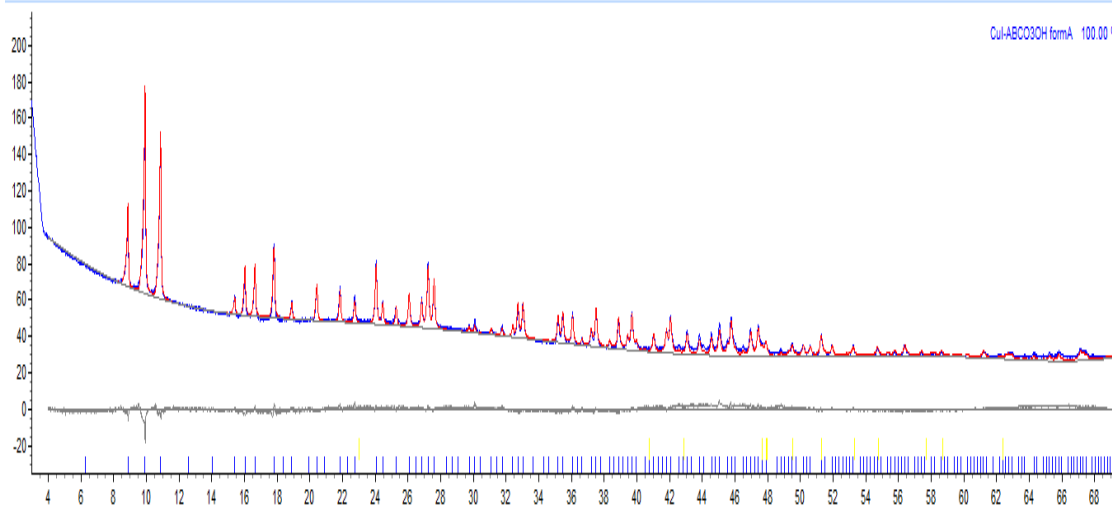


Figure C.13 | Rietveld analysis output graph of 5a.

The data set was background subtracted and truncated to  $50^\circ 2\theta$  for Pawley fitting ( $\chi^2 = 1.9$ ). A shifted Chebyshev function with 12 parameters and Pseudo-Voigt (type II) were used to fit respectively background and peak shape. A scale-only Rietveld refinement, performed with TOPAS 4.2 software package,<sup>1</sup> against the original data set in the range  $4^\circ$ – $65^\circ 2\theta$  to give a good final fit,  $R_{wp} = 2.89$ . No preferred orientation model have been used while rigid-body was built to model the chemical entities. An overall thermal parameter for each atom species was adopted.

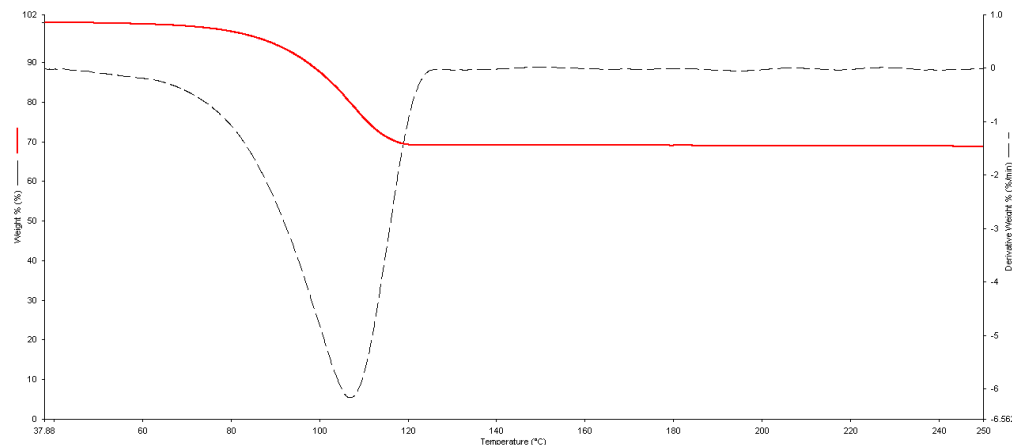


Figure C.14 | TGA analysis of 3

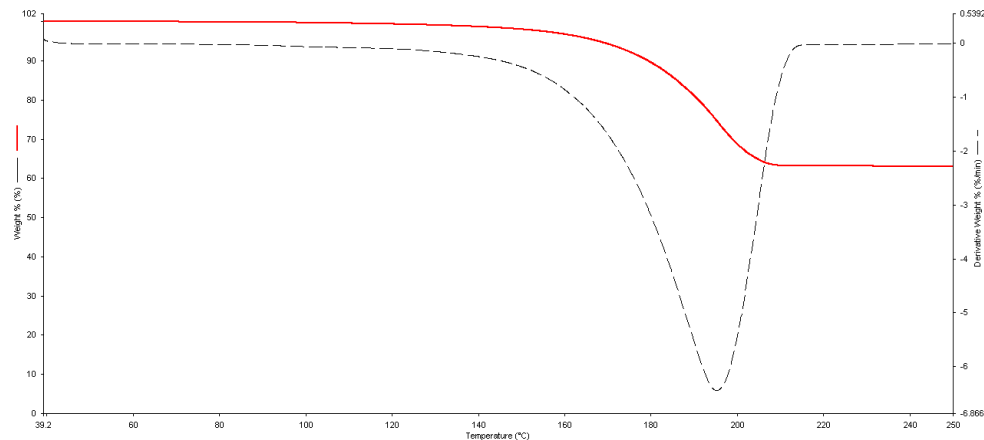


Figure C.15 | TGA analysis of 4

---

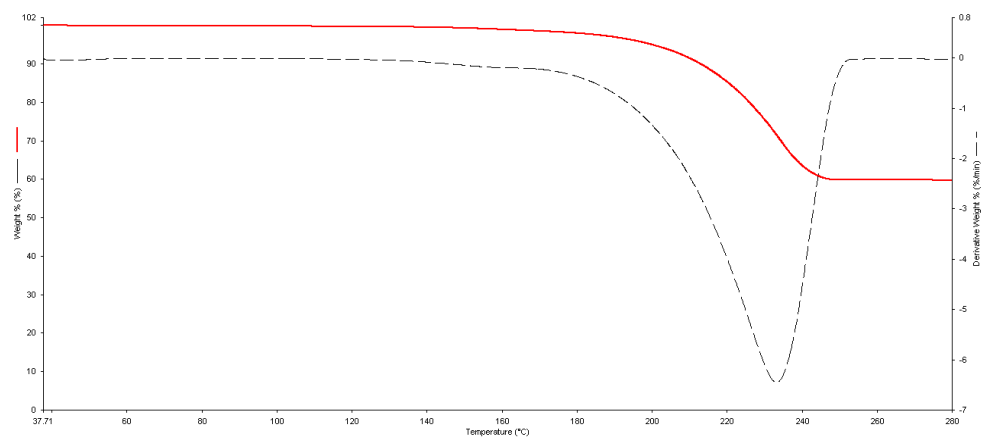


Figure C.16 | TGA analysis of 5a

---

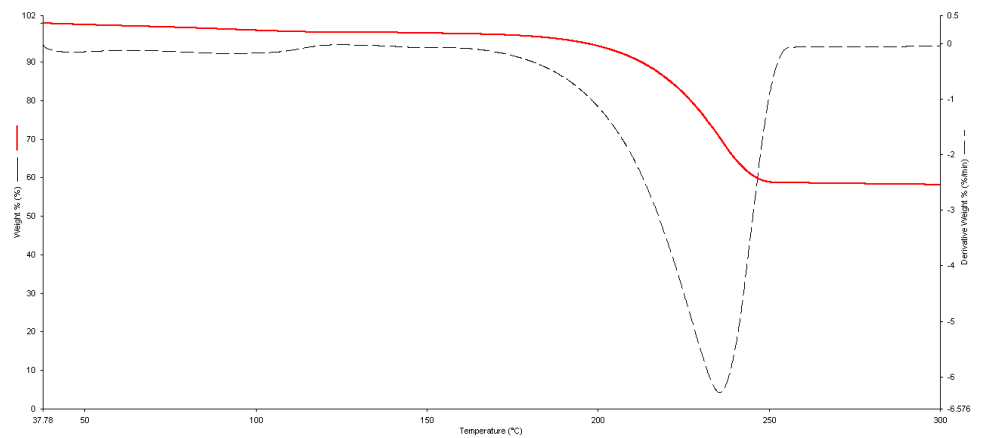


Figure C.17 | TGA analysis of 5b

---

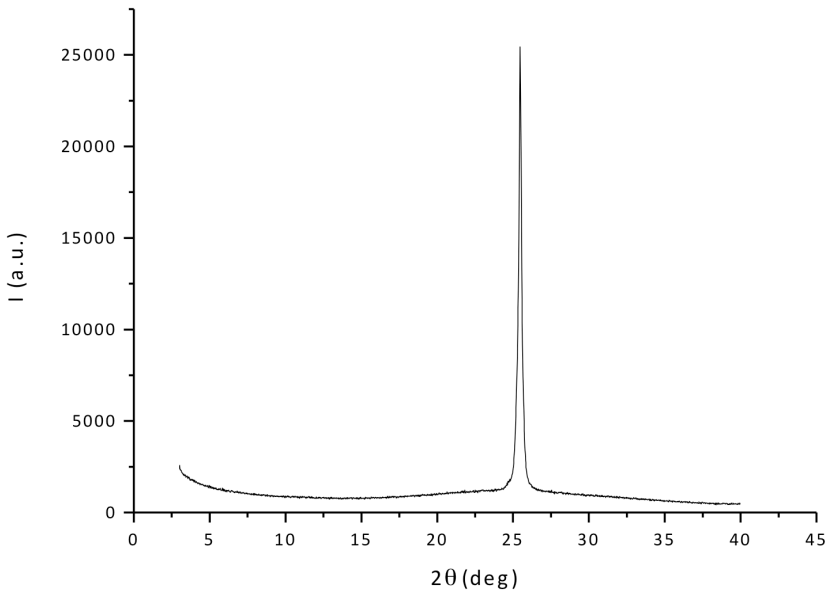


Figure C.18 | XRPD analysis performed in Bragg-Brentano geometry on a silica glass slide vacuum-deposited CuI thin film. The peak at  $25.45^\circ$  corresponds to the preferentially oriented (111) plane of the  $\gamma$ -CuI phase.

---

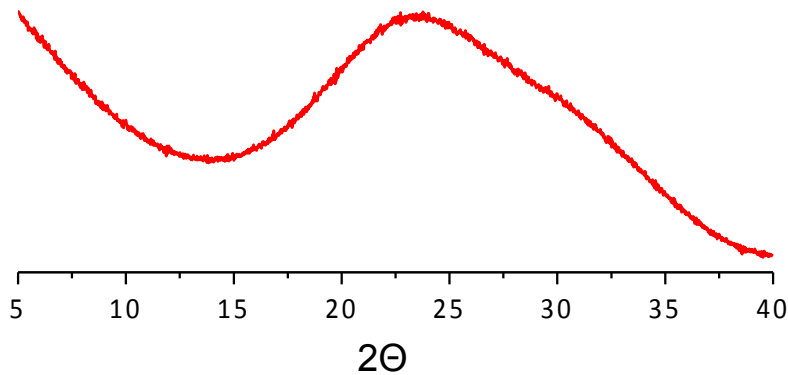


Figure C.19 | XRPD analysis performed in Bragg-Brentano geometry directly on silica glass slice after gas-solid reaction between 35nm deposited CuI and quinuclidine vapours.

---

Table C.1 | Crystal data and structure refinement for **3**, **4**, **5a**, **5b**

	<b>3</b>	<b>4</b>	<b>5a</b>	<b>5b</b>
Empirical formula	C <sub>24</sub> H <sub>56</sub> Cu <sub>4</sub> I <sub>4</sub> N <sub>4</sub>	C <sub>28</sub> H <sub>52</sub> Cu <sub>4</sub> I <sub>4</sub> N <sub>4</sub>	C <sub>28</sub> H <sub>48</sub> Cu <sub>4</sub> I <sub>4</sub> N <sub>4</sub> O <sub>4</sub>	C <sub>28</sub> H <sub>48</sub> Cu <sub>4</sub> I <sub>4</sub> N <sub>4</sub> O <sub>4</sub>
Formula weight	1162.49	1206.50	1266.46	1266.46
Temperature	293(2) K	293(2) K	293(2) K	293(2) K
Wavelength	0.71073		1.54056	0.71073
Crystal system	Tetragonal	Cubic	Monoclinic	
Space group	I -42m	P-43n	C 1 2/c 1	
Unit cell dimensions	a = 9.9963(7) b = 9.9963(7) c = 18.114(2) b = 90 1810.1(3)	a = 19.7281(6) b = 19.7281(6) c = 19.7281(6) b= 90 7678.1(4)	a = 19.9032(4) b = 19.9032(4) c = 19.9032(4) b= 90 7884.4 (1)	a = 37.444(4) b = 12.2662(8) c = 19.9994(19) b=113.379(12) 8431.6(13)
Volume	2	8	8	8
Z	Density (calculated)	2.133 Mg/m <sup>3</sup>	2.087 Mg/m <sup>3</sup>	2.106 Mg/m <sup>3</sup>
Absorption coefficient	5.749 mm <sup>-1</sup>	5.426 mm <sup>-1</sup>	-	1.995 Mg/m <sup>3</sup>
F(000)	11112	4608	-	4.953 mm <sup>-1</sup>
Crystal size	0.06 x 0.04 x 0.03 mm <sup>3</sup>	0.5 x 0.1 x 0.08 mm <sup>3</sup>	-	0.06 x 0.05 x 0.05 mm <sup>3</sup>
Reflections collected	2132	7799	-	21503
Independent reflections	1700 [R(int) = 0.0408]	2484 [R(int) = 0.0486]	-	9738 [R(int) = 0.0720]
Max. and min. transmission	1.00000 and 0.96619	1.00000 and 0.85425	-	1.00000 and 0.63350
Data / restraints / parameters	1700 / 38 / 82	2484 / 0 / 122	-	9738 / 245 / 383
Goodness-of-fit on F <sup>2</sup>	0.934	1.043	-	0.962
Final R indices [I>2sigma(I)]	R1 = 0.0766, wR2 = 0.1133	R1 = 0.0489, wR2 = 0.0669	-	R1 = 0.0798, wR2 = 0.1847-
Rwp	-	-	-	-
Rp	-	-	-	-
R(F <sup>2</sup> )	-	-	-	1.498

Crystal structures of **4** and **5b** present disorder on organic ligand; all the thermal parameters have been refined anisotropically but static or dynamic disorder are still present and neither SIMU or DELU command instructions during the refinement are able to model it.

## References

1. *Bruker AXS, Karlsruhe, Germany, 2008, TOPAS v.4.2: General Profile and Structure Analysis Software for Powder Diffraction Data.*
2. Spek, A. L., *Acta Cryst.* **1990**, *A46*, C34.

# Appendix D

## Measurements of photoluminescence quantum yield in solid state

For the measurements of photoluminescence quantum yield in solid state the SPEX Fluorolog spectrofluorometer equipped with an integrating sphere was employed and measurements after the De Mello's method were done [4]. This method, proposed in 1997 by De Mello et al, represents an improvement of the Greenham's method [5] for measuring the absolute quantum yields. Five experiments are needed in order to determine the absolute luminescence quantum yield of the sample (Figure D.1). In the first experiment, the excitation beam directly strikes the inner wall of the empty sphere, and the total amount of the excitation energy,  $L_a$ , is obtained.

In the second experiment, the sample is positioned inside the sphere but off the excitation beam pathway, the detected signal is composed by the scattered excitation light,  $L_b$ , plus the light emitted by the sample,  $P_b$ , after absorption of scattered excitation light. A fraction  $\mu$  of the excitation light scattered from the sphere wall is absorbed by the sample and so:

$$L_b = L_a (1 - \mu)$$

In the third experiment the excitation beam directly hits the sample surface and a fraction  $A$  of excitation light is absorbed. The unabsorbed fraction ( $1-A$ ) is either transmitted or reflected and a fraction  $\mu$  of this scattered light is then reabsorbed by the sample. The area of the detected excitation light spectrum,  $L_c$ , can be expressed by the equation:

$$L_c = L_a (1 - A)(1 - \mu)$$

Combining the two equations above an expression for the absorption coefficient  $A$  is obtained.

$$A = (1 - \frac{L_c}{L_b})$$

The emission profile measured in this experiment has two contributions: 1)  $\eta AL_a$ , where  $\eta$  is the photoluminescence efficiency, is due to the absorption of the excitation light, 2) is due to the light emitted after absorption of the scattered excitation light, given by:

$$P_b(1 - A)$$

Thus

$$P_c = \eta AL_a + P_b(1 - a)$$

Rearranging this equation, an expression for the PLQY is obtained. Equation 1

$$\eta = \frac{P_c - (1 - A)P_b}{AL_a}$$

The use of a spectrometer in these efficiency measurements provides several advantages:

- I. Absorption and luminescence are recorded simultaneously, so the effects of sample degradation are minimized
- II. The method can be applied even to highly scattering samples, because no separate measurements of reflectance and transmittance are requested.

For each sample five emission profiles were collected with the geometry schematized in Figure D.1: A, B, C, B<sub>2</sub>, C<sub>2</sub>. The excitation beam wavelength correspond to the maximum of the excitation spectrum or is close to it. For the first three profiles we used a grey filter at 1% of transmittance to weaken the light intensity on the fluorometer detector and prevent its saturation, and a cut-off filter at an appropriate wavelength to cut the exciting light when collecting the profiles B<sub>2</sub> and C<sub>2</sub>. The spectra were corrected for the baseline and the instrument errors. To obtain L<sub>a</sub>, L<sub>b</sub>, L<sub>c</sub> the integral value of the spectra A, B, C were corrected for the transmittance of the grey filter, while for P<sub>b</sub> and P<sub>c</sub> the integral values of the spectra B<sub>2</sub> and C<sub>2</sub> were corrected for the transmittance of the cut-off filter. At the end of this procedure we obtained the values for L<sub>a</sub>, L<sub>b</sub>, L<sub>c</sub>, P<sub>b</sub>, P<sub>c</sub> which were used to determine the absolute photoluminescence quantum yields.

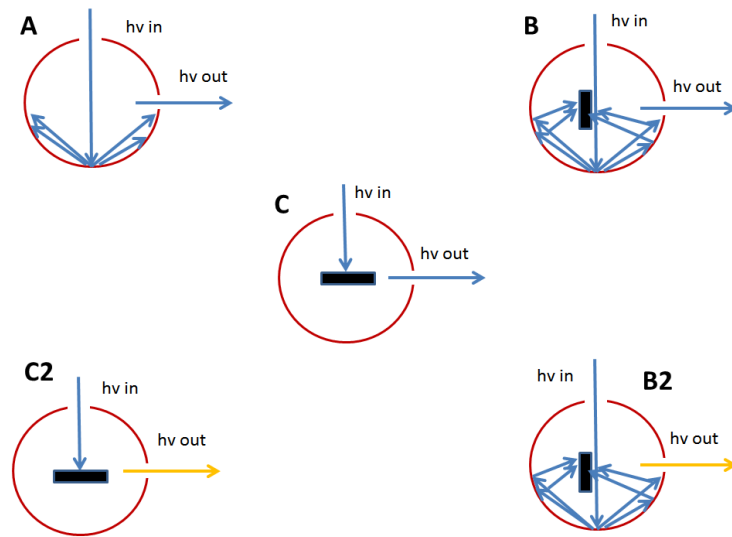


Figure D.1 | Schematic representation of the experiment needed to obtain the PLQY. In yellow the emission of the sample and in blue the incident beam

---

In Figure D.2 the spectra relative to the measures previously described are shown. It has to be specified that the area under  $L_{a,b,c}$  is related to the amount of unabsorbed light, and the area under  $P_{b,c}$  instead, is related to the amount of emitted light. For both measurements we set the instrumentation to read an emission spectrum.

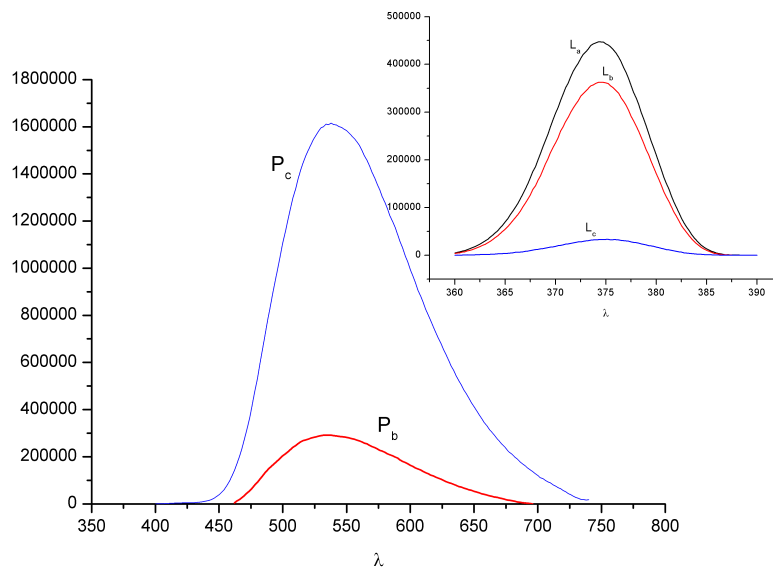


Figure D.2 | Representation of the spectral profiles obtained with the five measurements mentioned in the text.

---

# Appendix E

## Single-phase white-emitter copper iodide based Metal-Organic Framework

Supplementary information

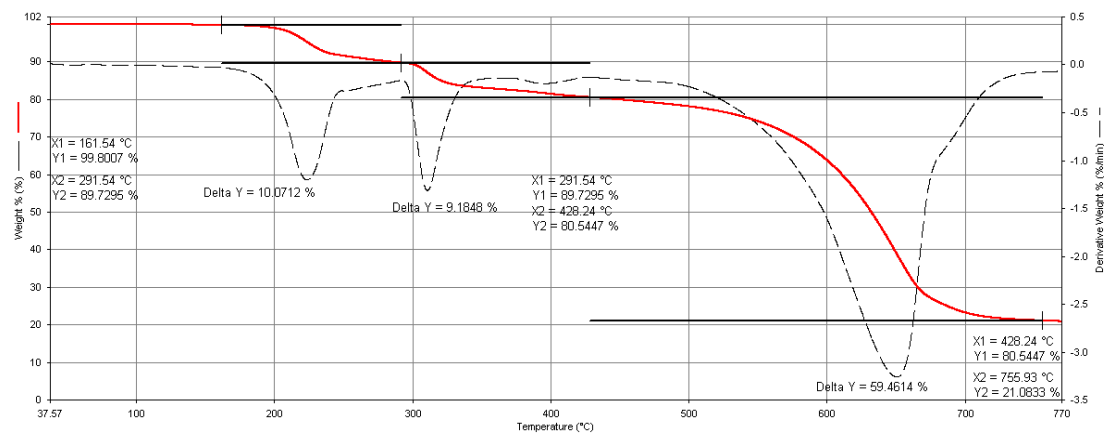


Figure E.1 | Thermogravimetric analysis of **1**. Scan rate 5°C/min. The first weight loss correspond to one ligand molecule loss in compound with  $\text{Cu}_2\text{I}_2(3\text{picolamine})_2$  stoichiometry.

---

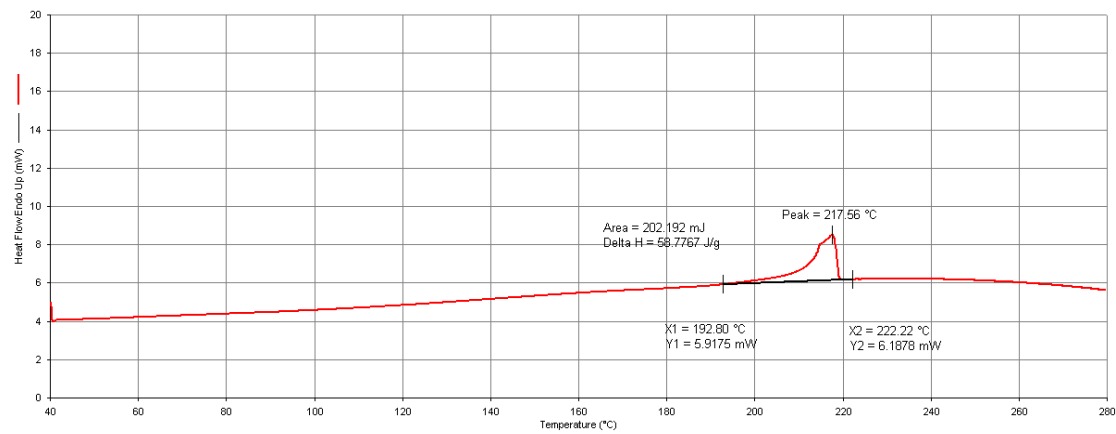


Figure E.2 | Differential Scanning Calorimetry analysis of **1**. Scan rate 5°C/min. Melting at 183°C

---

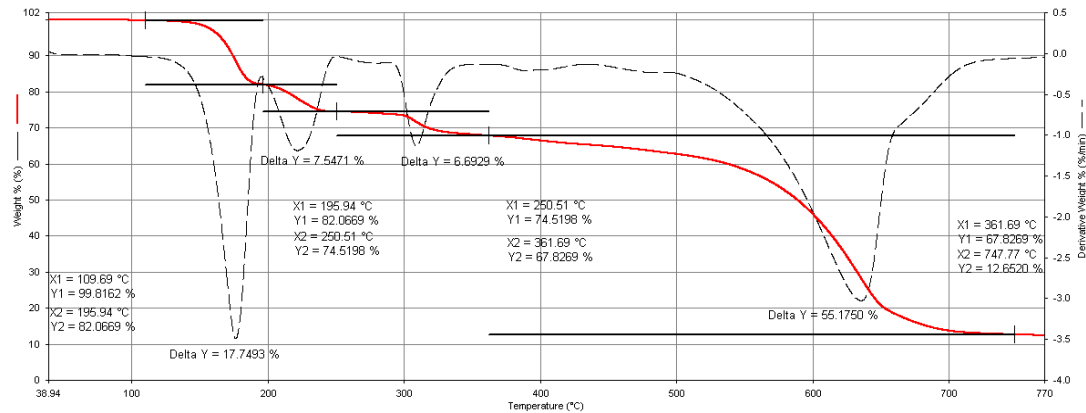


Figure E.3 | Thermogravimetric analysis of **2**. Scan rate 5°C/min. The first weight loss correspond to one ligand molecule loss in compound with  $\text{Cu}_2\text{I}_2(3\text{picolamine})_2$  stoichiometry.

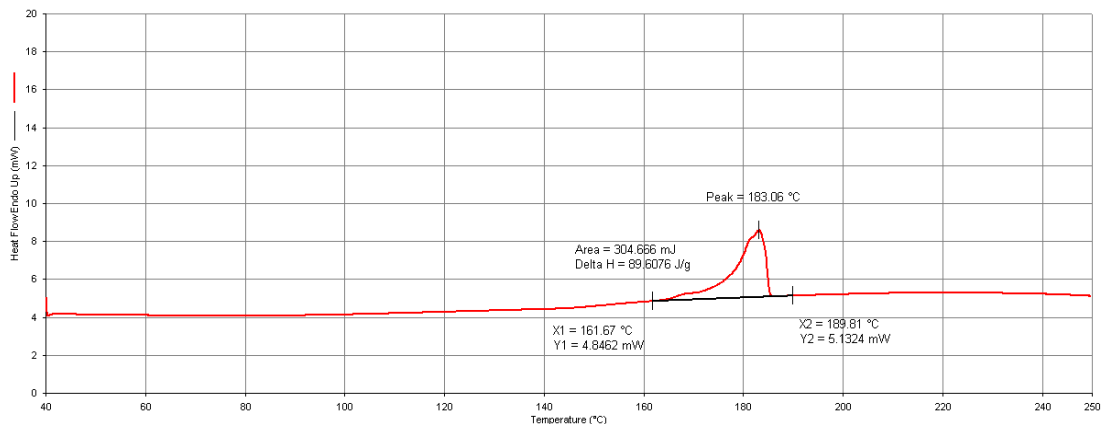


Figure E.4 | Differential Scanning Calorimetry analysis of **2**. Scan rate 5°C/min. Melting at 183°C



# Appendix F

Tuning the colour and efficiency in OLEDs by  
using amorphous or polycrystalline emitting  
layers

Supplementary Information

### Electrochemistry

The redox properties of the target Pt(II) complexes were investigated by cyclic voltammetry. Unfortunately, the solubility of Pt(ppy)(2-PTZ) in  $\text{CH}_2\text{Cl}_2$ , which is one of the preferred solvents for electrochemistry, is rather low, while the fluorinated analogue Pt(F<sub>2</sub>ppy)(2-PTZ) proved almost completely insoluble also in DMSO. Even though this feature limit the significance of the obtained results, it was possible to obtain a voltammetric curve for the complex Pt(ppy)(2PTZ) in  $\text{CH}_2\text{Cl}_2$  by using a glassy carbon (GC) working electrode coupled to a Platinum counter and in the presence of a saturated calomelane electrode (SCE) as the reference. In the region of the positive potentials, a Pt(II)-based and electrochemically and, likely, chemically irreversible process that is roughly centered at 0.9 V is observed. Relative to reductions, the voltammetric wave consist of one electrochemically irreversible process centered at -1.8 V that is assigned to the formation of a ligand (ppy or 2-PTZ)-based radical anion.

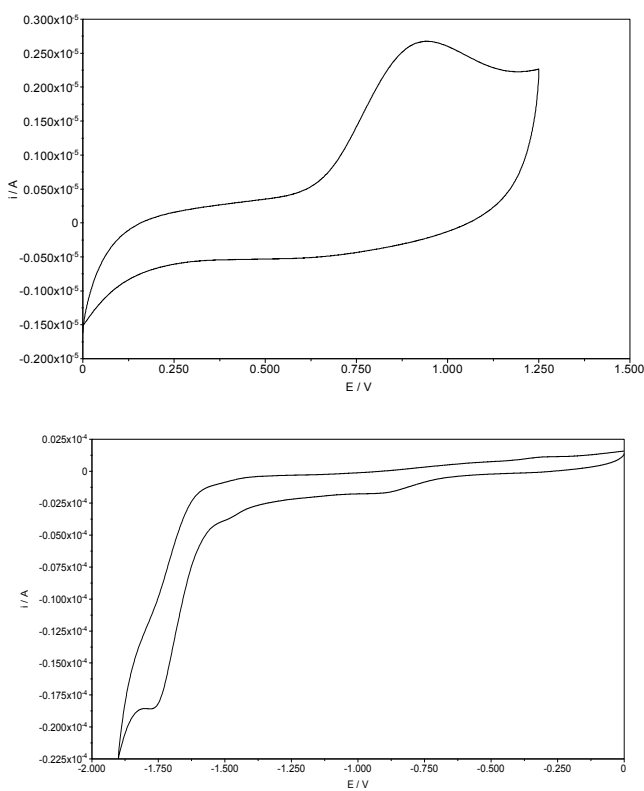


Figure F.1. | Experimental - Cyclic voltammetries were carried out using a mAutolab Type III potentiostat with computer control and data storage via GPES 110 Manager software. Solutions of concentration 1 mM in  $\text{CH}_2\text{Cl}_2$  were used, containing  $[\text{Bu}_4\text{N}][\text{BF}_4]$  as the supporting inert electrolyte. A three-electrode assembly was employed, consisting of a Glassy Carbon (GC) working electrode, platinum wire counter electrode and saturated calomelane (SCE) reference electrode. Solutions were purged for 5 min with solvent-saturated nitrogen gas with stirring, prior to measurements being taken without stirring.

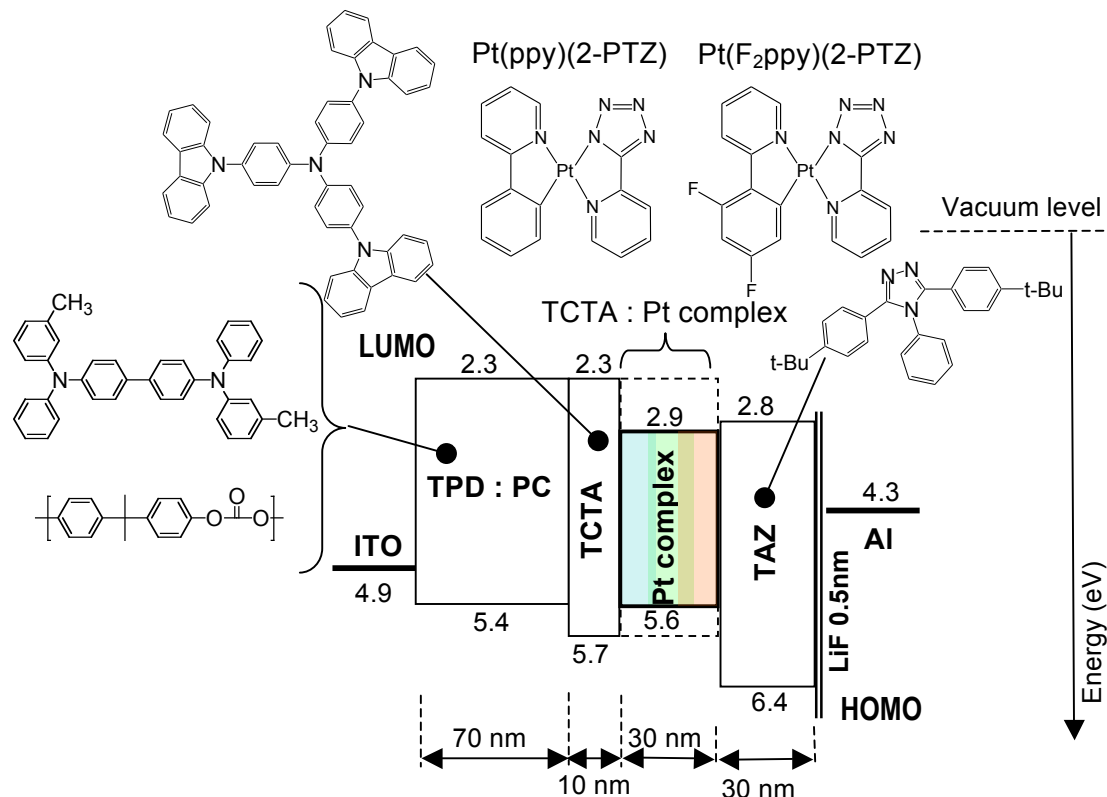
*OLED configuration*

Figure F.2 | Architecture of the LEDs manufactured, and molecular structures of the materials used. These are completed with energy level diagram shown for understanding the exciton and electronic traffic within the devices. The highest occupied molecular orbital (HOMO) obtained for each material corresponds to its ionization potential. The lowest unoccupied orbital (LUMO) is equal to the molecular electronic affinity. The Fermi level positions for ITO and Al electrode contacts are added for completion. The positions of all the levels are indicated by the numbers in electronvolts relative to the vacuum level at energy zero. HOMO and LUMO levels (eV) as calculated from redox potentials.

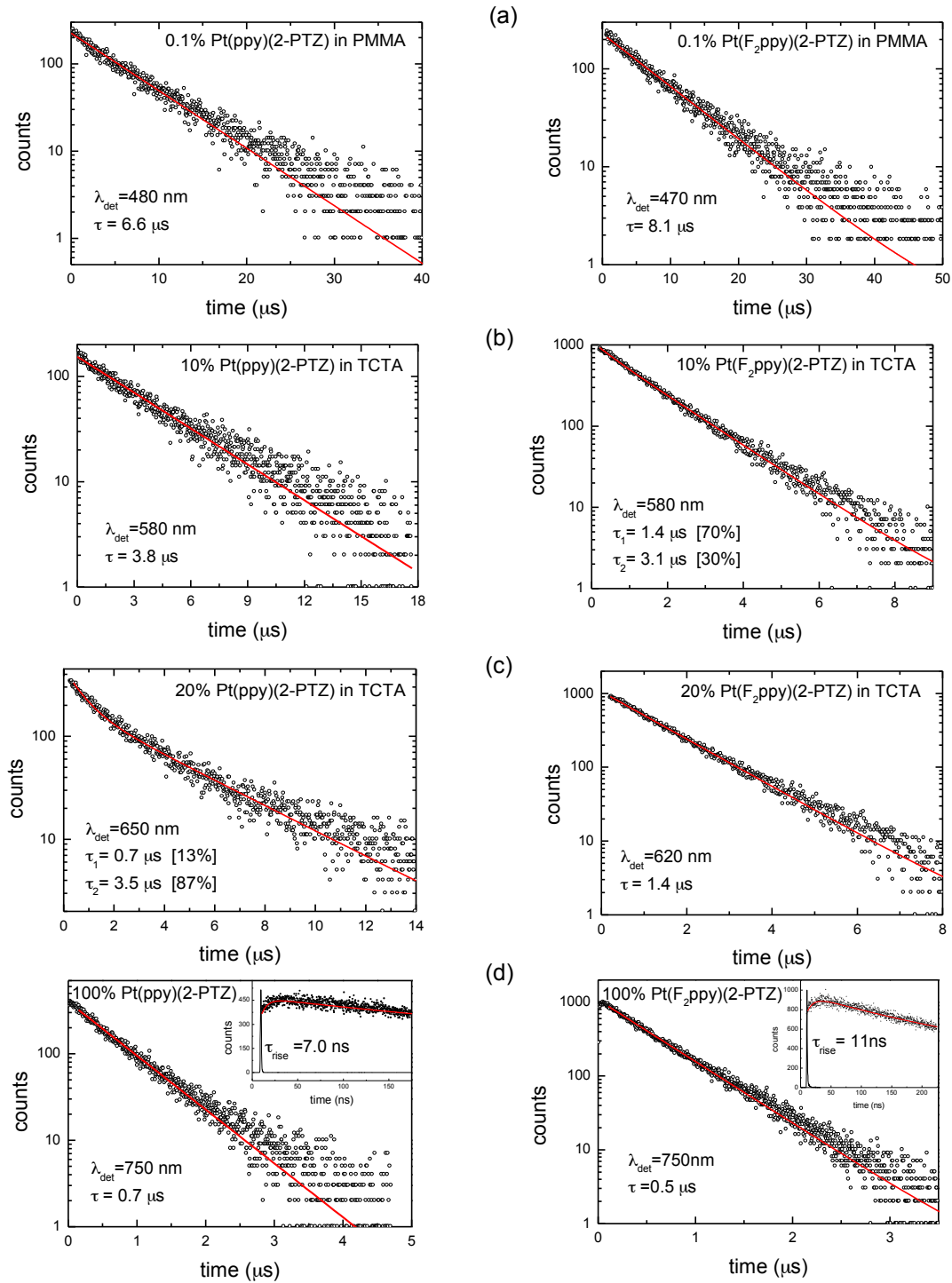
*Transient Decay Analysis*

Figure F.3 | Room temperature transient PL decays from both [4 wt% Pt complex:TCTA] blends (a), from both [10 wt% Pt complex :TCTA] blends (b) , from both [20 wt% Pt complex :TCTA] blends (c) and from neat films of both Pt complexes (d) on the microsecond time scale after excitation using light pulses of duration 1ns at  $\lambda_{\text{exc}} = 373$  nm. Also shown is the response time of the dimer phosphorescence from the neat films on a decimal nanosecond scale (inset) detected at  $\lambda_{\text{det}} = 750$  nm. Open circles represent the experimental data and solid lines are decay fits. Single-photon IBH model 5000 counter were employed for the time resolved luminescence measurements.

### X ray diffraction

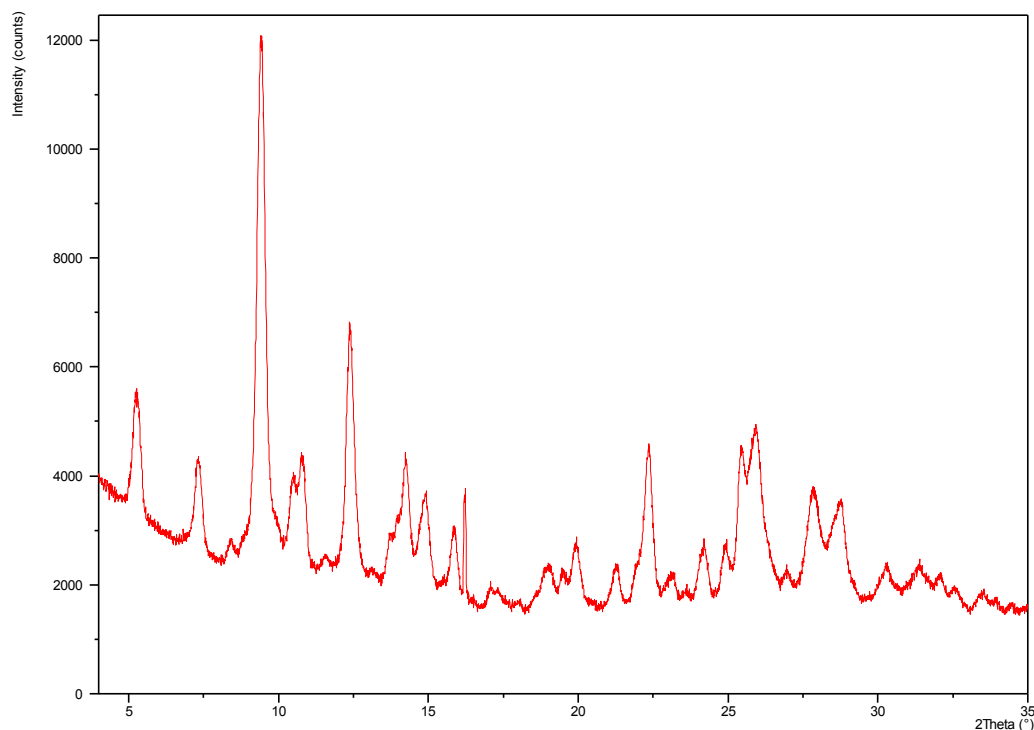


Figure F.4 | Diffractogram of the starting bulk Pt(ppy)(2-PTZ). The powder is crystalline, the sharp peak at  $2\theta = 16.3^\circ$  is due to the sample holder.

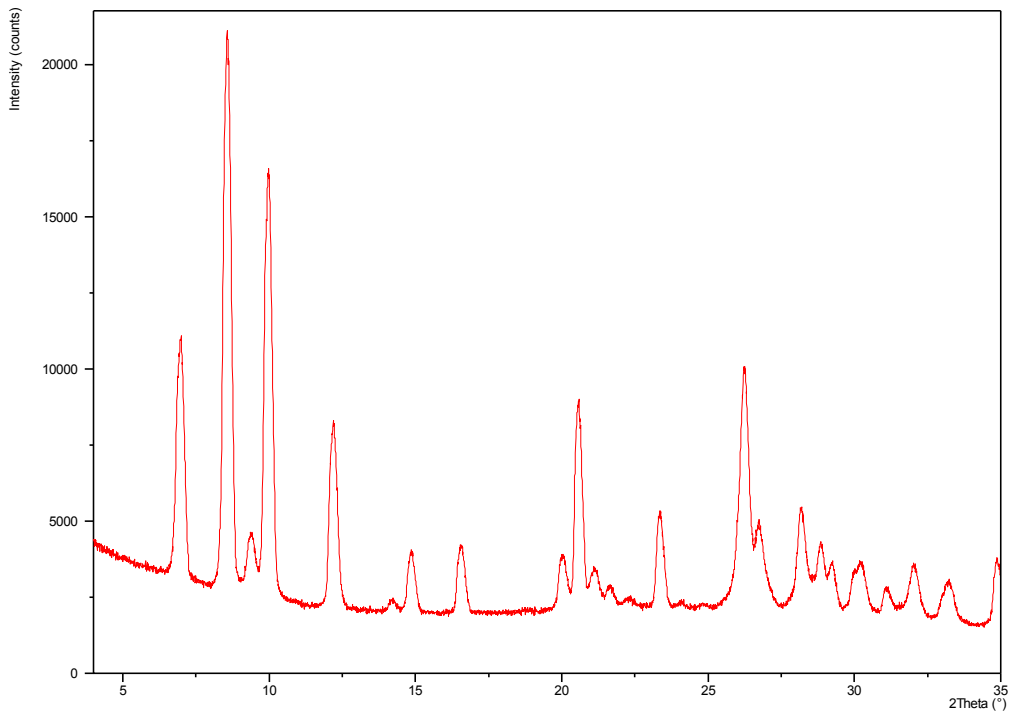


Figure F.5 | Diffractogram of the starting bulk Pt(F2ppy)(2-PTZ).

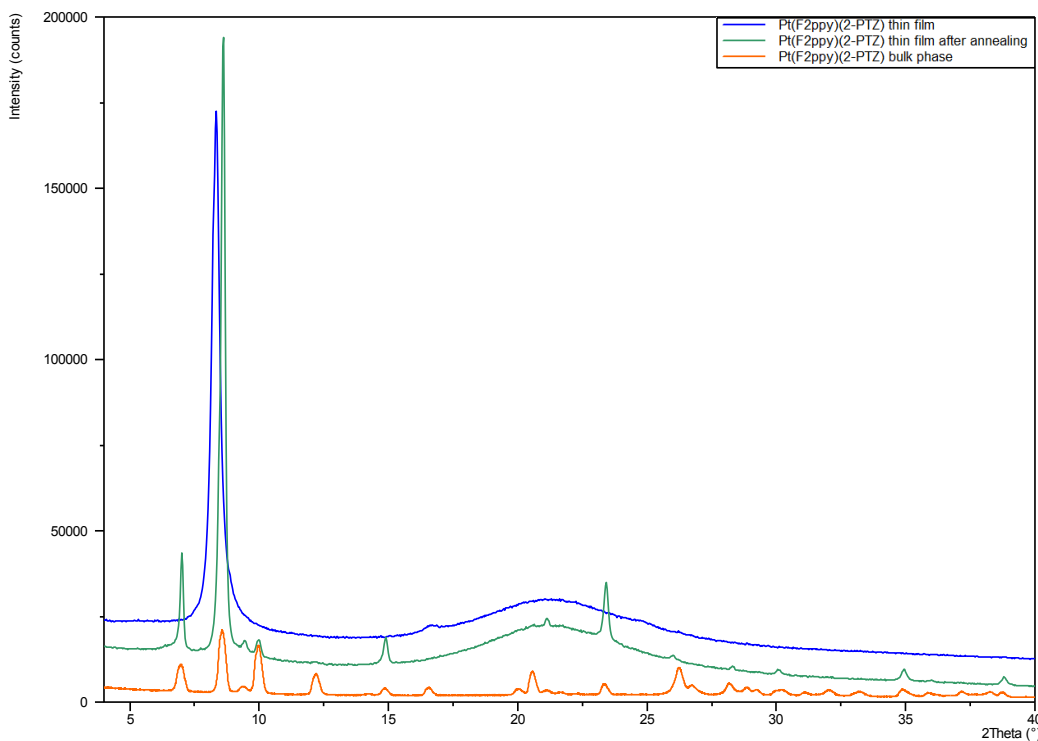


Figure F.6 | Comparison of the diffractograms of: the as-deposited Pt(F2ppy)(2-PTZ) thin film (blue line), the thin film after heating at 160°C for 30 minutes (green line) and the starting crystalline powder (red line). The as-deposited Pt(F2ppy)(2-PTZ) thin

film presents a strong peak at  $d=10.6\text{ \AA}$  which is not present in the starting material, suggesting the formation of a new form. Upon heating at  $160^\circ\text{C}$  the film converts into the bulk phase which can be easily detected by its colour change (from light yellow into pink) and confirmed by the presence of several peaks which correspond the starting powder structure.

---